University College London

The Migration of Plasticisers and Interaction of Nitrogen Dioxide and Water in Nitrocellulose Binder Systems

Thesis submitted for the degree of Doctor of Philosophy (PhD) by

Lisa A. Richards

Supervisor:

Professor Nora H. De Leeuw

UCL
Department of Chemistry

Sept. 2018

Declaration

I, Lisa A. Richards confirm that the work presented in this thesis is my own. Where information has been derived from other sources, I confirm that this has been indicated in the thesis.

Signature: Sept. 2018

Lisa A. Richards

Abstract

A nitrocellulose binder holds the explosive ingredients together in a polymer bonded explosive or propellant. The binder dissipates energy from hazardous stimuli with the aim of producing a less sensitive explosive. To improve the overall mechanical properties of a binder a plasticiser is added, however plasticiser migration from the binder polymer matrix deteriorates the mechanical properties and reduces the service life of the energetic material. To assess the migration of the plasticisers 2,4-dinitroethylbenzene, 2,4,6-trinitroethylbenzene and 1-nitramino-2,3-dinitroxypropane from each of the nitrocellulose binders, diffusion coefficients and activation energies of diffusion were obtained for each plasticiser molecule via molecular dynamics simulation. The two nitrocellulose binder systems also underwent molecular dynamics simulations to investigate the interaction of water and nitrogen dioxide in each system. Reaction of nitrogen dioxide with water produces nitric acid which is thought to further react and degrade the nitrocellulose. Plasticiser migration was found to be faster in a nitrocellulose binder plasticised with 2,4-dinitroethylbenzene and 2,4,6-trinitroethylbenzene compared to a nitrocellulose binder plasticised with 2,4-dinitroethylbenzene and 1-nitramino-2,3-dinitroxypropane. The formation of nitric acid was more likely in a nitrocellulose binder plasticised with 2,4-dinitroethylbenzene and 2,4,6-trinitroethylbenzene compared to a nitrocellulose binder plasticised with 2,4-dinitroethylbenzene and 1-nitramino-2,3-dinitroxypropane. Force fields were parameterised for each binder component. Force fields were derived for the plasticiser molecules, the stabiliser ethyl centralite, nitrogen dioxide and nitrocellulose. The Lennard-Jones parameters were refined for each individual binder ingredient and the overall nitrocellulose binder systems until the simulated densities were within 2% of the experimental values.

Impact Statement

This research is advantageous to the defense sector as it gives an important insight into plasticiser migration and the interaction of nitrogen dioxide and water in nitrocellulose binders, both of which can reduce the shelf-life of an energetic material. Any extra information which helps prolong the shelf-life of energetic materials used in public sector industries is beneficial to the wider public in terms of cost savings and safety. Molecular docking has become an important tool in drug discovery and design, it is the study of how two or more molecular structures for example, drug and receptor bind together. One docking method involves the estimation of affinities by summing the strength of the electrostatics and van der Waals interactions between all atoms of the two molecules bound together by using a force field. In this research force fields were parameterised for organic molecules which could be used for similar organic molecules in the molecular docking process, a useful contribution to the field of drug discovery in academia and the pharmaceuticals sector.

Acknowledgements

I would like to thank my supervisor Prof. Nora De Leeuw and post doc. Dr. Anthony Nash for their excellent research advice and guidance given throughout my PhD. Thank you to Dr. Thomas Collier for his technical guidance in the early stages of my project and Dr. Jamie Richards and Dr. Saul Lanyado for their suggestions on the preparation of my thesis. I would also like to thank the Atomic Weapons Establishment for their expertise, input and funding of this project. Finally, a big thank you to my family and friends especially my mum for their support throughout my PhD, especially in the final sixth months of my research.

List of Publications

1. Accepted - Richards, L. A.; Nash, A.; Willetts, A.; Entwistle, C.; de Leeuw, N. H. Modelling Water Diffusion in Plasticisers: Development and Optimisation of a Force Field for 2,4-Dinitroethylbenzene and 2,4,6-Trinitroethylbenzene. RSC Adv., 2018, 8 (11), 5728–5739 DOI: 10.1039/C7RA12254C.

2. Accepted - Richards, L. A.; Nash, A.; Phipps, M.; de Leeuw, N. H. A Molecular Dynamics Study of Plasticiser Migration in Nitrocellulose Binders. RSC New J. Chem., 2018, 42, 17420-17428 DOI: 10.1039/c8nj03464h.

3. Conference Proceedings - Lai, A.; Richards, L. A.; Nash, A.; de Leeuw, N. H. Investigating the Transport of Gases and Decomposition Pathways in Plasticised Nitrocellulose Materials. NTREM, International Seminar New Trends in Research of Energetic Materials, 2017, 20; 752-757

Table of Contents

Table of Tables

Chapter 3 - Parameterisation of Force Fields for the Plasticiser and Stabiliser molecules, Nitrocellulose and Nitrogen Dioxide

Chapter 4 - Migration of the Energetic Plasticisers 1-Nitramino-2,3-Dinitroxypropane, 2,4-Dinitroethylbenzene and 2,4,6-Trinitroethylbenzene in two Nitrocellulose Binder Mixtures

Table of Figures and Graphs

Chapter 1 - Introduction

Chapter 2 - Methodology

Chapter 3 - Parameterisation of Force Fields for the Plasticiser and Stabiliser molecules, Nitrocellulose and Nitrogen Dioxide

Chapter 5 - The Interaction of Water and Nitrogen Dioxide in the two Nitrocellulose Binder Systems

1. Introduction

1.1 Propellants and Energetic Materials

1.1.1 Explosives

One of the earliest known explosives thought to have been discovered in the 7th century was black powder a mixture of potassium nitrate, charcoal and sulfur.[1] The Chinese used black powder as a propellant, explosive and in fireworks as it undergoes a reactive combustion which releases large amounts of heat and gas in the process.[1,2] Development of nitrocellulose (NC) and nitroglycerine (NG) in Europe in the 1800s produced a new type of explosive which combusted slowly in a contained manner releasing a large volume of hot gases which could launch a projectile, this new type of explosive was named a propellant.[2] Later, research and development led to the production of much more powerful high explosives such as trinitrotoluene (TNT), cyclotetramethylene tetranitramine (high melting explosive, HMX) and cyclotrimethylene trinitramine (research department explosive, RDX).[2] An explosive can be defined as a substance which when detonated undergoes a very fast decomposition releasing a large amount of energy and a volume of gases substantially greater than the original volume of the explosive. Any material that can reach a highly energetic state mainly by chemical reactions is commonly known as a high energy material (HEM) or an energetic material (EM).[2]

1.1.2 Energetic Binders, Propellants and Polymer Bonded Explosives

Solid rocket propellants can be considered as highly filled polymers, typically containing approximately 85 wt. % explosive suspended in approximately 15 wt. % elastomeric binder.[3] NC was one of the first polymers used as a binder in homogeneous propellants, the NC enabled the propellant to be shaped to fit a wide range of motor geometries.[4] Various polymers began to

be investigated as potential binders for solid propellants and they were also considered as binders for high explosives, primarily for desensitisation.[4] This research eventually led to the development of polymer bonded explosives (PBX), highly filled composite materials consisting of explosive crystals and a polymeric binder approximately 5-10% by weight.[5] The polymeric binder in a PBX dissipates energy from hazardous stimuli with the aim of producing a less sensitive explosive.[6] The first PBX, PBX 9205 consisted of RDX crystals embedded in a polystyrene matrix plasticised with dioctyl phthalate.[7] The creation of PBX reduced the problem of explosive sensitivity, however the use of a non-energetic binder reduced the energetic output of the EM.[4] This resulted in the development of energetic binders containing energetic polymers, these polymers contain energetic functional groups such as nitro and azido groups.[4] The use of an energetic binder in a propellant or PBX enhances the energetic performance and enables the formulation to have comparatively less explosive filler thereby reducing sensitivity.[4] Therefore, a number of energetic polymers were synthesised specifically for use in binders of PBX and propellants. Examples of energetic polymers are nitrato polyethers such as poly(3-nitratomethyl-3-methyloxetane) known as polyNIMMO and poly(glycidyl nitrate) known as polyGLYN.[6] Energetic polymers like glycidyl azide polymer (GAP) use the positive heats of formation of the azido chemical groups to enhance energetic output.[4]

1.1.3 Insensitive Munitions

The development of Insensitive Munitions (IM) began in the 1970s with the aim of producing munitions which gave the required performance without violent response when subject to enemy action or accident.[8] The sensitivity of an EM to external stimuli and the response of the EM is determined by chemical characteristics such as the explosive compound used as well as physical

features such as the composition of the formulation. One approach in the design of insensitive munitions is to select explosive compounds that have inherently lower thermal decomposition and/or lower sensitivity to shock.[8] The composition of a formulation can significantly affect the response of an EM, in particular the binder ingredients. Binder ingredients which lessen the susceptibility of the EM to shatter, so that available burning surface is reduced will decrease the resulting EM response. An energetic binder can also reduce the amount of explosive compound required, decreasing sensitivity.[2]

1.1.4 Plasticisers

Plasticisers are added to a binder to alter the mechanical properties, primarily to improve safety characteristics.[6] The mechanical properties are altered by softening the polymer matrix of the binder which makes it more flexible. A plasticiser also enhances other properties such as tensile strength and softening point (T_g) which eases processing at lower temperatures.[2,6] Non-energetic plasticisers can modify toughness, softening point and tensile strength but do not contribute to the energetic output of an EM. Energetic plasticisers like energetic polymers contain functional groups such as azido, nitro and fluoroamino which add to the energy of the system, this combined with their modification of the mechanical properties of an EM means they are often favoured over non-energetic plasticisers.[2] Together with a positive influence on safety, performance and mechanical properties additionally the chemical stability, toxicity, compatibility with other constituents and the cost of a plasticiser must be considered.[6] Overall, the efficiency of a plasticiser is determined by the plasticiser's capability to produce the desired effect.[2] Due to the demand for plasticisers that meet certain requirements research into new and

improved plasticisers is ongoing.[9–12] Some of the main classes of energetic plasticiser are outlined below:[6]

- GLYN dimer – A glycidyl nitrate derivative which is used as a plasticiser of polyether binder systems such as polyNIMMO and polyGLYN.
- Nitrato Ethyl Nitramine (NENA) – NENAs contain both nitamine and nitrate ester functional groups and are particularly good at plasticising NC systems.
- Azido plasticisers – Plasticisers containing energetic azido functionalities.
- Nitrate esters – One of the first nitrate ester plasticisers was glycerol trinitrate or nitroglycerine (NG). However, NG was found to have many undesirable characteristics so compounds structurally similar to NG have been synthesised such as ethyleneglycol dinitrate (EGDN) and butanetriol trinitrate (BTTN).

1.1.5 Plasticiser Migration

Another important characteristic a plasticiser should possess is a low migration or exudation rate. Plasticisers have the tendency to seep out of EM formulations during storage which is known as plasticiser migration or exudation.[2] It has been suggested that even under moderate storage conditions most plasticisers used in PBXs migrate from the binder matrix.[13] The extent of plasticiser migration can depend on the degree of polymer crosslinking, the polymer-plasticiser system and the molecular weight of the plasticiser.[14] The mobility of a plasticiser molecule in a medium is inversely proportional to the plasticiser molecule's molecular weight.[13] A small amount of plasticiser migration is thought not to adversely affect mechanical properties of an EM, but considerable migration has severe effects.[15] Evaporation of plasticisers from a propellant can weaken the propellant grains, cause cracking at stress points, induce variations in

the burning rate and cause poor operation of the rocket motor.[16] It is critical that a plasticiser has sufficiently low-volatility to enable long-term storage of the EM formulation without significant alteration of properties and composition.[17] Techniques have been employed to prevent or reduce migration of plasticisers,[2] one approach is to use a plasticiser with structural similarity to the energetic polymer to increase miscibility.[13]

1.2 Nitrocellulose

1.2.1 Nitrocellulose Structure and History

Nitrocellulose was first discovered in 1833. Henri Braconnot found that when he mixed wood fibres or starch with nitric acid a lightweight explosive material was produced, he named this substance xyloïdine.[18] Théophile-Jules Pelouze made the same discovery in 1838 and gave the NC a different name, nitramidine.[19] In 1846, the first practical preparation of nitrocellulose (NC) was performed by Schönbein.[20] NC is prepared by nitrating cellulose, in Schönbein's patented procedure sulfuric acid was included in the mixture of nitric acid and cellulose.[4] He had discovered a method of nitrating cellulose which is used today, which increases the degree of nitration. By changing the reaction conditions and acid concentration, NC can be synthesised with varying nitrogen content from 12.0%-13.5%. As the nitrogen content increases the NC becomes less stable.[2] In fully nitrated NC all three hydroxyl groups in a celluose glucapyranose unit have been nitrated.

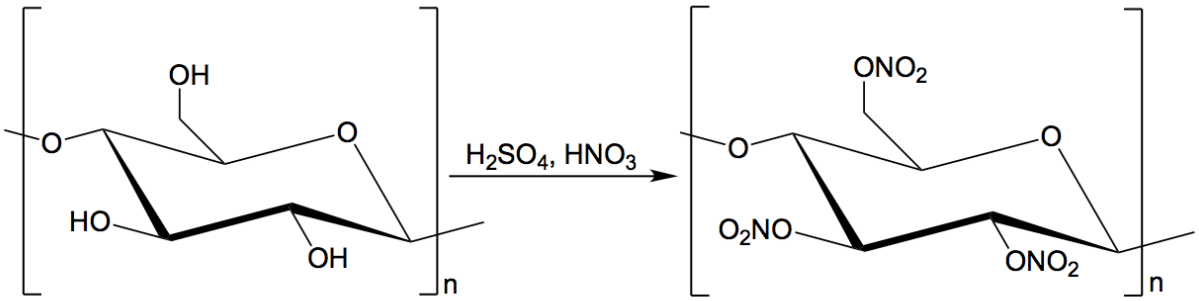

Figure 1 Diagram showing the synthesis of fully nitrated nitrocellulose from cellulose using a nitrating mixture.

The nitrogen content of NC in the dry state is used to find the degree of substitution, one of the characteristics used to determine the suitability of NC for a particular application. In Figure 1, all three hydroxyl groups in the cellulose glucapyranose unit have been substituted with a nitro group which would give a nitrogen content of 14.14%.[21] However, in practice only a 13.6% nitrogen content is achieved. Once the nitrogen content is above 12.6% NC is considered to be an explosive.[21]

1.2.2 Nitrocellulose in Binders and Propellants

The earliest binders used for propellants contained NC and later a mixture of NC and NG was used. NC thickened NG and reduced friction and impact sensitivity.[6] A single-base (SB) propellant contains NC as the only explosive ingredient. NC with a content of 12.5 – 13.25 % makes up more than 90 % of the mixture which also contains a plasticiser and a stabiliser.[2] In 1888 Alfred Nobel invented Ballistite, a combination of NG and soluble NC with a small amount of stabiliser and this was followed by the development of Cordite by Nobel and James Dewar a mixture of 37 % NC, 58 % NG and 5 % Vaseline.[4] Propellants which contain NG and NC are

known as double base (DB) propellants, DB propellants are of higher energy than SB propellants because NG is highly energetic and adds to the energetic output. The NG also has a positive oxygen balance which results in the complete oxidation of NC.[4]

1.2.3 Nitrocellulose Decomposition

NC decomposes even under normal storage conditions.[22] The decomposition of NC over time can lead to self-ignition which has led to fatal disasters being reported globally.[23–25] Due to the use of NC as an explosive ingredient in propellants, PBX, other energetic material formulations and in many non-explosive applications such as inks, lacquers and coatings the degradation mechanisms leading to NC decomposition have been widely investigated. Research in the 1950s indicated NC degradation started with an initial reaction followed by secondary reactions,[26] gaseous products from the initial reaction capable of reacting further with the solid residue were also reported.[27] It is now generally accepted that NC decomposition is initiated by the breaking of the O-NO_2 bond.[22,28–30] Successive reactions occur after the initial breaking of the O-NO_2 bond which have been termed 'autocatalytic',[29] however there is still some discussion over the complex reaction pathway which follows.[31,32] Two mechanisms of NC degradation proposed by Chin et al. are hydrolysis and thermolysis.[28] Cleavage of the O-NO_2 bond is initiated by acid hydrolysis in the hydrolysis mechanism,[28]

Initial Steps

$$RONO_2 + H_2O \rightarrow ROH + HNO_3 \quad (1)$$

$$ROH + HNO_3 \rightarrow RCHO + HNO_2 + H_2O \quad (2)$$

Propagation Steps

$$HNO_3 + HNO_2 \rightarrow N_2O_4 + H_2O \quad (3)$$

$$N_2O_4 \rightleftharpoons 2NO_2 \quad (4)$$

$$ROH + NO_2^{\cdot} \rightarrow {}^{\cdot}ROH + HNO_2 \quad (5)$$

$${}^{\cdot}ROH + HNO_3 \rightarrow RCHO + H_2O + NO_2 \quad (6)$$

Heat breaks the O-NO_2 bond in the thermolysis mechanism:[28]

Initial Step

$$RONO_2 \rightarrow RO^{\cdot} + NO_2 \quad (7)$$

Propagation Steps

$$RO^{\cdot} + NO_2^{\cdot} \xrightarrow{RONO_2} RONO_2 + NO + N_2O_4 + NO_2^{\cdot} + H_2O + N_2O + CO_2 + CO + C_2H_2O + \text{other organic fragments} \quad (8)$$

$$2NO + O_2 \rightarrow 2NO_2 \rightleftharpoons N_2O_4 \quad (9)$$

A number of products are formed during the decomposition of NC, as shown in equations 1-9. The nitrogen oxides, particularly NO_2 are considered to be the most detrimental.[33] Nitrogen dioxide is very reactive and can catalyse exothermic reactions leading to self-ignition, nitrogen dioxide also reacts with water to produce HNO_3 which is also thought to contribute to further degradation.[22,28] The changes in EM properties during production and storage are called aging. Various methods are used to study the aging of EMs containing NC to gain a better understanding of the nature and rate of decomposition.[34] For example, heat tests measure the weight loss of NC at elevated temperatures and NOx chemiluminescence detects nitrogen oxides produced during the heating of NC.[34] These tests, often termed stability tests can be used to predict the shelf life of an EM.

1.2.4 Stabilisers of Nitrocellulose

The storage life or shelf life is the length of time an EM can be stored safely without risk of self-ignition. The ballistic shelf life is the period of time in which ballistic properties are maintained, which usually ends before shelf life.[22] As an EM containing NC ages, decomposition will produce nitrogen oxides. Stabilisers are added which react easily with nitrogen oxides to prevent the autocatalytic reactions which further decomposition,[33] the addition of a stabiliser therefore increases the shelf life and safety of an EM. Instead of 2-4 days in the case of unstabilised NC, propellants that contain stabiliser in some instances have been stored at 70 °C for years without further degradation.[35] Conventional stabilisers for NC-based propellants are either aromatic urea derivatives or aromatic amines.[36,37] Aromatic amine and aromatic urea derivative stabilisers react with nitrogen oxides and in the process are converted to a range of nitrosamines and nitroamines.[38] Over time the stabiliser depletes completely due to reaction with more and more nitrogen oxides released during NC decomposition.[38] Often a stabiliser is unevenly distributed through an energetic material formulation, however this should not affect stability as it is thought the stabiliser migrates to where it is required.[22] The nitrogen oxides produced by NC decomposition are also likely to be mobile in the EM formulation. Ethyl Centralite (EC) displayed in Figure 2, is an aromatic urea-based stabiliser. EC depletes as it reacts with nitrogen oxides via a complex process to produce a mixture of N-nitroso and nitro derivatives.[38]

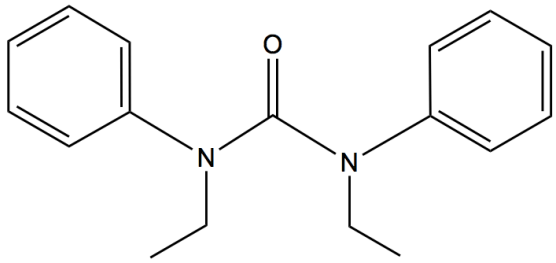

Figure 2 – Diagram of the stabiliser Ethyl Centralite.

1.2.5 Plasticisers of Nitrocellulose

A range of energetic plasticisers have been found to be particularly good at plasticising NC. Nitrate ester based plasticisers such as NG, triethylene glycol nitrate (TEGDN), 1,2,4-butane triol trinitrate (BTTN) and trimethylol ethane tri nitrate (TMETN) are effective plasticisers of NC. As mentioned previously NG was used as a plasticiser in one of the earliest NC binder formulations, however it is unstable at temperatures above 70-80°C and when heated to above 200°C it will explode.[6] Alternative nitrate esters were synthesised to overcome the shortcomings of NG. TEGDN has lower impact sensitivity than NG, TMETN has low volatility and is chemically stable and BTTN has shown increased stability compared to NG.[2,6] The nitroethyl nitramines (NENAs) have shown effective plasticising ability particularly for NC systems, displaying properties such as high burning rates and reduction in product gas molecular mass and flame temperature.[6] Alternative plasticisers for NC are continually being investigated. More recent studies have shown glycidyl azide polymer (GAP) to be an effective plasticiser in NC powders used for propellants and azidomethyl-dinitroxydimethyl-nitromethane (AMDNNM) was combined with NC to create a thermally stable plastic with low impact sensitivity suitable for propellants.[12,39] The energetic plasticisers that have been investigated in this research are 2,4-

dinitroethylbenzene (2,4-DNEB), 2,4,6-trinitroethylbenzene (2,4,6-TNEB) and 1-nitramino-2,3-dinitroxypropane (NG-N1). As early as 1934, nitroderivatives of ethylbenzene were found to have a gelatinising effect on NC of any nitrogen content,[40] the energetic plasticiser K10 is still used in NC energetic material formulations and is a mixture of 65% 2,4-DNEB and 35% 2,4,6-TNEB (Fig 3). The compound NG-N1 is a primary amine related to NG which has shown good potential as an energetic filler in EM formulations with reduced impact sensitivity from 0.2 J for NG to 14 J for NG-N1 (Fig 3).[41] The feasibility of NG-N1 as a plasticiser ingredient in an NC binder for 1,3,5,7-Tetranitro-1,3,5,7-tetrazocane (HMX) has been investigated.[42] The energy of a NC binder plasticised with a mixture of 33.3% NG-N1 and 66.6% 2,4-DNEB exceeded that of a NC binder plasticised with K10.[42] The NG-N1 and 2,4-DNEB plasticiser mixture was successful in gelatinising NC, but some phase separation was apparent in the proportions studied.[42] Testing of the entire HMX formulation containing the NC, 2,4-DNEB and NG-N1 binder showed improved performance in velocity and pressure of detonation.[42]

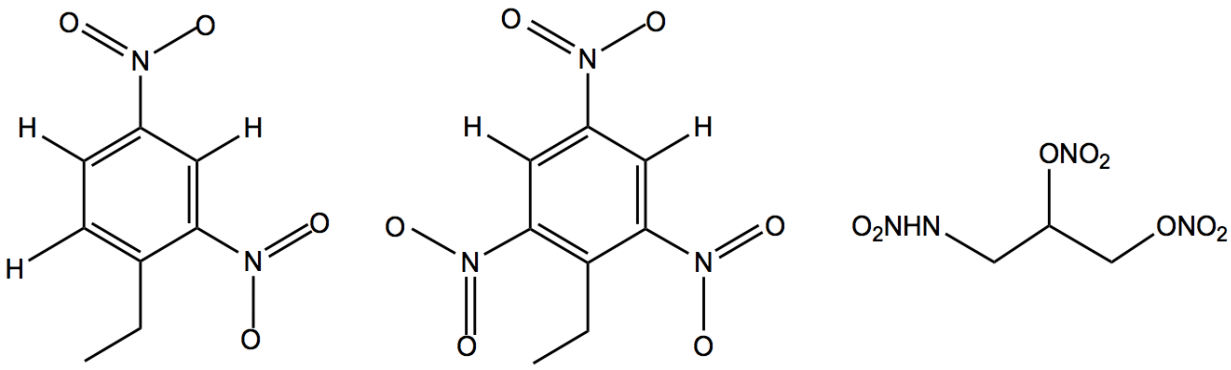

Figure 3 – Diagram displaying the plasticiser molecules 2,4-dinitroethylbenzene (2,4-DNEB), 2,4,6-trinitroethylbenzene (2,4,6-TNEB) and 1-nitramino-2,3-dinitroxypropane (NG-N1), respectively.

1.2.6 Storage of Nitrocellulose

The decomposition of NC can lead to self-ignition. Fatal disasters have occurred in relation to NC storage and the likelihood of fire or even explosion is greatly increased when NC is dry.[23,24] For this reason industrial NC is required by law to contain at least 18% plasticiser or 25% wetting agent, for example water or alcohol.[21] The plasticiser or wetting agent, phlegmatises the NC to deactivate the hazardous properties of dry NC such as high flammability.[21] Similar caution is required for transportation and storage of NC used in explosives, especially as the nitrogen content is likely to be greater than NC used for non-explosives such as inks and lacquers. NC to be used in explosives may also be transported and stored in a wetting agent, although there are alternative methods such as fine particle NC slurry formation using a solvent such as hexane.[43,44] Organisations storing and processing NC must ensure strict guidelines are followed regarding the material's treatment and storage. Poor safety awareness and not following the correct protocols contributed to the catastrophic NC explosion at Tianjin Port, China.[25] Evaporation of the wetting agent from the NC due to incorrect storage dried the NC and decomposition and heat release followed. Spontaneous combustion of the NC occurred and the fire spread to other flammable materials stored in too close proximity.[25]

1.3 Molecular Dynamics Studies of Energetic Materials containing Nitrocellulose

Various molecular dynamics (MD) studies have been performed on EMs containing NC.[9,45,46] The COMPASS force field has been extended to include high-energy nitro functional groups which has been implemented in some studies of EMs containing NC.[47] The COMPASS force field was employed in MD simulations to investigate the plasticising ability of 1,5-diazido-3-nitrazapene (DIANP) on NC.[46] Another implementation of the COMPASS force field was in a

MD study of the mechanical properties of NC, NG and the double base propellant consisting of NC and NG.[48] MD simulations using the ReaxFF reactive force field calculated the decomposition products of gunpowder containing NC, NG and the nitrate ester stabilisers diphenylaniline and EC.[49] To the best of my knowledge there have been no MD investigations into plasticiser migration or the diffusion of nitrogen dioxide and water in EMs containing NC.

1.4 Previous Investigations of Plasticiser Migration in Energetic Materials

A number of studies have used isothermal thermogravimetric analysis (TGA) to investigate plasticiser migration in propellants and energetic binder systems. During isothermal TGA the sample is maintained at constant temperature for a period of time and the change in mass recorded. The results obtained from isothermal TGA of a NC and NG DB propellant was used to calculate an activation energy of 89 kJ mol^{-1} for NG evaporation.[50] Cartwright also employed isothermal TGA to obtain diffusion coefficients and activation energies for plasticisers in NC propellants, concluding that NENA plasticisers had lower migration rates than NG or DEGDN.[17] Other systems studied using the isothermal TGA technique are a polyGLYN binder plasticised with GLYN oligomer and a polyGLYN binder plasticised with K10.[13] The diffusion coefficients of K10 and the GLYN oligomer showed an inverse relationship with molecular mass, whereby the GLYN oligomer with a higher molecular mass diffused at a slower rate than the lower molecular mass K10.[13] Diffusion coefficients for the plasticiser dioctyl azelate in a hydroxyl-terminated polybutadiene propellant were obtained by Libardi et al. using an alternative method.[51] Samples of the propellant were aged at 80 °C for 31 days and plasticiser concentration data collected from gas chromatography analysis, the diffusion coefficients for the plasticiser were calculated via a computer program using Fick's 2nd Law of diffusion.[51] Another study into

plasticiser migration focused on the diffusion of the curing agent and plasticiser across the bondline between the propellant formulation and the insulation in solid propellant rocket motors.[52] The weight uptake of the plasticiser and curing agent into the insulating material was measured and diffusion coefficients calculated from the results via Fick's 2nd Law of diffusion.[52] The effect of the degree of crosslinking and the amount of polymer in the polymer matrix on the diffusion rate of the plasticiser is a finding highlighted in research into plasticiser migration in propellants.[17,52–55] The evaporation rate of NG from a DB propellant was found to decrease with increased crosslink density, in a crosslinked polymer the plasticiser molecules are trapped resulting in less plasticiser migrating to the surface of the propellant.[53] Research by Phillips observed greater plasticiser diffusion rates in more highly plasticised NC propellants, Phillips' explanation being that the ability of NC to restrict the movement of plasticiser is lessened at higher plasticiser concentrations.[55]

1.5 Previous Investigations into Nitrogen Dioxide Formation and Interaction in Nitrocellulose

Many studies have investigated the aging and decomposition of NC. Research has identified products formed during the NC degradation process, with some research focusing specifically on the formation of NO_2 and the subsequent interaction of NO_2 within NC. Luo et al. studied the thermal decomposition of NC at different temperatures using X-ray photoelectron spectroscopy analysis and identified that high temperatures led to the rupture of the O-NO_2 bond.[56] An investigation using isothermal high temperature infrared spectroscopy found a rapid decrease in the O-NO_2 band intensity also suggesting breakage of the O-NO_2 bond.[29] Chemiluminescence has been employed to identify the decomposition products of NC, Vogelsanger and Sopranetti found

NOx was produced immediately after heating NC to 65.5 °C and Volltrauer and Fontijn reported NO_2 as the primary NC decomposition product which was rapidly reduced to NO.[34,57] Analysis of the spontaneous ignition mechanism of NC whilst pressure was altered during isothermal storage at 393 K indicated that NO_2 contributed to the decomposition process.[32] Another study into the interaction of NO_2 in NC during the decomposition process identified $RNO_2^{\bullet}$ radicals, it was proposed that the $RNO_2^{\bullet}$ radicals formed by reaction of NO_2 with NC.[58] Analysis using Fourier Transform Infrared Spectroscopy (FTIR) showed nitrocellulose can uptake a considerable amount of NO_2, which is even higher if water is also present.[34] A thorough search of the literature revealed that no diffusion coefficients have been calculated from experiment for NO_2 in NC or NO_2 in EMs containing NC.

1.6 Previous Investigations into the Interaction of Water in Nitrocellulose

Some previous studies have observed the possible effects of water on the NC degradation process, in particular the reaction of water with NO_2. In 1955 Oliver and Boyd reported that the decomposition of NC occurred rapidly if NO_2 was added to wet NC and the decomposition was even faster with the addition of a few drops of nitric acid.[59] Using FTIR Vogelsanger and Sopranetti reported that absorption of NO_2 by NC was consistent with the stoichiometry of the reaction of NO_2 with water to produce HNO_2 and HNO_3:[34]

$$2NO_{2\,(g)} + H_2O_{\,(l)} \rightarrow HNO_{2\,(aq)} + HNO_{3\,(aq)}$$

Chin et al. proposed that the reaction of water with NO_2 to produce HNO_3 is the initial step in the hydrolysis degradation mechanism, the HNO_3 is then involved in other steps of the degradation process.[28] Lindblom also highlighted that NO_2 together with the existence of moisture within NC further deteriorates stability due to the formation of reactive HNO_3.[22] Diffusion coefficients for

water in nitrocellulose have been measured experimentally. Long and Thompson used sorption and desorption studies to obtain diffusion coefficients.[60] The sorption studies were conducted by suspending an NC polymer film on a quartz spring balance in an evacuated chamber, water vapour was then introduced at the chosen pressure and the mass increase of the NC film measured as a function of time.[60] For desorption, the NC film was equilibrated with water vapour, the chamber opened, emptied and the mass loss of the NC film measured as a function of time.[60] The mass changes over time and film thickness were then used to calculate the diffusion coefficients. Diffusion coefficients were calculated via the experimental solubility and permeability constants in a study by Hsieh.[61] Lewis obtained diffusion coefficients for water in nitrocellulose by conducting sorption studies using a method very similar to that used by Long and Thompson.[61,62] The diffusion coefficient obtained by Hsieh for water in NC films of 2.62×10^{-9} cm^2 s^{-1} was in reasonable agreement with the value obtained by Lewis of 1.8×10^{-9} cm^2 s^{-1}.[61,62] The diffusion coefficients for water in NC calculated by Long and Thompson increased with film thickness, their values of $1.8 – 3.83 \times 10^{-8}$ cm^2 s^{-1} are an order of magnitude greater than those found by Hsieh and Lewis.[60] The films used in the study by Lewis were much thinner than those used by Long and Thompson, which may account for the lower diffusion coefficient obtained by Lewis for water in NC films.[60,62]

1.7 Nitrocellulose Binder Systems studied in this Research

Two NC binder systems which have been investigated in previous experimental work were studied in this research:[42]

- A NC binder containing 11% NC and 89% plasticiser by mass. The plasticiser component consisted of 67% 2,4-dinitroethylbenzene (2,4-DNEB) and 33% 1-nitramino-2,3-dinitroxypropane (NG-N1). The stabiliser EC was added in a proportion of 1% of the total binder mass.
- A NC binder containing 11% NC and 89% plasticiser by mass. The plasticiser component consisted of 65% 2,4-dinitroethylbenzene (2,4-DNEB) and 35% 2,4,6-trinitroethylbenzene (2,4,6-TNEB), also known as the plasticiser mixture K10. The stabiliser EC was added in a proportion of 1% of the total binder mass.

1.8 Practical Challenges in the Design, Production and Storage of Energetic Materials

When designing energetic materials (EM) enhanced performance (energy output) is required, however reduced vulnerability during storage and transportation is also critical.[6] EMs such as propellants and PBXs contain an explosive ingredient which is often crystalline suspended in a polymeric binder. The addition of the binder creates a rubber-like formulation which can be shaped but can also absorb and dissipate energy from hazardous stimuli, reducing vulnerability.[6] The length of time in which ballistic properties are preserved, known as the ballistic shelf-life proceeds the storage life or shelf-life which is the length of time an EM can be stored safely. When designing and producing EMs any factors which may impact the ballistic shelf-life, storage-life and overall safety and sensitivity of the formulation must be considered. The two nitrocellulose (NC) binder systems studied in this research each consist of the energetic polymer

NC and a plasticiser mixture, the plasticiser mixture is added to modify the physical and mechanical properties of the binder. In previous experimental work the NC binders were investigated as potential binders of the explosive HMX for use in a propellant.[42] Plasticiser loss or migration from these binders was not investigated. Plasticiser migration in a propellant can weaken the propellant grains, cause cracking at stress points, induce variations in the burning rate and cause poor operation of the rocket motor.[16] Significant plasticiser migration will reduce the ballistic shelf-life of a PBX or propellant and if the physical properties of the EM are changed greatly the sensitivity of the EM to hazardous stimuli may be increased.[2,8] NC decomposes even under normal storage conditions.[22] When formulating a binder which contains the energetic polymer NC, the degradation of NC and interaction of the products of NC degradation with the overall binder and its ingredients should be considered. A number of products are formed during the decomposition of NC of which the nitrogen oxides, particularly NO_2 are considered to be the most detrimental.[36] Nitrogen dioxide is very reactive and can catalyse exothermic reactions leading to self-ignition, also water already present in the system or absorbed by the formulation can react with nitrogen dioxide to produce HNO_3 which is thought to react with NC and cause further decomposition.[22,28,34] Nitric acid present in the binder from the reaction of NO_2 and water could reduce the stability and effectiveness of NC leading to a reduction in the shelf-life and ballistic shelf-life of the formulation, therefore any interactions of NO_2 and water within the NC binders and whether different plasticiser combinations facilitate their mobility is of interest.

1.9 Research Objectives

Molecular Dynamics Simulations were to be used to investigate plasticiser migration and the interaction of water and NO_2 in the two different NC binder systems. The overall research objectives:

1. Parameterise and validate force fields for the NC binder systems.
2. Assess plasticiser migration in the NC, 2,4-DNEB and NG-N1 binder and in the NC and K10 binder by calculation of diffusion coefficients and activation energies of diffusion for each plasticiser molecule in both systems.
3. Investigate and compare the interaction of water and NO_2 in the NC, 2,4-DNEB and NG-N1 binder and in the NC and K10 binder by calculation of diffusion coefficients for water and NO_2 in each system and calculation of radial distribution functions.

2. Methodology

2.1 Molecular Mechanics Methods

Many chemical and biological systems are too large to be investigated using quantum mechanical methods. Quantum mechanical calculations deal with the electrons in a system and are too time consuming due to the large number of particles that must be contemplated in large systems, even if semi-empirical methods are used in which some of the electrons are ignored.[63] The basis for molecular mechanics methods lies in the Born-Oppenheimer approximation that the motion of the atomic nuclei and electrons in a molecule can be separated and that the motion of the electrons is rapid compared to the nuclei meaning the 'permanent' geometric parameters of the molecule are the nuclear coordinates.[63] The molecular mechanics model represents molecules as a set of spheres (the atoms) connected by springs (the bonds). The energy of the molecule changes with geometry because the bonds resist being bent or stretched away from their 'equilibrium' length or angle and the atoms resist being pushed too closely together.[63] The bond stretching and angle bending constituent the bonding terms in the mathematical expression to calculate energy, there is also a term that describes how the energy changes as bonds are rotated and terms that describe the non-bonded interactions in the system. A force field is often used to describe the mathematical expression for the energy and the parameters in it because the force on a particle is the negative of the first derivative of the potential energy of the particle with respect to displacement along a certain direction. One functional form of a force field is,

$$E_{total} = \sum_{bonds} K_r (r - r_{eq})^2 + \sum_{angles} K_\theta (\theta - \theta_{eq})^2 + \sum_{dihedrals} \frac{V_n}{2}[1 + \cos(n\phi - \gamma)] + \sum_{i<j} \left[\frac{A_{ij}}{R_{ij}^{12}} - \frac{B_{ij}}{R_{ij}^{6}} + \frac{q_i q_j}{\epsilon R_{ij}} \right] \quad (1)$$

where the E_{total} is the total potential energy.[64]

2.1.1 Bonding Terms

Bond stretching is based on Hooke's law formula and treats the bonds as springs. The increase in energy of the spring when it is stretched is approximately proportional to the square of the extension. Bond length when stretched is denoted by r and r_{eq} is the equilibrium bond length or 'reference' length. If the energy corresponding to the equilibrium length r_{eq} is taken as zero energy the term for bond stretching is:[64]

$$E_{bond\ \ stretching} = \sum_{bonds} K_r (r - r_{eq})^2 \qquad (2)$$

The force constant (K_r) is the stiffness of the bond, the larger the force constant the more the bond resists being stretched. Hooke's law is also frequently used to describe the shift of angles away from their reference values.[63] The increase in energy of a triatomic unit A-B-C, where A and C are both bonded to central atom B is approximately proportional to the square of the increase in the angle:[64]

$$E_{angle\ \ bending} = \sum_{angles} K_\theta (\theta - \theta_{eq})^2 \qquad (3)$$

The bond angle is denoted by θ, the equilibrium bond angle is θ_{eq} and K_θ is the angle bending force constant. When modelling flexible molecules large changes in conformation are due to rotations about bonds; dihedral or torsional terms are needed so the force field correctly

represents the energy profiles of these changes.[63] The term to model dihedral angles is as follows,[64]

$$E_{dihedral} = \sum_{dihedrals} \frac{V_n}{2}[1 + \cos(n\phi - \gamma)] \quad (4)$$

where V_n is described as the barrier to free rotation or barrier height. It is realistic to view V_n as a qualitative indication of relative barriers to rotation as often other terms contribute such as non-bonded interactions between atoms 1,4, for example V_n will be smaller for a bond between two sp3 carbon atoms than for an amide bond. The multiplicity, n is the number of minima as the bond is rotated through 360° and γ is the angle where the potential passes through its minimum value.[65]

2.1.2 Non-Bonding Terms

Repulsion or attraction between atoms that are not directly bonded is described by the van der Waals energy, E_{vdW}. Atoms are non-bonded if they are in different molecules or if atoms A and B are in the same molecule they are non-bonded if they are separated by at least two atoms, are not directly bonded to each other and are not both bonded to a common atom (ie. A-X-B).[65] At short interatomic distances overlap of the electron clouds of the two atoms results in E_{vdW} becoming very repulsive due to the negatively charged electrons repelling each other. The van der Waals energy is zero at large interatomic distances. At intermediate distances the instantaneous movement of electrons induces dipole-dipole interactions creating a slight attraction between the electron clouds of the two atoms. The attraction can be derived theoretically and varies as the inverse sixth power of the distance between the two atoms. At

small interatomic distances E_{vdW} is positive, at distances where atoms are just about close enough to touch E_{vdW} has a minimum which is slightly negative and as the distance becomes large E_{vdW} approaches zero. The Lennard-Jones (LJ) potential can be used to model the changes in E_{vdW} with interatomic distance, where the functional form for repulsion which cannot be derived theoretically is given an R^{-12} dependence.[66] The van der Waals energy in the functional form of the LJ potential in the Amber force field represents the pair-wise sum of E_{vdW} of all possible interacting non-bonded atoms i and j: [64]

$$E_{vdW} = \sum_{i<j}^{atoms} \left[\frac{A_{ij}}{R_{ij}^{12}} - \frac{B_{ij}}{R_{ij}^{6}} \right] \quad (5)$$

The A and B coefficients are calculated for pairs of atoms using the atomic radius in Å and the well depth (ε) in kcal/mol for each atom and the interatomic distance is represented by R_{ij}.

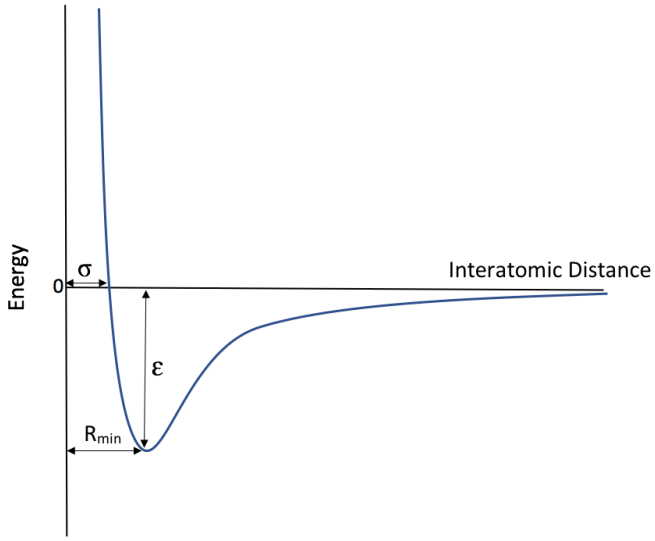

Figure 4 Diagram of the Lennard-Jones 6-12 potential. The potential well depth is denoted by epsilon (ε). Sigma (σ) is the distance where the potential equals zero which is twice the van der Waals radius of the atom. The distance where the potential reaches a minimum or the equilibrium position of the two particles is denoted by R_{min}.[65]

The electrostatic interactions can be modelled using a Coulombic term, whereby the electrostatic potential is represented by the sum of electrostatic potentials created by charges placed on atomic nuclei, i.e., partial charges. The electrostatic potential can be calculated by, [64]

$$E_{electrostatic} = \sum_{i<j}^{atoms} \frac{q_i q_j}{\varepsilon R_{ij}} \quad (6)$$

where q_i and q_j are the partial charges on atoms, R_{ij} is the interatomic distance and ε is the dielectric constant typically set to 1, corresponding to the permittivity of a vacuum.

2.1.3 Partial Charges

The electron distribution in the covalent bond between two different atoms is not shared evenly. Electronegative atoms attract the electron pair in a covalent bond more than less electronegative atoms resulting in an unequal charge distribution in a molecule. To model the electrostatic interaction in a molecular dynamics simulation the charge distribution in a molecule needs representation, one way is to arrange fractional point charges throughout the molecule. Charges assigned to the nuclear centres are known as net atomic charges or partial charges.[65] Many methods have been developed to estimate partial charges as they are not observable and cannot be determined exactly by quantum mechanical (QM) calculations or experiment.[67] One way to assign partial charges to atoms in a molecule is by population analysis of QM calculation results whereby the electron density between the nuclei is partitioned so that each nucleus has a number of electrons associated with it (the number is not necessarily an integer).[65] Mulliken population analysis distributes charge according to atomic orbital occupation. All of the electron density in an orbital is allocated to the atom on which it is located and the overlap between pairs of atoms is

divided equally between the two atoms. Mulliken charges do not consider different atom types or the electronegativity of an atom and depends heavily on the basis set used in the QM calculation.[67] Partial charges can also be estimated by deriving them from a least-squares fit to the electrostatic potential (ESP) calculation in a large number of points around the molecule. The charges from electrostatic potentials (CHELP) scheme selects points symmetrically on spherical shells around each atom.[68] The charges from electrostatic potentials using a grid based method (CHELPG) calculates the molecular electrostatic potential (MEP) at a number of grid points regularly spaced 0.3-0.8 Å apart in a cube. The molecule is positioned in the centre of the cube and points are left out of the fitting procedure if they are inside the Van der Waals radius of the molecule and if they are further than 2.8 Å away from any atom.[69] The algorithm to derive partial charges implemented in Amber uses points on a series of molecular surfaces on which the Van der Waals radii for the atoms gradually increases.[70] The Amber program also implements a restrained electrostatic potential fit (RESP) algorithm which includes restraints on non-hydrogen atoms. The RESP algorithm seeks to address the problem of artificially high charges being assigned to some atoms such as buried sp3 carbon atoms by reducing their charges with restraints.

2.1.4 Parameterisation of Force Fields

Classical molecular dynamics aims to approximate the potential energy surface of a system with mathematical functions from which forces between atoms can easily be calculated. The functions and parameters in them can be freely chosen, however despite more complex functions being developed classical pairwise additive force fields as displayed in equation 1 are still widely used due to their effectiveness.[71,72] A number of published force fields such as Amber,

Optimized Potentials for Liquid Simulations (OPLS) and Chemistry at Harvard Macromolecular Mechanics (CHARMM) are available for simulations of biological macromolecules. The idea behind the parameterisation of published force fields is that similar chemical groups in different molecules interact in the same way,[72] often these force fields are developed based on approximating the energy surfaces for a small number of molecules that contain the functional groups that are present in all biological macromolecules. Parameterisation of the bond angles and lengths in a molecule is less critical than the non-bonded interactions as bonded terms tend not to couple strongly to other terms.[72] Vibrational spectroscopy and crystallographic data can be used for bond lengths and angles or increasingly quantum mechanical calculations performed on small compounds can supply bond lengths and angles as well as force constants. Experimental data on the exact shape of a dihedral potential is unattainable, however quantum mechanical methods can be used to parameterise dihedral terms. Parameterisation of the non-bonded terms is more difficult, neither LJ parameters or partial charges are related directly to experiment or quantum mechanics.[72] Also, the non-bonded contributions may have some effect on the dihedral terms. The non-bonded interactions between atoms 1-4 separated by three covalent bonds do have non-bonded contributions as well as being included in the dihedral term. Some biomolecular force fields scale the non-bonded interaction to address the possible non-bonded interactions with the dihedral terms, the Amber molecular dynamics package scales the 1-4 vdW interactions by 2.0 and the electrostatic 1-4 terms by a factor of 1.2. The biomolecular force fields tend to define a number of atom types for each element for example, sp2 carbon and sp3 carbon and then assign each atom type individual LJ parameters and charges. Once the LJ parameters are assigned to atoms optimisation is usually always required especially when parameterising new molecules. Optimisation can be achieved by adjusting the LJ parameters and

performing simulations in an iterative manner until experimental data such as densities, heats of vaporisation or heat capacities are reproduced.[71] The validation of the entire parameter set is performed by comparing simulation results with experimental data not used in the parameterisation procedure. Parameters can be adjusted until simulation results are in good agreement with the experimental values. Different force fields may recreate the same potential energy surface of a molecule by addition of different contributions, for this reason parameters taken from different force fields and mixed must have been obtained using the same methodology.[72]

2.2 Quantum Mechanical Methods

Molecular mechanics methods do not treat the electrons explicitly. The main aim of quantum mechanical methods is to determine the electronic structure – the probability distribution of electrons in chemical systems. In this research quantum mechanical methods have been used for geometry optimisation and frequency calculations, all of which were performed using density functional theory (DFT). This section will outline the core principles relevant to the calculations that have been performed.

2.2.1 Density Functional Theory

The electron probability density, ρ is the central focus of density functional theory (DFT) rather than the wavefunction. The energy of the molecule is a function of the electron density and the electron density is a function of the electron positions, ρ(r). A function of a function is a functional, in DFT the energy is written as the functional [ρ].[73] Kohn-Sham self-consistent field theory built on earlier DFT methods by finding trial densities and determining energies from trial densities.[74] The energy functional can be divided into specific components:

$$E[\rho(r)] = T_{ni}[\rho(r)] + V_{ne}[\rho(r)] + V_{ee}[\rho(r)] + \Delta T[\rho(r)] + \Delta V_{ee}[\rho(r)] \quad (7)$$

Where T_{ni} is the kinetic energy of non-interacting electrons, V_{ne} is the nuclear-electron interaction and V_{ee} is the classical electron-electron repulsion. The last two terms constituent the exchange-correlation energy; ΔT applies small corrections to the kinetic energy that arise from electron-electron interactions and ΔV_{ee} takes into account all the non-classical electron-electron effects due to spin. Equation 8 combines the three terms T_{ni}, V_{ne} and V_{ee} from equation 7 into $E_{classical}[\rho]$ and combines ΔT and ΔV_{ee} into one term for the exchange-correlation energy:

$$E[\rho] = E_{classical}[\rho] + E_{XC}[\rho] \tag{8}$$

The electron density, ρ can be expressed as a contribution from each electron present in the molecule:[73]

$$\rho(r) = \sum_{i=1}^{N_e} |\Psi_i(r)|^2 \tag{9}$$

ψ is a Kohn-Sham orbital found by solving the Kohn-Sham equation.[73] The first step in finding the energy of the system is to assume the electron density is a sum of the atomic electron densities arising from the presence of electrons in atomic orbitals. Various basis functions can be used for the initial orbitals including Slater-type and Gaussian-type orbitals.[73] Secondly, by assuming an approximate form of the dependence of the exchange-correlation energy on the electron density the exchange-correlation potential is evaluated.[73] Next, the Kohn-Sham equations are solved to obtain an initial set of orbitals, ψ_i. The Kohn-Sham equation for a two-electron system:[73]

$$h_1\Psi_i(1) + j_0 \int \frac{\rho(2)}{r_{12}} d\tau_2 \Psi_i(1) + V_{XC}(1)\Psi_i(1) = \varepsilon_i \Psi_i \tag{10}$$

The first term combines the kinetic energy of the electrons with the potential energy of attraction between each electron and each of the nuclei. The second term is the classical electron-electron interaction and the third term considers exchange effects and is the exchange correlation potential. The Kohn-Sham orbital energies are ε_i.[73] The initial orbitals are used to calculate the electron density and this replaces the original electron density in equation 9.[73] This density is then used to solve the Kohn-Sham equation again to obtain improved orbitals, ψ_i. The whole

process is repeated until the density and exchange-correlation energy remain constant to within a specified tolerance. When convergence of the iterations has been achieved the electronic energy, E [ρ(r)] is calculated.[73]

2.2.2 Basis sets

A basis set is a set of one-particle functions used to build molecular orbitals. A set of basis functions can be used to expand the Kohn-Sham orbitals and equation 10 can then be solved by finding the coefficients in the expansion. The molecular orbitals can be built from atomic orbitals using the LCAO-MO approximation. To build one-electron wavefunctions several dozen basis functions are required resulting in a large number of integrals to evaluate.[73] A minimal basis set can be used in which one basis function represents each of the orbitals, however these often produce results in poor agreement with experiment. Increasing the number of basis set functions improves agreement between experiment and electronic structure calculations, where atomic orbitals can be represented by atom-centred Gaussians. A benefit of Gaussian-type orbitals is that the product of two Gaussian functions on different atomic centres is equal to a single Gaussian function at a point between the two atomic centres.[73] The integrals are easier to evaluate numerically, as two electron integrals on three or four different atomic centres can be decreased to integrals over two different centres. A 6-311G basis set is a split-valance basis set in which each core atomic orbital is represented by one function, a linear combination of six Gaussians.[73] Each valance atomic orbital is represented by three basis functions, a linear combination of three Gaussians and two consisting of one Gaussian function each. Polarisation functions often improve the accuracy of electronic structure calculations because atomic orbitals are distorted or polarised by neighbouring atoms when bonds form in

molecules. For non-hydrogen atoms d-type polarisation functions can be added and further p-type polarisation functions can be added for hydrogen atoms, each are represented by a * in a 6-311G** basis set. The 6-311++G** also has diffuse s- and p-type Gaussians each represented with a + on hydrogen and non-hydrogen atoms.[73]

2.2.3 Exchange-Correlation Functionals

Density functional theory (DFT) calculations require approximation of the exchange-correlation energy (E_{XC}). The quality of the results of a DFT calculation will depend on the quality of the E_{XC} approximation.[75] The simplest density functional is the local density approximation (LDA), in which the E_{XC} density depends solely on the density at a point and is that of the uniform electron gas of that density.[74] Generalised gradient approximations (GGAs) use both the density and it's gradient at each point to approximate E_{XC}.

2.2.4 B3LYP Functional

The B3LYP functional is a hybrid functional. The B3LYP functional mixes some exact exchange with a GGA and some empirical parameters determined by fitting to experimental data.[76,77]

2.3 Energy Minimisation

Arrangements of atoms which result in a structure of minimum energy are those which correspond to stable states of the system. A minimisation algorithm is used to identify geometries of the system that correspond to minimum points on the energy surface. Energy minimisation techniques can be placed in three general groups: methods that use only the energy, methods which use the gradient and methods which utilise second derivatives.[78] Gradient based methods often give the best balance between rate of convergence and computational cost.[78] Geometry optimisation using density functional theory was performed on all molecules requiring force field parameterisation. Prior to molecular dynamics simulation, minimisation may be performed to ensure a sensible starting configuration in which atoms are not overlapping. In this research prior to molecular dynamics simulations two first-order minimisation algorithms were employed, the steepest descents method and the conjugate gradient method. The direction of the first derivative of the energy (the gradient) identifies where the minimum lies and the magnitude of the gradient identifies the steepness of the slope. Both algorithms gradually change the coordinates of the atoms moving the system closer and closer to a minimum energy.[63]

2.3.1 The Steepest Descent Method

This method moves in the direction parallel to the net force and is named steepest descent because the direction in which the geometry is first minimised is the one in which the gradient is steepest. A line search can be used to locate the minimum along a specified direction. Three points can be found along the line, with the point in the middle having lower energy than the two outer points, gradually the distance is decreased between the three points restricting the minimum to a smaller region.[65] Alternatively, differentiation of a function such as a quadratic

fitted to the three points can be used to approximate the minimum. The new gradient at the minimum point of any line search is perpendicular to the direction just traversed, therefore with this method you must make a right angle turn at each point which is unlikely to reach the minimum, as shown in Figure 5.[79] Later steps reintroduce errors corrected in earlier steps. Rather than use a line search new coordinates can be obtained by taking steps of arbitrary length along the gradient. The first step usually has a predefined default value, if it leads to a reduction in energy the size of the step is increased by a multiplicative amount.[65] This procedure is continued so long as each step reduces the energy. If a step increases the energy, then the step size is decreased by a multiplicative amount. The arbitrary step method often needs more steps to reach a minimum but requires less function evaluations compared to a line search.[65]

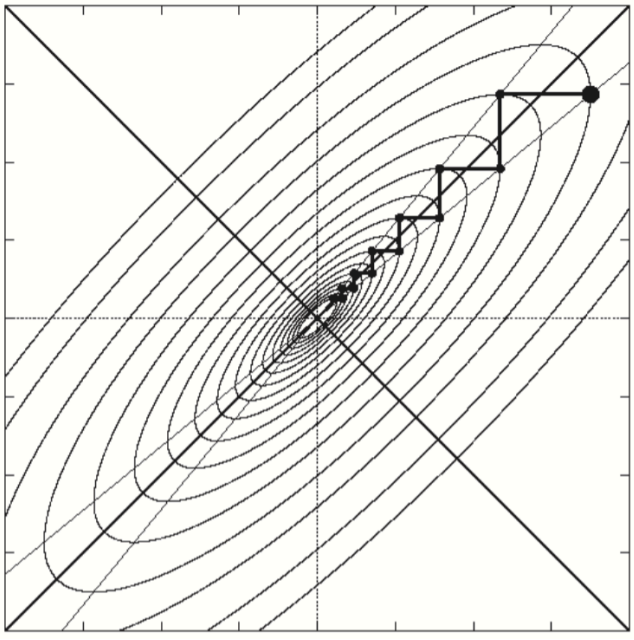

Figure 5 A diagram illustrating the steepest descents method. A right-angle turn made at each point gives the characteristic zig-zagging pattern produced by the steepest descent method.[79]

2.3.2 The Conjugate Gradient Method

A disadvantage of the steepest descent method is both the gradient and the direction of successive steps are orthogonal. The conjugate gradient method instead chooses a new direction of movement which depends on the previous direction, resulting in the gradients at each point being orthogonal but the directions conjugate.[65] This method requires the direction from the previous step to obtain the subsequent direction, so the first step follows the largest gradient as in the steepest descents method.

2.3.3 Geometry Optimisation using DFT

Geometry optimisation algorithms based on the Newton-Raphson method use the information of the Hessian, the second derivative of the energy. The Newton-Raphson method uses the gradient (the first derivative) to find the direction and the curvature (the second derivative) to predict where along the gradient the function will change direction and pass through a minimum. As the Newton-Raphson method depends on the second derivative it only works well near a minimum, therefore it is often used to locate the minimum in the last step in a refinement process of many stages.[65] Computing the Hessian is the most computationally expensive part of the Newton-Raphson method, the gradient history is therefore often used to approximate the Hessian using the Broyden-Fletcher-Goldfarb-Shanno (BFGS) technique.[80] The Hessian is also required to be non-singular with no negative eigenvalues using the basic Newton-Raphson method. To ensure this the algorithm is prevented from taking steps that are too large by scaling them to stay within a trust radius, known as the trust radius method (TRM) or by rational function optimisation (RFO) which introduces a step size dependent denominator.[80,81] In Gaussian '09 the geometry optimisation algorithm uses techniques from the Berny algorithm, other published and

unpublished algorithms and the Newton-Raphson method and implements the BFGS, TRM and RFO procedures.[82,83] Geometry optimisation using a quasi-newton algorithm is outlined in the flow chart in Figure 6.[78,83,84]

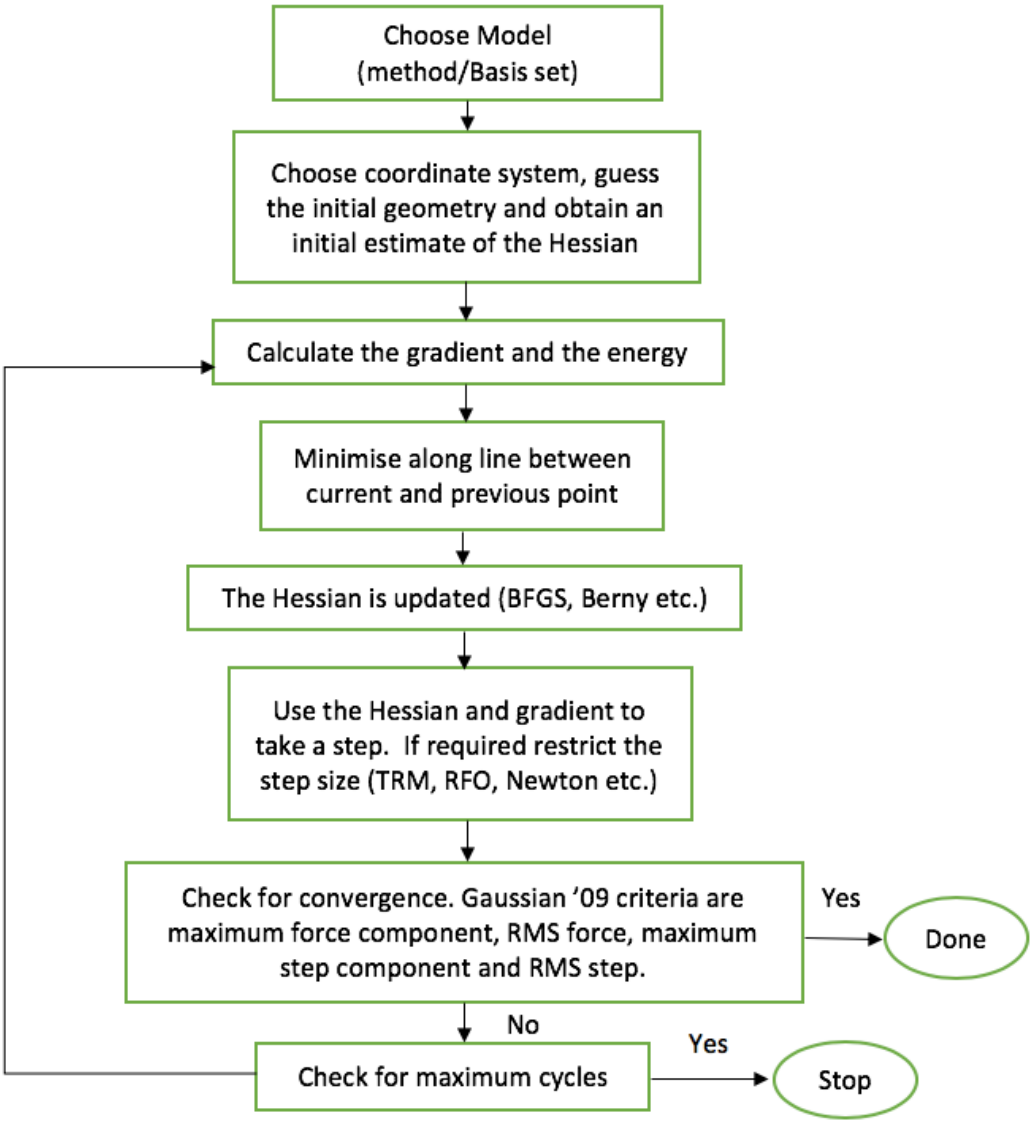

Figure 6 Flow chart showing the stages in a quasi-Newton Geometry Optimisation.[84]

2.4 Vibrational Frequency Calculations

Vibrational frequency analysis performed on an optimised structure generates a Hessian matrix containing the second derivative of the energy with respect to change in atomic position.[85] The vibrational frequencies are calculated by transforming the second derivatives of the energy with respect to the Cartesian nuclear coordinates to mass-weighted coordinates.[82] The transformation to mass-weighted coordinates to calculate the frequencies must be at a stationary point, therefore frequencies must be calculated for a molecule using the same method used to optimise the molecule's geometry.[82] Software employed in this research uses Seminario's method to diagonalise the Hessian in Cartesian coordinates to generate bond length and bond angle force constants for force field parameterisation.[85,86]

2.5 Molecular Dynamics

In a molecular dynamics simulation the 'real' dynamics of the system are calculated and then time averages of properties are calculated from these. Newton's equations of motion are used to derive sets of atomic positions in sequence. Early molecular dynamics simulations used very simple hard-sphere potentials where particles move in straight lines at constant velocity between collisions, collisions are perfectly elastic and happen when the distance between a pair of spheres equals the sum of their radii.[65] The principle of conservation of linear momentum is used to calculate the new velocities of the spheres after collision. In potentials such as the LJ potential where the force between two atoms or molecules changes continuously with the varying distance between them, the equations of motion need to be integrated by splitting the calculation into a series of very short time steps.[65] At each step, the forces on the atoms are calculated and along with the current positions and velocities used to produce new positions and velocities a short time ahead. It is assumed the force on each atom stays constant between steps. The atoms are then moved to the new positions, a new set of forces are calculated, and so on. This process creates a trajectory throughout the simulation that describes how the dynamic variables change with time.[65] The trajectory is obtained by solving Newton's second law (F = ma):

$$m\frac{d^2 r_i}{dt^2} = F_i\,(r_{1,}\, r_{2,}\, \cdots,\; r_{i,}\, \cdots,\; r_N),\;\; i=1,N \tag{11}$$

This equation describes the motion of a particle of mass m, along coordinate (ri) with a force (Fi) being applied on the particle in that direction. The force is calculated from the negative gradient of the potential energy (V), the sum of the potential energy of the intermolecular and intramolecular interactions:[65]

$$F_i = -\nabla_{r_i} V \tag{12}$$

2.5.1 Finite Difference Methods

Finite difference methods are used to generate trajectories from molecular dynamics simulations performed with a continuous potential such as the LJ potential used in this research. The fundamental idea is that the integration is broken down into many small stages, each separated in time by a fixed time Δt. There are various algorithms used in molecular dynamics simulations which integrate the equations of motion using finite difference methods. All algorithms assume that the positions and dynamic properties (velocities, accelerations etc.) can be approximated using Taylor series expansions. As the equations used in the algorithms are truncated Taylor expansions errors are introduced which may be minimised by using smaller time steps.

2.5.2 Verlet Algorithm

The Verlet algorithm in its simplest form uses the positions r(t) and acceleration (a) at time step t and previous step t - Δt to update positions at t + Δt.[87] The velocity is v and b is the third derivative of r with respect to t,

$$r(t+\Delta t) = r(t) + v(t)\Delta t + \frac{1}{2}a(t)\Delta t^2 + \frac{1}{6}b(t)\Delta t^3 + O(\Delta t^4) \tag{13}$$

$$r(t-\Delta t) = r(t) - v(t)\Delta t + \frac{1}{2}a(t)\Delta t^2 - \frac{1}{6}b(t)\Delta t^3 + O(\Delta t^4) \tag{14}$$

adding the two expressions gives:

$$r(t+\Delta t)=2r(t)-r(t-\Delta t)+a(t)\,\Delta t^2\ +\mathrm{O}(\Delta t^4) \tag{15}$$

where acceleration is calculated by,

$$a(t)=\ -\left(\frac{1}{m}\right)\nabla V\ \ (r_{1,}r_{2,}\cdots,r_N) \tag{16}$$

In the basic Verlet equation the velocities are not explicitly given, but they are required for the calculation of certain physical quantities like kinetic energy. The velocity can be estimated using the position terms and mean value theorem, however this requires an extra computation.[87]

$$v(t)=\frac{r(t+\Delta t)\ -\ r(t-\Delta t)}{2\Delta t}\mathrm{O}(\Delta t^2) \tag{17}$$

The truncation error is of order $O(\Delta t^4)$ for positions update whilst velocities are subject to errors of $O(\Delta t^2)$.

2.5.3 Leap-Frog Algorithm

The leap-frog scheme obtains the positions and velocities. In this algorithm, the velocities are first calculated at time t + ½ Δt from available quantities: [87]

$$v\left(t+\frac{\Delta t}{2}\right)\ =\ v\left(t-\frac{\Delta t}{2}\right)\ +\ \frac{\Delta t}{m}\ \ F(t) \tag{18}$$

these are then used to calculate the positions, r, at time t + Δt,

$$r(t+\Delta t) = r(t) + \Delta t\ v\left(t+\frac{\Delta t}{2}\right) \tag{19}$$

The velocities are updated at ½ time steps meaning the velocities leap over the positions, then the positions leap over the velocities, hence the name leap frog algorithm.[65] Compared to the Verlet algorithm velocity is explicitly calculated, however velocities are known accurately at t + ½ Δt and positions at t + Δt so they are not calculated at the same time as one another.[65] The current velocities at time t can therefore be obtained from:

$$v(t) = \frac{v\left(t-\frac{\Delta t}{2}\right)+ v\left(\Delta t+\frac{\Delta t}{2}\right)}{2} \tag{20}$$

2.5.4 Ensembles

The microcanonical or NVE ensemble is traditionally sampled when performing a molecular dynamics simulation in which the number of particles (N), volume (V) and energy (E) are constant. Molecular dynamics can be adapted to simulate other ensembles. In this work the experimental data compared to simulated properties was obtained under conditions of constant temperature and constant pressure, so simulations in the isothermal-isobaric (NPT) ensemble were most directly relevant. The NPT ensemble describes a system in contact with a thermostat to maintain the temperature (T) and a barostat to maintain the pressure (P). The system

exchanges volume with the barostat and heat with the thermostat. The total number of particles (N) remains constant, but the volume (V) and total energy (E) fluctuate at thermal equilibrium. Another ensemble, the canonical or NVT ensemble describes a system which is in contact with a thermostat to maintain the temperature (T). The number of particles (N) and the volume (V) remain fixed, but the energy fluctuates.

2.5.5 Berendsen Thermostat

The Berendsen thermostat couples the system to an external bath fixed to the desired temperature. To maintain the temperature the bath acts as a reservoir of thermal energy that supplies or removes temperature as necessary.[88] The velocities are rescaled at each time step, where the rate of change in temperature is proportional to the difference in the temperature in the system and the temperature of the external bath. [88] The amount of control that the thermostat imposes on the simulation is controlled by a coupling constant.

2.5.6 Anderson Thermostat

The Anderson thermostat is a stochastic-coupling method based on the reassignment of a randomly chosen particle's velocity.[89] If a particle is selected by chance for velocity reassignment each Cartesian element of the new velocity is selected at random from the Maxwell-Boltzman distribution. This is the equivalent of particles in the system randomly colliding with an imaginary heat bath at the desired temperature.[89] With the Anderson method, often a collision is not performed with each molecular dynamics time step instead a collision frequency (ν) or collision time $r = 1/\nu$ is adopted instead as implemented in the Amber 14 molecular dynamics package.[90]

2.5.7 Berendsen Barostat

The Berendsen barostat maintains a constant pressure by allowing the volume of the system to fluctuate.[88] For an isotropic system, this is achieved by changing the cell size uniformly but not the cell shape.

2.5.8 Constraint Algorithm

The maximum length of the time step for integration of the equations of motion in a molecular dynamics simulation is determined by the frequency of the fastest motion in the system. Time steps must be small enough for the fastest modes such as bond stretches involving hydrogen to be handled accurately. Imposing constraints integrates out the rapid vibrational modes allowing the use of a longer time step resulting in greater computational efficiency.[91] In constraint dynamics the equations of motion are solved whilst simultaneously fulfilling the imposed constraints. The SHAKE procedure was applied to bonds involving hydrogen in all simulations.[91]

2.5.9 Periodic Boundary Conditions

The behaviour of finite systems is very different to that of infinite systems. Even in the largest of systems that can be simulated the number of particles is negligible compared to the number of particles in a macroscopic system. To simulate a system with a relatively small number of particles so that each particle encounters forces as if they were in a macroscopic system, periodic boundary conditions (PBC) are implemented.[65] Using PBCs involves replicating a box to infinity by rigid translation in all three Cartesian directions. A cubic box is easiest to visualise, however cells of different shapes can be used. When a particle enters or leaves the box an image

particle enters or leaves from the opposite side meaning the number of particles in the central box is always conserved, this is shown in the two-dimensional representation of PBCs displayed in Figure 7.[65]

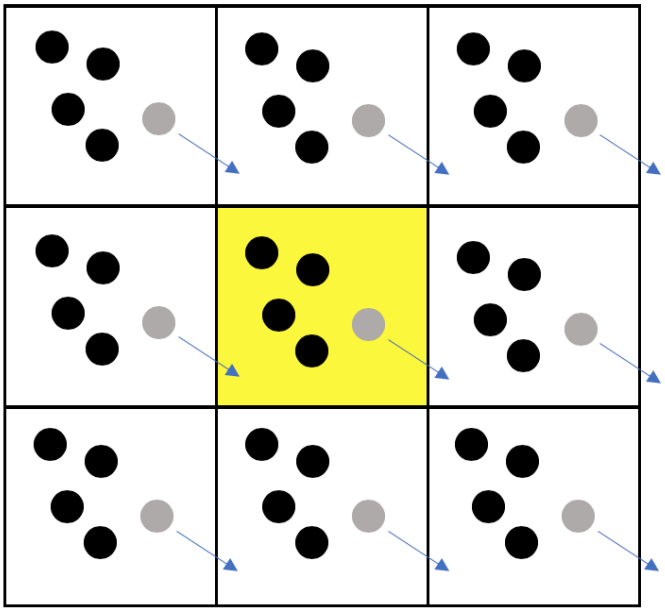

Figure 7 Two-dimensional schematic of periodic boundary conditions. The particle trajectories in the central simulation box are copied in every direction.[92]

2.5.10 Cut-offs and the Minimum Image Convention

The non-bonded interactions are the most time consuming to calculate, in theory the non-bonded interactions are calculated between every pair of atoms in the system. However, for many interaction models such as the LJ potential where attractive forces fall off very quickly with distance this is not necessary.[65] This problem can be overcome by using the potential in a finite range such that the interaction of two distant particles at or beyond a finite length or cut-off can

be neglected. This cut-off length must be equal to or less than the half of the box length used in the simulation.

2.6 Diffusion

Diffusion can be described as the net movement of particles from a high chemical potential to a lower chemical potential due to the random movement of particles. The chemical potential gradient drives the process of diffusion.

2.6.1 Fick's First Law of Diffusion

The flow of matter (as in diffusion) can be described as matter flux (J) of a number of particles per square metre per second.[73] Fick's first law of diffusion relates the proportionality of the flux of matter to the concentration gradient:

$$J = -D\frac{dC}{dx} \tag{21}$$

where D is the diffusion coefficient ($m^2\ s^{-1}$) and dC/dx is the change in concentration due to the change in position in $cm^{-3}\ cm^{-1}$.

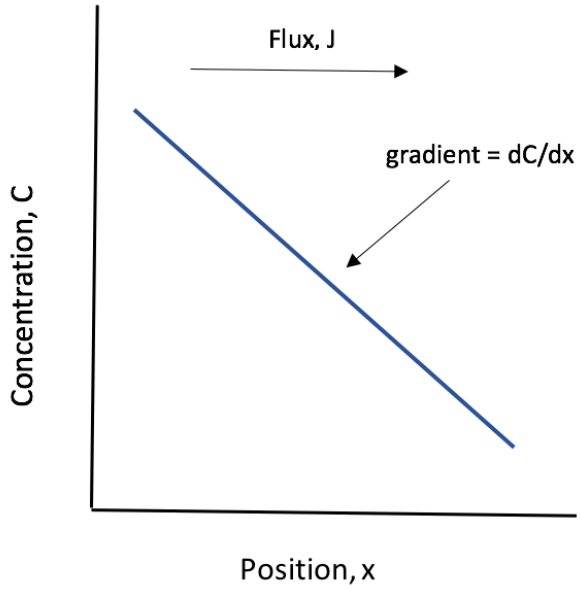

Figure 8 Graph illustrating the proportionality of the flux of matter to the concentration gradient.[93]

The negative sign means that J is positive when movement is down the gradient, i.e., the negative sign cancels the negative gradient along the direction of positive flux.[93] Fick's first law indicates that, if the concentration changes steeply with position, then diffusion will be fast.[73]

2.6.2 Fick's Second Law of Diffusion

Fick's first law of diffusion applies when the concentration is constant, however in many cases the concentration changes with time. Fick's second law of diffusion correlates the rate of change of concentration at a point to the spatial variation of the concentration at that point:

$$\frac{\partial c}{\partial t} = D\frac{\partial^2 c}{\partial x^2} \qquad (22)$$

The equation for Fick's second law of diffusion shows that the rate of change of concentration is proportional to the second derivative of the concentration with respect to distance.[73]

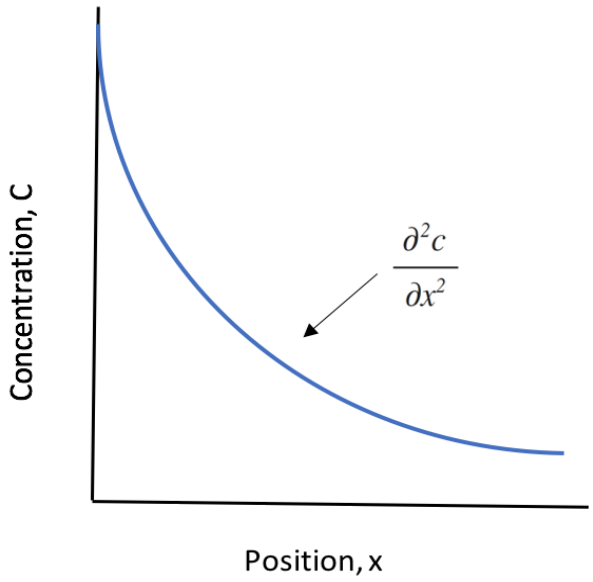

Figure 9 Graph showing how the rate of change of concentration at a point relates to the spatial variation of the concentration at that point.[93]

2.6.3 Einstein's Diffusion Equation

The diffusion coefficient is related to the mean square displacement (MSD), which Einstein determined was equal to 2Dt,[94]

$$2nDt = \langle |r_i(t) - r_i(0)|^2 \rangle \tag{23}$$

where $r_i(t) - r_i(0)$ is a measure of particle displacement between 0 and time t.[94] The Einstein relation can therefore be used to calculate D by plotting the MSD as a function of time,

$$2nD = \frac{d}{dt} \langle |r_i(t) - r_i(0)|^2 \rangle \tag{24}$$

where for three spatial dimensions, n=3. The gradient of the plot of MSD versus time can be calculated and the diffusion coefficient determined using,[94]

$$6D = \lim_{t \to \infty} \frac{MSD}{t} \tag{25}$$

The Einstein derivation is based on the assumption that a single particle is on a random walk, meaning that a particle's motion at a particular time t is entirely uncorrelated with the particle's motion at any previous time t'. For the Einstein relation to be valid the particle must have no memory of previous steps, which holds true if there is adequate time between t and t'. The Einstein relation is therefore often described as being correct in the long-time limit, $t \rightarrow \infty$. If the simulation time is too short a particle's motion may be correlated, the MSD follows a different power law and D cannot be calculated correctly using the Einstein equation.[95] In a molecular dynamics simulation the MSD's are calculated from initial positions meaning diffusion calculated for a small number of particles would be inherently stochastic, to reduce statistical error the MSD can be averaged over all the particles in the system. Diffusion coefficients calculated in this research were averaged over all molecules using the Cpptraj module in Amber 14.[96] When using the Einstein relation to calculate D the MSD should not be limited to the edges of the periodic box. A set of positions that have not been translated back into the central simulation cell can be generated in Amber 14 using the unwrap command in the Cpptraj module.[96]

2.7 The Radial Distribution Function

The radial distribution function (RDF) can be described as the number of particles a distance r from a reference particle compared with the number at the same distance in an ideal gas at the same density.[97] The RDF is calculated by taking the centre of a reference particle as being r = 0 and creating a histogram of the particles at a given distance r from the reference.[98] For example, the number of neighbours between 2.0 and 2.25 Å, 2.25 and 2.50 Å and so on are counted and sorted into distance bins. The distance is limited to less than some maximum, for example half of the simulation box length.[97] The process is repeated for every particle in the simulation and the number of neighbours in each distance bin is averaged over the entire simulation. To obtain g (r) the data is normalised by division of the average number of neighbours in each distance bin by the volume of the distance bin and then division by the particle number density.[99] Particles located in the first distance bin or spherical shell with the radius between r0 and r1 around the reference particle are in the first coordination shell. The first coordination shell would appear as a prominent first peak in an RDF. Particles in the second spherical shell around the central reference particle would be indicated by a less prominent peak in an RDF, the second coordination shell (Figure 10).[100]

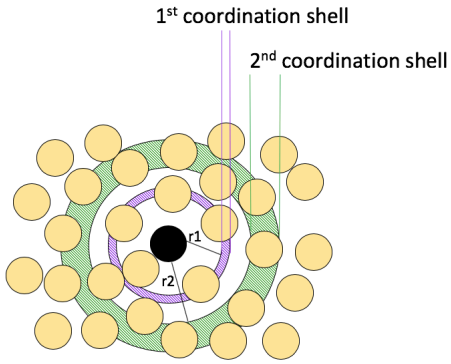

Figure 10 Schematic showing particles coloured yellow in the first and second coordination shells at distances r1 and r2, respectively from the reference particle in black.[100]

3. Parameterisation of Force Fields for the Plasticiser and Stabiliser molecules, Nitrocellulose and Nitrogen Dioxide

To perform molecular dynamics simulations on the nitrocellulose binder mixtures force fields were required for all of the constituents.[64,101] Bonding and non-bonding parameters are available in generic published force fields. Although there are parameters available for molecules with structural similarity to those studied in this research to the best of my knowledge there are no force fields available specifically for 1-nitramino-2,3-dinitroxypropane (NG-N1), 2,4-dinitroethylbenzene (2,4-DNEB), 2,4,6-trinitroethylbenzene (2,4,6-TNEB) or ethyl centralite (EC). The calculation of diffusion coefficients via molecular dynamics simulation is sensitive to properties of the system such as density, [102] to accurately model these experimentally observed properties force fields were developed and optimised for the individual NG-N1, 2,4-DNEB, 2,4,6-TNEB, EC and nitrogen dioxide (NO_2) molecules and nitrocellulose (NC). The Lennard-Jones parameters were also refined for the two NC binder systems and the plasticiser mixtures K10 and R8002. There are force field parameters in the literature for NC and NO_2,[47] however for consistency the NC and NO_2 were parameterised using the same procedure as NG-N1, 2,4-DNEB, 2,4,6-TNEB and EC.

3.1 Parameterisation Methodology

3.1.1 Parameterisation of Force Fields

The functional form of the force field implemented in the Amber 14 molecular dynamics package is displayed in equation 1 and is used to describe the parameterisation procedure.[90]

$$E_{total} = \sum_{bonds} K_r(r - r_{eq})^2 + \sum_{angles} K_\theta (\theta - \theta_{eq})^2 + \sum_{dihedrals} \frac{V_n}{2}[1 + \cos(n\phi - \gamma)] + \sum_{i<j} \left[\frac{A_{ij}}{R_{ij}^{12}} - \frac{B_{ij}}{R_{ij}^{6}} + \frac{q_i q_j}{\epsilon R_{ij}} \right] \quad (1)$$

Geometry optimisation using density functional theory was performed on the NG-N1, 2,4-DNEB, 2,4,6-TNEB, EC and NO_2 molecules and a fully nitrated NC dimer.[82] The geometry optimised 2,4-DNEB and 2,4,6-TNEB structures are shown in Figures 16A and 16B, respectively and the geometry optimised EC, NG-N1 structures and NC dimer in Figures 17A, 17B and 17C, respectively. The stretching of bonds and bending of angles is represented by terms one and two in equation 1. For all molecules and the NC dimer the equilibrium bond lengths, r_{eq}, and bond angles, θ_{eq} were obtained from the optimised structures and the program ForceGen generated the bond stretching, K_r and angle bending, K_θ force constants.[85,86] A fully nitrated NC dimer was chosen for geometry optimisation as this exhibited all the possible bonding environments that exist in the fully nitrated NC polymer. NC used in energetic binders needs explosive properties meaning a nitrogen content of more than 12.6% is required, full nitration of the NC dimer ensures this. The dihedral term is displayed in term 3 of equation 1. The General Amber Force Field (GAFF) was used for all of dihedral angles for the NG-N1 and

EC molecules and the NC dimer.[64] The GAFF was also used for the majority of the torsional terms for 2,4-DNEB and 2,4,6-TNEB, however other terms available in the literature which are more specific to nitro aromatic compounds were also used. Parameters available in the literature for nitrobenzene were used for the C – C – C – N torsion.[103] Nitrotyrosine contains an aromatic ring with a nitro group attached. The X-ray structures of nitrotyrosine have displayed rotation of the C-NO_2 bond and out-of-plane deformation of the NO_2 group, Myung and Han developed parameters to accurately model this behavior which can used with other nitro aromatic compounds.[104] The parameters for nitrotyrosine were used for the improper dihedral C – O – N – O and the proper dihedral C – C – N – O in both 2,4-DNEB and 2,4,6-TNEB.[104] The non-bonded interactions are represented by the fourth term of equation 1, the first part being the Lennard Jones (LJ) 12-6 potential. The GAFF and the Optimised Potentials for Liquid Simulations (OPLS) force field provided all the LJ parameters for NO_2, NC, EC and NG-N1.[64,101] LJ parameters from the GAFF were used for the aliphatic hydrogen and carbon atoms in 2,4-DNEB and 2,4,6-TNEB and values for nitrobenzene were taken from the OPLS force field for the aromatic ring and nitro group.[64,101] The symbols q_i and q_j are the atomic partial charges and ε is the dielectric constant in the final term representing the electrostatic potential. The restricted electrostatic potential (RESP) method was used to obtain the partial charges for all of the molecules and the NC dimer via the RED Server Development package.[70,105–107] Figure 11 displays the QM bond lengths and partial charges for 2,4,6-TNEB and Figure 12 displays the QM bond angles for 2,4,6-TNEB. The QM bond lengths and partial charges for 2,4-DNEB are displayed in Figure 13 and Figure 14 contains the QM bond angles for 2,4-DNEB. Finally, the QM bond lengths, the partial charges and the QM bond angles for EC are displayed in Figure 15. All force field parameters are supplied in Appendix 2 (p.180) and Appendix 4 (p.206).

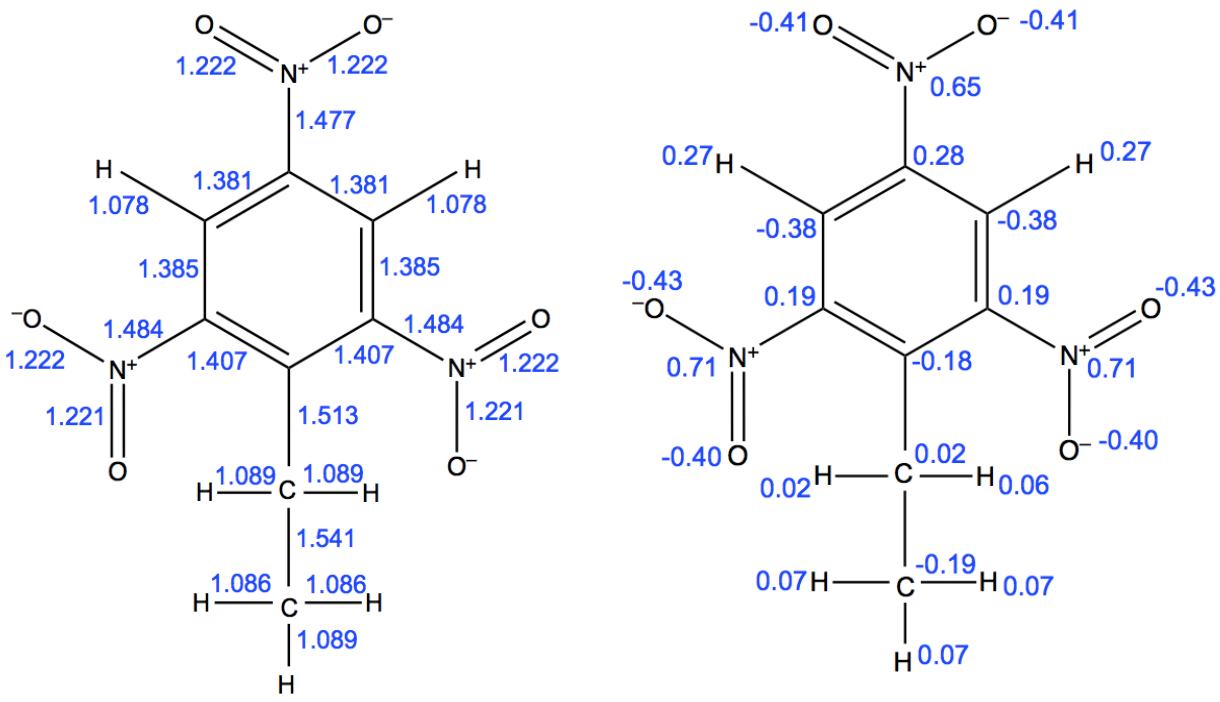

Figure 11 QM bond lengths and partial charges for 2,4,6-TNEB

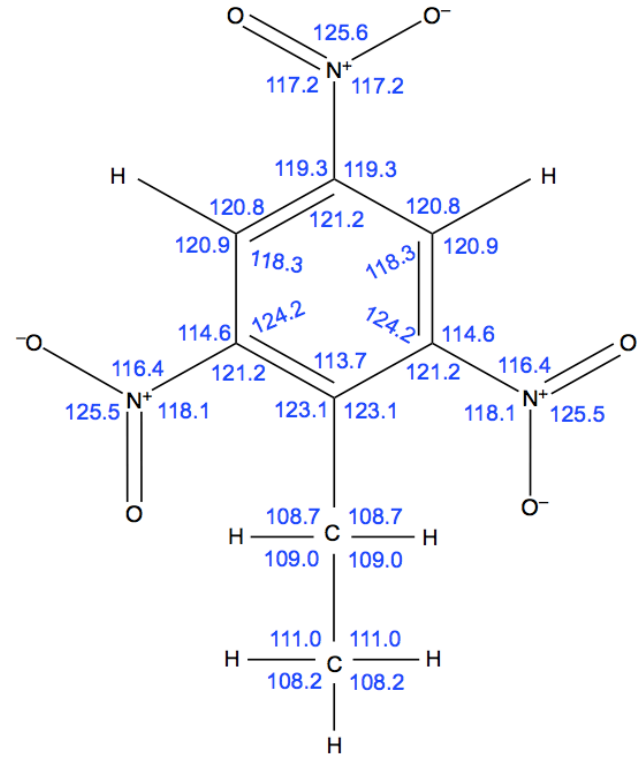

Figure 12 QM bond angles for 2,4,6-TNEB

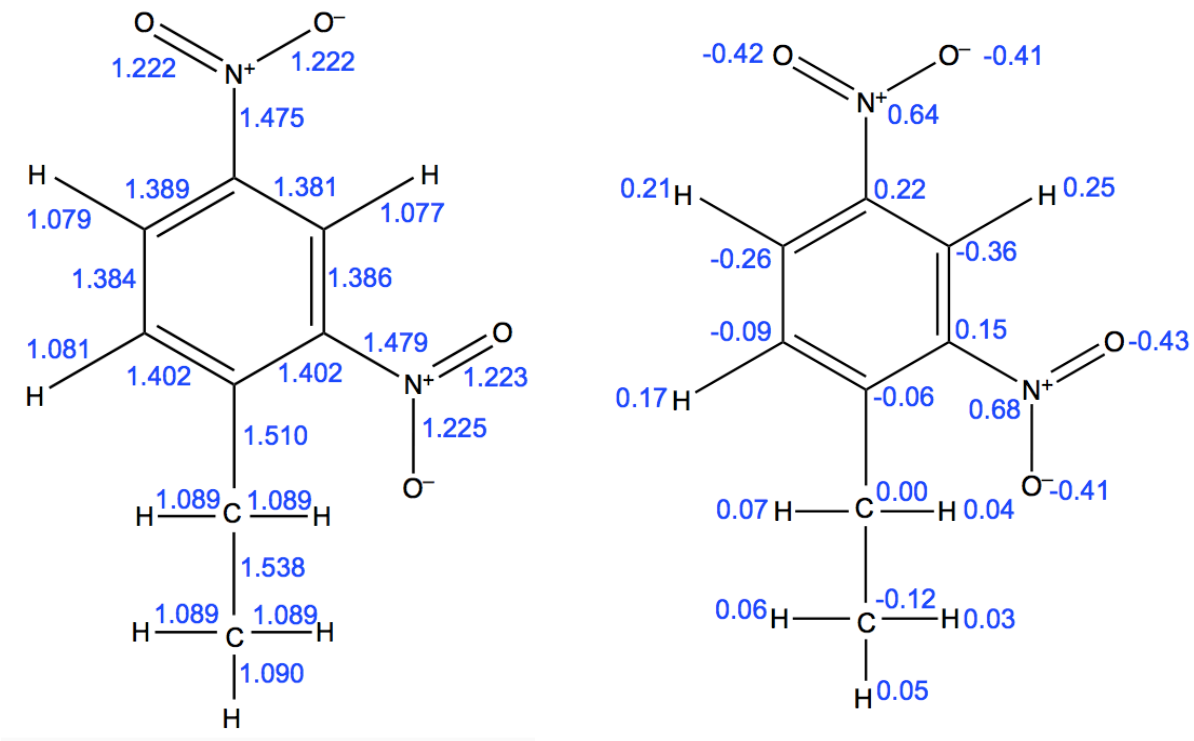

Figure 13 QM bond lengths and partial charges for 2,4-DNEB

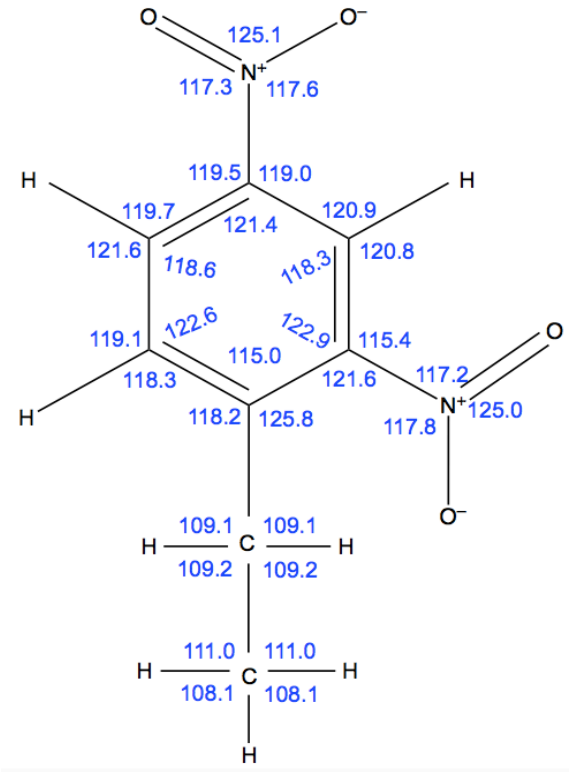

Figure 14 QM bond angles for 2,4-DNEB

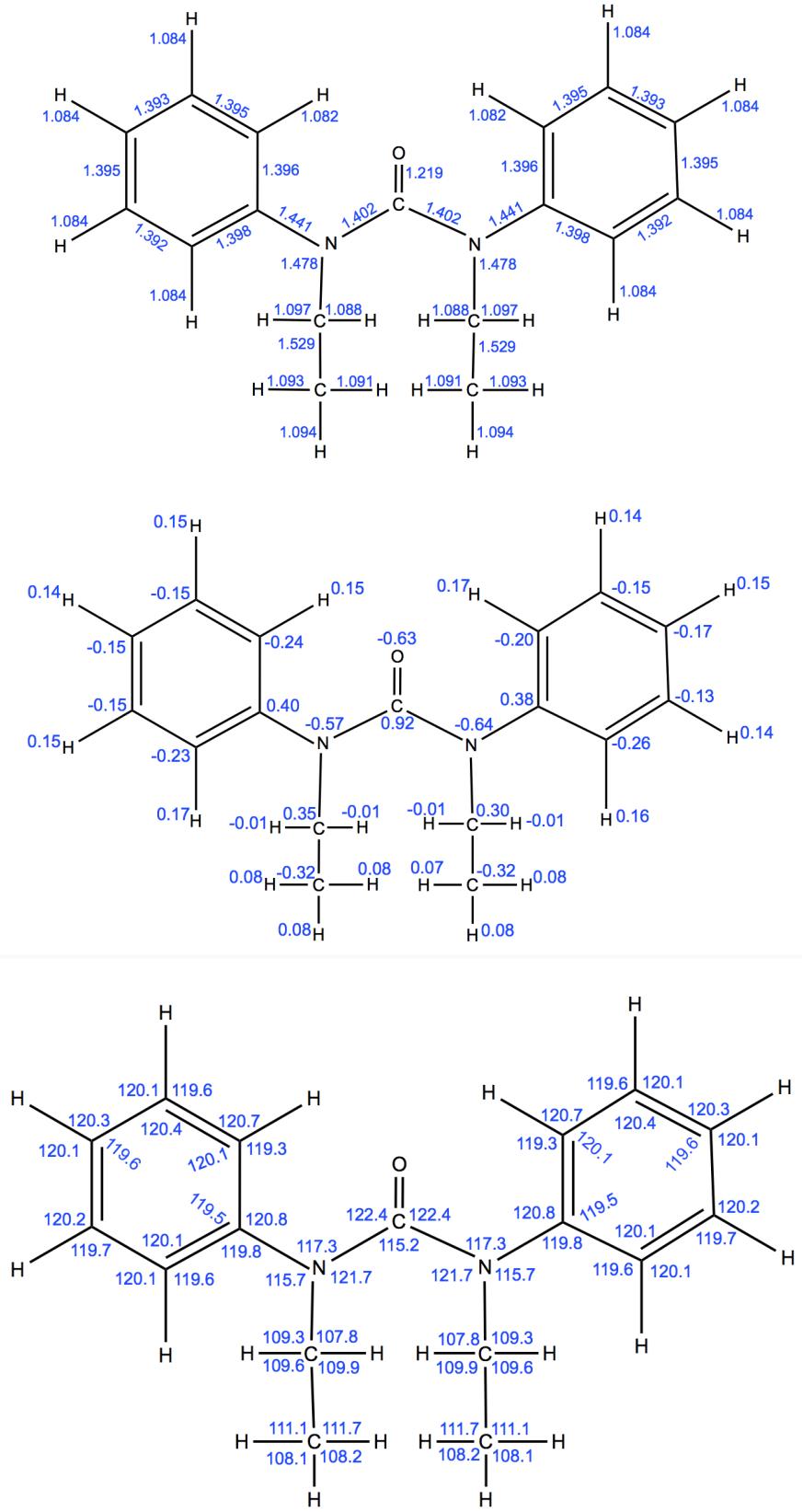

Figure 15 QM bond lengths, partial charges and QM bond angles for EC

3.1.2 Quantum Mechanical Calculations

All DFT calculations were performed using Gaussian '09.[82] Each 2,4-DNEB, 2,4,6-TNEB, NG-N1, NO_2 and EC molecule and the NC dimer underwent geometry optimisation followed by frequency calculations. The B3LYP/6-311^{++}G** functional was used for all geometry optimisations and frequency calculations were performed at the same level.

3.1.3 Validation of Parameters

Firstly, the bonding parameters were validated by comparing the quantum mechanical (QM) bond lengths and angles to experimental data. Experimental values specifically for bond lengths and angles in NC, 2,4-DNEB and 2,4,6-TNEB were not available in the literature so the QM values were compared to experimental data for structurally similar compounds. The QM bond angles and lengths obtained for the nitrate ester group of the NC dimer were compared to experimental values for ethyl nitrate and those of the nitro group to the experimental bond lengths and angles of methyl nitrate.[108,109] The experimental bond lengths and angles for ethylbenzene and trinitrobenzene were used to validate the QM values obtained for 2,4-DNEB and 2,4,6-TNEB.[110–113] The QM bond lengths and angles obtained from the DFT optimised EC and NG-N1 structures were compared to X-ray diffraction data for EC and NG-N1 respectively.[41,114,115] The bond angle and bond lengths in NO_2 were compared to experimental values.[116] An additional check was performed with the QM bonding terms of 2,4-DNEB and 2,4,6-TNEB by using them in single molecule MD simulations. The dynamic MD bond lengths and angles from the single molecule simulations of 2,4-DNEB and 2,4,6-TNEB were compared to experimental data to see if they had altered significantly.[110–113] The QM bond lengths and angles were used in MD simulations if they were considered to be in good agreement with the

experimental data. Once complete parameter sets had been obtained for each molecule, simulation cells were constructed for 2,4-DNEB, 2,4,6-TNEB, NG-N1, NO_2 and EC respectively and their densities calculated from MD simulations under vacuum at 298 K. An NC polymer chain was constructed from the parameterised NC dimer and the density calculated from MD simulation under vacuum at 298 K. For each of the 2,4-DNEB, 2,4,6-TNEB, NG-N1, NO_2, EC and NC parameter sets the LJ parameters were altered where necessary until values were obtained which simulated densities comparable to experimental values.[41,115,117–120]

NC binder simulation boxes were created, one consisting of NC, EC and a plasticiser mixture of 2,4-DNEB and NG-N1 which is displayed in Figure 17F and another containing NC, EC and the plasticiser K10 which is presented in Figure 17G. The densities of these two binder mixtures were simulated under vacuum at 298 K and the LJ parameters adjusted until the calculated densities of the overall mixtures agreed with experimental data.[42] Next the densities of the plasticiser mixtures R8002 and K10 were simulated under vacuum at 298 K and the same iterative procedure used to refine the LJ parameters to reproduce the experimental density.[121,122] Simulated densities were deemed acceptable if they were within ~2% of the experimental values. For all molecules, the NC and the binder and plasticiser mixtures LJ optimisation was achieved by directly altering the A and B coefficients in the input parameter files. Finally, the density of a plasticiser mixture of 67% 2,4-DNEB and 33% NG-N1 was obtained from simulation at 298 K. The LJ parameters were not altered as no exact experimental density of this mixture is available, a rough comparison of the simulated density was made with the experimental density of the NC, 2,4-DNEB and NG-N1 binder. To determine the performance of the force field the densities of NG-N1, EC, 2,4-DNEB and 2,4,6-TNEB obtained after refinement of the LJ parameters were

compared with those obtained using the original LJ parameters before their alteration.[64,101] An additional comparison was made between the simulated densities of 2,4-DNEB and 2,4,6-TNEB and those obtained using parameters solely from a published force field.[64,103,104] The published force field was parameterised using the same non-bonding parameters and dihedral angles as those used for 2,4-DNEB and 2,4,6-TNEB before their alteration,[64,103,104] but the GAFF was used for all the bonding terms.[64] Partial charges are not readily available in GAFF for specific molecules and need to be obtained via geometry optimisation of the molecule, therefore the RESP charges generated in this work previously for 2,4-DNEB and 2,4,6-TNEB were used. To evaluate if the interactions of 2,4,6-TNEB and 2,4-DNEB with themselves and in the mixtures were as expected considering the simulated densities the self-diffusion coefficients of 2,4,6-TNEB and 2,4-DNEB in the pure systems and in K10 and R8002 were calculated.

3.1.4 Construction of Simulation Cells

For each of the 2,4-DNEB, 2,4,6-TNEB, NG-N1, EC, R8002 and K10 systems and the 2,4-DNEB and NG-N1 plasticiser mixture, simulation cell dimensions of 40 Å × 40 Å × 40 Å were used assuming cubic geometries. The NG-N1 simulation cell contained 306 molecules calculated using the unit cell proposed by Altenburg et al. and the unit cell dimensions reported by Betz et al. were used to add 149 molecules to the EC simulation box.[41,114] The unit cell parameters for 2,4-DNEB and 2,4,6-TNEB were unavailable so the unit cells of the structurally similar 2,4,6-trinitrotoluene (TNT) and 2,4-dinitrotoluene (2,4-DNT) were used to construct the simulation cells. An estimate of 238 2,4,6-TNEB molecules were added to a simulation box using the monoclinic unit cell of TNT determined by Vrcelj et al (Figure 16C).[123] An estimate of 283 2,4-DNEB molecules were added to a simulation box based on the monoclinic unit cell

reported by Hanson et al. for 2,4-DNT.[124] To create the 35%/65% composition of the plasticiser K10, a mixture of 78 2,4,6-TNEB molecules and 144 2,4-DNEB molecules was added to the simulation cell. The 50%/50% mixture of the plasticiser R8002 was made by adding 111 2,4-DNEB and 2,4,6-TNEB molecules each to the simulation cell. To construct the simulation cell for the 67% 2,4-DNEB and 33% NG-N1 plasticiser mixture 118 2,4-DNEB molecules and 58 NG-N1 molecules were added to a simulation cell. The density of NO_2 was used to estimate the number of molecules that could be added to the simulation cell, 22 NO_2 molecules were added to a cubic box with the dimensions 77 Å × 71 Å × 76 Å.[119] The molecules were added to each of the 2,4-DNEB, 2,4,6-TNEB, NG-N1, EC, R8002, K10 and NO_2 boxes using the program Packmol with a tolerance of 2 Å between molecules.[125]

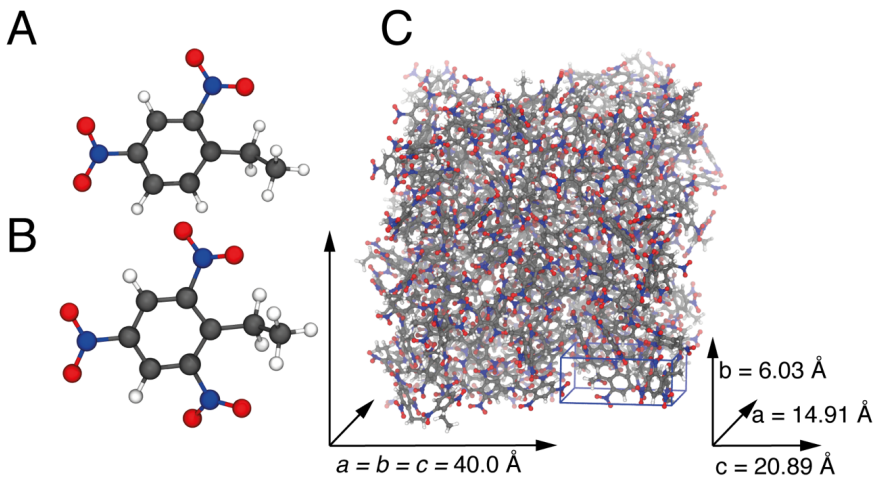

Figure 16 The geometry optimised 2,4-DNEB (A) and 2,4,6-TNEB (B) structures. The simulation cell for 2,4,6-TNEB (C), constructed from the TNT unit cell. Carbon atoms are displayed in grey, nitrogen atoms in blue, oxygen atoms in red and hydrogen atoms in white.

The NC was built using the dimensions determined by Meader et al.[126] A molecular chain of 5 geometry optimised fully nitrated NC dimers was constructed using the UCSF Chimera package and added to a box with the lattice dimensions a = 5.20 nm, b = 0.73 nm and c = 0.90 nm and the lattice angles $\alpha = \beta = \gamma = 90°$ (Figure 17D).[126–128] The box of 5 dimers was replicated once more in the x direction and the resulting chain replicated three times in the y and z directions to build the simulation cell containing only NC (Figure 17E).[128] The NC model used in the binder mixtures was constructed by firstly replicating the 5 dimers in the x direction to create a chain of 10 dimers, then duplicating this chain in the z direction and then the resulting two chains in the y direction.[128] The NC model used in the binder mixtures has been numbered for clarity in both Figures 17F and 17G. The ratios of the NC binder mixture components were obtained from experimental studies to compare the energetic output of K10 as a plasticiser of NC to the energetic output of NG-N1 combined with 2,4-DNEB as a plasticiser of NC.[42] The binder mixtures contained 11% NC and 89% plasticiser, the K10 plasticiser mixture contained 35% and 65% 2,4,6-TNEB and 2,4-DNEB respectively and the NG-N1 and 2,4-DNEB plasticiser proportions were 33% and 67%, respectively. The first binder mixture was built by adding the NC model, 286 NG-N1 molecules and 640 2,4-DNEB molecules to a simulation cell with the dimensions 115.5 Å × 84.4 Å × 68.9 Å (Figure 17F). To construct the K10 plasticiser and NC binder system the NC model, 276 2,4,6-TNEB molecules and 630 2,4-DNEB molecules were added to a simulation cell with the dimensions 115.5 Å × 89.4 Å × 70.9 Å (Figure 17G). To simulate a continuous NC polymer chain, the NC was positioned in both of the simulation cells so as to pass through the x-dimension periodic boundary. A stabiliser is added to NC binder mixtures and usually equals ~1% of the total ingredients by weight, in both cases this equaled the

addition of 8 EC molecules to each mixture.[16,17] The program Packmol was used to build both of the binder mixture simulation cells with a tolerance of 2.5 Å between the molecules.[125]

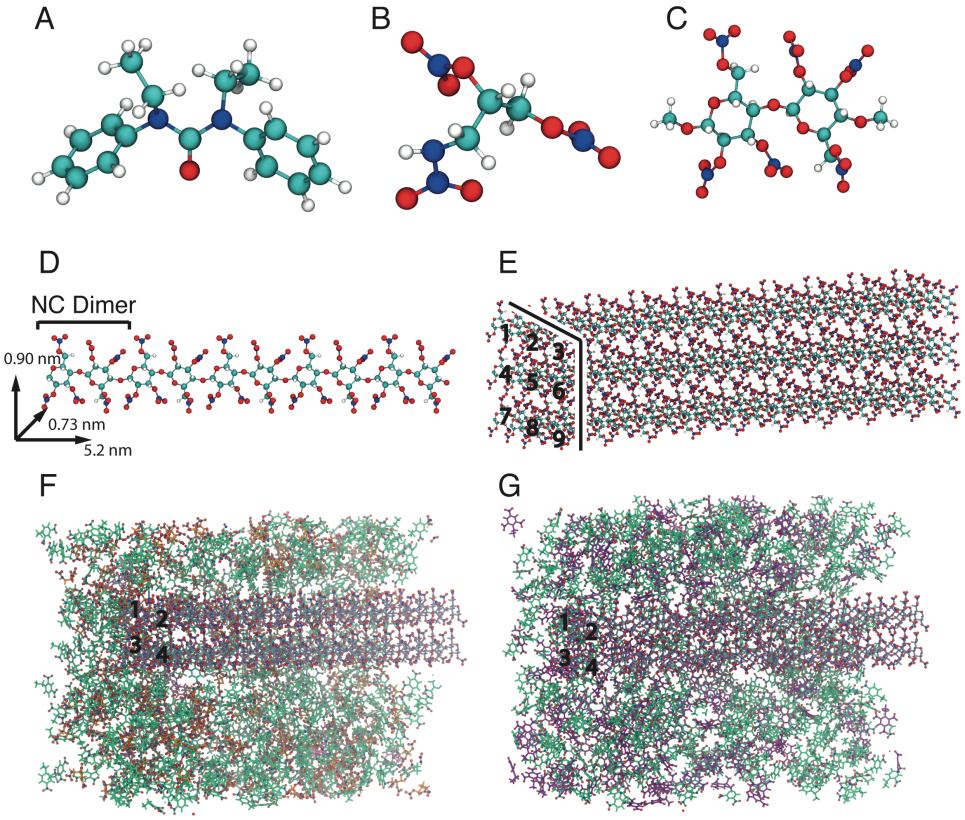

Figure 17 The optimised electronic structure of A) ethyl centralite (EC), B) 1-nitramino-2,3-dinitroxypropane (NG-N1), and C) methyl-capped nitrocellulose (NC) dimer. D) The unit cell of five NC dimers presented with unit cell periodic boundary dimensions, lattice angles of $\alpha = \beta = \gamma = 90°$, and E) an extended unit cell of nine NC chains. Both constructs repeat across the unit cell. F) The pre-equilibration NC binder configuration of four extended NC chains within a 2,4-dinitroethylbenzene (2,4-DNEB) and NG-N1 plasticiser mixture with EC, and G) within a K10 plasticiser mixture with EC. Individual NC chains have been numbered for clarity, running horizontal to the page. Molecules of EC are depicted with pink bonds, 2,4-DNEB with green bonds, NG-N1 with orange bonds and 2,4,6-TNEB with purple bonds. Oxygen and nitrogen have been visualised in red and blue, respectively.

The construction of all simulation cells is outlined in Appendix 1 (p.177).

3.1.5 Integration of Parameters into Amber

To perform molecular dynamics simulations the Sander module of Amber requires two input files, a prmtop and an inpcrd file.[90] The force field parameters for all of the atoms in the system, the atom and residue names and the periodic box type are incorporated in the prmtop file. The inpcrd file contains the initial coordinates and periodic box size. To prepare these files the LEaP and Antechamber modules of Amber 14 were used.[90] As the force fields for all molecules used bonding terms and non-bonding terms from various sources and were not entirely from Amber, the atom types to label the atoms in all files had to be different to those in Amber. Firstly, the Gaussian output file of the optimised geometry for a molecule was converted to a protein database (PDB) file and each atom given a unique type.[82] Antechamber converted the PDB files into mol2 files and these generated the frcmod and library files.[90] Each frcmod file for 2,4-DNEB, 2,4,6-TNEB, NC, EC, NG-N1 and NO_2 contained the parameter set created for that system with the unique atom types whilst the geometry information, RESP charges, atom types and details of connectivity for NC were contained in the library file for each molecule. For each pure system, the two plasticiser mixtures R8002 and K10 and the two NC binder systems inpcrd and prmtop files were built by loading the required frcmod, library and PDB files into the LEaP program.[90] The prmtop files contained the LJ A and B coefficients which were refined to optimise the densities for each system.

3.1.6 Molecular Dynamics Simulations

The Sander module of the Amber 14 package was used for all the molecular dynamics simulations. For all simulations periodic boundary conditions were defined in the x, y and z directions to approximate an infinite system. A minimisation was performed before all MD simulations firstly using the steepest descents method and then the conjugate gradient method for a larger number of cycles. Minimisation ensured molecules had adopted a conformation at a local minimum and was deemed complete when the RMS of the Cartesian element of the gradient was less than 1.0×10^{-4} kcal^{-1} mol^{-1} Å^{-1}. The equations of motion were integrated with a 0.001 ps time step using the Velocity Verlet algorithm.[87] The SHAKE algorithm constrained bonds to hydrogen. Prior to MD production runs the systems were heated to the required temperatures.[91] Anderson temperature-coupling maintained the temperature in equilibration simulations at constant volume (NVT) and constant pressure (NPT) and to maintain constant pressure in the NPT simulations the Berendsen barostat was used.[88,89]

In order to compare the dynamic bond lengths of 2,4-DNEB and 2,4,6-TNEB with the QM values the single molecules underwent MD simulations in a vacuum at 298 K for 3.5 ns. To enable accurate measurement of bond angles and lengths snapshots were taken every 400 steps over the last 2 ns and no constraints were applied so bonds and angles could equilibrate.

Simulations were performed under vacuum at 298 K of the pure 2,4-DNEB, 2,4,6-TNEB, NC, EC, NG-N1 and NO_2 systems. Simulations of the energetic plasticiser mixtures K10 and R8002 and the two binder mixtures, NC plasticised with NG-N1 and 2,4-DNEB and NC plasticised with K10 were also performed. All systems underwent a 30 ps NVT equilibration, prior to a 400 ps NPT equilibration in order to stabilise the pressure and therefore the density. Finally, for each of

the 2,4-DNEB, 2,4,6-TNEB, EC, NG-N1, R8002 and K10 systems a 12 ns NPT production run was performed. For NC and NO_2 18 ns and 7 ns production simulations were performed, respectively and for both of the NC binder mixtures NPT production runs were extended to 20 ns.

3.1.7 Calculation of Diffusion Coefficients using the Einstein equation

The production simulations of 2,4,6-TNEB, 2,4-DNEB, R8002 and K10 at 298 K were divided into two 6 ns halves. The thermostat was switched to the Berendsen scheme for the latter half of the production runs,[88] as the use of Langevin dynamics or the Anderson Thermostat may lead to inaccurate diffusion coeffcients.[129] To calculate the diffusion coefficients for the 2,4,6-TNEB and 2,4,-DNEB molecules in the systems, the latter half of the production simulations were also used to obtain the mean square displacements (MSD) to make certain that system parameters, such as box volume, pressure, temperature and density, had equilibrated. To find the diffusion coefficients using the Einstein equation (EE) the gradient of the plot of MSD versus time for the molecules was calculated in $Å^2$/ps. Because the MSDs for the molecules were calculated from initial positions, diffusion coefficients calculated for a small number of molecules would be intrinsically stochastic. To obtain reliable diffusion coefficients the MSDs were therefore averaged over all molecules in each of the 2,4,6-TNEB, 2,4-DNEB, R8002 and K10 systems.[96]

3.2 Parameterisation Results

3.2.1 Validation of Parameterisation

The validation of the parameterisation of 2,4-DNEB, 2,4,6-TNEB, NG-N1, EC, NC, NO_2, the plasticiser mixtures K10 and R8002 and the NC binder systems is outlined in this section. A comparison of the QM and MD bond lengths and angles of 2,4,6-TNEB and 2,4-DNEB with the experimental values is displayed in Table 1, Table 2 displays the comparison of the QM bonding terms of NG-N1, EC and NC with experimental values and the QM and experimental bond angle and lengths of NO_2 are in Table 3. The comparison of the QM, MD and experimental bonding terms is outlined in Appendix 3 (p.193). Simulated densities were compared to the experimental densities where available to assess the validity of the entire parameter sets for each of the pure systems, the plasticiser mixtures R8002 and K10, the 2,4-DNEB and NG-N1 mixture and the NC binder mixtures (Tables 4 and 5). The root mean squared deviation (RMSD) was averaged over simulation time to give the root mean square fluctuation (RMSF). Tables 4 and 5 display the RMSF for the simulated densities. The self-diffusion coefficients of 2,4,6-TNEB and 2,4-DNEB in the pure systems, and the diffusion coefficients of 2,4,6-TNEB and 2,4-DNEB in R8002 and K10, calculated at 298 K using the Einstein equation (EE) are displayed in Table 6. The standard deviation of the gradient of the MSD versus time graphs was used to calculate the standard errors for the diffusion coefficients calculated via the EE equation given in Table 6.

The QM-derived bonding terms for 2,4,6-TNEB and 2,4-DNEB were compared to experimental data; if the majority were in agreement with the experimental values they were then used in single molecule MD simulations of 2,4,6-TNEB and 2,4-DNEB. The single molecule 2,4,6-

TNEB and 2,4-DNEB bonding terms from the MD simulations were then compared back to the experimental data.[110–113]

Table 1 The Percentage of Bonds and Angles obtained from QM and MD Simulations of 2,4-DNEB and 2,4,6-TNEB respectively within 3%, 4-5% and 6-10% of the Experimental data.

	Percentage of QM and MD Bonds and Angles within 3%, 4-5% and 6-10% of the experimental data			
	2,4-DNEB		2,4,6-TNEB	
	QM	MD	QM	MD
[0% - 3%].	82	61	86	67
[4% - 5%].	9	23	8	13
[6% - 10%].	9	16	6	20

a. Experimental bond lengths and angles referenced in section 3.1.3.

The majority of 2,4,6-TNEB and 2,4-DNEB QM bond lengths and angles were in good agreement with the experimental data, 82% of bond lengths and 86% of bond angles were within 3% of the experimental values, respectively (Table 1.). The dynamic MD bond lengths and angles for 2,4,6-TNEB and 2,4-DNEB were also in close agreement with the experimental values, with 80% of the 2,4,6-TNEB values and 84% of the 2,4-DNEB values falling within 5% of the experimental bond lengths and angles.

Table 2 The Percentage of Bonds and Angles obtained from QM calculations of NG-N1, EC and NC respectively within 3%, 4-5%, 6-10% and >11% of the Experimental data.

	Percentage of QM Bonds and Angles of NG-N1, EC and NC respectively within 3%, 4-5%, 6-10% and >11% of the experimental data.		
	NG-N1	EC	NC
[0% - 3%].	63	79	92
[4% - 5%].	23	4	6
[6% - 10%].	4	4	2
> 11%	10	14	0

a. Experimental bond lengths and angles referenced in section 3.1.3.

The QM-derived bond lengths and angles of NC were in excellent agreement with experiment, 92% of the QM bond lengths and angles compared to the experimental values available were within 3% (Table 2). Of the QM bond lengths and angles for NG-N1 and EC, 86% and 83% were within 5% of the experimental values, respectively (Table 2).

Table 3 The QM and Experimental Bond Lengths and Angles of Nitrogen Dioxide, NO_2.

	QM and experimental NO_2 bond lengths and angles	
	bond length N-O (Å)	bond angle O-N-O (°)
Experimental	1.188	134.1
QM	1.193	134.4

a. Experimental bond lengths and angles referenced in section 3.1.3.

As shown in Table 3, the NO_2 QM bond angle differs from the experimental value by only 0.3°. The N-O QM bond lengths were slightly overestimated by 0.005 Å compared to the experimental bond lengths of NO_2.

The QM bonding terms for 2,4,6-TNEB, 2,4-DNEB, NC and NO_2 were considered in good agreement with the experimental values, simulations of these systems at 298 K were therefore performed using the QM-derived parameters for the bond lengths and angles, without adjustment. For NG-N1 5 of the 20 QM bond lengths, accounting for 10% of the total bonds and angles were significantly overestimated compared to experiment. For EC 8 of the 21 QM bond lengths, accounting for 14% of the total bonds and angles were significantly overestimated compared to experiment (Table 2). To see if this affected the overall bulk properties, simulations of NG-N1 and EC were performed at 298 K using the QM-derived bond lengths. If simulated densities of NG-N1 and EC within 2% of the experimental densities were not obtained after refinement of the LJ parameters, the overestimated QM bonding terms would be readjusted.

Table 4 Experimental and Simulated Densities in g cm^{-3} for the pure systems 2,4-DNEB, 2,4,6-TNEB, NG-N1, EC, NC and NO_2 measured at 298 K and 100kPa. Simulation errors are the RMSF.

	Simulated Density (g cm^{-3})	Experimental Density (g cm^{-3})
2,4,6-TNEB (optimised)	1.515	1.528
2,4,6-TNEB (original LJ)	1.338 +/- 0.01	
2,4,6-TNEB (published)	1.377 +/- 0.01	
2,4-DNEB (optimised)	1.304 +/- 0.01	1.317
2,4-DNEB (original LJ)	1.263 +/- 0.01	
2,4-DNEB (published)	1.270 +/- 0.01	
NG-N1 (optimised)	1.801 +/- 0.009	1.799
NG-N1 (original LJ)	1.592 +/- 0.009	
EC (optimised)	1.159 +/- 0.01	1.16
EC (original LJ)	1.054 +/- 0.01	
NC (optimised)	1.619 +/- 0.01	1.60
NO_2 (optimised)	0.003 +/- 0.0002	0.003

a. Experimental densities referenced in section 3.1.3.

As shown in Table 4 the optimised force field reproduces the densities of 2,4-DNEB and 2,4,6-TNEB very well, differing by only 1% and 0.9%, respectively, from the experimental values. The simulated density of 2,4,6-TNEB was significantly underestimated when using the original LJ parameters with a 12.4% difference compared to the experimental value, whilst the simulated

density for 2,4,6-TNEB using published force field parameters was marginally better with a 9.9% difference from the experimental value.[64,101] The optimised force field for 2,4-DNEB performs well compared to the 2,4-DNEB force field with the original LJ parameters and the force field parameterised with published force field values, where the simulated densities were underestimated by 4.1% and 3.6% respectively.[64,101] The optimised force fields for NG-N1 and EC performed very well, the simulated densities of both systems being within 0.1% of the experimental values. The simulated densities of EC and NG-N1 were again underestimated using the force field with the original LJ parameters, the simulated densities differing from experiment by 9.1% for EC and 11.6% for NG-N1.[64,101] The simulated density of NC using the GAFF LJ parameters was within 1.2% of experiment and the force field using GAFF LJ parameters reproduced the experimental density exactly for NO_2, the GAFF LJ parameters were therefore not adapted in both cases.[64]

Table 5 Experimental and Simulated Densities in g cm^{-3} for the Plasticisers K10 and R8002 and the NC Binder Mixtures measured at 298 K and 100kPa. Simulation errors are the RMSF.

	Simulated Density (g cm^{-3})	Experimental Density (g cm^{-3})
K10 - 35%:65% 2,4,6-TNEB & 2,4-DNEB	1.338 +/- 0.01	1.363 +/- 0.003
R8002 - 50%:50% 2,4,6-TNEB & 2,4-DNEB	1.357 +/- 0.01	1.380 +/- 0.002
67%:33% 2,4-DNEB & NG-N1	1.485 +/- 0.02	not available
NC binder - NG-N1 & 2,4-DNEB	1.412 +/- 0.02	1.428
NC binder - 2,4,6-TNEB & 2,4-DNEB	1.385 +/- 0.02	1.400

a. Experimental densities referenced in section 3.1.3.

The simulated densities of K10, R8002, the 2,4-DNEB and NG-N1 mixture, the NC binder mixture plasticised with NG-N1 and 2,4-DNEB and the NC binder mixture plasticised with K10 are displayed in Table 5. The simulated densities are in good agreement with experimental values. The differences between the simulated and experimental densities for the R8002 and K10 plasticiser mixtures are 1.7% and 1.8%, respectively.[121,122] The simulated densities of the NC binder mixture plasticised with NG-N1 and 2,4-DNEB and the NC binder mixture plasticised with K10 differ from their experimental densities by only 1.1% in both cases.[42] The simulated density of the 2,4-DNEB and NG-N1 mixture was obtained using the optimised LJ parameters for 2,4-DNEB and NG-N1. The mixture consists of 67% 2,4-DNEB and 33% NG-N1, so a simulated density between 1.304 g cm^{-3} the simulated density of 2,4-DNEB and 1.801g cm^{-3} the simulated density of NG-N1 would be expected and the simulated density of the mixture of 1.485 g cm^{-3} is between these two values. However, the simulated density of the 2,4-DNEB and NG-N1 mixture of 1.485 g cm^{-3} does appear high considering the simulated density of the NC binder containing 89% of the 2,4-DNEB and NG-N1 mixture is 1.412 g cm^{-3}. Although the simulated density of the 2,4-DNEB and NG-N1 mixture seems high compared to the NC 2,4-DNEB and NG-N1 binder, the LJ parameters for the mixture were not altered as no exact experimental density for the mixture minus the NC was available.

Overall the simulated densities of the 2,4-DNEB, 2,4,6-TNEB, NG-N1, EC, NO_2, and NC systems and the plasticiser and NC binder mixtures were in excellent agreement with the experimental densities. There was however some underestimation of the simulated densities of 2,4-DNEB and 2,4,6-TNEB which is likely to have contributed to the slight underestimation of the K10, R8002 and NC binder mixtures simulated densities compared to the experimental values. To obtain the simulated densities the LJ parameters were derived; one possible

explanation for the underestimation of the densities may therefore be due to the intramolecular terms, rather than the intermolecular parameters. Closer scrutiny of the dynamic bond lengths and bond angles from the single molecule simulations of 2,4,6-TNEB and 2,4-DNEB revealed a somewhat equal distribution of bond angles that were slightly above and below the experimental values. However, in both molecules all bond lengths were slightly greater than the experimental values. Even a small lengthening of the desired intramolecular bond lengths would lead to an overestimation of volume in the bulk simulations of 2,4,6-TNEB and 2,4-DNEB at 298 K and would result in a decrease in the system density. Although there was significant overestimation of some of the bond lengths and angles in the EC and NG-N1 molecules it possibly was not a great enough number of bonds to cause a decrease in the simulated densities of these systems. The slight underestimation of the K10 and R8002 simulated densities is likely due to these systems consisting of 2,4,6-TNEB and 2,4-DNEB molecules. The simulated densities of the NC binder systems were both slightly underestimated, although the simulated density of NC was slightly larger than the experimental value and the simulated density of the plasticiser NG-N1 present in one of the binder mixtures was slightly greater than experiment also. This is likely due to the large proportion of plasticiser molecules (~89%) in both the NC binder mixtures. The NC binder plasticised with K10 contained only 2,4,6-TNEB and 2,4-DNEB plasticiser molecules which likely decreased the simulated density. In the NC binder plasticised with NG-N1 and 2,4-DNEB, 66% of the plasticiser mixture consisted of 2,4-DNEB which again is likely to have resulted in a slightly lower simulated density overall for this NC binder mixture. However, as the variations in densities from the experimental values are very small and well within acceptable errors, simulations were continued with the parameters.

3.2.2 Diffusion of 2,4-DNEB and 2,4,6-TNEB

Table 6 The Self-Diffusion Coefficients calculated using the Einstein Equation of 2,4-DNEB and 2,4,6-TNEB in the pure systems and the Diffusion Coefficients of 2,4-DNEB and 2,4,6-TNEB in K10 and R8002 at 298 K.

Diffusion Coefficients (D) calculated at 298 K using the Einstein equation		
	D 10^{-9} m^2 s^{-1}	Standard Error 10^{-10} m^2 s^{-1}
2,4-DNEB	0.083	± 0.005
2,4,6-TNEB	0.006	± 0.001
2,4-DNEB in K10	0.014	± 0.001
2,4,6-TNEB in K10	0.010	± 0.001
2,4-DNEB in R8002	0.008	± 0.001
2,4,6-TNEB in R8002	0.005	± 0.001

Calculation of diffusion coefficients in Appendix 5 (p.211)

The self-diffusion coefficients of 2,4-DNEB and 2,4,6-TNEB and the diffusion coefficients of 2,4-DNEB and 2,4,6-TNEB in the plasticiser mixtures R8002 and K10 (Table 6) are as predicted when the simulated densities and molecular masses of the molecules are considered. The self-diffusion coefficient of 2,4,6-TNEB is much lower than that of 2,4-DNEB and the rate of diffusion of 2,4,6-TNEB is also lower in the K10 and R8002 mixtures compared to 2,4-DNEB, however in the plasticiser mixtures the difference between the diffusion coefficients of the two molecules is much smaller. The diffusivity of a substance is inversely proportional to molar mass, which is observed in these simulations.[130] At the same temperature and therefore equivalent average kinetic energy, 2,4-TNEB with a greater molecular mass of 221 u moves at a slower rate through its pure system and both the K10 and R8002 mixtures compared to 2,4,6-

DNEB, which has a lower molecular mass of 196 u.[130] The higher density of 2,4,6-TNEB compared to 2,4-DNEB also adds to the much lower self-diffusion of 2,4,6-TNEB as the molecules are arranged more tightly, imposing some restriction on their movement. The difference in diffusion coefficients of 2,4-DNEB and 2,4,6-TNEB in the K10 and R8002 mixtures is as expected considering the simulated densities; both molecules diffuse at a faster rate through the slightly lower density K10 mixture compared to R8002, likely due to the molecules being slightly more spaced apart which facilitates movement. The self-diffusion coefficient of 2,4-DNEB of 0.083 10^{-9} m^2 s^{-1} is higher than the values of 0.014 10^{-9} m^2 s^{-1} and 0.008 10^{-9} m^2 s^{-1} obtained for 2,4-DNEB in K10 and R8002, respectively. Hale describes 2,4-DNEB as a liquid at ordinary atmospheric temperatures and 2,4,6-TNEB as having a melting point of 37°C.[40] The diffusion of 2,4-DNEB in 2,4-DNEB alone is likely to be faster as it is a liquid at room temperature, it is possible that the addition of 2,4,6-TNEB with a higher melting point to 2,4-DNEB to create the K10 and R8002 mixtures raises the density significantly slowing the diffusion rate of 2,4-DNEB in these mixtures. Conversely the addition of liquid 2,4-DNEB to 2,4,6-TNEB to formulate K10 increases the diffusivity of 2,4,6-TNEB in K10 compared to 2,4,6-TNEB alone. The diffusion of 2,4,6-TNEB in R8002 is slightly slower than in 2,4,6-TNEB, which suggests this diffusion coefficient may have been underestimated. Faster diffusion of 2,4,6-TNEB in R8002 would be expected compared to 2,4,6-TNEB alone as R8002 has a lower density due to the addition of liquid 2,4-DNEB to make this mixture.

3.3 Conclusion

To investigate plasticiser migration and the interaction of nitrogen dioxide and water in a nitrocellulose (NC) binder system plasticised with 2,4-dinitroethylbenzene (2,4-DNEB) and 2,4,6-trinitroethylbenzene (2,4,6-TNEB) and a NC binder system plasticised with 2,4-DNEB and 1-nitramino-2,3-dinitroxypropane (NG-N1) force field parameterisation was required for the plasticiser molecules and NC. Force field parameters were also derived for nitrogen dioxide and the stabiliser molecule ethyl centralite which was added to each binder system. Geometry optimisation of the 2,4-DNEB, 2,4,6-TNEB, NG-N1, ethyl centralite and nitrogen dioxide molecules and the NC dimer generated the bonding parameters and partial charges. Either all or the majority of torsional terms for each molecule and the NC were taken from the General Amber Force Field. For 2,4-DNEB and 2,4,6-TNEB dihedral terms to specifically model out-of-plane deformation of the nitro group with the aromatic ring and rotation of the C-NO_2 bond were also employed. Initial Lennard-Jones parameters for each of the molecules and the NC dimer were taken from the literature. The quantum mechanical bond lengths and angles derived for the 2,4-DNEB, 2,4,6-TNEB, NG-N1, ethyl centralite and nitrogen dioxide molecules and the NC dimer were compared to experimental values. Readjustment of bond angles and lengths was only to be considered after the entire parameter set for each molecule and the NC had been validated. Bulk simulations of each compound were performed and the Lennard-Jones parameters adjusted iteratively until the experimental density of each compound was reproduced. The Lennard-Jones parameters from the General Amber Force Field reproduced the experimental densities of the NC and nitrogen dioxide to an acceptable degree of accuracy and were therefore left unaltered. The simulated densities of NG-N1 and ethyl centralite were in excellent agreement with experiment, the simulated densities of both systems being within 0.1% of the

experimental values. The force field also reproduced the experimental densities of 2,4-DNEB, 2,4,6-TNEB to a good level of accuracy, with the simulated densities differing by only 1% and 0.9%, respectively, from the experimental values. Simulated densities of 2,4-DNEB, 2,4,6-TNEB, NG-N1 and ethyl centralite obtained using the original unadjusted Lennard-Jones parameters were underestimated by 4.3%, 12.4%, 11.6% and 9.1% respectively, compared to experimental values. As the complete force field parameter sets reproduced the experimental densities of 2,4-DNEB, 2,4,6-TNEB, NG-N1, ethyl centralite, NC and nitrogen dioxide the bond lengths and angles were left unchanged. The plasticiser mixtures R8002 and K10 consisting of different proportions of 2,4-DNEB and 2,4,6-TNEB were simulated and after adjustment of the Lennard-Jones parameters the simulated densities were within 1.7% and 1.8% of experiment, respectively. The NC binder system plasticised with 2,4-DNEB and 2,4,6-TNEB (K10) and the NC binder system plasticised with 2,4-DNEB and NG-N1 were simulated and after alteration of the Lennard-Jones parameters the simulated densities of both systems were within 1.1% of experiment. A mixture of 67% 2,4-DNEB and 33% NG-N1 was simulated with the optimised 2,4-DNEB and NG-N1 LJ parameters. The simulated density of the 2,4-DNEB and NG-N1 mixture of 1.485 g cm^{-3} seems high compared to 1.412 g cm^{-3} the simulated density of the NC, 2,4-DNEB and NG-N1 binder, however the LJ parameters for the mixture were not altered as no exact experimental density for the mixture minus the NC was available. After closer examination of the 2,4-DNEB and 2,4,6-TNEB bond lengths it appears a number were overestimated, this may have led to the densities of the plasticiser mixtures and NC binder systems being slightly underestimated compared to experiment although they still are within an acceptable margin of error. The diffusion coefficients of 2,4-DNEB and 2,4,6-TNEB are as predicted considering the simulated densities and molecular masses of the molecules. The self-

diffusion coefficient of 2,4,6-TNEB is lower than that of 2,4-DNEB due to 2,4,6-TNEB having a higher density. Both molecules have lower diffusion rates in R8002 compared to K10 owing to R8002 having a higher simulated density. 2,4,6-TNEB also has a lower diffusion rate compared to 2,4-DNEB due to 2,4,6-TNEB having a greater molecular mass.

4. Migration of the Energetic Plasticisers 1-Nitramino-2,3-Dinitroxypropane, 2,4-Dinitroethylbenzene and 2,4,6-Trinitroethylbenzene in two Nitrocellulose Binder Mixtures

A binder holds the explosive ingredients together in a polymer bonded explosive (PBX) or propellant. The binder usually consists of a polymer mixed with a plasticiser.[6] The plasticiser alters the mechanical properties of the binder with the aim of improving the overall safety of the energetic material (EM). Many plasticisers migrate from the binder matrix which alters the mechanical properties of the EM and reduces the shelf-life.[13] The energetic output of an EM containing the explosive ingredient 1,3,5,7-Tetranitro-1,3,5,7-tetrazocane (HMX) mixed with a NC, NG-N1 and 2,4-DNEB binder was greater than an EM containing HMX suspended in a NC, 2,4-DNEB and 2,4,6-TNEB (K10) binder.[42] The migration of the concentrations of the energetic plasticiser molecules NG-N1, 2,4-DNEB and 2,4,6-TNEB as part of these two NC binder mixtures of 89% plasticiser and 11% NC has not been investigated experimentally or using computational studies.[42] In this chapter diffusion coefficients were calculated for each plasticiser in the two NC binder systems at five temperatures followed by calculation of activation energies of diffusion in order to compare the migration of NG-N1, 2,4-DNEB and 2,4,6-TNEB. The diffusion coefficients of NC in both binder systems were calculated to see if the behaviour of NC was as expected when compared to that of the plasticiser molecules. The radial distribution functions for each NC binder mixture were used to observe any ordering of the plasticiser molecules.

4.1 Migration of Energetic Plasticisers Methodology

4.1.1 Construction of NC Binder Systems

The NC binder systems simulated in the Parameterisation Chapter were used to determine diffusion coefficients at five temperatures for each of the energetic plasticiser molecules. The NC binder systems are displayed in Figures 17F and 17G on page 70 in the Parameterisation Chapter. The simulation cells for each binder mixture are outlined in Tables 7 and 8.

Table 7 – The Number and Percentage of Plasticiser molecules in the NC Binder plasticised with 2,4-DNEB and NG-N1 and the Simulation Cell dimensions (Å).

	Nitrocellulose binder plasticised with 2,4-DNEB and NG-N1				
Plasticiser Molecule	Amount of plasticiser in plasticiser mixture		Amount of plasticiser mixture in binder	Amount of NC in binder	Simulation Cell Dimensions
	(Number)	(%)	(%)	(%)	(Å)
2,4-DNEB	640	67	89	11	115.5 × 84.4 × 68.9
NG-N1	286	33			

Table 8 – The Number and Percentage of Plasticiser molecules in the NC Binder plasticised with K10 and the Simulation Cell dimensions (Å).

	Nitrocellulose binder plasticised with 2,4-DNEB and 2,4,6-TNEB				
Plasticiser Molecule	Amount of plasticiser in plasticiser mixture		Amount of plasticiser mixture in binder	Amount of NC in binder	Simulation Cell Dimensions
	(Number)	(%)	(%)	(%)	(Å)
2,4-DNEB	630	65	89	11	115.5 × 89.4 × 70.9
2,4,6-TNEB	276	35			

The stabiliser EC was added to each binder mixture, 8 molecules of EC were added to each binder system simulation cell.

4.1.2 Molecular Dynamics Simulations

The MD simulations and minimisations were performed using the Sander module of the Amber 14 package.[90] The steepest descent method followed by a larger number of conjugate gradient cycles were used for minimisation. The minimisation was deemed complete once the RMS of the Cartesian element of the gradient was less than 1.0×10^{-4} kcal^{-1} mol^{-1} Å^{-1}. To effectively approximate an infinite system of plasticiser molecules containing a continuous NC polymer chain, periodic boundary conditions were implemented for all simulations. A non-bonded cutoff of 8 Å was used for the pairwise LJ interactions and the Particle Mesh Ewald (PME) was used for treatment of long-range electrostatics. Bonds to hydrogen atoms were constrained using the SHAKE algorithm.[91] The Velocity Verlet algorithm integrated the equations of motion with a 0.001 ps time step.[87]

Equilibration was performed by simulation of each binder system using the NVT ensemble (constant temperature, volume and number of particles) and then simulation of each binder system using the NPT ensemble (constant temperature, pressure and number of particles). Equilibration of each binder system was performed for 30 ps using the NVT ensemble, followed by a 400 ps simulation using the NPT ensemble. The simulations utlised the Anderson temperature-coupling to calculate temperature and an isotropic implementation of the Berendsen barostat was used to maintain constant pressure in the NPT simulations.[88,89] For both binder mixtures 20 ns production run simulations were performed at 298 K, 323 K, 348 K, 373 K and 398 K using the NPT ensemble.

4.1.3 Calculation of Diffusion Coefficients using the Einstein equation

The NC binder systems were heated and equilibrated using the Anderson thermostat and then the thermostat was switched to the Berendsen scheme for production runs,[88] as the use of Langevin dynamics or the Anderson Thermostat can result in unreliable diffusion coefficients.[129] The gradients of the MSD over time for the NG-N1, 2,4-DNEB and 2,4,6-TNEB molecules and NC in the two NC binder systems were calculated to find the diffusion coefficients using:

$$6D = \lim_{t \to \infty} \frac{MSD}{t} \quad (1)$$

Diffusion coefficients calculated for a small number of molecules would be inherently stochastic as the MSD for the molecules were calculated from initial positions. Therefore, to obtain accurate diffusion coefficients the MSD was averaged over all molecules in each of the NC binder mixtures.[131] Diffusion is a temperature dependent process, which can be described by the Arrhenius relationship. Activation energies (E_a) were calculated for NG-N1 and 2,4-DNEB in the first of the NC binders and for 2,4,6-TNEB and 2,4-DNEB in second NC binder using the diffusion coefficients for each molecule of interest:

$$lnD = lnD_0 - \frac{E_a}{RT} \quad (5)$$

The diffusion constant ($cm^2\ s^{-1}$) is denoted by D_0, Ea is the activation energy, T is the temperature in Kelvin and R is the real gas constant.[132]

4.1.4 Radial Distribution Functions

A radial distribution function (RDF), displays the probability g (r) of finding a particle at distance r from another particle. To observe the distribution and arrangement of plasticiser

molecules in the NC and K10 binder and the NC, 2,4-DNEB and NG-N1 binder, RDF's were obtained for both systems at 298 K, 348 K and 398 K using the cpptraj module of Amber 14.[131] The RDF was calculated to show how the relative density of C2 atoms in the 2,4,6-TNEB molecules varies as a function of distance from the C1 atoms in 2,4-DNEB molecules in the NC and K10 binder. RDF's were also calculated to find how the relative density of C2 atoms in the NG-N1 molecules varies as a function of distance from the C1 atoms in 2,4-DNEB molecules in the NC, 2,4-DNEB and NG-N1 binder.

4.2 Migration of Energetic Plasticisers Results

The diffusion coefficients (*D*) of 2,4-DNEB and 2,4,6-TNEB in the NC binder plasticised with K10 are displayed in Table 9 and Graph 1. The diffusion coefficients of 2,4-DNEB and NG-N1 in the NC binder system plasticised with the 2,4-DNEB and NG-N1 mixture are displayed in Table 9 and Graph 2. Graph 3 shows D versus temperature for 2,4-DNEB in each NC binder system. The standard errors for the diffusion coefficients given in Table 1 were calculated from the standard deviations of the gradients of the MSD versus time graphs. For comparison of the results with experimental values, simulated values of *D* at ~398 K for NG-N1 are displayed alongside experimental values for NG in Table 10. Table 11 contains the diffusion coefficient simulated at ~373 K and ~398 K for K10 with the experimental value of the diffusion coefficient for K10 in a similar system. Tables 12 and 13 and Graphs 4 and 5 display the natural log of diffusion coefficient versus reciprocal temperature for 2,4-DNEB and NG-N1 in the NC, 2,4-DNEB and NG-N1 binder and for 2,4-DNEB and 2,4,6-TNEB in the NC K10 binder, respectively. The activation energies of diffusion calculated for each plasticiser molecule (in kJ mol^{-1}) are presented in Table 14 with the associated errors calculated from the standard errors of the gradients of the natural logarithm versus 1/T graphs. The diffusion coefficients calculated for NC in both binder systems are displayed in Table 15 and Graph 6. Graphs 7, 8 and 9 are the RDFs for the NC and K10 binder system and the RDFs for the NC, 2,4-DNEB and NG-N1 binder system are displayed in Graphs 10, 11 and 12.

Table 9 The Diffusion Coefficients ($cm^2\ s^{-1}$) for molecules 2,4-DNEB and 2,4,6-TNEB in a NC Binder Plasticiser of K10 and Diffusion Coefficients for molecules 2,4-DNEB and NG-N1 in a NC Binder Plasticiser of 2,4-DNEB and NG-N1 calculated at 5 different temperatures (K).

	NC Binder: 2,4-DNEB and 2,4,6-TNEB (K10)				NC Binder: 2,4-DNEB and NG-N1			
	2,4-DNEB		2,4,6-TNEB		2,4-DNEB		NG-N1	
T (K)	D 10^7 $cm^2\ s^{-1}$	Std. Err $cm^2\ s^{-1}$	D 10^7 $cm^2\ s^{-1}$	Std. Err $cm^2\ s^{-1}$	D 10^7 $cm^2\ s^{-1}$	Std. Err $cm^2\ s^{-1}$	D 10^7 $cm^2\ s^{-1}$	Std. Err $cm^2\ s^{-1}$
298	0.33	2.72×10^{-10}	0.30	4.66×10^{-10}	0.16	3.13×10^{-10}	0.19	5.63×10^{-10}
323	2.17	5.20×10^{-09}	1.27	2.08×10^{-9}	0.45	1.49×10^{-9}	0.22	3.09×10^{-10}
348	3.75	4.26×10^{-9}	1.85	1.43×10^{-9}	0.85	1.53×10^{-9}	0.56	6.56×10^{-10}
373	4.30	9.30×10^{-10}	3.08	1.13×10^{-9}	1.50	6.17×10^{-10}	0.96	3.57×10^{-10}
398	9.31	9.90×10^{-10}	5.76	1.48×10^{-9}	3.38	8.67×10^{-10}	2.48	1.03×10^{-9}

Calculation of diffusion coefficients displayed in Appendix 6 (p.212-213)

4.2.1 The Effect of Temperature, Density and Molecular Mass on the Diffusion Coefficients of the Plasticisers

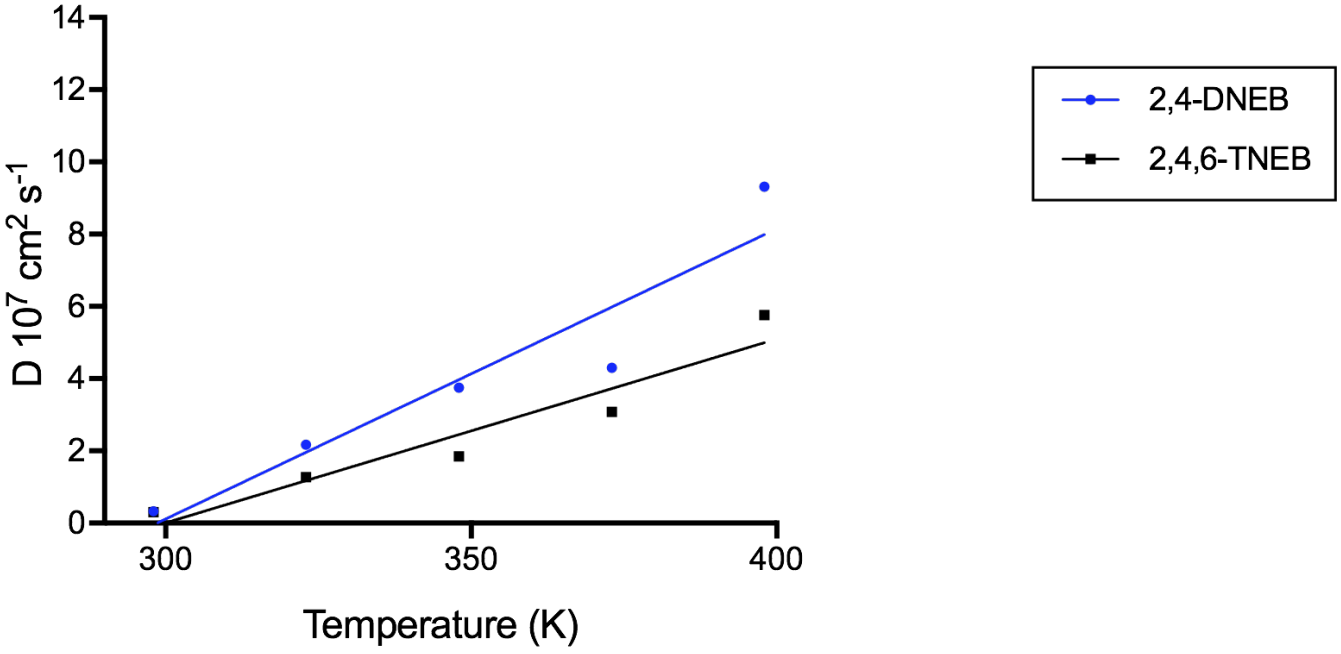

Graph 1 Plot of diffusion coefficients (D) versus temperature for 2,4-DNEB and 2,4,6-TNEB in the NC binder plasticised with K10.

The diffusion coeffcients for 2,4,6-TNEB and 2,4-DNEB in the NC binder plasticised with K10 increase with temperature, as would be predicted due to the increased kinetic energy of the binder system (Table 9, Graph 1). Diffusion coefficients are inversely proportional to the molecular weight of the molecule.[130] This inverse law is clear in the NC binder plasticised with K10; 2,4,6-TNEB with a greater molecular mass of 241 u has a smaller diffusion coefficient at all temperatures compared to 2,4-DNEB, which has a molecular mass of 196 u. The same trends in diffusion coefficients are found in the NC binder plasticised with a mixture of NG-N1 and 2,4-

DNEB (Table 9, Graph 2). The diffusion coefficients for NG-N1 and 2,4-DNEB increase with temperature and are lower for NG-N1 compared to 2,4-DNEB across the 323 K – 398 K temperature range. This is explained by the greater molecular mass of NG-N1 (226 u) compared to 2,4-DNEB (196 u).

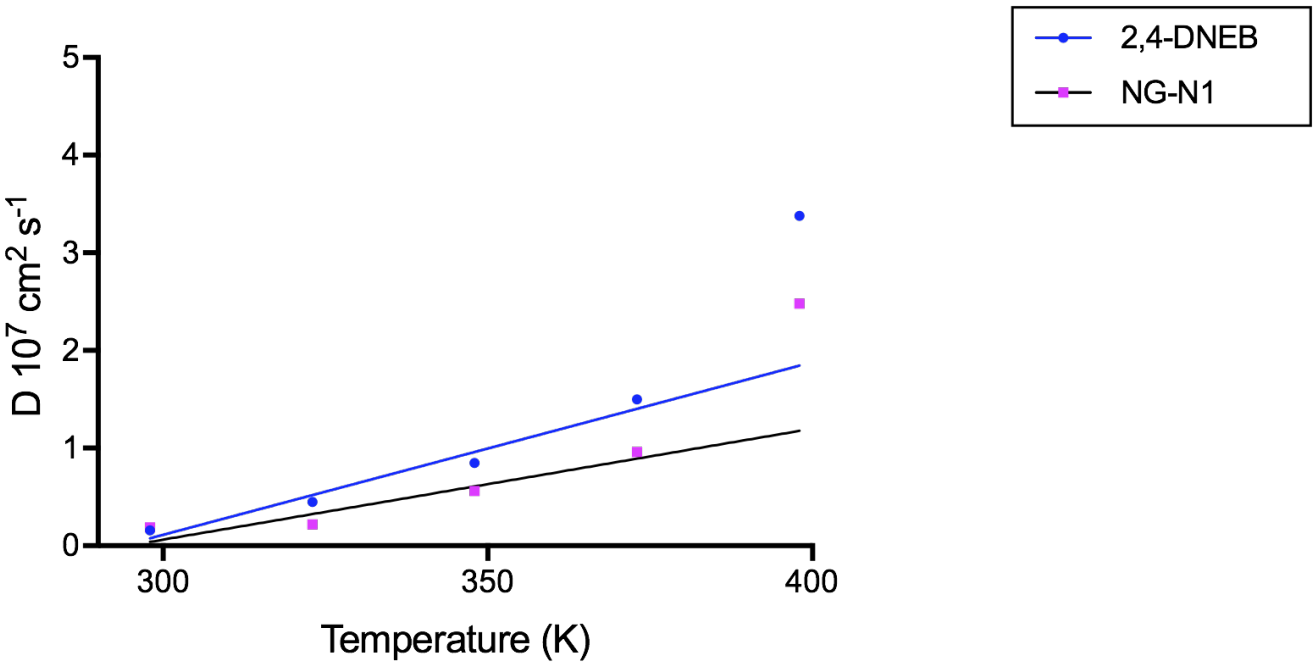

Graph 2 Plot of diffusion coefficients (*D*) versus temperature for 2,4-DNEB and NG-N1 in the NC binder system plasticised with the 2,4-DNEB and NG-N1 mixture.

Small changes in density can affect calculated diffusion coefficients,[102] this has been shown in these NC binder systems where the diffusion coefficients of 2,4-DNEB and NG-N1 in the NC binder plasticised with the 2,4-DNEB and NG-N1 mixture are lower than those of 2,4-DNEB and 2,4,6-TNEB at the corresponding temperatures in the NC binder plasticised with K10 (Graphs 1 and 2). The slower diffusion of the 2,4-DNEB and NG-N1 molecules in the NC binder plasticised with the 2,4-DNEB and NG-N1 mixture can be attributed to the higher

simulated density of 1.412 g cm^{-3} compared to the simulated density of 1.385 g cm^{-3} for the NC and K10 binder. This trend is further reinforced by comparison of the values of D for 2,4-DNEB in both binder mixtures (Graph 3), the molecular mass which affects the rate of diffusion is no longer contributing to the differing diffusion rates as the same molecule is being observed in each mixture. The larger diffusion coefficients for 2,4-DNEB in the NC binder mixture plasticised with K10 compared to those obtained for the NC binder plasticised with 2,4-DNEB and NG-N1 are therefore due to the lower simulated density of the NC and K10 binder.

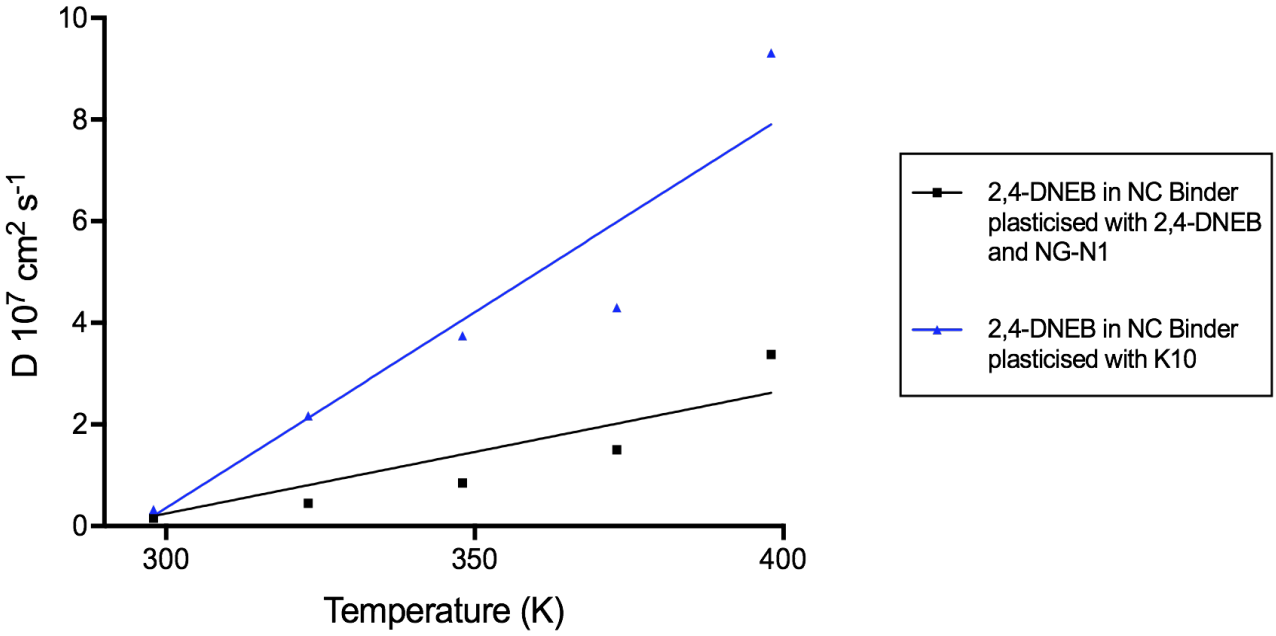

Graph 3 Plot of diffusion coefficients (D) versus temperature for 2,4-DNEB in each NC binder system.

4.2.2 Comparison of the Diffusion Coefficients of the Plasticisers with Experimental Values

Experimental diffusion coefficients for NG-N1, 2,4,6-TNEB and 2,4-DNEB in the NC binder mixtures studied in this work are not available. However, there are experimental diffusion coefficients calculated for plasticiser molecules in similar systems which have been used to determine the reliability of the values. Cartwright measured the mass loss of various plasticised propellants due to plasticiser vaporisation using thermogravimetric analysis (TGA) at constant temperature and used the results to calculate the diffusion coefficients and activation energies for the plasticisers.[17] One of the studies calculated diffusion coefficients for nitroglycerin (NG) at three temperatures in a NC propellant with a plasticiser content of 40%, NC with a 13.25% nitrogen content and 1% EC by weight of the total propellant ingredients.[17] The molecular mass of NG-N1 is 226 u and NG has a molecular mass of 227 u, therefore considering their structural similarity and mass a comparison was made between the experimental value for NG at 125.4ºC (~398 K) in the experimental NG and NC propellant mixture and the diffusion coefficient for NG-N1 at 398 K (~125ºC) calculated from simulation of the NC, 2,4-DNEB and NG-N1 binder system (Table 10).[17]

Table 10 The Experimental Diffusion Coefficient for NG at ~398 K and the Diffusion Coefficient calculated from Simulation for NG-N1 at 398 K ($cm^2\ s^{-1}$).

	Diffusion Coefficients for NG-N1 and NG ($cm^2\ s^{-1}$)	
T (K)	NG-N1	NG
~398	2.48×10^{-7}	1.09×10^{-7}

The diffusion coefficient calculated at ~398 K for NG-N1 in the NC, 2,4-DNEB and NG-N1 binder system is 2.48 $\times 10^{-7}$ cm^2 s^{-1} which is the same order of magnitude as the value of the diffusion coefficient calculated from experiment at ~398 K for NG in the NC propellant (1.09 $\times 10^{-7}$ cm^2 s^{-1}). The diffusion coefficient calculated for NG-N1 of 2.48 $\times 10^{-7}$ cm^2 s^{-1} is higher than the experimental value for NG. Diffusion coefficients are inversely proportional to molecular mass, however the molecular masses of the molecules are unlikely to cause this difference in the diffusion coefficients as NG has a molecular mass of 227 u and NG-N1 has a molecular mass of 226 u.[130] The reason for the larger diffusion coefficient at ~398 K for NG-N1 compared to NG is most likely to be the proportions of NC and plasticiser in the simulated NC binder. The rate of diffusion is greater in a more highly plasticised propellant or binder due to greater mobility within the macromolecular network;[17] it has been suggested that at higher plasticiser levels the ability of NC to immobilise plasticiser molecules is reduced.[55] The diffusion coefficient of NG-N1 is nearly 2.3 times greater than the experimental diffusion coefficient obtained for NG. It is likely that the larger diffusion coefficient is due to the NC binder system plasticised with 2,4-DNEB and NG-N1 containing 89% plasticiser, roughly 2.2 times the 40% plasticiser content of the NC and NG propellant investigated experimentally.[17,42]

An experimental study by Provatas used TGA to investigate plasticiser migration rates in a polyGLYN binder containing 15% plasticiser by weight.[13] Diffusion coefficients were calculated for K10 and the GLYN oligomer at 4 different temperatures, diffusion coefficients for two of the temperatures were compared with the results from this research.[13] In the experimental study separate diffusion coefficients for 2,4-DNEB and 2,4,6-TNEB the constituents of K10 were not given, Provatas reported diffusion coefficients for the overall plasticiser mixture K10.[13] To approximate values for simulated diffusion coefficients of K10 in the NC binder which could be

compared to Provatas' experimental values, the diffusion coefficients for 2,4,6-TNEB and 2,4-DNEB were multiplied by their K10 plasticiser proportions (0.35 and 0.65, respectively) and added together. The estimations of the diffusion coefficients for K10 obtained in this work at 373 K and 398 K and the experimental diffusion coefficients for K10 at ~373 K and ~398 K in a polyGLYN binder are displayed in Table 11.

Table 11 The Experimental and Simulated Diffusion Coefficients calculated for K10 at ~373 K and ~ 398 K.

	Experimental and simulated diffusion coefficients for K10 ($cm^2\ s^{-1}$)	
T (K)	Experimental	Simulated
~373	1.32×10^{-7}	3.88×10^{-7}
~398	7.01×10^{-7}	8.07×10^{-7}

The simulated diffusion constants calculated for K10 are the same order of magnitude as those obtained for K10 at ~373 K and ~398 K from TGA of the polyGLYN binder.[13] The diffusion coefficients for K10 calculated from simulation at ~373 K and ~398 K are both higher than the experimental values. The differences are possibly due to the different plasticiser proportions and densities of the experimental polyGLYN binder and simulated NC K10 binder. The polyGLYN binder contained 15% plasticiser by weight compared to 89% for the simulated NC K10 binder and the simulated NC and K10 binder density is 1.385 g cm^{-3} compared to a polyGLYN binder which typically has a density of 1.42 g cm^{-3}.[42,133] Calculated diffusion coefficients are sensitive to small changes in density, the lower density of the simulated NC and K10 binder compared to the polyGLYN binder means plasticiser molecules can move with less restriction.[102] A higher

plasticiser level results in a faster diffusion rate for the plasticiser molecules.[17] The lower density of the simulated NC and K10 binder combined with a much higher plasticiser content would explain the larger diffusion coefficient values for K10 compared to the experimental study.

The diffusion coefficients calculated for all plasticiser molecules in both NC binder systems increase steadily from 298 K to 373 K, but it is apparent that there is a large increase in the diffusion coefficient value from 373 K to 398 K (Table 9 and Graphs 1 and 2). The diffusion coefficients for 2,4-DNEB and NG-N1 at 398 K in the NC binder system plasticised with the 2,4-DNEB and NG-N1 mixture were left out the least-squares fit in Graph 2 so the general trend of increasing D with temperature could be observed. However the increase in diffusion coefficient at higher temperatures is also observed in the experimental studies of the K10 and polyGLYN binder and the NC and NG propellant.[17] The experimental diffusion coefficient for K10 in polyGLYN increases by ~5.3 from 1.32×10^{-7} cm^2 s^{-1} to 7.01×10^{-7} cm^2 s^{-1} between ~373 K and ~398 K and the diffusion coefficient for K10 in the simulated NC K10 binder increases from 3.88×10^{-7} cm^2 s^{-1} at 373 K to 8.07×10^{-7} cm^2 s^{-1} at 398 K.[13] In the simulated NC binder plasticised with NG-N1 and 2,4-DNEB, the D value for NG-N1 increases from 9.59×10^{-8} cm^2 s^{-1} at 373 K to 2.48×10^{-7} cm^2 s^{-1} at 398 K. A large increase is also noticeable between 381 K and 398 K in the experimental NC and NG propellant, where the diffusion coefficient increases from 3.54×10^{-8} cm^2 s^{-1} to 1.09×10^{-7} cm^2 s^{-1}.[17] At 398 K the kinetic energy of the molecules has increased compared to ~373 - 380 K, resulting in increased mobility of molecules and significantly higher diffusion coefficients.

4.2.3 The Activation Energies of the Plasticisers

The Arrhenius relationship was used to calculate activation energies (E_a) of diffusion for NG-N1 and 2,4-DNEB in the NC binder plasticised with this mixture and for 2,4,6-TNEB and 2,4-DNEB in the NC and K10 binder using the diffusion coefficient at each temperature for each molecule of interest.

Table 12 Natural Logarithms of the Diffusion Coefficients of 2,4-DNEB and NG-N1 in the NC Binder plasticised with 2,4-DNEB and NG-N1.

		ln D ($cm^2 s^{-1}$) for 2,4-DNEB and NG-N1 in the NC binder	
T (K)	1/T (K)	2,4-DNEB	NG-N1
298	0.00336	-17.92	-17.81
323	0.00310	-16.92	-17.65
348	0.00287	-16.28	-16.69
373	0.00268	-15.71	-16.16
398	0.00251	-14.90	-15.21

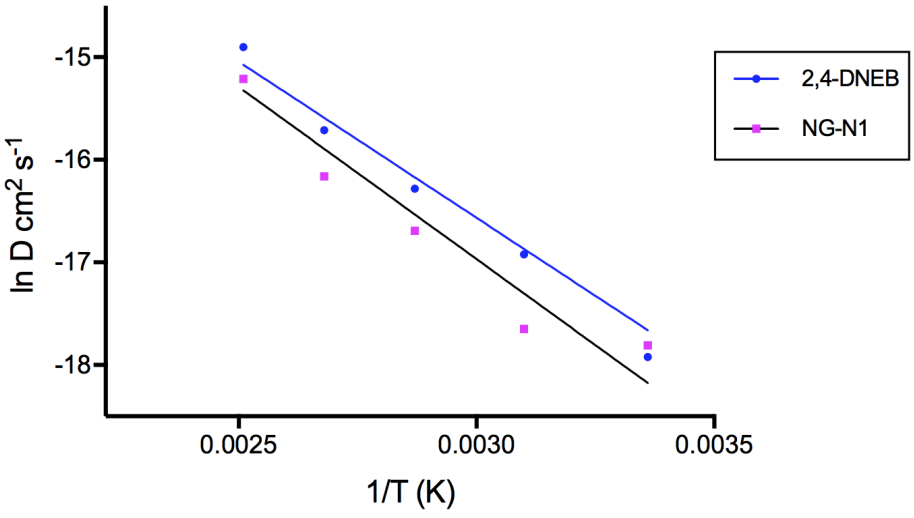

Graph 4 Least-squares best-fit of ln D of 2,4-DNEB and NG-N1 versus the reciprocal of temperature (K).

Table 13 Natural Logarithms of the Diffusion Coefficients of 2,4-DNEB and 2,4 TNEB in the NC K10 Binder.

		ln D ($cm^2 s^{-1}$) for 2,4-DNEB and 2,4 TNEB in the NC binder	
T (K)	1/T (K)	2,4-DNEB	2,4,6-TNEB
298	0.00336	-17.23	-17.32
323	0.00310	-15.35	-15.88
348	0.00287	-14.80	-15.50
373	0.00268	-14.66	-14.99
398	0.00251	-13.89	-14.37

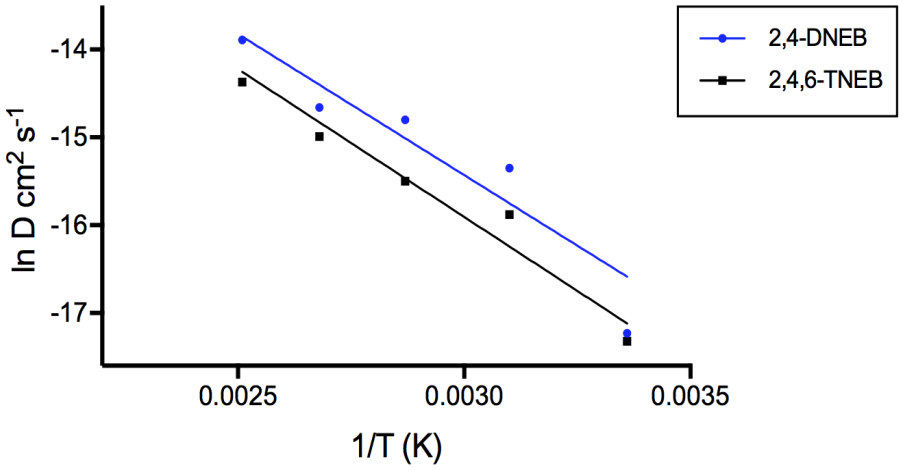

Graph 5 Least-squares best-fit of ln D of 2,4-DNEB and NG-N1 versus the reciprocal of temperature (K).

Good linearity was shown in the plots of the natural logarithms of the diffusion coefficients versus reciprocal temperature (1/T) for the plasticisers in both of the binder systems. The gradients of the linear fits were used to calculate the activation energies of diffusion for each

plasticiser and the associated errors were calculated from the standard errors of the gradients of the linear fits.

Table 14 Activation Energies (E_a) of Diffusion for the Plasticiser molecules (kJ mol^{-1}).

NC Binder	Plasticiser	Activation Energy (kJ mol^{-1})
NC, 2,4-DNEB & NG-N1 binder	2,4-DNEB	25.3 ± 1.2
	NG-N1	27.9 ± 2.2
NC & K10 binder	2,4-DNEB	26.7 ± 2.8
	2,4,6-TNEB	28.0 ± 1.7

Calculation of activation energies of diffusion and errors displayed in Appendix 7 (p.216)

As would be expected due to a higher molecular mass, the activation energy of NG-N1 is slightly higher than that of 2,4-DNEB in the NC binder mixture plasticised with a mixture of these two molecules. The same trend in activation energies of diffusion are observed in experimental studies of low molecular mass migrants in Poly(ethylene terephthalate): the greater the mass of a molecule, the lower the diffusion rate and the higher the activation energy of diffusion.[13] The same trend occurs in the NC and K10 binder, where 2,4,6-TNEB with a greater molecular mass than 2,4-DNEB has a slightly higher activation energy of diffusion. The activation energy of 2,4-DNEB is 26.7 kJ mol^{-1} in the NC and K10 binder compared to 25.3 kJ mol^{-1} in the NC binder plasticised with 2,4-DNEB and NG-N1. This would not be expected as the higher simulated density of the NC, 2,4-DNEB and NG-N1 binder should reduce the rate of diffusion leading to a higher activation energy compared to the value obtained for the NC and K10 binder, however the difference in activation energy is only 1.4 kJ mol^{-1}. The activation energy of diffusion of NG in the experimental study of an NC propellant containing a plasticiser content of 40% and NC with

a 13.25% nitrogen content was calculated as 89 kJ mol^{-1}, approximately three times the value obtained for NG-N1.[17] The NC propellant used in the experimental study by Cartwright contained 60% NC whereas the NC, 2,4-DNEB and NG-N1 binder simulated in this study contained 11% NC. The ability of the NC polymer in a binder to immobilise diffusant molecules has been discussed previously and the larger amount of NC in Cartwright's propellant certainly would have had an impact on the activation energy of diffusion obtained for NG which is much greater than the 27.9 kJ mol^{-1} obtained for NG-N1. An activation energy calculated from the rate constant of a chemical reaction can suggest a diffusion-controlled reaction which is determined by the rate the reactant molecules diffuse through a medium or if the activation energy is considerable an activation-controlled reaction is more likely.[134] In contrast activation energies of diffusion calculated from diffusion coefficients indicate the relative 'ease' and energy required for a species or diffusant to diffuse through a material. The diffusion of organic substances through polymers is controlled by the ability and frequency with which molecules 'jump' from one hole to another.[135] The temperature dependence of diffusion is governed by the activation energy needed for the diffusant to make this jump. As this jump requires space in the polymer matrix, its activation energy will be dependent on intra- and interchain forces in the polymer structure.[136–138] The activation energy of diffusion, E_a is calculated as follows,

$$lnD = lnD_0 - \frac{E_a}{RT} \tag{3}$$

and depends on the ease with which the diffusant can move from hole to hole. The diffusion constant, D_0 is a preexponential factor associated with the number of holes in which the diffusant can be held (dependent on diffusant size and polymer density).[135] Therefore the temperature-dependent E_a, includes the enthalpic factors, whereas the temperature-independent

D_0, thus includes entropic factors.[135] Diffusivity decreases with increasing crosslinking and polymer density, because the number of holes able to contain the diffusant is reduced. The lower number of holes increases the distance of a "jump" from one hole to another making it more difficult. [136] The experimental propellant studied certainly had a greater NC polymer density compared to the simulated NC binder which would result in a lower number of holes in which the diffusing NG molecules could potentially occupy. The ease at which the NG molecules could 'jump' from hole to hole in Cartwright's propellant would therefore be reduced meaning the NG molecules would require a greater activation energy of diffusion compared to the NG-N1 molecules in the simulated NC, 2,4-DNEB and NC binder. The activation energy will be greater if the diffusant is less flexible, more branched or larger.[138] The structures of NG and NG-N1 are very similar, NG has a molecular mass of 227 u and NG-N1 has a molecular mass of 226 u, the molecular mass and amount of branching are therefore unlikely to contribute significantly to the difference in the activation energies of diffusion. A factor that will result in differing activation energies of diffusion is the likelihood of hydrogen bond formation between the partially positive hydrogen atoms in the plasticiser molecules and the partially negatively charged oxygen atoms in the NC. Radial distribution functions of a double base propellant consisting of NC and NG obtained by Ma and et al. indicated hydrogen bonding action and strong vdW force between NC and NG, with most of the hydrogen bonding action existing between O(NC) and H(NG).[48] It is likely a greater number of hydrogen bonds will form between the hydrogen atoms in the NG and oxygen atoms in the NC in the experimental propellant compared to the number formed between hydrogen atoms in the NG-N1 and the oxygen atoms in the NC in the simulated binder. This is due to the experimental propellant studied by Cartwright containing 60% NC compared to the 11% NC contained in the simulated binder. A greater number of NG molecules hydrogen

bonded to the NC in the experimental propellant would reduce the ease at which the NG molecules could 'jump' from hole to hole in the NC resulting in a larger the activation energy of diffusion for NG in the experimental propellant than that obtained for NG-N1 in the simulated NC, 2,4-DNEB and NG-N1 binder.

4.2.4 Diffusion of Nitrocellulose in the Nitrocellulose Binder Systems

Diffusion coefficients were calculated for NC at five temperatures in the NC binder plasticised with 2,4-DNEB and NG-N1 and in the NC binder plasticised with K10, as displayed in Table 15. The standard deviations of the gradients of the MSD versus time graphs were used to calculate the standard errors for the diffusion coefficients given in Table 15. Graph 6 is a least-squares best fit of the diffusion coefficients versus temperature for NC in each binder mixture.

Table 15 Diffusion Coefficients for NC in the NC, 2,4-DNEB and NG-N1 Binder and in the NC and K10 Binder

	NC in the NC and K10 binder		NC in the NC, 2,4-DNEB and NG-N1 binder	
T (K)	D 10^7 cm^2 s^{-1}	Standard Error cm^2 s^{-1}	D 10^7 cm^2 s^{-1}	Standard Error cm^2 s^{-1}
298	0.196	7.01×10^{-10}	0.034	1.81×10^{-10}
323	0.219	5.55×10^{-10}	0.132	5.71×10^{-10}
348	0.298	1.81×10^{-9}	0.193	1.25×10^{-9}
373	0.362	1.17×10^{-9}	0.317	5.72×10^{-10}
398	1.192	5.56×10^{-9}	0.470	1.08×10^{-9}

Calculation of diffusion coefficients displayed in Appendix 6 (p.214)

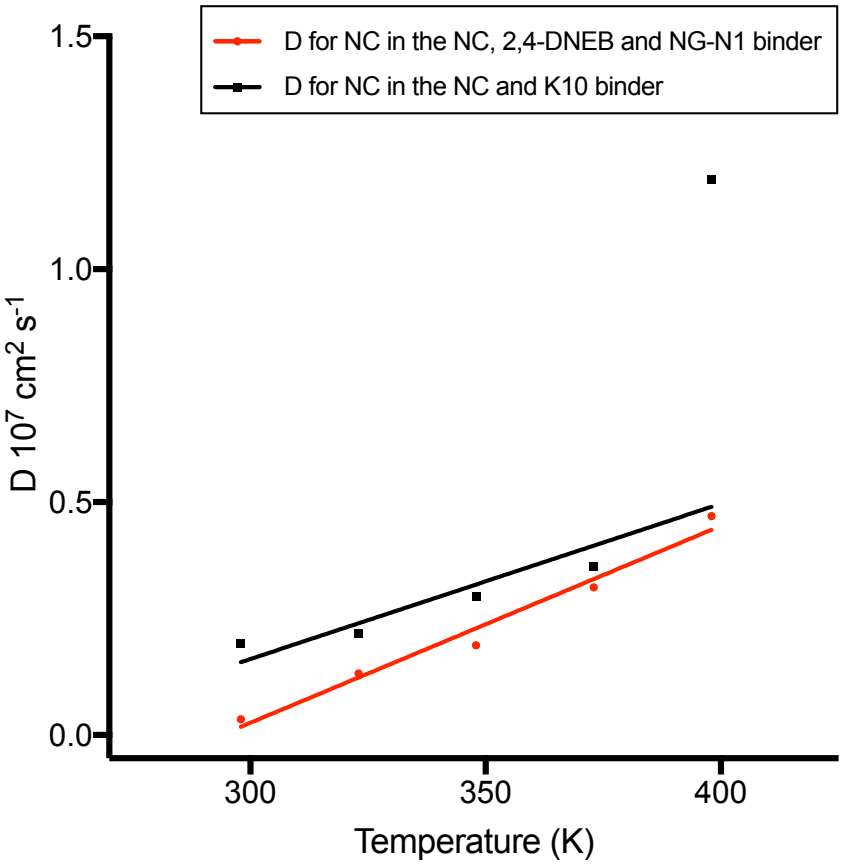

Graph 6 Plot of diffusion coefficients (D) versus temperature for NC in each NC binder system.

There was a large jump in diffusion coefficient values at 398 K for the plasticiser molecules in both of the simulated NC binder mixtures and in the values of D obtained for the plasticisers studied in the experimental work conducted by Provatas and Cartwright.[13,17] Graph 6 shows the diffusion coefficient for NC in the NC and K10 binder at 398 K is also much greater than the other values, however the difference between this and the other values is so much larger it was treated as anomalous and excluded from the least-squares best fit. As discussed previously calculated diffusion coefficients are sensitive to small changes in density.[102] This is observed in the two NC binder mixtures where the calculated diffusion coefficients for NC are higher in the NC and K10 binder with a lower simulated density of 1.385 g cm^{-3} compared to the values of D

for NC in the NC, 2,4-DNEB and NG-N1 binder which has a simulated density of 1.412 g cm^{-3} (Graph 6). The NC diffusion is less restricted in the NC and K10 binder due to the molecules being slightly more spaced apart resulting in higher D values. The diffusion coefficients for NC in the NC, 2,4-DNEB and NG-N1 binder are lower than those of 2,4-DNEB and NG-N1 in this mixture. Comparison of the diffusion coefficients for different molecules in the same binder mixture means the simulated density is unlikely to be the cause of the different diffusion rates. Diffusion coefficients are inversely proportional to molecular mass, the values of D for NC are lower than the plasticiser molecules due to the greater molecular mass of the NC polymer chain.[130] The same explanation applies to the NC K10 binder where the diffusion coefficients are lower for NC compared to the 2,4-DNEB and 2,4,6-TNEB molecules due to the greater molecular mass of the NC polymer chain.

4.2.5 Radial Distribution Functions of the NC Binder Systems

The RDF was calculated between the C2 atoms in the 2,4,6-TNEB molecules and the C1 atoms in the 2,4-DNEB molecules in the NC and K10 binder, the C2 atom in 2,4,6-TNEB and C1 atom in 2,4-DNEB were chosen to try and obtain similar points in each molecule (Figure 18). The RDFs for the NC and K10 binder systems at 298 K, 348 K and 398 K are displayed in Graphs 7, 8 and 9 respectively.

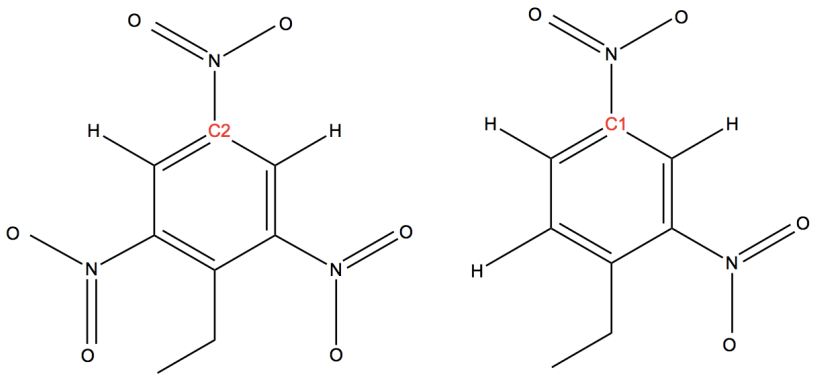

Figure 18 Diagram of 2,4,6-TNEB molecule with the C2 atom highlighted in red and 2,4-DNEB molecule with the C1 atom highlighted in red.

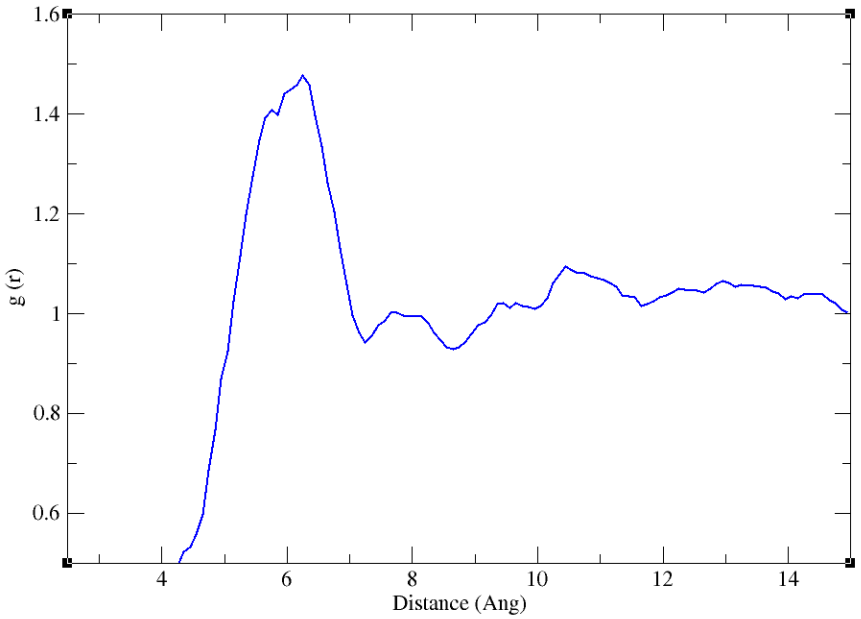

Graph 7 The RDF between the C2 atom in 2,4,6-TNEB and C1 atom in 2,4-DNEB in the NC and K10 binder at 298 K.

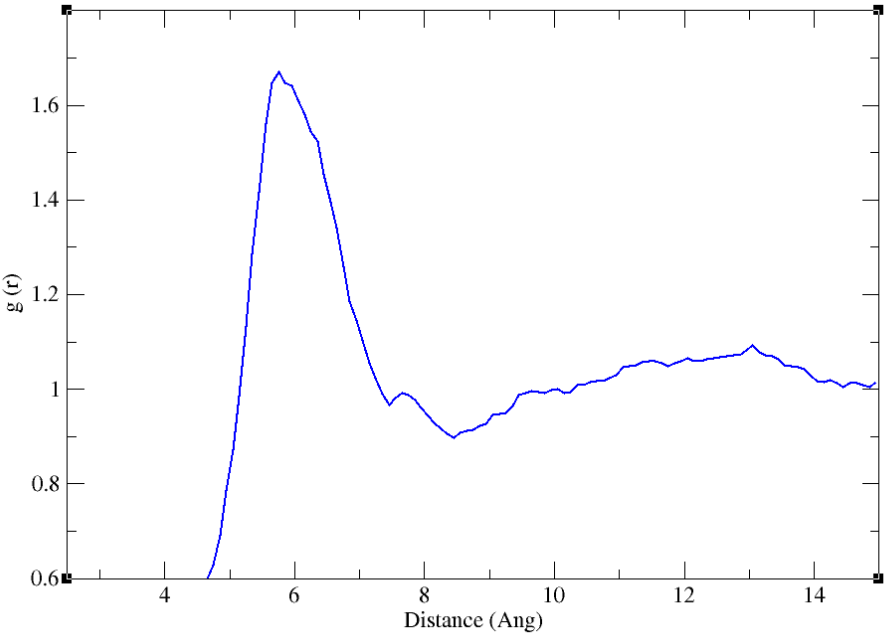

Graph 8 The RDF between the C2 atom in 2,4,6-TNEB and C1 atom in 2,4-DNEB in the NC and K10 binder at 348 K.

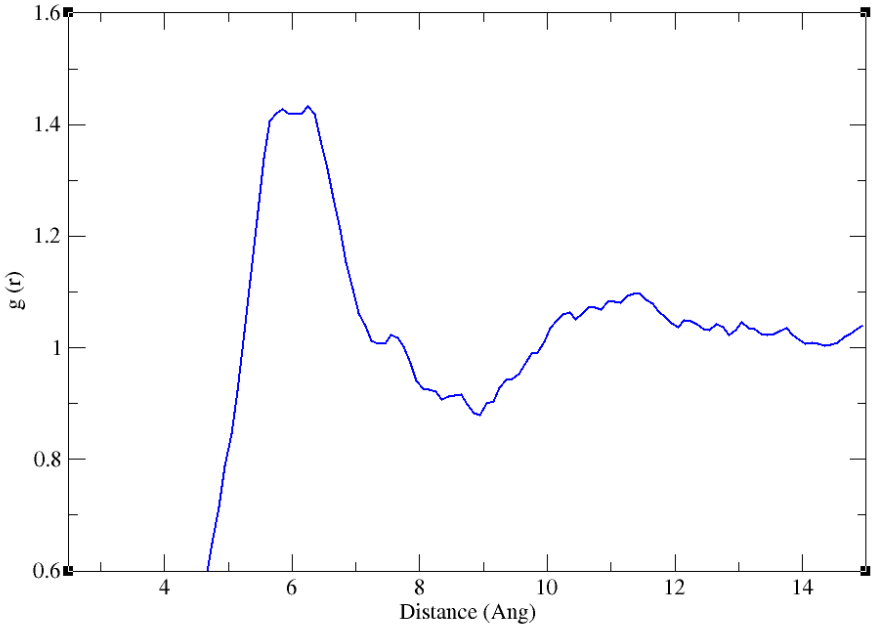

Graph 9 The RDF between the C2 atom in 2,4,6-TNEB and C1 atom in 2,4-DNEB in the NC and K10 binder at 398 K.

In graphs 7,8 and 9 the radial distribution functions show clear first peaks at ~ 6 Å, this peak indicates the first coordination shell. There is a high probability of finding a C2 atom in a 2,4,6-TNEB molecule approximately 6 Å from a C1 atom in a 2,4-DNEB molecule in the NC and K10 binder. At 398 K the first peak is slightly broader and g (r) is a lower, at this higher temperature the molecules will have spread part a little due to them having increased kinetic energy therefore finding a C2 atom in a 2,4,6-TNEB molecule ~ 6 Å from a C1 atom in a 2,4-DNEB molecule is less probable. Further peaks are not apparent enough to indicate a second coordination shell showing long-range order is not present in the NC and K10 binder system.

The RDF was calculated between the C2 atoms in the NG-N1 molecules and the C1 atoms in the 2,4-DNEB molecules in the NC, 2,4-DNEB and NG-N1 binder (Figure 19). The C2 atom was chosen in NG-N1 to try and obtain the most central part of the molecule. The RDFs for the NC, 2,4-DNEB and NG-N1 binder systems at 298 K, 348 K and 398 K are displayed in Graphs 10, 11 and 12 respectively.

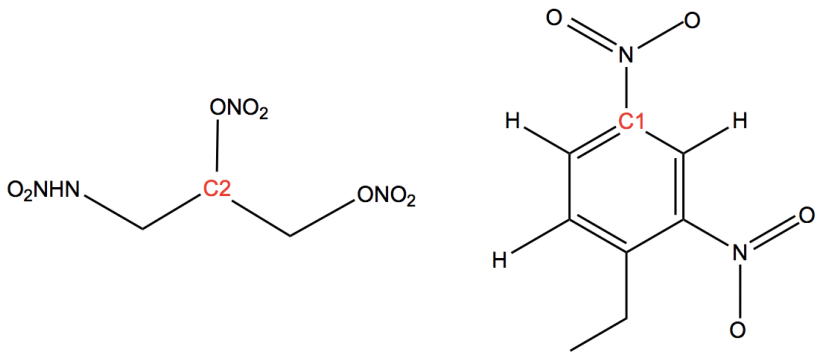

Figure 19 Diagram of NG-N1 molecule with the C2 atom highlighted in red and 2,4-DNEB molecule with the C1 atom highlighted in red.

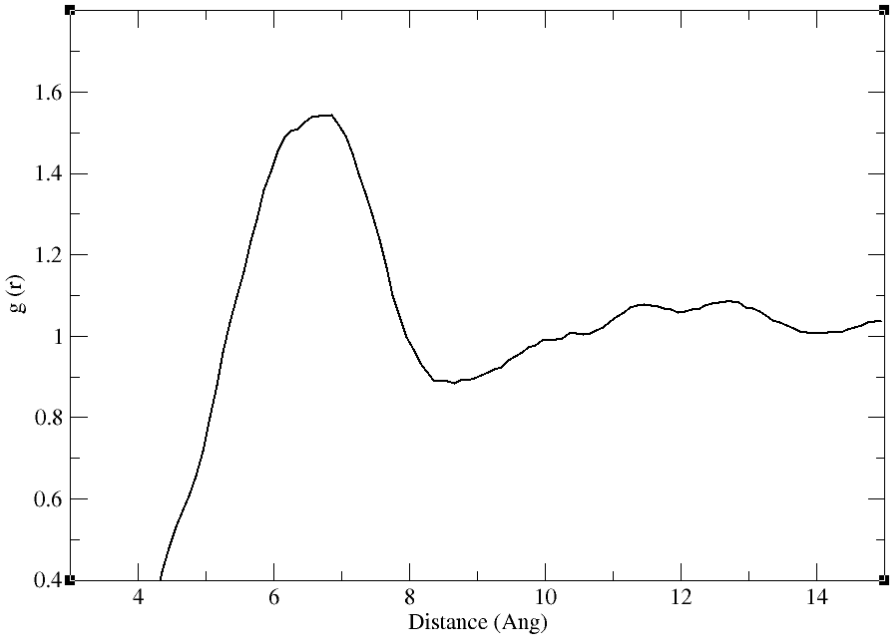

Graph 10 The RDF between the C2 atom in NG-N1 and C1 atom in 2,4-DNEB in the NC, 2,4-DNEB and NG-N1 binder at 298 K.

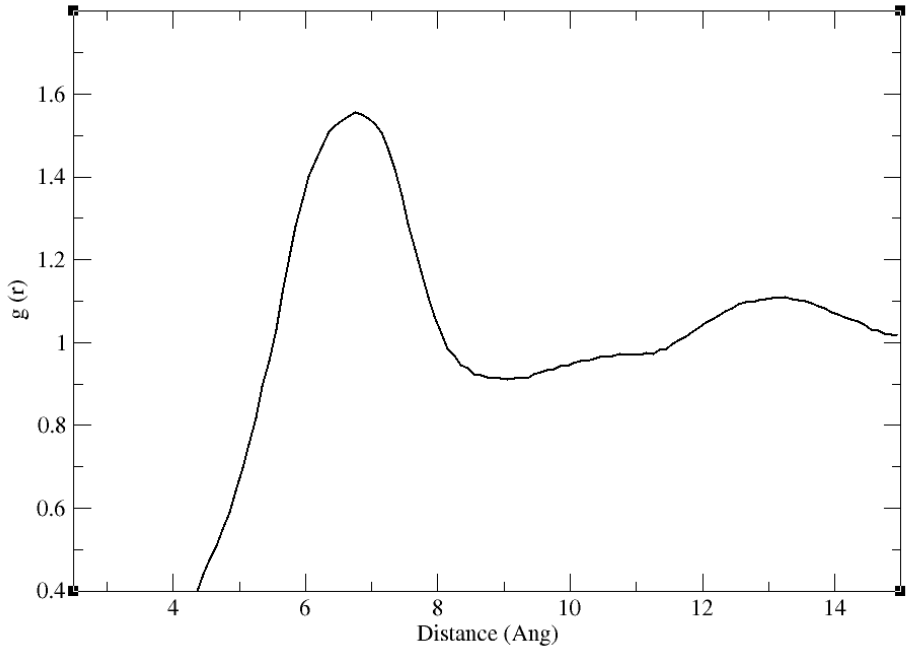

Graph 11 The RDF between the C2 atom in NG-N1 and C1 atom in 2,4-DNEB in the NC, 2,4-DNEB and NG-N1 binder at 348 K.

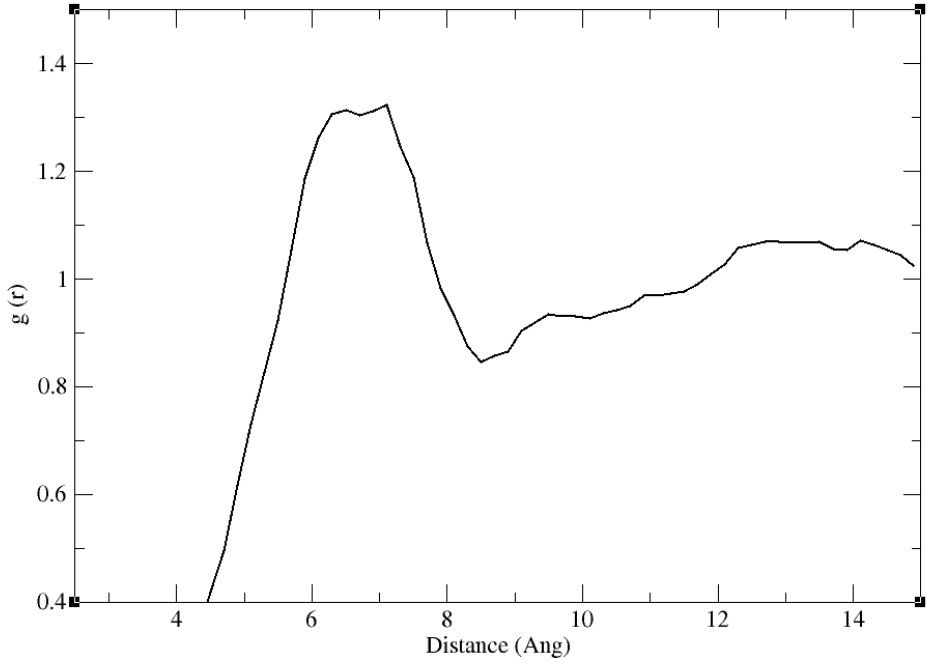

Graph 12 The RDF between the C2 atom in NG-N1 and C1 atom in 2,4-DNEB in the NC, 2,4-DNEB and NG-N1 binder at 398 K.

The RDFs at 298 K and 348 K contain peaks at ~6.5 Å with g (r) values just under 1.6. These peaks show a first coordination shell where it is likely a C2 atom in NG-N1 is a distance of 6.5 Å away from a C1 atom in 2,4-DNEB. At 398 K the RDF contains a peak at ~6.5 Å which has a lower g (r) value than the peaks at ~6.5 Å in the RDFs at 298 K and 348 K. At a higher temperature it is less likely a C2 atom in NG-N1 is a distance of 6.5 Å away from a C1 atom in 2,4-DNEB because the molecules have spread apart slightly. The energetic outputs of the NC and K10 binder and the NC, 2,4-DNEB and NG-N1 binder were investigated experimentally.[3] The experimental binders were formulated by addition of NC in solution to plasticiser in a 1:8 ratio and were reported as having a gel like consistency.[3] In the RDFs for both of the NC binder systems the coordination shell nearest to the reference particle is visible, however at distances

greater than at ~6 - 6.5 Å coordination shells are not apparent indicating no long range order is present. The RDFs are consistent with the order of a gelatinous mixture, where long-range order and tightly packed molecules would not be expected. In contrast, in a densely packed solid the RDF would display clear peaks indicating additional coordination shells which would be further from the reference particle than the first and second coordination shells.[100]

4.3 Conclusion

The migration of the energetic plasticisers 1-nitramino-2,3-dinitroxypropane (NG-N1), 2,4-dinitroethylbenzene (2,4-DNEB) and 2,4,6-trinitroethylbenzene (2,4,6-TNEB) from two nitrocellulose (NC) binder mixtures was assessed by calculation of diffusion coefficients and activation energies of diffusion from molecular dynamics simulations. In order to calculate the diffusion coefficients from the mean squared displacements, molecular dynamics simulations were performed on a NC binder plasticised with K10 (2,4-DNEB and 2,4,6-TNEB) and a NC binder plasticised with 2,4-DNEB and NG-N1 at five different temperatures. The Arrhenius relationship was used to calculate activation energies of diffusion.

The diffusion coefficients for NG-N1 are lower than those of 2,4-DNEB at the corresponding temperatures, indicating that NG-N1 will migrate at a slower rate than 2,4-DNEB when a mixture of these two molecules is used as a plasticiser in a NC binder with an 89% NC:11% plasticiser composition. The lower migration rate is further confirmed by the activation energies of diffusion, the activation energy of diffusion calculated for NG-N1 is 2.6 kJ mol^{-1} higher than that of 2,4-DNEB. These results suggest that a greater proportion of NG-N1 versus 2,4-DNEB would be favourable when formulating a NC binder of this composition as plasticiser migration is likely to be reduced which should increase the ballistic shelf-life of the overall energetic material. Experimental data available for the migration of nitroglycerine, a molecule with a molecular mass close to that of NG-N1 from a NC propellant compares positively with the simulated diffusion coefficient for NG-N1 at 398 K. The diffusion coefficient of NG-N1 (2.48×10^{-7} cm^2 s^{-1}) calculated from simulation of the NC, 2,4-DNEB and NG-N1 binder at 398 K is the same order of magnitude as 1.09×10^{-7} cm^2 s^{-1} the experimental value obtained for nitroglycerine at ~ 398 K. The diffusion coefficient of NG-N1 is greater than that of

nitroglycerine, however the NC, 2,4-DNEB and NG-N1 binder contained more than twice as much plasticiser and less NC than the NC and nitroglycerine propellant investigated experimentally. Greater mobility of plasticiser molecules due to less NC immobilising the plasticiser molecules resulted in larger diffusion coefficients for NG-N1 in the simulated NC binder. The diffusion coefficients obtained for 2,4-DNEB and 2,4,6-TNEB in the simulated NC and K10 binder were compared to a diffusion coefficient for K10 in in a poly(GLYN) binder obtained from experiment. The diffusion coefficient for K10 at 398 K in the simulated NC and K10 binder was the same order of magnitude as that of K10 in the experimental poly(GLYN) binder at ~398 K. The simulated diffusion coefficient for K10 was slightly higher than the diffusion coefficient for K10 in the poly(GLYN) binder but was reasonable considering the simulated density of the NC and K10 binder was lower and contained a greater proportion of plasticiser compared to NC. The diffusion coefficients for NC in of the both binder systems are as predicted considering the diffusion rates of the plasticiser molecules. In both of the binder mixtures the NC has a lower diffusion rate than the plasticiser molecules, this is due to the NC polymer chain having a much greater molecular mass than NG-N1, 2,4-DNEB and 2,4,6-TNEB. Radial distribution functions of both binder systems were consistent with the gelatinous consistency of the mixtures. The first coordination shell was visible in the RDFs for both NC binder systems, but there was no indication of long-range ordering of the plasticiser molecules.

5. The Interaction of Water and Nitrogen Dioxide in the two Nitrocellulose Binder Systems

Nitrocellulose decomposes over time via a complex degradation process.[28] The NO_2 is considered to be the most detrimental decomposition product due to its involvement in a series of complex reactions leading to autocatalysis.[29] In order to investigate how an increase in the amount of NO_2 produced during degradation affects the diffusion rate of NO_2 in the NC binder systems the diffusion coefficients for different concentrations of NO_2 in the NC, 2,4-DNEB and NG-N1 binder and the NC and K10 binder have been calculated at 298 K, 323K, and 348 K. The detection of NO_2 during nitrocellulose aging has been widely studied experimentally[34,57] however, quantifying the exact amount of NO_2 given off during the degradation process is difficult. Here the concentrations of NO_2 were approximated by using the number of nitrate ester bonds that could break in a fully nitrated nitrocellulose dimer to liberate NO_2.

NC degradation can result in self-ignition.[23–25] Water is added to NC as a wetting agent during storage and transportation as the possibility of explosion or fire is greatly increased when the NC is dry.[24,25] After the wetting agent has been removed some residual water is often left in the NC or whilst NC based propellants or PBXs are in storage, water from the atmosphere may also be absorbed by the formulation.[117,139] The NO_2 produced in the NC degradation process may react with any residual water to produce nitric acid which is thought to contribute to further NC degradation.[22,28] The interaction of water within the NC binder systems is of interest, especially if different plasticiser mixtures either facilitate or inhibit diffusion. The temperature inside containers of wetted NC reached 338 K in a recent NC-related explosion,[25] the behaviour of water in the plasticisers was therefore investigated at this critical temperature compared to

room temperature by calculation of diffusion coefficients at 298 K and 338 K. Diffusion coefficients were also calculated for water in the two NC binder systems at 298 K, 323 K, 338 K and 348 K. Finally, the NC, 2,4-DNEB and NG-N1 binder and the NC and K10 binder were simulated with the addition of both NO_2 (40%) and water. The 96 NO_2 molecules (40% concentration) were positioned around the NC polymer chain in each NC binder system with water, the most likely initial position of the NO_2 molecules when they are produced by O-NO_2 bond scission in the NC. Radial distribution functions were used to observe the interactions between the NO_2 molecules and the NC polymer chain in each NC binder system. Diffusion coefficients were also calculated for water and NO_2 in these NC binder systems at 298 K, 323 K, 338 K and 348 K.

5.1 Interaction of Water and Nitrogen Dioxide Methodology

5.1.1 Construction of NC Binder Systems with different Concentrations of Nitrogen Dioxide

The unit cell dimensions and number of molecules used for the NC binder simulation cells with NO_2 were the same as those used in the simulations of the nitrocellulose binders in the Parameterisation and Migration Chapters. As the exact amount of NO_2 produced during the degradation process is difficult to quantify exactly, the concentrations of NO_2 were approximated based on the maximum number of O-NO_2 bonds that could break and liberate a NO_2 molecule in a fully nitrated NC dimer. The total number of O-NO_2 bonds that can break in a fully nitrated NC dimer is 6, theoretically producing 6 NO_2 molecules. The NC, 2,4-DNEB and NG-N1 binder and NC and K10 binder each contain 40 fully nitrated NC dimers. If all of the O-NO_2 bonds were broken in the NC in each of the NC binder system 240 NO_2 molecules would be liberated in each NC binder system. Therefore, 240 NO_2 molecules were considered a 100% concentration in the NC binder systems and the other percentage concentrations were calculated from this. The program Packmol was used to construct the simulation cells with a tolerance of 2 Å.[125] The number of molecules of NO_2 added to each of the NC binder simulation cells is outlined in Table 16.

Table 16 The Concentrations (%) and Number of NO_2 molecules added to each of the NC Binder Simulation Cells. (The total number of NO_2 molecules for the 100% concentration was calculated from the maximum number of O-NO_2 bonds that could break a fully nitrated NC dimer.)

Concentration of NO_2 (%)	Theoretical number of NO_2 molecules liberated and added to each NC binder simulation cell
100	240
75	180
40	96
15	36
5	12

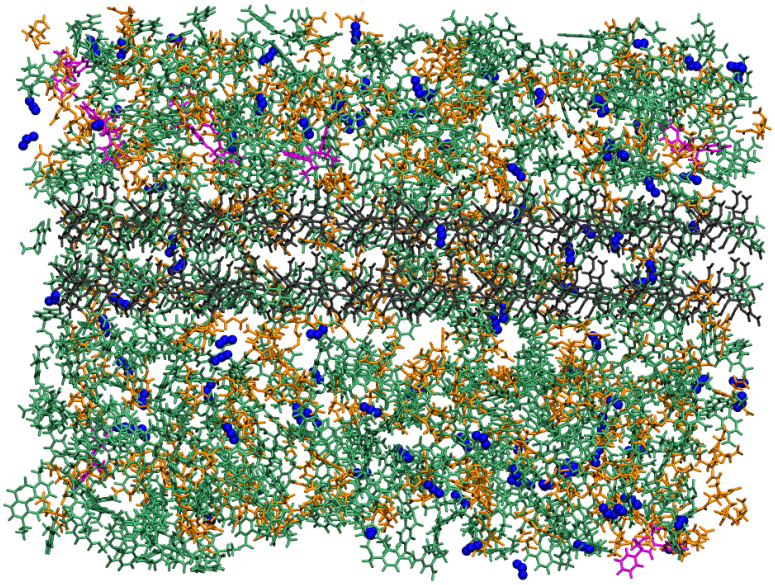

Figure 20 The simulation cell containing the NC, 2,4-DNEB, NG-N1 and EC binder system mixed with 40% (96) NO_2 molecules. The NC is displayed in grey, the 2,4-DNEB molecules in green, the NG-N1 molecules in orange, the EC molecules in pink and the NO_2 molecules in blue.

5.1.2 Construction of Plasticiser Systems and NC Binder Systems with Water

The unit cell dimensions and number of molecules used for the simulation of the plasticisers 2,4-DNEB, 2,4,6-TNEB, NG-N1, K10 and R8002 with water were the same as those used in the simulations of the plasticisers in the Parameterisation Chapter. The residual water in nitrocellulose in plasticised energetic material formulations may be as much as 5% by mass.[117] Each simulation box contained ~5% water by mass, 155 water molecules were added to the 2,4,6-TNEB, 2,4-DNEB, R8002 and K10 boxes and 190 water molecules were added to the NG-N1 box. An additional simulation cell containing 33% NG-N1 and 67% 2,4-DNEB was constructed with ~5% water by mass to enable comparison between water diffusion in this plasticiser mixture and water diffusion in the NC binder plasticised with this mixture. A 40 Å × 40 Å × 40 Å simulation cell was constructed with 208 2,4-DNEB molecules, 90 NG-N1 molecules and 170 water molecules. In all plasticiser and water simulation cells the water molecules were spread throughout the plasticiser. The dimensions of the two NC binder simulation cells and the number of molecules added were the same as those used in the simulations in the Parameterisation and Migration Chapters. The NC binder system consisting of NC, 2,4-DNEB and NG-N1 and the NC and K10 binder system each contained 600 water molecules, ~5% by mass which were distributed throughout the mixtures. Packmol was used to construct all simulation boxes with a tolerance of 2 Å and the extended single point charge (SPC/E) model was used to describe the water molecules in all simulations.[125,140] The construction of all simulation cells with water is outlined in Appendix 8 (p.217).

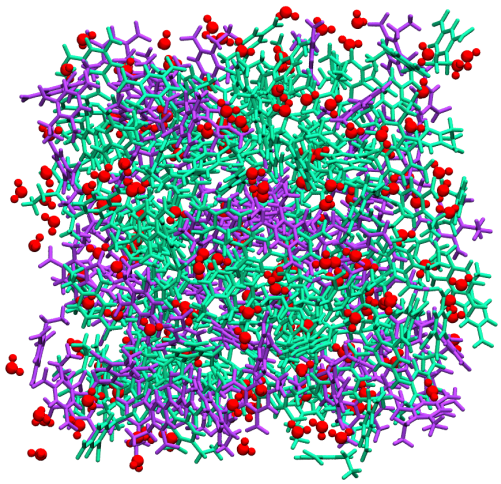

Figure 21 The K10 and water simulation cell with the 2,4,6-TNEB molecules displayed in purple, the 2,4-DNEB molecules displayed in green and the water molecules displayed in red.

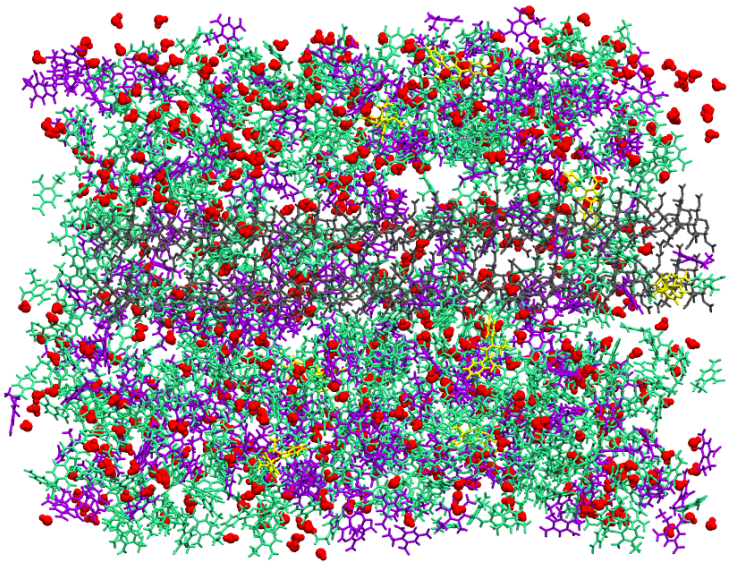

Figure 22 The simulation cell containing the NC, K10 and EC binder system mixed with water. The NC is displayed in grey, the 2,4-DNEB molecules in green, the 2,4,6-TNEB molecules in purple, the EC molecules in yellow and the water molecules in red.

5.1.3 Construction of NC Binder Systems with Nitrogen Dioxide and Water

The same number of molecules and the same dimensions used for the NC binder systems containing ~ 5% water, outlined in 5.1.2 were used here. In addition to water, 96 NO_2 molecules (40% NO_2) were added to the NC, 2,4-DNEB, NG-N1 and water binder system and the NC, K10 and water binder system. Packmol was used to construct the simulation cells with a tolerance of 2 Å, the 96 NO_2 molecules were positioned around the NC polymer chain in each NC binder system with water.[125] The water molecules were distributed throughout both of the binder systems.

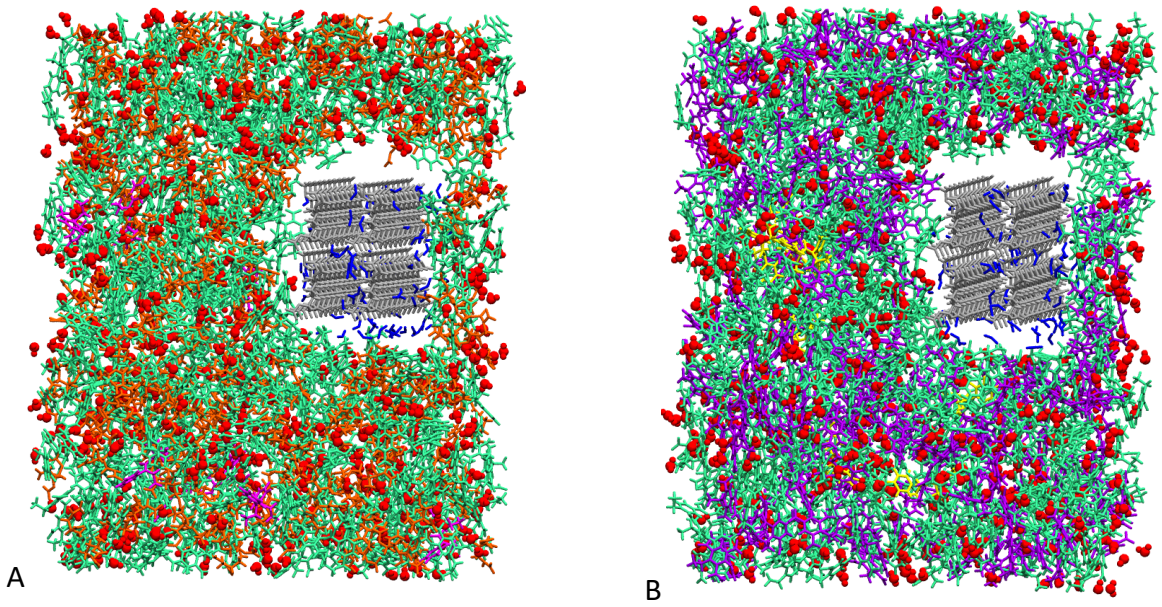

Figure 23 The NC binder simulation cells containing water and NO_2 viewed from the side to show the NO_2 molecules displayed in blue positioned around the NC polymer chains in grey. A. The NC, 2,4-DNEB and NG-N1 binder system with the 2,4-DNEB molecules displayed in green, the NG-N1 molecules in orange, the EC molecules in pink and the water molecules in red. B. The NC and K10 binder system with the 2,4-DNEB molecules displayed in green, the 2,4,6-TNEB molecules in purple, the EC molecules in yellow and the water molecules in red.

5.1.4 Molecular Dynamics Simulations

All molecular dynamics simulations were performed using the Sander module of Amber 14. A non-bonded cut-off of 8 Å was used for the LJ interactions and the Particle Mesh Ewald (PME) was used for the treatment of the long-range electrostatics. Periodic Boundary Conditions were employed to model the infinite systems. The steepest descents method followed by a larger number of cycles of the conjugate gradient method were used for minimisation. Minimisation was deemed complete once the Cartesian element of the gradient was 1.0×10^{-4} kcal^{-1} mol^{-1} Å^{-1} or less. A 0.001 ps time step was used and the Velocity Verlet algorithm integrated the equations of motion.[87] Bonds to hydrogen were constrained using the SHAKE algorithm.[91]

Firstly, each system was heated to the required temperature and then a 30 ps NVT equilibration, followed by a 400 ps NPT equilibration was performed. Production runs of 25 ns were performed on the NC, 2,4-DNEB, NG-N1 and NO_2 binder system and the NC, K10 and NO_2 binder system under vacuum at 298 K, 323 K and 348 K, respectively. Production runs of 18 ns were performed on the NG-N1 and 2,4-DNEB mixture and the 2,4-DNEB, 2,4,6-TNEB, NG-N1, K10 and R8002 plasticiser systems with water under vacuum at 298 K and 338 K, respectively. The NC, 2,4-DNEB, NG-N1, and water system and the NC, K10, and water system both underwent 25 ns production runs under vacuum at 298 K, 323 K, 338 K and 348 K. Lastly, production runs of 25 ns at 298 K, 323 K, 338 K and 348 K under vacuum were performed on the two NC binder systems containing both 40% NO_2 and ~5% water. Anderson temperature-coupling maintained constant temperature during equilibration at constant volume (NVT).[89] The Berendsen barostat maintained constant pressure in the NPT simulations.[88] Due to the possibility of unreliable diffusion coefficients being calculated with Langevin dynamics or the

Anderson Thermostat, the thermostat was switched to the Berendsen scheme for production runs.[88,129]

5.1.5 Calculation of Diffusion Coefficients

The production simulations were used to obtain the mean square displacements (MSD) of the NO_2 and/or water molecules in each system. The slope of the MSD versus time for the NO_2 and water molecules was calculated in $Å^2$/ps and the diffusion coefficients were calculated using equation 1.

$$6D = \lim_{t \to \infty} \frac{MSD}{t} \tag{1}$$

The cpptraj module of Amber 14 was used to obtain the MSDs which were averaged over all molecules in each of the systems.[96]

5.1.6 Radial Distribution Functions

The probability (g) r of finding a particle at a distance r from another particle in a system can be found by calculating the radial distribution function (RDF). RDFs were calculated between the NC and NO_2 molecules for the both NC binder systems containing 40 % NO_2 and water prior to simulation, at 298 K and 348 K using the cpptraj module of Amber 14.[96]

5.2 Interaction of Water and Nitrogen Dioxide Results

The diffusion coefficients for different concentrations of NO_2 at 298 K, 323 K and 348 K in the NC binder plasticised with K10 are displayed in Table 17 and Graph 13. The diffusion coefficients for different concentrations of NO_2 at 298 K, 323 K and 348 K in the NC binder plasticised with NG-N1 and 2,4-DNEB are presented in Table 18 and Graph 14. Table 19 and Graph 15 display the diffusion coefficients for water in the different plasticisers at 298 K and 338 K. The diffusion coefficients for water in the NC binders with water and no NO_2 at 298 K, 323 K, 338 K and 348 K are displayed in Table 20 and Graph 16. The diffusion coefficients for water and 40 % NO_2 in the NC binders with water and 40 % NO_2 at 298 K, 323 K, 338 K and 348 K are presented in Table 21. Graph 17 displays the diffusion coefficients for water in the NC binders with water and 40 % NO_2 and Graph 18 displays the diffusion coefficients for 40 % NO_2 in the NC binders with water and 40 % NO_2. For all diffusion coefficients, displayed in Tables 17-21 the standard deviation of the gradient of the MSD versus time graphs was used to calculate the standard errors. Graphs 19, 20 and 21 display the RDFs between the C2 atoms in the NC and the NO_2 molecules in the NC, 2,4-DNEB, NG-N1, 40% NO_2 and water binder system prior to simulation, at 298 K and 348 K, respectively. The RDFs between the C2 atoms in the NC and the NO_2 molecules in the NC, K10, 40% NO_2 and water binder system prior to simulation, at 298 K and 348 K are presented in Graphs 22, 23 and 24, respectively.

5.2.1 The Diffusion of different Concentrations of NO_2 in the NC Binder Systems

Table 17 The Diffusion Coefficients (cm^{-2} s^{-1}) for 5%, 15%, 40%, 75% and 100% NO_2 in the NC Binder plasticised with K10 at 298 K, 323 K and 348 K.

	Diffusion Coefficients (cm^2 s^{-1}) for NO_2 in the NC Binder plasticised with 2,4-DNEB and 2,4,6-TNEB (K10)					
	298 K		323 K		348 K	
NO_2 (%)	D 10^7 cm^2 s^{-1}	Std. Err cm^2 s^{-1}	D 10^7 cm^2 s^{-1}	Std. Err cm^2 s^{-1}	D 10^7 cm^2 s^{-1}	Std. Err cm^2 s^{-1}
5	1.57	2.3×10^{-09}	1.28	7.2×10^{-09}	11.21	2.9×10^{-08}
15	1.12	4.9×10^{-09}	4.09	4.6×10^{-09}	14.69	1.8×10^{-08}
40	2.27	1.9×10^{-09}	8.71	2.3×10^{-09}	24.47	1.2×10^{-08}
75	3.39	4.1×10^{-09}	9.03	2.7×10^{-09}	29.57	2.2×10^{-08}
100	4.17	1.5×10^{-09}	15.63	3.7×10^{-09}	37.25	1.6×10^{-08}

Table 18 The Diffusion Coefficients (cm^{-2} s^{-1}) for 5%, 15%, 40%, 75% and 100% NO_2 in the NC Binder plasticised with NG-N1 and 2,4-DNEB at 298 K, 323 K and 348 K.

	Diffusion Coefficients (cm^2 s^{-1}) for NO_2 in the NC Binder plasticised with 2,4-DNEB and NG-N1					
	298 K		323 K		348 K	
NO_2 (%)	D 10^7 cm^2 s^{-1}	Std. Err cm^2 s^{-1}	D 10^7 cm^2 s^{-1}	Std. Err cm^2 s^{-1}	D 10^7 cm^2 s^{-1}	Std. Err cm^2 s^{-1}
5	0.05	7.1×10^{-08}	0.36	4.7×10^{-09}	0.94	3.4×10^{-09}
15	0.02	2.5×10^{-10}	0.62	3.0×10^{-09}	3.13	6.5×10^{-09}
40	0.94	1.8×10^{-09}	0.86	1.5×10^{-09}	4.82	1.5×10^{-09}
75	1.64	1.9×10^{-09}	2.32	1.2×10^{-09}	10.02	1.3×10^{-09}
100	2.18	3.6×10^{-09}	3.72	2.9×10^{-09}	10.84	1.5×10^{-09}

Calculation of diffusion coefficients displayed in Appendix 9 (p.218-219).

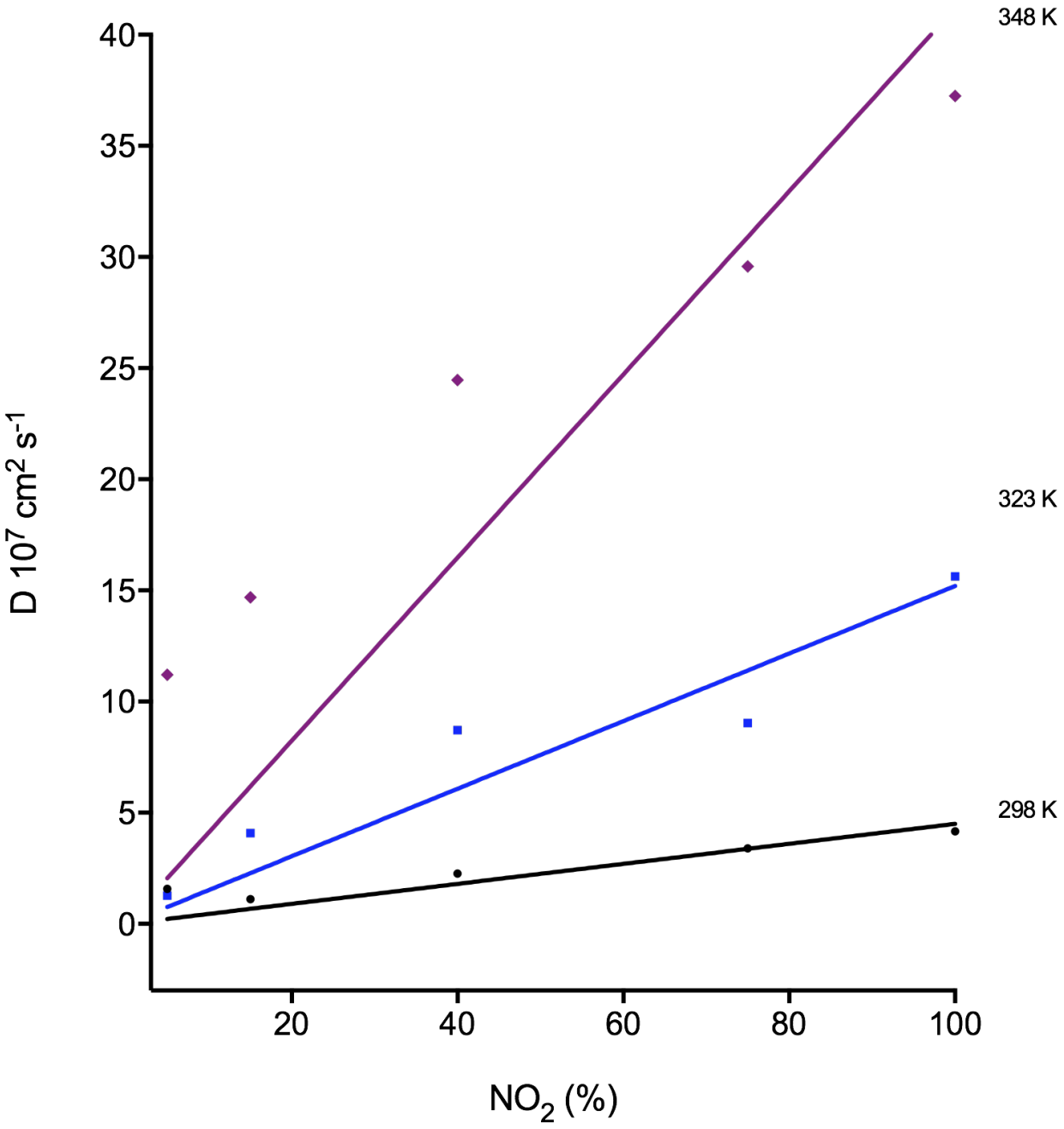

Graph 13 The diffusion coefficients (cm^{-2} s^{-1}) for 5%, 15%, 40%, 75% and 100% NO_2 in the NC binder plasticised with K10 at 298 K, 323 K and 348 K.

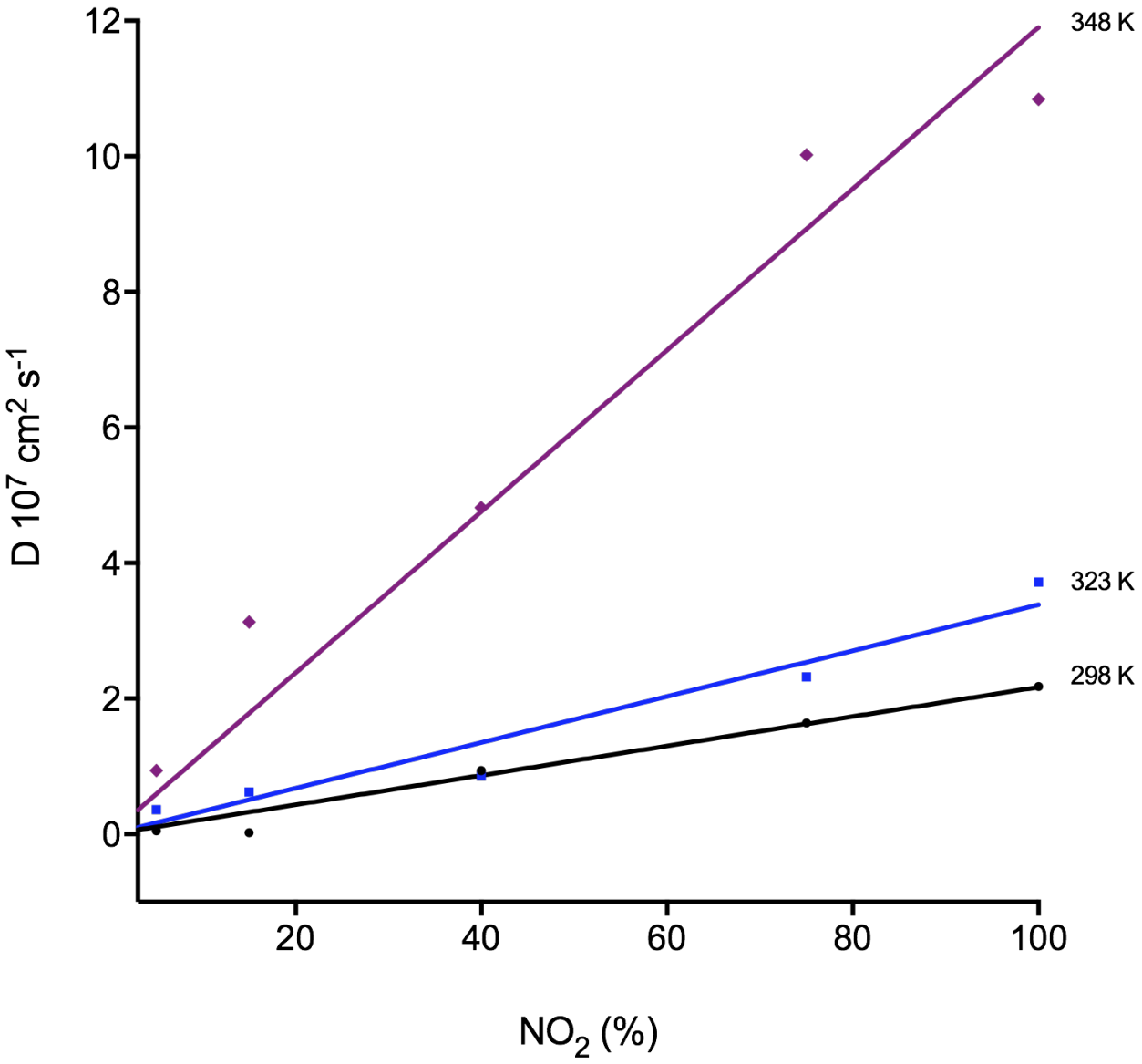

Graph 14 The diffusion coefficients (cm^{-2} s^{-1}) for 5%, 15%, 40%, 75% and 100% in the NC binder plasticised with NG-N1 and 2,4-DNEB at 298 K, 323 K and 348 K.

The diffusion coefficients for the different concentrations of NO_2 in the NC and K10 binder (Table 17, Graph 13) are greater than those obtained for the different concentrations of NO_2 in the NC, 2,4-DNEB and NG-N1 binder (Table 18, Graph 14). This is foreseeable considering the

lower simulated density of the NC and K10 binder, where the NO_2 molecules will be able to move more freely compared to the NC, 2,4-DNEB and NG-N1 binder. As predicted the values of D for all concentrations of NO_2 in both binder systems increase as temperature increases due to the increased kinetic energy of the molecules. Crank explained that concentration dependent diffusion exists in most systems, but in dilute solutions for example the dependence is small and for practical purposes the diffusion coefficient can be considered constant.[141] However, the literature reports a relationship between concentration and diffusion coefficient in the diffusion of vapours in high-polymer substances.[141–143] The relationship between concentration and diffusion coefficient is complex. A number of methods have been used to reach numerical solutions with some relevant to any type of concentration-dependent diffusion and some relevant to linear dependence.[141] After observation of the results a linear relationship has been assumed between NO_2 concentration and diffusion coefficient in both NC binder systems. In both of the NC binder systems the diffusion coefficients for NO_2 increase as concentration increases. In the NC and K10 binder the relationship between the concentration of NO_2 and diffusion coefficient at 298 K displays good linearity, however the linearity is poorer at 323 K and 348 K (Graph 13). Good linearity at all temperatures is shown between the concentration of NO_2 and diffusion coefficient in the NC, 2,4-DNEB and NG-N1 binder (Graph 14). According to Fick's first law of diffusion if the concentration changes steeply with position, then diffusion will be fast.[73] In both NC binder systems as the concentration of NO_2 increased the rate of diffusion increased. This can be explained in terms of the NO_2 concentration gradients, where the NC binder systems with a greater number of NO_2 molecules would have steeper concentration gradients compared to the systems with less NO_2 and steeper concentration gradients would result in faster rates of diffusion of NO_2 molecules.

5.2.2 The Diffusion of Water in the Plasticisers

Table 19 The Diffusion Coefficients (cm^{-2} s^{-1}) for H_2O in the Plasticisers at 298 K and 338 K.

	Diffusion Coefficients (cm^2 s^{-1}) for H_2O in the different Plasticisers			
	298 K		338 K	
Plasticiser	D 10^7 cm^2 s^{-1}	Std. Err cm^2 s^{-1}	D 10^7 cm^2 s^{-1}	Std. Err cm^2 s^{-1}
2,4-DNEB	44.13	2.6×10^{-8}	82.60	2.2×10^{-8}
2,4,6-TNEB	8.56	4.1×10^{-9}	10.34	1.4×10^{-8}
K10 (65 % 2,4-DNEB & 35 % 2,4,6-TNEB)	21.75	9.8×10^{-9}	37.02	1.3×10^{-8}
R8002 (50 % 2,4-DNEB & 50 % 2,4,6-TNEB)	20.52	1.1×10^{-8}	55.20	5.5×10^{-8}
NG-N1	0.02	1.7×10^{-11}	0.16	7.8×10^{-11}
67 % 2,4-DNEB and 33 % NG-N1	4.05	3.7×10^{-9}	18.5	1.4×10^{-8}

Calculation of diffusion coefficients displayed in Appendix 9 (p.220)

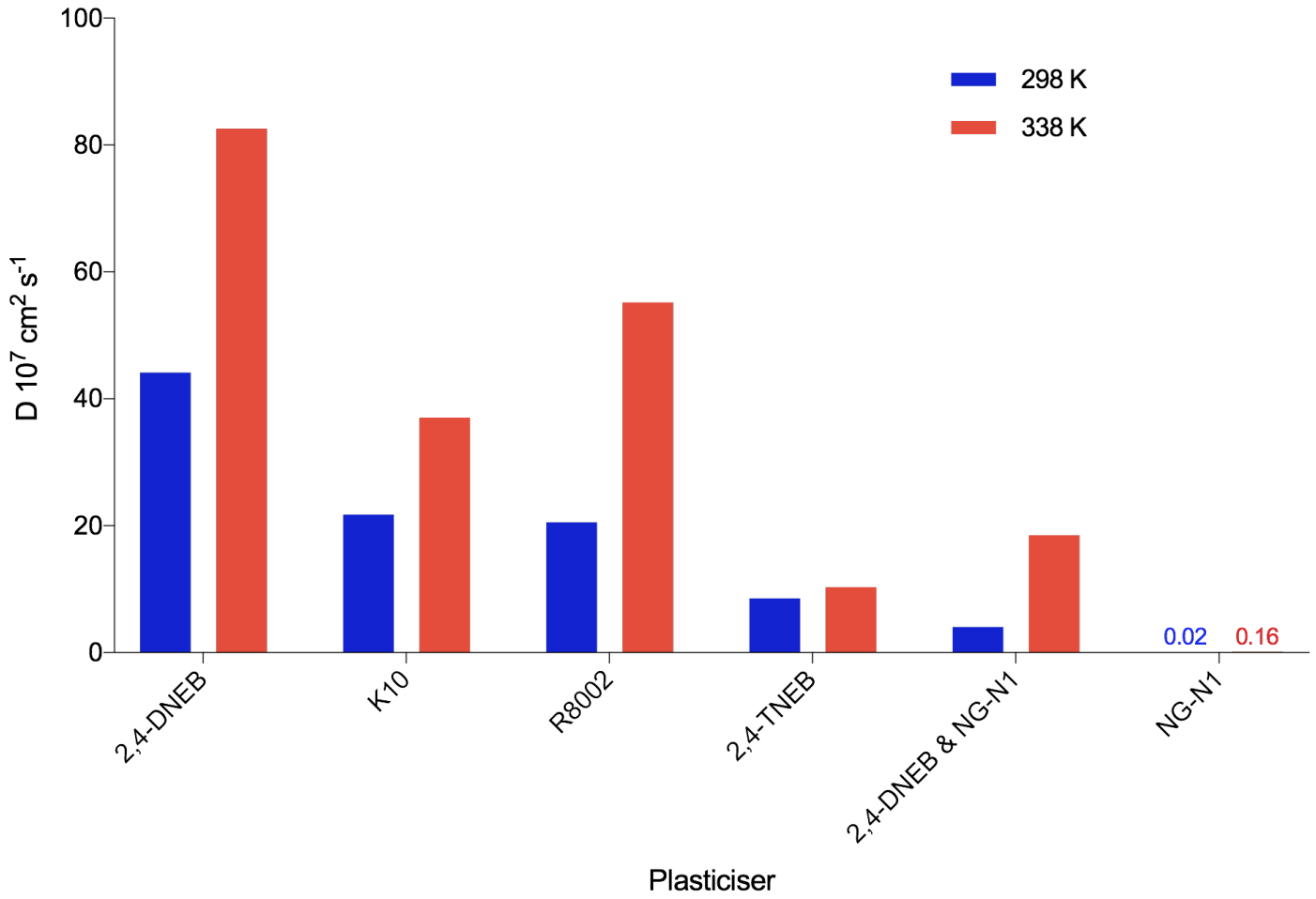

Graph 15 Bar chart displaying the diffusion coefficients for water ($cm^2\ s^{-1}$) in the different plasticisers at 298 K and 338 K.

The diffusion coefficients for water in the plasticisers are displayed in Table 19 and Graph 15. The simulated densities of the plasticisers obtained from the parameterisation simulations at 298 K were 1.30 g cm^{-3} for 2,4-DNEB, 1.34 g cm^{-3} for K10, 1.36 g cm^{-3} for R8002, 1.52 g cm^{-3} for 2,4,6-TNEB, 1.49 g cm^{-3} for the 2,4-DNEB and NG-N1 mixture and 1.80 g cm^{-3} for NG-N1. Greater diffusion coefficients for water in the plasticisers with lower densities would be predicted, due to more space between molecules allowing the water molecules to move more freely. Lower diffusion coefficients would be predicted for water in the plasticisers with a higher density due to the tightly packed molecules imposing some restriction on the movement of the water. The diffusion coefficient for water of 44 10^7 cm^2 s^{-1} in 2,4-DNEB at 298 K is the highest compared to the values obtained for the other plasticisers at this temperature which is expected considering it has the lowest simulated density. The diffusion coefficients for water in K10 of 22 10^7 cm^2 s^{-1} and for water in R8002 of 21 10^7 cm^2 s^{-1} at 298 K are lower than that of water in 2,4-DNEB which is correct as the densities of these mixtures are both higher than 2,4-DNEB. The difference between the D value for water in 2,4-DNEB and the D values for water in K10 and R8002 is quite large considering the difference in simulated densities is 0.04 g cm^{-3} between 2,4-DNEB and K10 and 0.06 g cm^{-3} between 2,4-DNEB and R8002, although the sensitivity of diffusion coefficients to small changes in density has been mentioned in the literature.[144] The diffusion coefficient of water in 2,4,6-TNEB is smaller than those obtained for water in 2,4-DNEB, K10 and R8002 as the simulated density of 2,4,6-TNEB is higher than these plasticisers. The diffusion coefficient for water in 2,4,6-TNEB is also greater than that of water in NG-N1 as 2,4,6-TNEB has a lower simulated density compared to this plasticiser. The diffusion coefficient for water in NG-N1 is very low, however it has a simulated density which is quite a bit higher than the densities of the other plasticisers. The diffusion coefficient for water in the NG-N1 and

2,4-DNEB mixture may be too low, the value is lower than the D values for water in 2,4-DNEB, K10 and R8002 as expected due to the greater simulated density compared to these plasticisers. However, it is lower than the diffusion coefficient for water in 2,4,6-TNEB which is not expected as 2,4,6-TNEB has a greater simulated density compared to the NG-N1 and 2,4-DNEB mixture. As predicted due to an increase in kinetic energy at 338 K there is an increase in the diffusion coefficients for water at 338 K in each plasticiser compared to the values obtained for water in the same plasticiser at 298 K. Some of the trends at 338 K are the same as at 298 K, for example the diffusion coefficient of 83 10^7 cm^2 s^{-1} for water in 2,4-DNEB is again the highest compared to the values obtained for the other plasticisers at this temperature. The diffusion coefficient for water in R8002 of 55 10^7 cm^2 s^{-1} and in K10 of 37 at 338 K is unusual, R8002 has a larger simulated density compared to K10 which would make water diffusion in R8002 slower than in K10. The same unexpected behaviour is observed in the diffusion coefficients of water in R8002 and K10 at 298 K, however at 298 K the difference in values was very small whereas at 338 K it is more pronounced. The diffusion coefficients for water in the other plasticisers follow the trends expected considering their simulated densities. The diffusion coefficient for water in NG-N1 is the lowest compared to the values obtained for the other plasticisers which given that NG-N1 has the largest simulated density of all the plasticisers is correct. The plasticiser 2,4,6-TNEB has a simulated density of 1.52 g cm^{-3} which is greater than the simulated densities of 2,4-DNEB, K10 and R8002 and the diffusion coefficient for water in 2,4,6-TNEB is therefore lower than those calculated for 2,4-DNEB, K10 and R8002 as predicted. The diffusion coefficient for water in the NG-N1 and 2,4-DNEB mixture of 18.5 10^7 cm^2 s^{-1} is smaller than the values obtained for 2,4-DNEB, K10 and R8002 which is foreseeable seeing as the NG-N1 and 2,4-DNEB mixture has a greater simulated density than 2,4-DNEB, K10 and R8002. Finally, the

diffusion of water in the NG-N1 and 2,4-DNEB mixture is faster than in 2,4,6-TNEB and NG-N1 as predicted due to the simulated density of the NG-N1 and 2,4-DNEB mixture of 1.49 g cm^{-3} is being lower than 1.52 g cm^{-3} and 1.80 g cm^{-3} the simulated densities of 2,4,6-TNEB and NG-N1, respectively.

5.2.3 Diffusion of Water the NC Binder Systems

Table 20 The Diffusion Coefficients (cm^{-2} s^{-1}) for H_2O in the NC and K10 Binder and NC, 2,4-DNEB and NG-N1 Binder at 298 K, 323 K, 338 K and 348 K.

	Diffusion Coefficients (cm^2 s^{-1}) and their associated errors (cm^2 s^{-1}) for H_2O in the NC and K10 binder and the NC, 2,4-DNEB and NG-N1 binder							
	298 K		323 K		338 K		348 K	
	D 10^7	Std. Err	D 10^7	Std. Err	D 10^7	Std. Err	D 10^7	Std. Err
NC, 2,4-DNEB & NG-N1	2.35	1.3×10^{-9}	7.34	3.8×10^{-9}	5.73	4.1×10^{-9}	17.00	1.6×10^{-8}
NC & K10	8.38	9.5×10^{-9}	10.10	8.2×10^{-9}	12.19	9.9×10^{-9}	22.82	2.1×10^{-8}

Calculation of diffusion coefficients displayed in Appendix 9 (p.221)

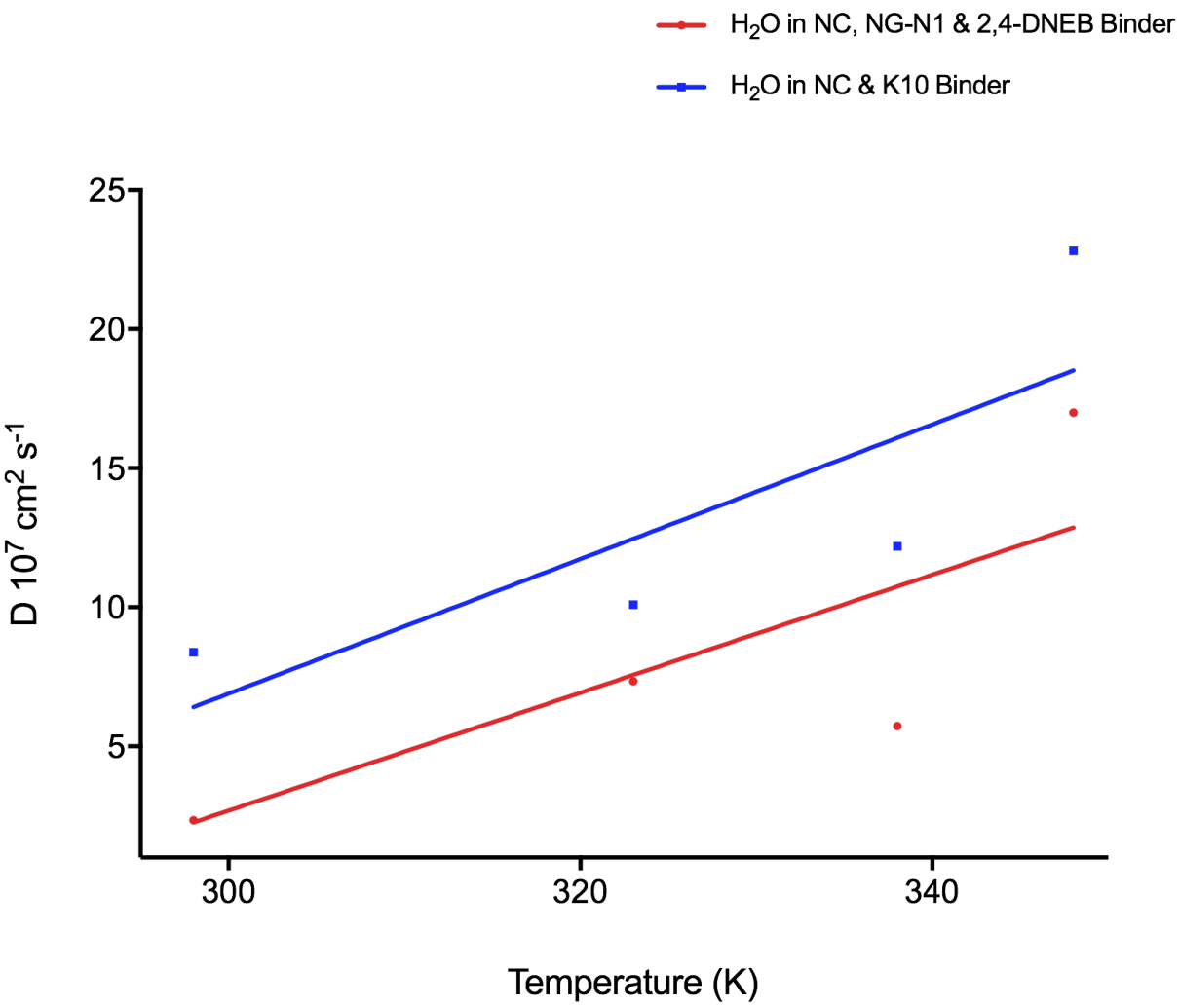

Graph 16 The diffusion coefficients for water ($cm^2\ s^{-1}$) in the NC binder systems.

The diffusion coefficients for water in the NC and K10 binder system are greater than those obtained for water in the NC, 2,4-DNEB and NG-N1 binder system, this would be predicted as the lower simulated density of the NC and K10 binder resulted in the molecules moving more freely in this system (Table 20, Graph 16). Graph 16 shows that in both NC binder systems there is a general trend of increasing water diffusion rate with increasing temperature. This is as expected owing to the molecules increased kinetic energy, however the value of D for water at 338 K of 5.73 10^7 $cm^2\ s^{-1}$ appears to have been underestimated and the value of D for water at

338 K of 12.19 10^7 cm^2 s^{-1} in the NC and K10 binder has been slightly underestimated. The diffusion coefficients for water are higher than those calculated in the Migration Chapter at the corresponding temperatures for the plasticiser molecules in the NC, 2,4-DNEB and NG-N1 binder system. The rate of diffusion is inversely proportional to molecular mass,[130] water has a molecular mass of 18 u which is much smaller than 226 u the molecular mass of NG-N1 and 196 u the molecular mass of 2,4-DNEB, explaining why water diffuses at a faster rate than these molecules. The same trend applies in the NC and K10 binder, where the diffusion coefficients for water in the system are greater at the corresponding temperatures than the higher molecular mass 2,4-DNEB and 2,4,6-TNEB plasticiser molecules. The diffusion coefficient for water at 298 K in the NC, 2,4-DNEB and NG-N1 binder is 2.35 10^7 cm^2 s^{-1}, in the 2,4-DNEB and NG-N1 plasticiser mixture at 298 K the D value for water is 4.05 10^7 cm^2 s^{-1}. The diffusion coefficient for water at 338 K in the NC, 2,4-DNEB and NG-N1 binder is 5.73 10^7 cm^2 s^{-1} whereas in the 2,4-DNEB and NG-N1 plasticiser mixture it is 18.5 10^7 cm^2 s^{-1} at 338 K. These results show that at both temperatures water diffusion is slower in the NC binder plasticised with 2,4-DNEB and NG-N1 compared to the 2,4-DNEB and NG-N1 plasticiser mixture alone with no NC present. The D value for water at 338 K in the NC, 2,4-DNEB and NG-N1 binder is likely to have been underestimated, however the diffusion coefficient for water of 18.5 10^7 cm^2 s^{-1} at 338 K in the 2,4-DNEB and NG-N1 plasticiser mixture is still greater than 17.00 10^7 cm^2 s^{-1}, the D value for water at 348 K in the NC, 2,4-DNEB and NG-N1 binder. The same trend can be observed in water diffusion in the NC and K10 binder and K10 plasticiser mixture alone, the diffusion coefficients for water in the NC and K10 binder are 8.38 10^7 cm^2 s^{-1} at 298 K and 12.19 10^7 cm^2 s^{-1} at 338 K compared to 21.75 10^7 cm^2 s^{-1} at 298 K and 37.02 10^7 cm^2 s^{-1} at 338 K in the K10 plasticiser mixture with no NC. The effect of the NC to plasticiser ratio on the mobility of

molecules in NC binders and propellants has been discussed in the literature. Molecules in highly plasticised NC propellants and binders are more mobile, and the addition of greater quantities of NC has the effect of immobilising molecules.[17,55] A possible explanation is that the presence of NC in both of the binder mixtures resulted in reduced water diffusion due to decreased mobility of molecules compared to the plasticiser mixtures minus the NC.

5.2.4 Diffusion in the NC Binder Systems containing both Water and 40% Nitrogen Dioxide

Table 21 The Diffusion Coefficients (cm^{-2} s^{-1}) for H_2O and 40 % NO_2 in the NC and K10 Binder and the NC, 2,4-DNEB and NG-N1 Binder at 298 K, 323 K, 338 K and 348 K.

	Diffusion Coefficients (cm^2 s^{-1}) for H_2O and NO_2 and their associated errors (cm^2 s^{-1}) in the NC and K10 binder and the NC, 2,4-DNEB and NG-N1 binder							
	NC binder plasticised with K10				NC binder plasticised with 2,4-DNEB and NG-N1			
Temperature (K)	NO_2 D 10^7	NO_2 Std. Err	H_2O D 10^7	H_2O Std. Err	NO_2 D 10^7	NO_2 Std. Err	H_2O D 10^7	H_2O Std. Err
298	2.78	2.8×10^{-9}	3.92	4.8×10^{-9}	1.26	1.5×10^{-9}	3.10	1.9×10^{-9}
323	10.58	2.6×10^{-9}	7.50	1.3×10^{-8}	1.64	1.4×10^{-9}	3.90	1.6×10^{-9}
338	19.48	1.1×10^{-9}	18.60	1.2×10^{-8}	3.49	1.2×10^{-9}	7.80	3.2×10^{-9}
348	34.47	1.4×10^{-8}	29.40	3.9×10^{-8}	10.45	3.6×10^{-9}	8.10	9.8×10^{-9}

Calculation of diffusion coefficients displayed in Appendix 9 (p.222-223)

As in the NC binder systems containing water and no NO_2 in the NC binder systems containing both water and NO_2, water diffused at a faster rate in the binder plasticised with K10 compared to the binder plasticised with 2,4-DNEB and NG-N1 due to the NC and K10 binder having a lower simulated density (Table 21, Graph 17). In the NC, K10, 40% NO_2 and water system the diffusion coefficient for water of 7.50 10^7 cm^2 s^{-1} at 323 K may have been underestimated compared to the other values for water in this binder and compared to 10.10 10^7 cm^2 s^{-1}, the diffusion coefficient for water at 323 K in the NC and K10 binder with water only. In the NC,

2,4-DNEB, NG-N1 40% NO_2 and water binder the diffusion coefficient for water of 8.10 10^7

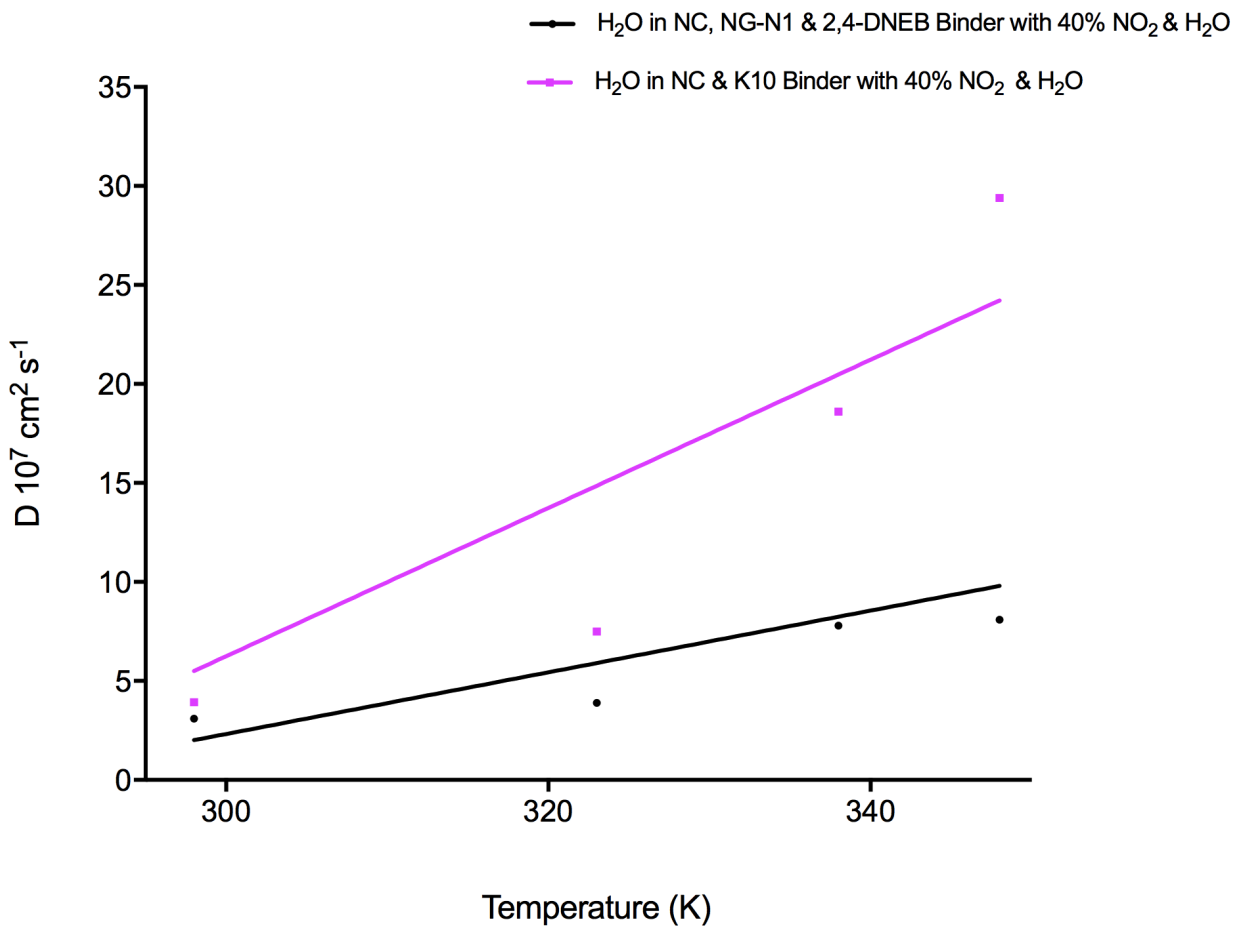

Graph 17 The diffusion coefficients for water (cm^2 s^{-1}) in the NC binder systems containing 40% NO_2 and H_2O.

cm^2 s^{-1} at 348 K could have been underestimated considering the value for water in this binder system containing water only and no NO_2 is 17.00 10^7 cm^2 s^{-1}. There is general trend of increasing rate of water diffusion with temperature in both NC binder systems containing water and NO_2 due to the increased kinetic energy of the molecules. Similarly, in these NC binder systems as those containing water and no NO_2, water diffusion is slower at 298 K and 338 K where NC is present compared to the constituent plasticiser mixtures alone with no NC. The

diffusion coefficients for water in K10 only at 298 K and 338 K are both higher than for water at 298 K and 338 K in the NC, K10, 40% NO_2 and water binder system. The same is true of the NG-N1 and 2,4-DNEB plasticiser mixture where the diffusion coefficients for water are higher than those at the corresponding temperatures in the NC, 2,4-DNEB, NG-N1, 40% NO_2 and water binder system. There are no experimental diffusion coefficients available for water in either of the NC binder systems simulated in this research. There are diffusion coefficients for water in NC films obtained via experiment. The experimental diffusion coefficient for water in NC at 25 °C determined by Hsieh was 2.62×10^{-9} cm^2 s^{-1} and the value determined by Lewis at 25 °C was 1.8×10^{-9} cm^2 s^{-1}.[61,62] The experimental diffusion coefficients for water in NC are much lower than the values obtained in this research. The diffusion coefficients for water in the NC, K10 and water binder and the NC, K10, 40% NO_2 and water binder at ~25°C are 8.38×10^{-7} cm^2 s^{-1} and 3.92×10^{-7} cm^2 s^{-1}, respectively. The diffusion coefficients for water in the NC, 2,4-DNEB, NG-N1 and water binder and the NC, 2,4-DNEB, NG-N1, 40% NO_2 and water binder at ~25 °C are 2.35×10^{-7} cm^2 s^{-1} and 3.10×10^{-7} cm^2 s^{-1}, respectively. The rate of water diffusion in the NC binder systems is much faster than in NC alone. It could be suggested that a comparison between the diffusion coefficients for water in the NC binders with those obtained in NC is not ideal as the NC binders only contain 11% NC. However, the results are useful in reinforcing the idea that in NC propellants and binders with much greater proportions of plasticiser compared to NC the mobility of molecules is much higher.[17,55] Research by Tompa into plasticiser migration in NC propellants suggested molecules can be trapped in a crosslinked polymer, this is much more likely to happen with water molecules in NC alone rather than in the NC binder systems with very little NC and high molecule mobility due to a high proportion of plasticiser.[53]

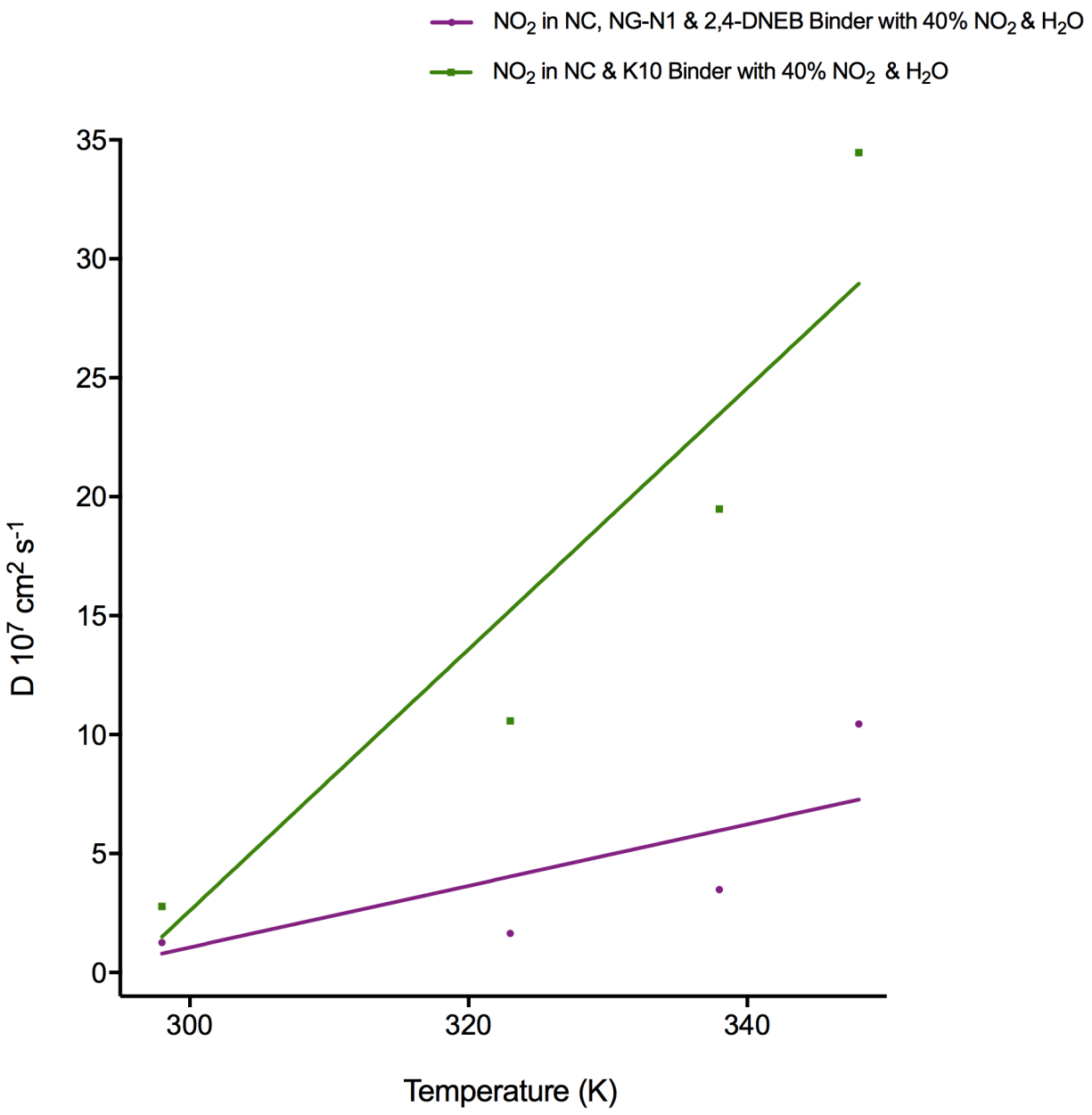

Graph 18 The diffusion coefficients for NO_2 (cm^2 s^{-1}) in the NC binder systems containing 40% NO_2 and H_2O.

The same trend of a higher rate of diffusion of molecules through the NC and K10 binder compared to the NC, 2,4-DNEB and NG-N1 binder applies to the diffusion of NO_2 in the NC

binders containing 40% NO_2 and water (Table 21, Graph 18). In both NC binder systems with 40% NO_2 and water some diffusion coefficients for NO_2 appear to be slightly underestimated whereas others appear to have been slightly overestimated. However, Graph 18 shows there is enough linearity between temperature and diffusion coefficient of NO_2 in both systems to conclude that the diffusion rate increases with temperature. Some of the diffusion coefficients are greater for NO_2 in the NC binder systems with both NO_2 and water than would be predicted. For example, the diffusion coefficients for NO_2 in the NC, K10, 40 % NO_2 and water system are 2.78 10^7 cm^2 s^{-1}, 10.58 10^7 cm^2 s^{-1} and 34.47 10^7 cm^2 s^{-1} at 298 K, 323 K and 348 K, respectively (Table 21). However, in the NC, K10 and 40 % NO_2 system with no water present the diffusion coefficient for NO_2 at 298 K is 2.27 10^7 cm^2 s^{-1} , at 323 K it is 8.71 10^7 cm^2 s^{-1} and at 348 K it is 24.47 10^7 cm^2 s^{-1} (Table 17). In the NC, 2,4-DNEB, NG-N1, 40% NO_2 and water system the diffusion coefficients for NO_2 are 1.26 10^7 cm^2 s^{-1}, 1.64 10^7 cm^2 s^{-1} , and 10.45 10^7 cm^2 s^{-1} at 298 K, 323 K and 348 K, respectively (Table 21) compared to 0.94 10^7 cm^2 s^{-1} , 0.86 10^7 cm^2 s^{-1}, and 4.82 10^7 cm^2 s^{-1} at the corresponding temperatures in the NC, 2,4-DNEB, NG-N1 and 40% NO_2 binder with no water present (Table 18). The diffusion coefficients for NO_2 in the the NC, K10, 40 % NO_2 and water system are greater at 298 K, 323 K and 348 K than those of water in this system at the same temperatures, the opposite would be expected considering diffusion coefficients are inversely proportional to molecular mass and NO_2 has a greater molecular mass than water.[130] The reason for the larger than expected diffusion coefficients for NO_2 in the NC binder systems with 40% NO_2 and water could be due to the arrangement of NO_2 molecules within these systems. In the NC binder systems with 40% NO_2 and water the NO_2 molecules are all arranged around the NC polymer chain (Figure 23), whereas those in the NC binders with 40% NO_2 and no water are distributed evenly thoroughout the binder system (Figure 20). The

water molecules in the NC, K10, 40 % NO_2 and water system (Figure 23B) are also distributed evenly in the binder system. Fick's first law of diffusion describes diffusion as fast if the concentration changes steeply with position.[73] The arrangement of all of the NO_2 molecules around the NC polymer chain in the NC binder systems with 40% NO_2 and water will result in a steeper NO_2 concentration gradient. The steeper NO_2 concentration gradient results in a faster rate of diffusion of NO_2 compared to the evenly spread NO_2 molecules in the NC binder systems containing 40% NO_2 and no water and the water molecules in the NC, K10, 40 % NO_2 and water system.

5.2.5 The Radial Distibution Functions between NC and NO_2 in the NC Binder Systems containing both Water and 40% Nitrogen Dioxide

RDFs were calculated between the C2 atoms in the NC polymer chain, as shown in Figure 24 and the centre of mass of the NO_2 molecules prior to simulation, at 298 K and at 348 K in the NC binder systems containing both water and 40% nitrogen dioxide.

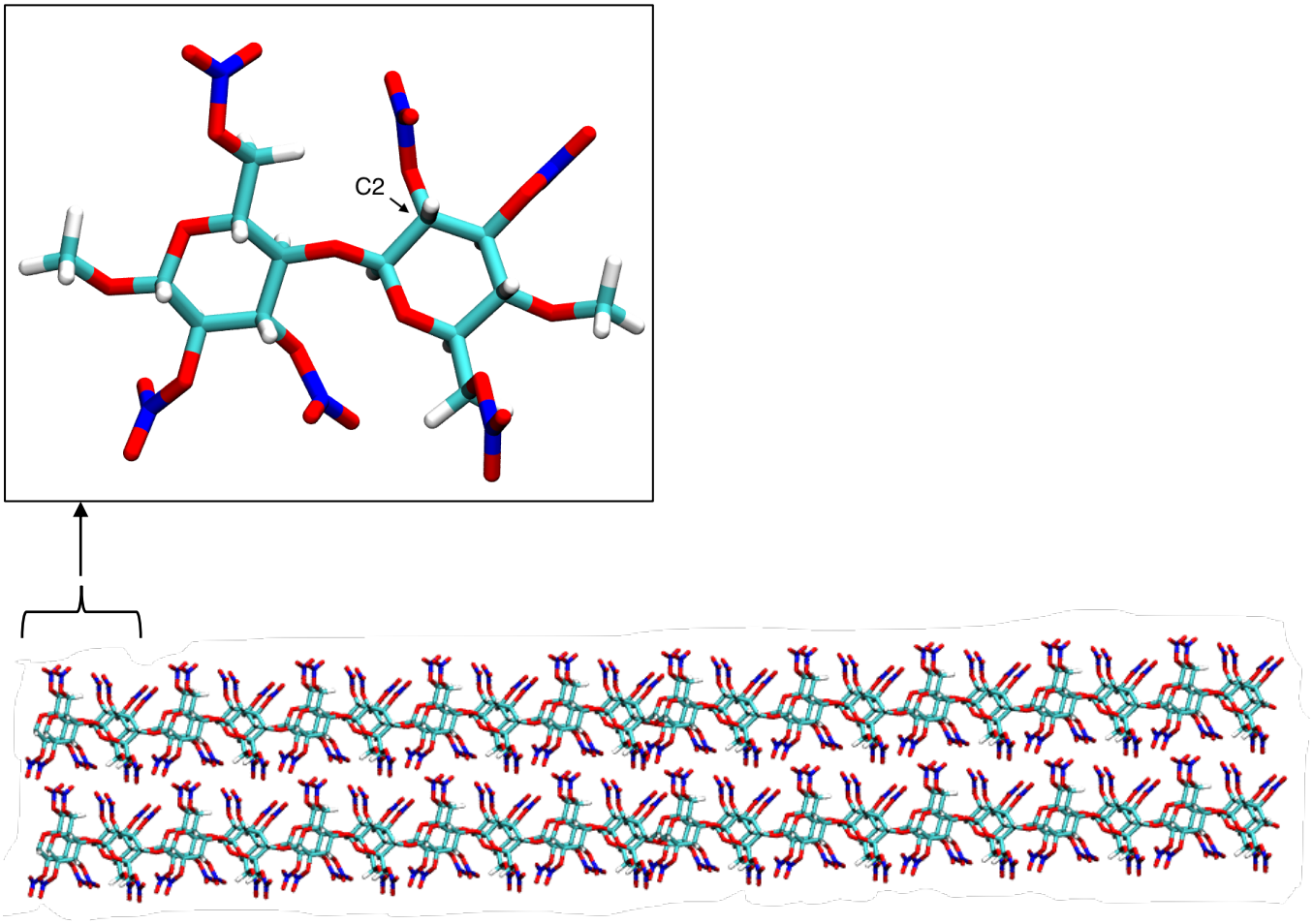

Figure 24 The nitrocellulose polymer within the binder systems with a C2 atom labelled within an enlarged nitrocellulose dimer.

The aim was to investigate how the NO_2 molecules produced during NC degradation would interact with the entire binder mixtures as temperature increased from 298 K to 348 K and to observe the difference between the NC and K10 binder and the NC, 2,4-DNEB and NG-N1 binder. Theoretically, the NO_2 molecules would initially be positioned around the NC chain when they are produced during NC degradation. RDFs were calculated prior to simulation for each NC binder to compare the distribution of NO_2 molecules at 298 K and at 348 K with their starting point.

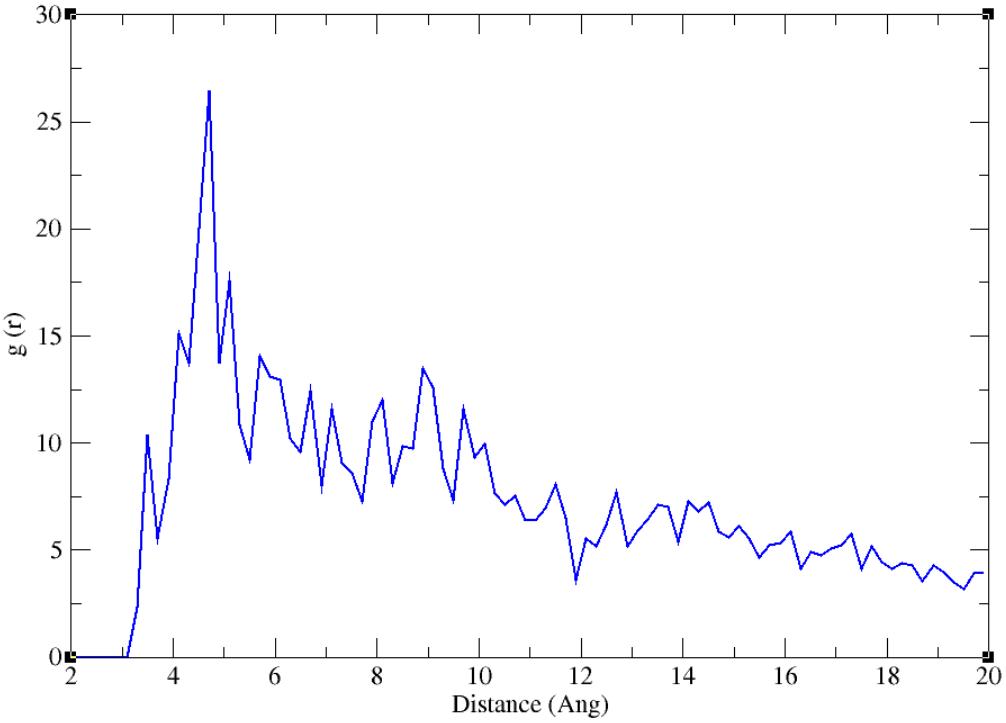

Graph 19 The radial distribution function prior to simulation between the C2 atoms in the NC and the NO_2 molecules in the NC, 2,4-DNEB, NG-N1, 40% NO_2 and water binder system.

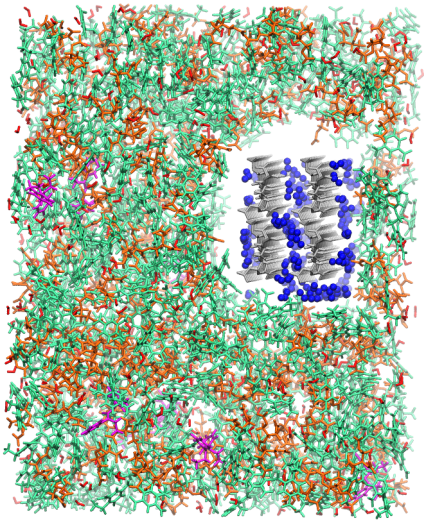

Figure 25 The NC, 2,4-DNEB, NG-N1, 40% NO_2 and water binder system pre equilibration. The 2,4-DNEB molecules are displayed in green, the NG-N1 molecules in orange, the EC molecules in pink, the water molecules in red, the NO_2 molecules in blue and the NC in grey.

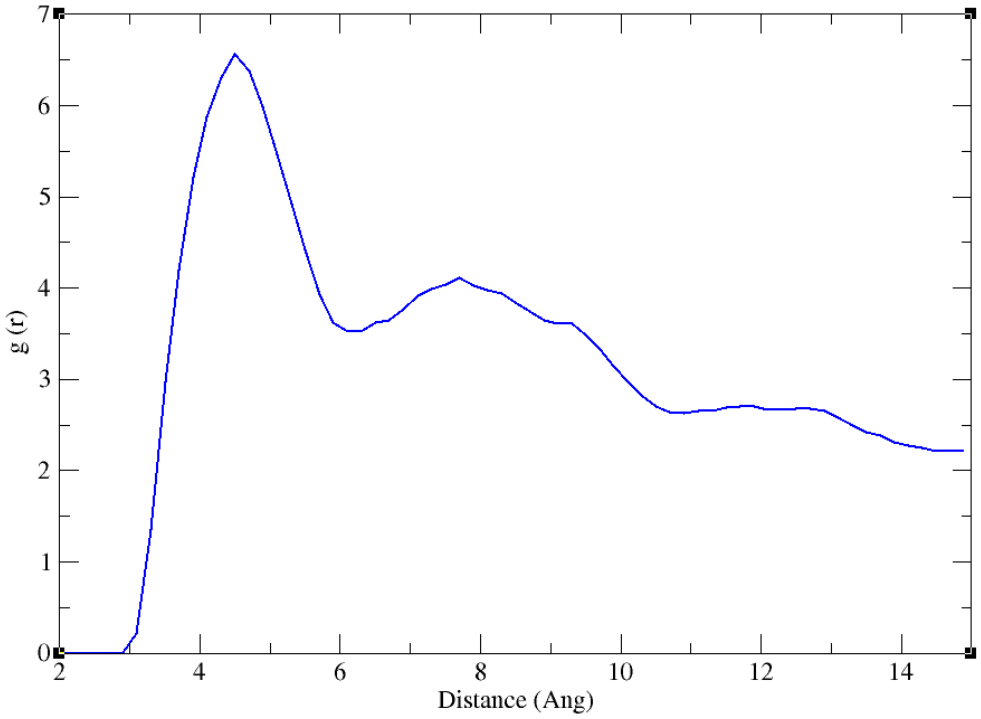

Graph 20 The radial distribution function at 298 K between the C2 atoms in the NC and the NO_2 molecules in the NC, 2,4-DNEB, NG-N1, 40% NO_2 and water binder system.

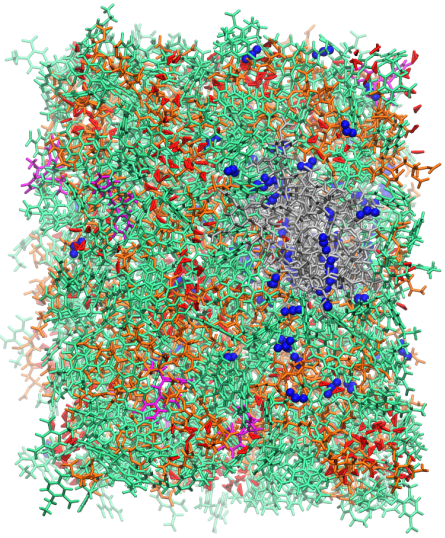

Figure 26 The NC, 2,4-DNEB, NG-N1, 40% NO_2 and water binder system at 298 K. The 2,4-DNEB molecules are displayed in green, the NG-N1 molecules in orange, the EC molecules in pink, the water molecules in red, the NO_2 molecules in blue and the NC in grey.

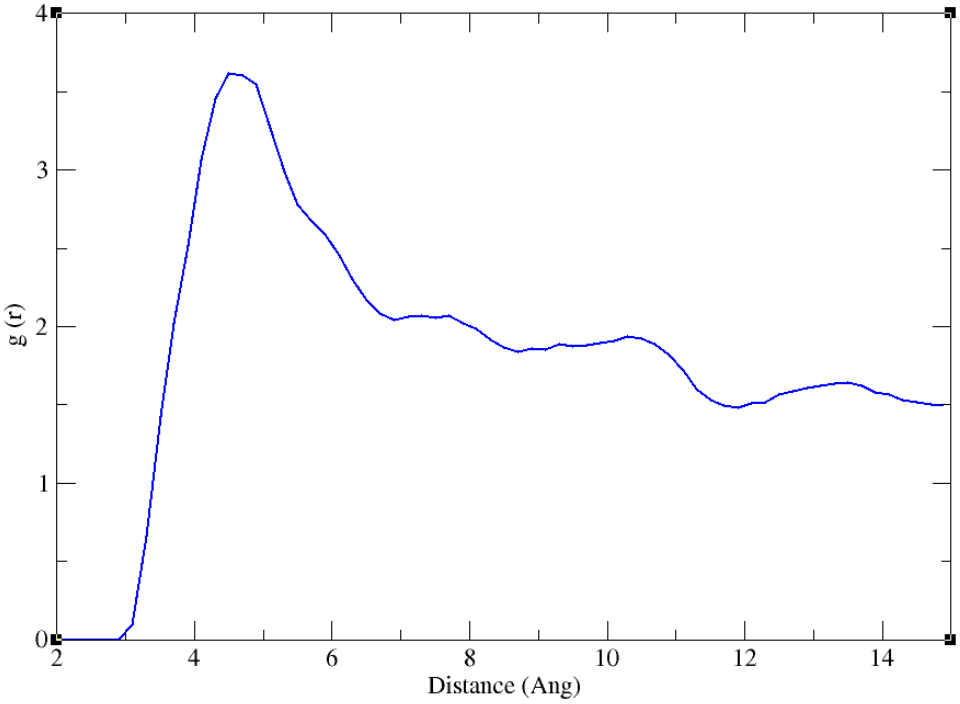

Graph 21 The radial distribution function at 348 K between the C2 atoms in the NC and the NO_2 molecules in the NC, 2,4-DNEB, NG-N1, 40% NO_2 and water binder system.

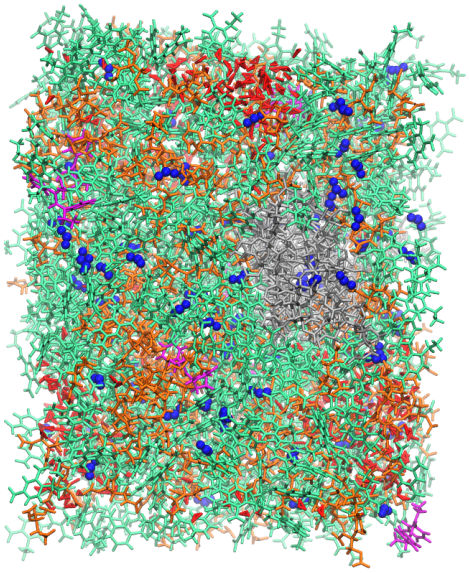

Figure 27 The NC, 2,4-DNEB, NG-N1, 40% NO_2 and water binder system at 348 K. The 2,4-DNEB molecules are displayed in green, the NG-N1 molecules in orange, the EC molecules in pink, the water molecules in red, the NO_2 molecules in blue and the NC in grey.

Graph 19 displays the RDF between the C2 atoms in the NC and the centre of mass of the NO_2 molecules in the NC, 2,4-DNEB, NG-N1, 40% NO_2 and water binder system prior to simulation where the NO_2 molecules have been intentionally placed around the NC polymer chain as shown in Figure 25. There is a very high probability of finding a NO_2 molecule 4.5 Å from a C2 atom in the NC, the peak indicating this has a g (r) value of approximately 27. As there are no peaks of less than 4.5 Å, it is unlikely many NO_2 molecules are closer to a C2 atom in the NC than 4.5 Å. There are also peaks at ~5.5 Å, ~6.5 Å, ~8 Å and ~ 9 Å with relatively high g (r) values of over 11, indicating that there are also NO_2 molecules at these distances away from a C2 atom in the NC. Graph 20 shows the RDF for the NC, 2,4-DNEB, NG-N1, 40% NO_2 and water binder system after simulation at 298 K. In Graph 20 there are far less peaks, but a prominent peak is still visible at 4.5 Å and a smaller peak is at ~7.5 Å. The g (r) value of 6.5 for the peak at 4.5 Å is much lower after simulation at 298 K than it was prior to simulation, therefore it is less likely a NO_2 molecule is this distance away from a C2 atom. As the simulation of the NC, 2,4-DNEB, NG-N1, 40% NO_2 and water binder system progressed at 298 K the NO_2 molecules have moved away from the NC polymer chain into the plasticiser mixture as shown in Figure 26 and indicated by the RDF. The radial distribution function at 348 K between the C2 atoms in the NC and the NO_2 molecules in the NC, 2,4-DNEB, NG-N1, 40% NO_2 and water binder system is displayed in Graph 21. In Graph 21 a peak is still visible at 4.5 Å, but it has a lower g (r) value of 3.5 after simulation at 348 K compared to the g (r) value of 6.5 after simulation at 298 K. It is now far less probable that a NO_2 molecule will be found 4.5 Å away from C2 atom in the NC polymer chain, a greater number of the NO_2 molecules have moved away from the NC into the plasticiser mixture which is also illustrated by Figure 27.

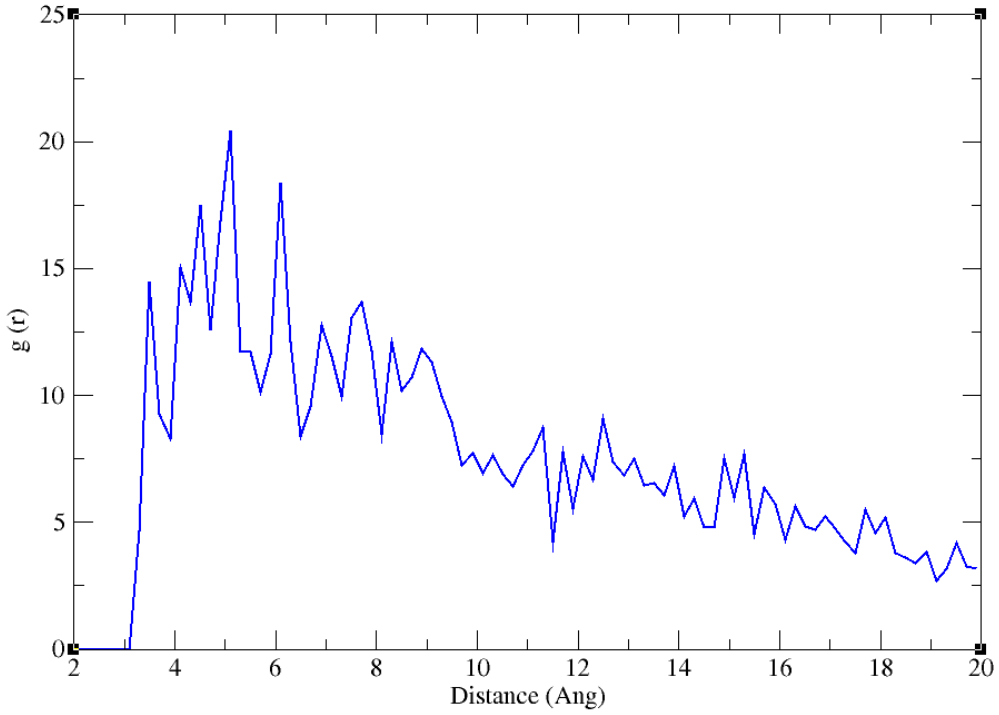

Graph 22 The radial distribution function prior to simulation between the C2 atoms in the NC and the NO_2 molecules in the NC, K10, 40% NO_2 and water binder system.

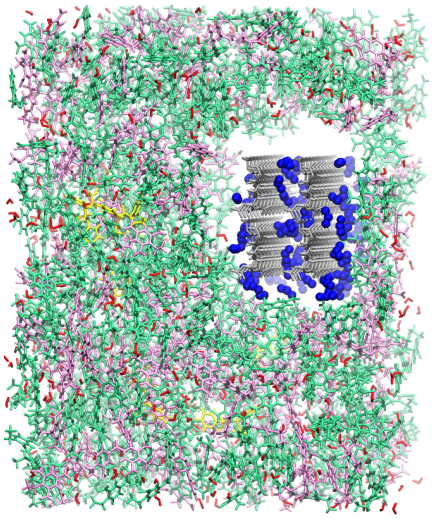

Figure 28 The NC, K10, 40% NO_2 and water binder system pre equilibration. The 2,4-DNEB molecules are displayed in green, the 2,4,6-TNEB molecules in pink, the EC molecules in yellow, the water molecules in red, the NO_2 molecules in blue and the NC in grey.

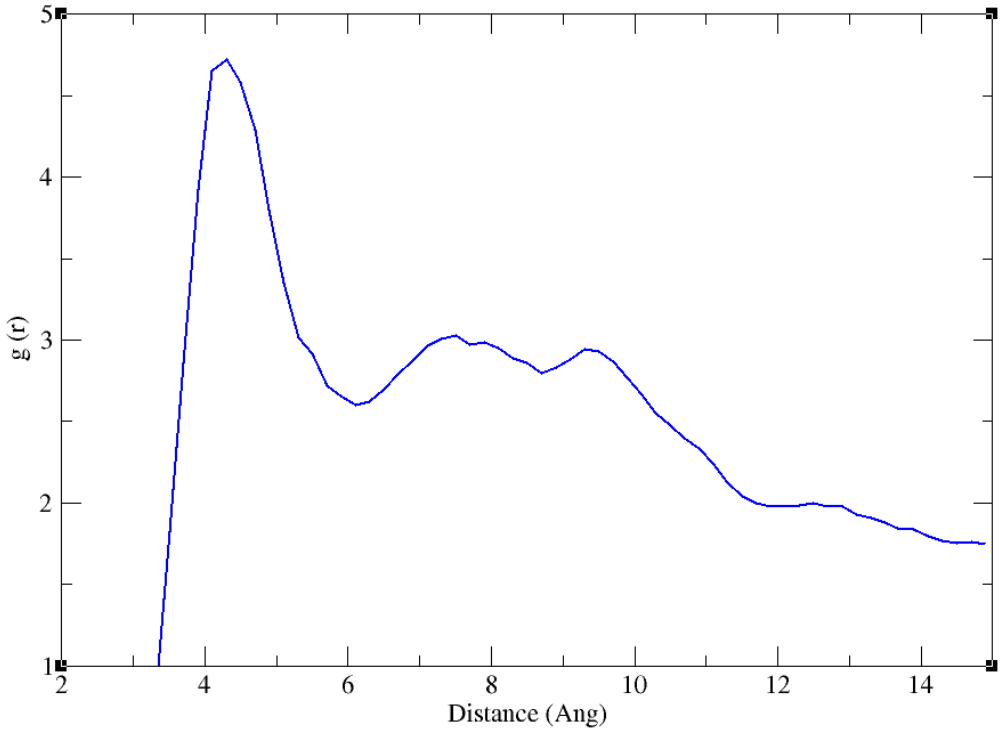

Graph 23 The radial distribution function at 298 K between the C2 atoms in the NC and the NO_2 molecules in the NC, K10, 40% NO_2 and water binder system.

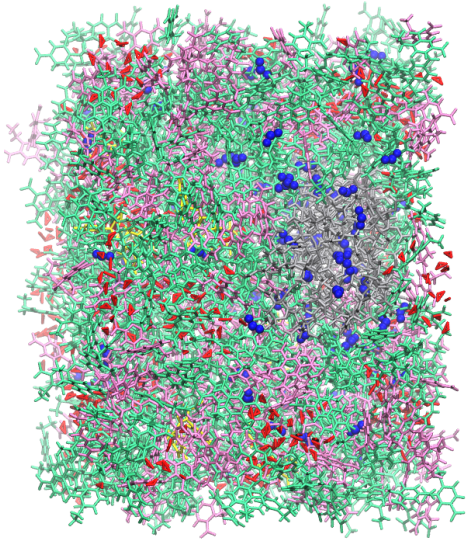

Figure 29 The NC, K10, 40% NO_2 and water binder system at 298 K. The 2,4-DNEB molecules are displayed in green, the 2,4,6-TNEB molecules in pink, the EC molecules in yellow, the water molecules in red, the NO_2 molecules in blue and the NC in grey.

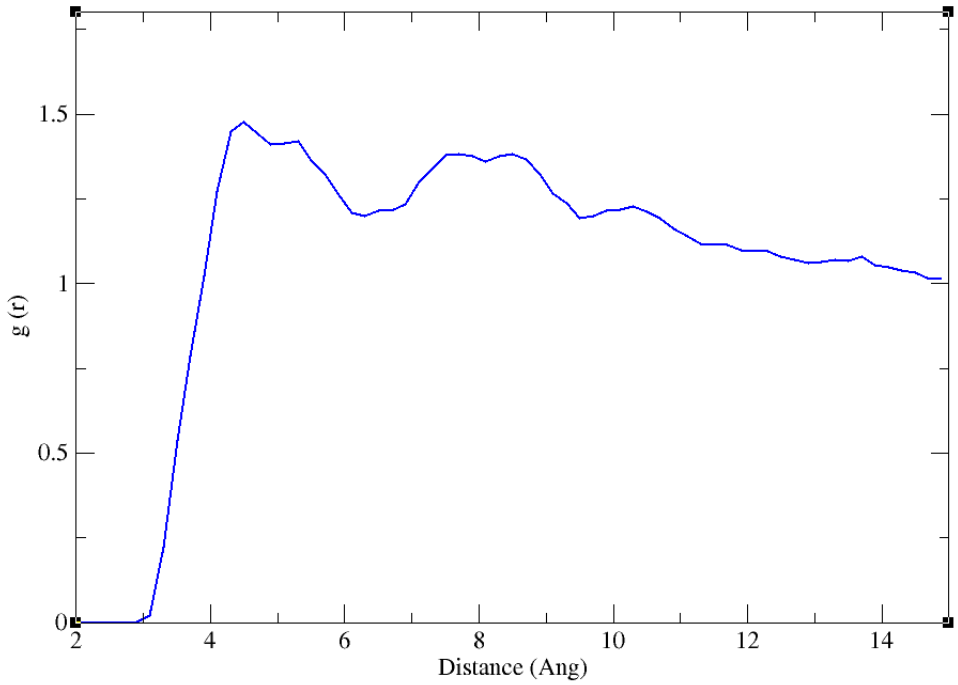

Graph 24 The radial distribution function at 348 K between the C2 atoms in the NC and the NO_2 molecules in the NC, K10, 40% NO_2 and water binder system.

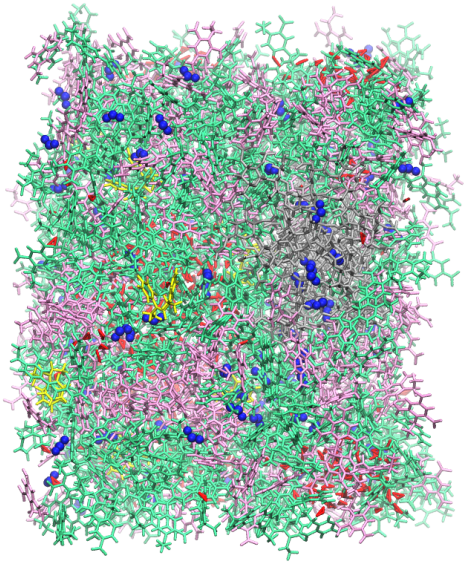

Figure 30 The NC, K10, 40% NO_2 and water binder system at 348 K. The 2,4-DNEB molecules are displayed in green, the 2,4,6-TNEB molecules in pink, the EC molecules in yellow, the water molecules in red, the NO_2 molecules in blue and the NC in grey.

The RDF prior to simulation between the C2 atoms in the NC and the NO_2 molecules in the NC, K10, 40% NO_2 and water binder system is displayed in Graph 22. The NO_2 molecules have all been arranged around the NC polymer chain as illustrated by Figure 28. The first peak has a g (r) value of ~15 at 3.5 Å suggesting NO_2 molecules could be found at this distance from a C2 atom in the NC. There are no peaks before 3.5 Å, therefore it is unlikely there are many NO_2 molecules closer to a C2 atom in the NC than 3.5 Å. The most prominent peaks are at ~4.5 Å, ~5 Å, and 6 Å indicating it is highly probable a NO_2 molecule is at these distances from a C2 atom in the NC. There are smaller peaks at ~7 Å, ~7.5 Å, and 9 Å showing NO_2 molecules are also at these distances from a C2 atom in the NC. The RDF after simulation at 298 K between the C2 atoms in the NC and the NO_2 molecules in the NC, K10, 40% NO_2 and water binder system is displayed in Graph 23. The most prominent peak is at 4.5 Å, but the g (r) value is now 4.75 rather than ~17.5 the g (r) value for the peak at 4.5 Å in the system prior to simulation. It is now most probable a NO_2 molecule will be found 4.5 Å away from a C2 atom in the NC after simulation at 298 K, but it is less likely compared to the system prior to simulation. At the end of the simulation of the NC, K10, 40% NO_2 and water binder system at 298 K the NO_2 molecules have diffused away from the NC polymer chain into the plasticiser mixture as indicated by the RDF and as shown in Figure 29. The RDF for this system at 348 K displayed in Graph 24 has peaks at 4.5 Å and ~7-9 Å, however compared to the system prior to simulation and at 298 K the g (r) value of approximately 1.5 means it is far less likely a NO_2 molecule will be found at these distances from a C2 atom in the NC. After simulation of the NC, K10, 40% NO_2 and water binder system at 348 K, an even greater number of the NO_2 molecules have moved into the plasticiser mixture, as shown in Figure 30.

The diffusion coefficients for NO_2 in the NC and K10 binders are greater than those obtained for NO_2 in the NC, 2,4-DNEB and NG-N1 binders at the corresponding temperatures. The likely explanation is the lower simulated density of 1.385 g cm^{-3} of the NC and K10 binder compared to 1.412 g cm^{-3} for the NC, 2,4-DNEB and NG-N1 binder, meaning the molecules can move more freely. The finding that the NO_2 molecules can move more freely in the NC and K10 binder is reinforced by the RDFs for both NC binder systems. After simulation at 298 K the NC, 2,4-DNEB, NG-N1, 40% NO_2 and water system displays a peak with the greatest g (r) value of 6.5 at 4.5 Å, the most prominent peak in the RDF for the NC, K10, 40% NO_2 and water system after simulation at 298 K is also at 4.5 Å but with a g (r) value of 4.75. The RDF values indicate it is possible in both systems that a NO_2 molecule will be found 4.5 Å from a C2 atom in the NC after simulation at 298 K, but as the NC and K10 binder has a lower g (r) value it suggests it is less likely in this system compared to the NC, 2,4-DNEB, NG-N1, 40% NO_2 and water system. After simulation at 348 K the most prominent peak in the RDFs is at 4.5 Å in both systems, however the g (r) value for this peak is 3.6 in the NC, 2,4-DNEB, NG-N1, 40% NO_2 and water system compared to 1.5 in the NC, K10, 40% NO_2 and water system. There is also some likelihood in both systems of finding a NO_2 molecule 4.5 Å from a C2 atom in the NC after simulation at 348 K, however it is less likely in the NC, K10, 40% NO_2 and water system. This suggests that it is easier for the NO_2 molecules to diffuse away from the NC into the K10 plasticiser mixture than it is for the NO_2 molecules to diffuse away from the NC into the 2,4-DNEB and NG-N1 plasticiser mixture.

5.3 Conclusion

Molecular dynamics simulations were performed to study the interaction of water and nitrogen dioxide in the nitrocellulose (NC), 2,4-dinitroethylbenzene (2,4-DNEB) and 1-nitramino-2,3-dinitroxypropane (NG-N1) binder and the NC binder plasticised with K10 a mixture of 2,4-DNEB and 2,4,6-trinitroethylbenzene (2,4,6-TNEB). Diffusion coefficients were calculated for different concentrations of nitrogen dioxide in NC and K10 binder and the NC, 2,4-DNEB and NG-N1 binder. Diffusion coefficients were obtained for water in the plasticisers 2,4-DNEB, 2,4,6-TNEB, NG-N1, K10, R8002 and a 2,4-DNEB and NG-N1 mixture and diffusion coefficients were obtained for water in both of the NC binder systems. A NC, 2,4-DNEB and NG-N1 binder system and a NC and K10 binder system were constructed with water molecules evenly distributed throughout the systems and 40% nitrogen dioxide molecules positioned solely around the NC polymer chain. The nitrogen dioxide molecules were arranged solely around the NC because this is the most likely initial position of the nitrogen dioxide molecules when they are produced from breaking of the O-NO_2 bonds in the NC, allowing their movement through each binder mixture after simulation to be studied. Radial distribution functions were calculated in the NC binder systems with water and 40% nitrogen dioxide between the C2 atom in the NC and the nitrogen dioxide molecules prior to simulation, at 298 K and at 348 K. Diffusion coefficients were also calculated for water and nitrogen dioxide in the NC binder systems with water and 40% nitrogen dioxide.

In both of the NC binder systems the diffusion coefficients for nitrogen dioxide increased as the concentration of nitrogen dioxide increased at 298 K, 323 K and 348 K. In terms of NC degradation this suggests that as more nitrogen dioxide is produced due to the breaking of the O-NO_2 bonds in the NC in both binder systems, the rate of diffusion of nitrogen dioxide will

increase due to there being a greater concentration of nitrogen dioxide. An increase in the rate of nitrogen dioxide diffusion means nitrogen dioxide molecules may interact and react with water molecules at a faster rate to produce nitric acid. Nitric acid is thought to react with the NC chain causing further degradation. Diffusion of nitrogen dioxide in the NC and K10 binder at all concentrations and temperatures was faster than nitrogen dioxide diffusion at the corresponding concentrations and temperatures in the NC, 2,4-DNEB and NG-N1 binder. The diffusion coefficients calculated for water in the plasticisers was mostly expected considering their simulated densities, water diffusion was faster in the plasticisers with lower simulated densities due to the water molecules being able to move more freely. The rate of water diffusion was faster in the plasticisers alone compared to when the plasticisers were combined with NC in the binders. For example, the diffusion coefficients for water were larger in the 2,4-DNEB and NG-N1 mixture at 298 K and 338 K compared to those obtained for water at the corresponding temperatures in the NC, 2,4-DNEB and NG-N1 binder. The same trend in water diffusion was found in the K10 plasticiser alone and the NC and K10 binder, where water diffusion was faster in the K10 plasticiser alone compared to the NC and K10 binder. Water diffusion in both of the NC binder systems containing water and 40% nitrogen dioxide was also slower than in the plasticisers without NC. It has been reported in the literature that the molecules in highly plasticised NC propellants and binders can move more freely and the addition of greater quantities of NC has the effect of immobilising molecules. A possible explanation for the higher diffusion coefficients for water in the plasticisers alone is that the presence of NC in both of the binder mixtures resulted in reduced water diffusion due to decreased mobility of molecules compared to the plasticiser mixtures minus the NC. The rate of diffusion of nitrogen dioxide in the NC, 2,4-DNEB and NG-N1 binder containing 40% nitrogen dioxide and water was faster

than in this binder with 40% nitrogen dioxide and no water. In the NC and K10 binder with 40% nitrogen dioxide and water, the diffusion coefficients for nitrogen dioxide were higher compared to those in the NC and K10 binder with 40% nitrogen dioxide and no water. The diffusion coefficients were also unexpectedly higher than those of water in the NC and K10 binder with 40% nitrogen dioxide and water. Diffusion coefficients are inversely proportional to molecular mass and owing to water having a lower molecular mass than nitrogen dioxide, higher diffusion coefficients would be predicted for water compared to nitrogen dioxide. A possible explanation is that the positioning of the nitrogen molecules solely around the NC polymer chain in the NC binder systems with 40% nitrogen dioxide and water resulted in a steeper nitrogen dioxide concentration gradients. The steeper nitrogen dioxide concentration gradients resulted in a faster rate of diffusion of nitrogen dioxide compared to the evenly spread nitrogen dioxide molecules in the NC binder systems containing 40% nitrogen dioxide and no water and the evenely spread water molecules in the NC, K10, 40 % nitrogen dioxide and water system. The diffusion coefficients for nitrogen dioxide in the NC and K10 binders are greater than those obtained for nitrogen dioxide in the NC, 2,4-DNEB and NG-N1 binders at the corresponding temperatures. This is likely due to the lower simulated density of 1.385 g cm^{-3} of the NC and K10 binder compared to 1.412 g cm^{-3} for the NC, 2,4-DNEB and NG-N1 binder, meaning the molecules can move more freely. The radial distribution functions calculated for both binder systems support the finding that the nitrogen dioxide molecules can move more freely in the NC and K10 binder. After simulation at 298 K the most prominent peak in the radial distribution function for the NC, 2,4-DNEB, NG-N1, 40% nitrogen dioxide and water binder is at 4.5 Å. The most prominent peak in the radial distribution function for the NC, K10, 40 % nitrogen dioxide and water system after simulation at 298 K is also at 4.5 Å but it has a lower g (r) value compared to the peak at

4.5 Å in the NC, 2,4-DNEB, NG-N1, and 40% nitrogen dioxide and water system. The same trend is observed after simulation at 348 K where the most prominent peak in the radial distribution functions is at 4.5 Å in both systems, however the g (r) value for this peak is higher in the NC, 2,4-DNEB, NG-N1, 40% nitrogen dioxide and water system compared to the NC, K10, 40% nitrogen dioxide and water system. It is possible in both systems a nitrogen dioxide molecule will be found 4.5 Å from a C2 atom in the NC after simulation at 298 K and 348 K. However, as the peaks at 4.5 Å in the radial distribution functions for the NC, K10, 40% nitrogen dioxide and water system have lower g (r) values compared to the corresponding peaks in the radial distribution functions for the NC, 2,4-DNEB, NG-N1, 40% nitrogen dioxide and water system it suggests it is less likely in the NC, K10, 40% nitrogen dioxide and water binder. It is appears that it is easier for the nitrogen dioxide molecules to diffuse away from the NC into the K10 plasticiser mixture than it is for the nitrogen dioxide molecules to diffuse away from the NC into the 2,4-DNEB and NG-N1 plasticiser mixture. All the diffusion coefficients obtained for water in the NC and K10 binder systems are greater than those calculated for water at the same temperatures in the NC, 2,4-DNEB and NG-N1 binder systems. The finding that water diffusion is faster in the NC and K10 binder combined with the finding that NO_2 diffuses into the K10 plasticiser at a faster rate than NO_2 diffuses into the 2,4-DNEB and NG-N1 plasticiser mixture, may result in faster NC degradation. The NO_2 molecules and water molecules in the NC and K10 binder can diffuse and react more quickly to produce nitric acid compared to the NO_2 and water molecules in the NC, 2,4-DNEB and NG-N1 binder. Diffusion of nitric acid in the NC and K10 binder is also likely to be faster than in NC, 2,4-DNEB and NG-N1 binder due to the lower density of the NC and K10 binder. Faster diffusion of nitric acid in the NC and K10 binder could mean the nitric acid will interact and react with the NC polymer chain at a faster rate in

this system leading to an increased NC degradation rate in the NC and K10 binder compared to the NC, 2,4-DNEB and NG-N1 binder. Taking the possible interaction between water molecules and NO_2 molecules to produce nitric acid into consideration, a NC binder plasticised with a 2,4-DNEB and NG-N1 mixture appears to be advantageous compared to a NC binder plasticised with K10. As with plasticiser migration, increasing the proportion of higher density NG-N1 (1.80 g cm^{-3}) compared to lower density 2,4-DNEB (1.32 g cm^{-3}) to increase the overall NC, 2,4-DNEB and NG-N1 binder density slightly could be beneficial in slowing down the diffusion of molecules. In the case of water and NO_2 diffusion, if the rate of diffusion of these molecules is slowed it could decrease the rate of nitric acid formation in the NC, 2,4-DNEB and NG-N1 binder system.

6. General Discussion and Key Conclusions

In this research plasticiser migration was investigated in two NC binder systems by obtaining diffusion coefficients and activation energies of diffusion for the plasticiser molecules via MD simulations. The interaction of nitrogen dioxide and water was explored in the NC binder systems by calculation of diffusion coeffcients for nitrogen dioxide and water in each system from MD simulations. Fox and Kollman have related the sensitivity of diffusion coefficient calculation to the density of the system.[144] Force fields specifically parameterised for the NC binders systems and their constituents were more likely to simulate densities closer to the experimental values. The simulated densities of the plasticisers 2,4,6-TNEB and 2,4-DNEB parameterised with bonding and non-bonding terms from the General Amber Force Field and Optimised Potentials for Liquid Simulations were 9.9% and 3.6% lower than the experimental densities, respectively.[64,101] Whilst the simulated densities of 2,4,6-TNEB and 2,4-DNEB obtained in this research using bonding terms and partial charges from electronic geometry optimsation of the molecules and adjusted LJ parameters from the literature were within 0.9% and 1% of the experimental densities, respectively. The simulated densities of the plasticiser NG-N1 and stabiliser EC obtained using bonding terms and partial charges from electronic geometry optimsation of the molecules but with LJ parameters from the literature before adjustment were underestimated compared to experiment by 9.1% for EC and 11.6% for NG-N1. The optimised force fields for NG-N1 and EC performed very well, the simulated densities of both systems being within 0.1% of the experimental values. The findings of this research show force fields optimised specifically for each molecule and system are advantageous compared to unadjusted generic force fields from the literature. The NC binder system plasticised with 2,4-DNEB and 2,4,6-TNEB (K10) and the NC binder system plasticised with 2,4-DNEB and NG-N1

were constructed using the force fields obtained for the individual constituents. After alteration of the Lennard-Jones parameters the simulated densities of both systems were within 1.1% of experiment. The plasticiser migration rate in a NC binder plastcised with 2,4-DNEB and NG-N1 was compared to the plasticiser migration rate in a NC binder plasticised with K10 (a 2,4-DNEB and 2,4,6-TNEB mixture) by calculation of diffusion coeffcients and activation energies of diffusion from MD simulations. Plasticiser migration rates in binders have been assessed using diffusion coefficients obtained from experiment in similar systems.[13,17] The diffusion coefficients for 2,4,6-TNEB and 2,4-DNEB in the NC and K10 binder were higher than those obtained for 2,4-DNEB and NG-N1 in the NC binder plasticised with these molecules. The activation energies of diffusion for 2,4,6-TNEB and 2,4-DNEB in the NC and K10 binder were lower than those obtained for 2,4-DNEB and NG-N1 in the NC binder plasticised with these molecules. The diffusion of organic substances through polymers is controlled by the ability and frequency with which molecules 'jump' from one hole to another.[135] The temperature dependence of diffusion is governed by the activation energy needed for the diffusant to make this jump. As this jump requires space in the polymer matrix, its activation energy will be dependent on intra- and interchain forces in the polymer structure.[136,137,145] The higher diffusion rate and lower activation energies of diffusion for 2,4,6-TNEB and 2,4-DNEB suggest the NC and K10 binder structure and intra- and interchain forces allows for easier migration of plasticiser molecules than the structure of the NC, 2,4-DNEB and NG-N1 binder. An increased plasticiser migration rate will change the mechanical properties and composition of the binder reducing the ballistic shelf-life and shelf-life. According to these findings the 2,4-DNEB and NG-N1 plasticiser mixture is preferential in a NC binder compared to the plasticiser K10 as the plasticiser migration rate will be slower leading to a prolonged ballistic shelf-life and shelf-life.

The diffusion coefficients obtained for the plasticisers in the NC binders simulated in this study were compared to those obtained via experiment for plasticisers in similar systems.[13,17] The diffusion coefficients obtained in this work were the same order of magnitude as those obtained for the plasticisers in the experimental binder and propellant. However, the diffusion coeffcients calculated for 2,4,6-TNEB and 2,4-DNEB in the simulated NC binder used in this study with 89% plasticiser were higher than those obtained for 2,4,6-TNEB and 2,4-DNEB in the experimental polyGLYN binder with 15% plasticiser.[13] The diffusion coefficients obtained for NG-N1 in the simulated NC, 2,4-DNEB and NG-N1 binder with 89% plasticiser were higher than those obtained for the structurally similar NG in a NC propellant studied experimentally containing 40% plasticiser.[17] The larger diffusion coefficients obtained in this work are most likely caused by the much lower amount of NC compared to plasticiser. The greater rate of diffusion in highly plasticised propellants or binders such as the ones simulated in this study has been discussed in the literature.[17] The larger amount of energetic polymer in the experimental formulations means a greater number of intra- and interchain forces in the polymer structure either between the polymer chains and/or between the polymer and plasticiser, therefore the 'ease' at which plasticiser molecules can diffuse through these materials compared to the simulated systems results in lower diffusion coeffcients compared to those obtained in this research.[136,137,145] The diffusion coefficients obtained for NO_2 and water in the NC and K10 binder were greater compared to those obtained for NO_2 and water at the corresponding temperatures in the NC, 2,4-DNEB and NG-N1 binder. These results are aligned with the plasticiser migration results where the diffusion coefficients were also greater for the plasticiser molecules in the NC and K10 binder compared to the NC, 2,4-DNEB and NG-N1 binder. If the NO_2 molecules and water molecules in the NC and K10 binder can diffuse and react more

quickly to produce nitric acid compared to the NO_2 and water molecules in the NC, 2,4-DNEB and NG-N1 binder, nitric acid may interact and react with the NC polymer chain at a faster rate in this system. This would lead to an increased NC degradation rate and a reduction in the stability and effectiveness of the NC in the NC and K10 binder compared to the NC, 2,4-DNEB and NG-N1 binder. This suggests as with plasticiser migration, that the 2,4-DNEB and NG-N1 plasticiser mixture in the NC binder may be advantageous in increasing ballistic shelf-life and shelf-life compared to the K10 plasticiser mixture.

Key Conclusions and Contributions:

1. Force fields have been parameterised for the plasticiser molecules 2,4,6-TNEB, 2,4-DNEB and NG-N1 and the stabiliser molecule EC. The simulated densities of these systems were in excellent agreement with experiment and were an improvement on those obtained with unaltered force field parameters taken from the literature. The simulated densities of the NC, K10 binder and NC, 2,4-DNEB and NG-N1 binder constructed using these force fields were within 1.1% of the experimental densities.

2. The findings show slower diffusion of plasticiser molecules in the NC, 2,4-DNEB and NG-N1 binder compared to the NC, K10 binder, indicating a slower plasticiser migration rate. The 2,4-DNEB and NG-N1 plasticiser mixture is preferential compared to the K10 plasticiser when considering plasticiser migration as slower plasticiser migration will lengthen the ballistic shelf-life and shelf-life of the overall NC binder plasticised with this mixture.

3. The findings show slower diffusion of NO_2 and water molecules in the NC, 2,4-DNEB and NG-N1 binder compared to the NC, K10 binder, indicating a lower likelihood of reaction of NO_2 and water to produce nitric acid. The 2,4-DNEB and NG-N1 binder is advantageous compared to the K10 plasticiser when considering nitric acid formation. Less nitric acid reacting with the NC will lengthen the period of NC effectiveness and stability, thus increasing the ballistic shelf-life and shelf-life of the overall NC binder plasticised with 2,4-DNEB and NG-N1.

7. Future Work

Parameterisation of the NC and K10 binder and NC, 2,4-DNEB and NG-N1 binder enables straightforward preparation of the systems for simulation in order to investigate other properties of interest in the study of energetic materials. Properties of the NC and K10 binder and NC, 2,4-DNEB and NG-N1 binder systems such as tensile modulus, heat of detonation and velocity of detonation could be obtained from molecular dynamics simulations. An experimental density is available for a NC, NG-N1 and BuNENA binder with an 89% plasticiser to 11% NC composition. Parameterisation of BuNENA and tuning of the LJ parameters of the overall binder system would enable simulation and investigation of this NC binder system also. Other energetic binder formulations studied in plasticiser migration experiments can contain 15-40% plasticiser versus energetic polymer compared to the 89% plasticiser to 11% NC ratio used in the NC binders investigated in this research. The NC and K10 binder and NC, 2,4-DNEB and NG-N1 binder could be constructed with different proportions of plasticiser and simulated if experimental densities were available and the effect of plasticiser proportion on migration rate could be determined. The interaction of nitric acid and other degradation products with the plasticiser and NC could be investigated through molecular dynamics simulation of both of the NC systems containing the degradation products of interest.

8. Bibliography

(1) Zhang, X.; Yun, Z. Explosive Chemistry. *Natl. Def. Ind. Press. Beijing* **1989**, No. 1, 1–3.

(2) Agrawal, J. P. *High Energy Materials*; Wiley-VCH Verlag GmbH & Co: Weinheim, 2010; Vol. 35.

(3) Ünver, A.; Dilsiz, N.; Volkan, M.; Akovali, G. Investigation of Acetyl Ferrocene Migration from Hydroxyl-Terminated Polybutadiene Based Elastomers by Means of Ultraviolet-Visible and Atomic Absorption Spectroscopic Techniques. *J. Appl. Polym. Sci.* **2005**, *96* (5), 1654–1661 DOI: 10.1002/app.21624.

(4) G. G. Ang; Pisharath Sreekumar. Polymers as Binders and Plasticizers - Historical Perspective. In *Energetic Polymers - Binders and Plasticizers for Enhancing Performance.*; 2012; Vol. 37, p 510.

(5) Chen, P.; Huang, F.; Ding, Y. Microstructure, Deformation and Failure of Polymer Bonded Explosives. *J. Mater. Sci.* **2007**, *42* (13), 5272–5280 DOI: 10.1007/s10853-006-0387-y.

(6) Arthur Provatas. *Energetic Polymers and Plasticisers for Explosive Formulations*; Melbourne, 2000.

(7) Daniel, M. A. *Polyurethane Binder Systems for Polymer Bonded Explosives*; 2006.

(8) Powell, I. J. Insensitive Munitions – Design Principles and Technology Developments. *Propellants, Explos. Pyrotech.* **2016**, *41* (3), 409–413 DOI: 10.1002/prep.201500341.

(9) Yang, J.; Gong, X.; Wang, G. A Promising Azido Nitrate Ester Plasticizer for Propellant. *Comput. Mater. Sci.* **2015**, *110*, 71–76 DOI: 10.1016/j.commatsci.2015.07.049.

(10) Tang, Y.; Shreeve, J. M. Nitroxy/Azido-Functionalized Triazoles as Potential Energetic Plasticizers. *Chem. - A Eur. J.* **2015**, *21* (19), 7285–7291 DOI: 10.1002/chem.201500098.

(11) Reese, D. A.; Groven, L. J.; Son, S. F. Formulation and Characterization of a New Nitroglycerin-Free Double Base Propellant. *Propellants, Explos. Pyrotech.* **2014**, *39* (2), 205–210 DOI: 10.1002/prep.201300105.

(12) Schulze, M. C.; Chavez, D. E. Synthesis and Characterization of Energetic Plasticizer AMDNNM. *J. Energ. Mater.* **2016**, *34* (2), 129–137 DOI: 10.1080/07370652.2015.1005774.

(13) Provatas, A. Energetic Plasticizer Migration Studies. *J. Energ. Mater.* **2003**, *21* (4), 237–245 DOI: 10.1080/713770435.

(14) Agrawal, J. P.; Singh, H. Qualitative Assessment of Nitroglycerin Migration from Double-base and Composite Modified Double-base Rocket Propellants: Concepts and Methods of Prevention. *Propellants, Explos. Pyrotech.* **1993**, *18* (2), 106–110 DOI: 10.1002/prep.19930180211.

(15) Kumari, D.; Balakshe, R.; Banerjee, S.; Singh, H. Energetic Plasticizers for Gun & Rocket Propellants. *Rev. J. Chem.* **2012**, *2* (3), 240–262 DOI: 10.1134/S207997801203003X.

(16) Zhao, B.; Zhang, T.; Wang, Z.; Sun, S.; Ge, Z.; Luo, Y. Kinetics of Bu-NENA Evaporation from Bu-NENA/NC Propellant Determined by Isothermal Thermogravimetry. *Propellants, Explos. Pyrotech.* **2017**, *42* (3), 253–259 DOI: 10.1002/prep.201600054.

(17) Cartwright, R. V. Volatility of NENA and Other Energetic Plasticizers Determined by Thermogravimetric Analysis. *Propellants, Explos. Pyrotech.* **1995**, *20* (2), 51–57 DOI: 10.1002/prep.19950200202.

(18) Fernández de la Ossa, M. ángeles; López-López, M.; Torre, M.; García-Ruiz, C.

Analytical Techniques in the Study of Highly-Nitrated Nitrocellulose. *TrAC - Trends Anal. Chem.* **2011**, *30* (11), 1740–1755 DOI: 10.1016/j.trac.2011.06.014.

(19) Pelouze, J. On the Products of the Action of Concentrated Nitric Acid on Starch and Wood. *Comptes Rendus* **1838**, No. 7, 713–715.

(20) Weir, J. Nitroglycerine and Gun-Cotton: A Double Centenary. *Nature* **1946**, *158* (4003), 83–85 DOI: 10.1038/158083a0.

(21) Dow Wolff Cellulosics. *Nitrocellulose Essential for an Extra-Special Finish*; Bomlitz, Germany.

(22) Lindbolm, T. Reactions in the System Nitrocellulose / Diphenylamine with Special Reference to the Formation of a Stabilizing Product Bonded to Nitrocellulose, Uppsala University, 2004.

(23) Hassan, M. A. Effect of Malonyl Malonanilide Dimers on the Thermal Stability of Nitrocellulose. *J. Hazard. Mater.* **2001**, *88*, 33–49.

(24) Zhao, B. Facts and Lessons Related to the Explosion Accident in Tianjin Port, China. *Nat. Hazards* **2016**, *84* (1), 707–713 DOI: 10.1007/s11069-016-2403-0.

(25) Fu, G.; Wang, J.; Yan, M. Anatomy of Tianjin Port Fire and Explosion: Process and Causes. *Process Saf. Prog.* **2016**, *35* (3), 216–220 DOI: 10.1002/prs.

(26) Gelernter, G.; Browning, L. C.; Harris, S. R.; Mason, C. M. The Slow Thermal Decomposition of Cellulose Nitrate. *J. Phys. Chem.* **1956**, *60* (9), 1260–1264 DOI: 10.1021/j150543a027.

(27) Phillips, R. W.; Orlick, C. A.; Steinberger, R. The Kinetics of the Thermal Decomposition of Nitrocellulose. *J. Phys. Chem.* **1955**, *59* (10), 1034–1039 DOI: 10.1021/j150532a011.

(28) Chin, A.; Ellison, D. S.; Poehlein, S. K.; Ahn, M. K. Investigation of the Decomposition

Mechanism and Thermal Stability of Nitrocellulose/Nitroglycerine Based Propellants by Electron Spin Resonance. *Propellants, Explos. Pyrotech.* **2007**, *32* (2), 117–126 DOI: 10.1002/prep.200700013.

(29) Makashir, P. S.; Mahajan, R. R.; Agrawal, J. P. Studies on Kinetics and Mechanism of Initial Thermal Decomposition of Nitrocellulose. *J. Therm. Anal.* **1995**, *45* (3), 501–509 DOI: 10.1007/BF02548782.

(30) Sun, Z. D.; Fu, X. L.; Yu, H. J.; Fan, X. Z.; Ju, X. H. Theoretical Study on Stabilization Mechanisms of Nitrate Esters Using Aromatic Amines as Stabilizers. *J. Hazard. Mater.* **2017**, *339*, 401–408 DOI: 10.1016/j.jhazmat.2017.06.025.

(31) Batten, J. J. The Agent of the Autocatalytic Thermal Decomposition of Aliphatic Nitrate Ester Explosives. *Int. J. Chem. Kinet.* **1985**, *17*, 1085–1090.

(32) Katoh, K.; Le, L.; Kumasaki, M.; Wada, Y.; Arai, M. Study on the Spontaneous Ignition Mechanism of Nitric Esters (III). In *Thermochimica Acta*; 2005; Vol. 431, pp 173–176.

(33) Lussier, L. S.; Gagnon, H.; Bohn, M. A. On the Chemical Reactions of Diphenylamine and Its Derivatives with Nitrogen Dioxide at Normal Storage Temperature Conditions. *Propellants, Explos. Pyrotech.* **2000**, *25* (3), 117–125 DOI: 10.1002/1521-4087(200006)25:3<117::AID-PREP117>3.0.CO;2-8.

(34) Vogelsanger, B.; Sopranetti, R. Nitrocellulose Ageing Processes and Their Consequences for Stability Testing. In *4th International Nitrocellulose Symposium*; 2010.

(35) Lindblom, T. Reactions in Stabilizer and between Stabilizer and Nitrocellulose in Propellants. *Propellants, Explos. Pyrotech.* **2002**, *27* (4), 197–208 DOI: 10.1002/1521-4087(200209)27:4<197::AID-PREP197>3.0.CO;2-W.

(36) Wilker, S.; Heeb, G.; Vogelsanger, B.; Petrzilek, J.; Skladal, J. Triphenylamine - A “new”

Stabilizer for Nitrocellulose Based Propellants - Part I: Chemical Stability Studies. *Propellants, Explos. Pyrotech.* **2007**, *32* (2), 135–148 DOI: 10.1002/prep.200700014.

(37) Fryš, O.; Bajerová, P.; Eisner, A.; Skládal, J.; Ventura, K. Utilization of New Non-Toxic Substances as Stabilizers for Nitrocellulose-Based Propellants. *Propellants, Explos. Pyrotech.* **2011**, *36* (4), 347–355 DOI: 10.1002/prep.201000043.

(38) Trache, D.; Tarchoun, A. F. Stabilizers for Nitrate Ester-Based Energetic Materials and Their Mechanism of Action: A State-of-the-Art Review. *J. Mater. Sci.* **2018**, *53* (1), 100–123 DOI: 10.1007/s10853-017-1474-y.

(39) Wu, Y.; Yi, Z.; Luo, Y.; Ge, Z.; Du, F.; Chen, S.; Sun, J. Fabrication and Properties of Glycidyl Azide Polymer-Modified Nitrocellulose Spherical Powders. *J. Therm. Anal. Calorim.* **2017**, *129* (3), 1555–1562 DOI: 10.1007/s10973-017-6387-0.

(40) Hale, G. Propellant Powder. 1963992, 1934.

(41) Altenburg, T.; Klapötke, T. M.; Penger, A. Primary Nitramines Related to Nitroglycerine: 1-Nitramino-2,3-Dinitroxypropane and 1,2,3-Trinitraminopropane. *Cent. Eur. J. Energ. Mater.* **2009**, *6* (3–4), 3–4.

(42) Willcox, M.; Padfield, J.; McAteer, D. *Demonstration of 1-Nitramino-2,3-Dinitroxypropane as an Energetic Plasticiser Component in an HMX-Based PBX*; Shrivenham.

(43) Seel, P. Process of Dehydrating Nitrocellulose and Reducing the Fire Risk Thereof. 1398911, 1921.

(44) Johnson, C. E.; Dendor, P. F. Process for Forming a Pourable Plastisol Nitrocellulose Slurry. 3962382, 1976.

(45) Ma, X.; Zhao, F.; Ji, G.; Zhu, W.; Xiao, J.; Xiao, H. Computational Study of Structure and

Performance of Four Constituents HMX-Based Composite Material. *J. Mol. Struct. THEOCHEM* **2008**, *851* (1–3), 22–29 DOI: 10.1016/j.theochem.2007.10.044.

(46) Yang, J.; Gong, X.; Wang, G. Theoretical Studies on the Plasticizing Effect of DIANP on NC with Various Esterification Degrees. *Comput. Mater. Sci.* **2014**, *95*, 129–135 DOI: 10.1016/j.commatsci.2014.07.024.

(47) Bunte, S. W.; Sun, H. Molecular Modeling of Energetic Materials: The Parameterization and Validation of Nitrate Esters in the COMPASS Force Field. *J. Phys. Chem. B* **2000**, *104* (11), 2477–2489 DOI: 10.1021/jp991786u.

(48) Ma, X.; Zhu, W.; Xiao, J.; Xiao, H. Molecular Dynamics Study of the Structure and Performance of Simple and Double Bases Propellants. *J. Hazard. Mater.* **2008**, *156*, 201–207 DOI: 10.1016/j.jhazmat.2007.12.068.

(49) Jensen, T. L.; Moxnes, J. F.; Unneberg, E.; Dullum, O. Calculation of Decomposition Products from Components of Gunpowder by Using ReaxFF Reactive Force Field Molecular Dynamics and Thermodynamic Calculations of Equilibrium Composition. *Propellants, Explos. Pyrotech.* **2014**, *39* (6), 830–837 DOI: 10.1002/prep.201300198.

(50) Suceska, M. Test Methods for Explosives. In *Test Methods for Explosives*; Springer Science & Business Media: New York, 2012; pp 11–64.

(51) Libardi, J.; Ravagnani, S. P.; Morais, A. M. F.; Cardoso, A. R. Diffusion of Plasticizer in a Solid Propellant Based on Hydroxyl-Terminated Polybutadiene. *Polim.: Cienc. Tecnol.* **2010**, *20* (4), 241–245 DOI: 10.1590/S0104-14282010005000048.

(52) Grythe, K. F.; Hansen, F. K. Diffusion Rates and the Role of Diffusion in Solid Propellant Rocket Motor Adhesion. *J. Appl. Polym. Sci.* **2007**, *103* (3), 1529–1538 DOI: 10.1002/app.25086.

(53) Tompa, A. S. Thermal Analysis of Liquid and Solid Propellants. *J. Hazard. Mater.* **1980**, *4* (1), 95–112 DOI: 10.1016/0304-3894(80)80026-4.

(54) Akhavan, J. Investigation into the Network Structure of Plasticized Rocket Propellant. *Polymer (Guildf).* **1998**, *39* (1), 215–221 DOI: 10.1016/S0032-3861(97)00259-0.

(55) Phillips, A. J. *Study of Factors Which Affect the Volatility of Smokeless Powder*; New Jersey, USA, 1940.

(56) Luo, Q.; Ren, T.; Shen, H.; Zhang, J.; Liang, D. The Thermal Properties of Nitrocellulose: From Thermal Decomposition to Thermal Explosion. *Combust. Sci. Technol.* **2018**, *190* (4), 579–590 DOI: 10.1080/00102202.2017.1396586.

(57) Volltrauer, H. N.; Fontijn, A. Low-Temperature Pyrolysis Studies by Chemiluminescence Techniques Real-Time Nitrocellulose and PBX 9404 Decomposition. *Combust. Flame* **1981**, *41* (C), 313–324 DOI: 10.1016/0010-2180(81)90065-1.

(58) Kon'kin, A. L.; Ershov, B. G.; Kargin, Y. M.; Chichirov, A. A.; Agafonov, M. N. Study of the Radical Products of the Thermal Decomposition of Nitrocellulose. *Bull. Acad. Sci. USSR Div. Chem. Sci.* **1989**, *38* (11), 2426–2428 DOI: 10.1007/BF01168105.

(59) Miles, F. D. Cellulose Nitrate. In *Cellulose Nitrate*; Interscience: New York, 1955; p 96–97,1 24–127, 131–133.

(60) Long, F. A.; Thompson, L. J. Diffusion of Water Vapor in Polymers. *J. Polym. Sci.* **1955**, *15* (80), 413–426 DOI: 10.1002/pol.1955.120158009.

(61) Hsieh, P. Y. Diffusibility and Solubility of Gases in Ethylcelluloee and Nitrocellulose. *J. Appl. Polym. Sci.* **1963**, *7*, 1743–1756.

(62) Lewis, T. J. Diffusion of Isopropyl Nitrate, Acetone and Water into Nitrocellulose. *Polymer (Guildf).* **1978**, *19* (3), 285–290 DOI: 10.1016/0032-3861(78)90222-7.

(63) Lewars, E. *Computational Chemistry: Introduction to the Theory and Applications of Molecular and Quantum Mechanics*; Kluwer Academic Publishers: New York, 2003.

(64) Wang, J.; Wolf, R. M.; Caldwell, J. W.; Kollman, P. A.; Case, D. A. Development and Testing of a General Amber Force Field. *J Comput Chem* **2004**, *25*, 1157–1174.

(65) Leach A.R. *Molecular Modelling. Principles and Applications*, 2nd editio.; Pearson Education: Harlow, 2001.

(66) Jensen, F. *Introduction to Computational Chemistry*, 2nd Ed.; John Wiley and Sons: Chichester, 2007.

(67) Sigfridsson, E.; Ryde, U. Comparison of Methods for Deriving Atomic Charges from the Electrostatic Potential and Moments. *J. Comput. Chem.* **1998**, *19* (4), 377–395 DOI: 10.1002/(SICI)1096-987X(199803)19:4<377::AID-JCC1>3.0.CO;2-P.

(68) Chirlian, L.; Francl, M. Atomic Charges Derived from Electrostatic Potentials; A Detailed Study. *J. Comp. Chem.* **1987**, *8* (6), 894–905 DOI: 10.1002/jcc.540080616.

(69) Breneman, C. M.; Wiberg, K. B. "Determining Atom-Centered Monopoles from Molecular Electrostatic Potentials. The Need for High Sampling Density in Formamide Conformational Analysis." *J. Comput. Chem.* **1990**, *11*, 361.

(70) Singh, U. C.; Kollman, P. A. An Approach to Computing Electrostatic Charges for Molecules. *J. Comput. Chem.* **1984**, *5* (2), 129–145 DOI: 10.1002/jcc.540050204.

(71) González, M. A. Force Fields and Molecular Dynamics Simulations. *Collect. SFN* **2011**, *12*, 169–200 DOI: 10.1051/sfn/201112009.

(72) Monticelli, L.; Salonen, E. *Biomolecular Simulations: Methods and Protocols*; Monticelli, L., Emppu, S., Eds.; Humana Press: New York, 2016.

(73) Atkins, P.; de Paula, J.; Friedman, R. *Quanta, Matter and Change*; Oxford University

Press: Oxford, 2009.

(74) Kohn, W.; Sham, L. J. Phys. Review. *Phys. Rev.* **1965**, *140*, A1133–A1138.

(75) Rappoport, D.; Crawford, N. R. M.; Furche, F.; Burke, K. Approximate Density Functionals: Which Should I Choose? In *Encyclopedia of Inorganic Chemistry*; Solomon, E. I., King, R. B., A., S. R., Eds.; Wiley: New Jersey, 2009.

(76) Becke, A. D. Density Functional Thermochemistry. III. The Role of Exact Exchange. *J. Chem. Phys.* **1993**, *98*, 5648 DOI: https://doi.org/10.1063/1.464913.

(77) Stephens, P. J.; Devlin, F. J.; Chabalowski, C. F.; Frisch, M. J. Ab Initio Calculation of Vibrational Absorption and Circular Dichroism Spectra Using Density Functional Force Fields. *J. Phys. Chem.* **1994**, *98* (45), 11623–11627.

(78) Hratchian, H. P.; Schlegel, H. B. Finding Minima, Transition States, and Following Reaction Pathways on Ab Initio Potential Energy Surfaces. In *Theory and Application sof Computational Chemistry: The First Forty Years*; Dykstra et al., C., Ed.; Elsevier B.V.: New York, 2005; pp 195–249.

(79) No Title http://komarix.org/ac/papers/thesis/thesis_html/node10.html (accessed Aug 11, 2018).

(80) Fletcher, R. *Practical Methods of Optimization*, 2nd ed.; John Wiley and Sons: New York, 1987.

(81) Simons, J.; Jørgensen, P.; Taylor, H.; Ozment, J. Walking on Potential Energy Surfaces. *J. Phys. Chem.* **1983**, *87*, 2745–2753.

(82) Frisch, M. J.; Trucks G. W. et al. Gaussian'09. Gaussian, Inc.,: Wallingford CT, 2009.

(83) Schlegel, H. B. Optimization of Equilibrium and Transition Structures. *J. Comput. Chem.* **1982**, *3* (2), 214–218.

(84) Foresman, J. B.; Frisch, A. *Exploring Chemistry with Electronic Structure Methods*, 2nd Ed.; Gaussian, Inc.,: Pittsburgh, PA, 1996.

(85) Nash, A.; Collier, T.; Birch, H.; De Leeuw, N. ForceGen: Atomic Covalent Bond Value Derivation for Gromacs. *J. Mol. Model.* **2017**, *24* (5), 1–11 DOI: https://doi.org/10.1007/s00894-017-3530-6.

(86) Seminario, J. M. Calculation of Intramolecular Force Fields from Second-Derivative Tensors. *Int. J. Quantum Chem. Quantum Chem. Symp.* **1996**, *30*, 1271–1277 DOI: 10.1002/(SICI)1097-461X(1996)60:7<1271::AID-QUA8>3.0.CO;2-W.

(87) Verlet, L. Computer "Experiments" on Classical Fluids. I. Thermodynamical Properties of Lennard-Jones Molecules. *Phys. Rev.* **1967**, *159* (1), 98–103 DOI: 10.1103/PhysRev.159.98.

(88) Berendsen, H. J. C.; Postma, J. P. M.; van Gunsteren, W. F.; DiNola, A.; Haak, J. R. Molecular Dynamics with Coupling to an External Bath. *J. Chem. Phys.* **1984**, *81* (8), 3684–3690 DOI: 10.1063/1.448118.

(89) Andersen, H. C. Molecular Dynamics Simulations at Constant Pressure and/or Temperature. *J. Chem. Phys.* **1980**, *72* (1980), 2384 DOI: 10.1063/1.439486.

(90) Case, D. A.; Babin, V. et al. Amber 14. University of California: San Francisco 2015.

(91) Ryckaert, J. P.; Ciccotti, G.; Berendsen, H. J. C. Numerical Integration of the Cartesian Equations of Motion of a System with Constraints: Molecular Dynamics of n-Alkanes. *J. Comput. Phys.* **1977**, *23* (3), 327–341 DOI: 10.1016/0021-9991(77)90098-5.

(92) Steinhauser, M. O. Introduction to Molecular Dynamics Simulations: Applications in Hard and Soft Condensed Matter Physics. In *Molecular dynamics - Studies of synthetic and biological macromolecules*; Wang, L., Ed.; IntechOpen, 2012; pp 4–28.

(93) Fick's 1st Law of Diffusion https://omlc.org/classroom/ece532/class5/ficks1.html (accessed Jun 27, 2018).

(94) Einstein, A. *Investigations on the Theory of the Brownian Movement*; Furth, R., Ed.; Methuen Publishing: London, 1926.

(95) Muller Plathe, F. Permeation of Polymers a Computational Approach. *Acta Polym.* **1994**, *45* (4), 259–293 DOI: 10.1002/actp.1994.010450401.

(96) Roe, D. R.; Cheatham, T. E. PTRAJ and CPPTRAJ: Software for Processing and Analysis of Molecular Dynamics Trajectory Data. *J Chem Theory Com* **2013**, *9* (7), 3084–3095 DOI: 10.1021/ct400341p.

(97) Allen, M. P.; Tildesley, D. J. *Computer Simulation of Liquids*, First Ed.; Oxford University Press: New York, 1987.

(98) The Thomas Group - PTCL, Oxford http://rkt.chem.ox.ac.uk/tutorials/molint/liquids.html (accessed Jun 28, 2018).

(99) Sinica http://w3.iams.sinica.edu.tw/lab/jlli/thesis_andy/node14.html (accessed Jun 28, 2018).

(100) No Title http://www.globalsino.com/EM/page3097.html (accessed Jun 28, 2018).

(101) Jorgensen, W. L.; Tirado-Rives, J. The OPLS [Optimized Potentials for Liquid Simulations] Potential Functions for Proteins, Energy Minimizations for Crystals of Cyclic Peptides and Crambin. *J. Am. Chem. Soc.* **1988**, *110* (6), 1657–1666 DOI: 10.1021/ja00214a001.

(102) Fox, T.; Kollman, P. A. Application of the RESP Methodology in the Parameterization of Organic Solvents. *J. Phys. Chem. B* **1998**, *102* (41), 8070–8079 DOI: 10.1021/jp9717655.

(103) Klauda, J. B.; Brooks, B. R. CHARMM Force Field Parameters for Nitroalkanes and

Nitroarenes. *J. Chem. Theory Comput.* **2008**, *4*, 107–115 DOI: 10.1021/ct700191v.

(104) Myung, Y.-C.; Han, S.-H. Force Field Parameters for 3-Nitrotyrosine and 6-Nitrotryptophan. *Bull. Korean Chem. Soc.* **2010**, *31* (9), 2581–2587 DOI: 10.5012/bkcs.2010.31.9.2581.

(105) Dupradeau, F.-Y.; Pigache, A.; Zaffran, T.; Savineau, C.; Lelong, R.; Grivel, N.; Lelong, D.; Rosanski, W.; Cieplak, P. The R.E.D. Tools: Advances in RESP and ESP Charge Derivation and Force Field Library Building. *Phys. Chem. Chem. Phys.* **2010**, *12* (28), 7821–7839 DOI: 10.1039/c0cp00111b.

(106) Vanquelef, E.; Simon, S.; Marquant, G.; Garcia, E.; Klimerak, G.; Delepine, J. C.; Cieplak, P.; Dupradeau, F. Y. R.E.D. Server: A Web Service for Deriving RESP and ESP Charges and Building Force Field Libraries for New Molecules and Molecular Fragments. *Nucleic Acids Res.* **2011**, *39* (2), 511–517 DOI: 10.1093/nar/gkr288.

(107) Cieplak, P.; Cornell, W. D.; Kollman, P. A. A Well-Behaved Electrostatic Potential Based Method Using Charge Restraints for Deriving Atomic Charges: The RESP Model. *J. Phys. Chem* **1993**, *97*, 10269–10280.

(108) Cox, P.; Waring, S. Microwave Spectrum, Structure, and Dipole Moment of Methyl Nitrate. *Trans. Faraday Soc* **1971**, *67*, 3441–3450 DOI: 10.1021/ja01038a006.

(109) Durig, J. R.; Sheehan, T. G. Raman Spectra, Vibrational Assignment, Structural Parameters and Ab Initio Calculations for Ethyl Nitrate. *J. Raman Spectrosc.* **1990**, *21* (April), 635–644.

(110) Choi, C. S.; Abel, J. E. The Crystal Structure of 1,3,5-Trinitrobenzene by Neutron Diffraction. *Acta Crystallogr.* **1972**, *B28*, 193–201.

(111) Bar I; Bernstein J. The Pi-Molecular Complex Stilbene-(Sym-Trinitrobenzene)2. *Acta*

Crystallogr. **1978**, *B34*, 3438–3441.

(112) Bar I, B. J. The Po -Molecular Complexes Trans-Azobenzene-(Sym-Trinitrobenzene) 2 and N-Benzylideneaniline-(Sym-Trinitrobenzene) 2. *Acta Crystallogr.* **1981**, *B37*, 569–575.

(113) Yufit, D. S. The Low-Melting Compounds 1,4-Diethyl-, 1,2-Diethyl- and Ethylbenzene. *Acta Crystallogr. Sect. C Cryst. Struct. Commun.* **2013**, *69* (3), 273–276 DOI: 10.1107/S0108270113003041.

(114) Betz, R.; Gerber, T.; Schalekamp, H. 1,3-Diethyl-1,3-Diphenylurea. *Acta Crystallogr. Sect. E Struct. Reports Online* **2011**, *67* (4), o827–o827 DOI: 10.1107/S1600536811008294.

(115) Ganis, P.; Avitable, G.; Benedetti, E.; Pedone, C.; Goodman, M. Proceedings of the National Academy of Sciences. In *Crystal and Molecular Structure of N,N'-Diethyl-N,N'-Diphenylurea*; 1970; Vol. 67, pp 426–433.

(116) *Tables of Interatomic Distances and Configuration in Molecules and Ions*; Sutton, L. E., Ed.; London: The Chemical Society, 1958.

(117) AWE. Personal Communication, 2016.

(118) Pristera, F.; Halik, M.; Castelli, A.; Fredericks, W. Analysis of Explosives Using Infrared Spectroscopy. *Anal. Chem.* **1960**, *32* (4), 495–508 DOI: 10.1021/ac60160a013.

(119) Nitrogen Dioxide https://www.mathesongas.com/pdfs/products/Nitrogen-Dioxide-Pure-Gas.pdf (accessed Feb 8, 2018).

(120) French, D. M. Journal of Polymer Science. In *Journal of Applied Polymer Science*; 1978; Vol. 22, pp 309–313.

(121) Hollands, R.; Fung, V. *High Performance Polymer-Bonded Explosive Containing*

PolyNIMMO for Metal Accelerating Applications; 2004.

(122) Garvey, A.; Price, D. W. *Energetic Plasticizer Evaluation in Cast-Cured Polymer Based Explosives (PBXs)*; 2014.

(123) Vrcelj, R. M.; Sherwood, J. N.; Kennedy, A. R.; Gallagher, H. G.; Gelbrich, T. Polymorphism in 2-4-6 Trinitrotoluene. *Cryst. Growth Des.* **2003**, *3* (6), 1027–1032 DOI: 10.1021/cg0340704.

(124) Hanson, J. .; Hitchcock, P. B.; Saberi, H. Steric Factors in the Preparation of Nitrostilbenes. *J. Chem. Res.* **2004**, 667–669.

(125) Steffen, C.; Thomas, K.; Huniar, U.; Hellweg, A.; Rubner, O.; Schroer, A. Packmol: A Package for Building Initial Configurations for Molecular Dynamics Simulations. *J. Comput. Chem.* **2008**, *31* (16), 2967–2970 DOI: 10.1002/jcc.

(126) Meader, D.; Atkins, E. D. T.; Happey, F. Cellulose Trinitrate: Molecular Conformation and Packing Considerations. *Polymer (Guildf).* **1978** DOI: 10.1016/0032-3861(78)90086-1.

(127) Humphrey, W.; Dalke, A.; Schulten, K. VMD - Visual Molecular Dynamics. *J. Molec. Graph.* **1996**, *14*, 33–38.

(128) Pettersen EF, Goddard TD, Huang CC, Couch GS, Greenblatt DM, Meng EC, F. T. UCSF Chimera--a Visualization System for Exploratory Research and Analysis. *J. Comput. Chem.* **2004**, *25* (13), 1605–1612.

(129) Basconi, J. E.; Shirts, M. R. Effects of Temperature Control Algorithms on Transport Properties and Kinetics in Molecular Dynamics Simulations. *J. Chem. Theory Comput.* **2013**, *9*, 2887–2899 DOI: 10.1021/ct400109a.

(130) Kirk, A. D. The Range of Validity of Graham ' s Law. *J. Chem. Educ.* **1967**, *44* (12), 745–

750.

(131) Roe, D. R.; Cheatham, T. E. "PTRAJ and CPPTRAJ: Software for Processing and Analysis of Molecular Dynamics Trajectory Data." *J. Chem. Theory Comput.* **2013**, *9* (7), 3084–3095.

(132) Welle, F.; Franz, R. Diffusion Coefficients and Activation Energies of Diffusion of Low Molecular Weight Migrants in Poly(Ethylene Terephthalate) Bottles. *Polym. Test.* **2012**, *31* (1), 93–101 DOI: 10.1016/j.polymertesting.2011.09.011.

(133) De Luca, L. T.; Shimada, T.; Sinditskii, V. P.; Calabro, M. Chemical Rocket Propulsion: A Comprehensive Survey of Energetic Materials; Springer Berlin Heidelberg, 2016; pp 863–887.

(134) Atkins, P.; de Paula, J. *Atkins' Physical Chemistry*, 10th ed.; Oxford University Press: Oxford, 2014.

(135) Hulscher, D.; Cornelissen, G. Effect of Temperature on Sorption Coefficients and Sorption Kinetics of Organic Micropollutants - a Review. *Chemosphere* **1996**, *32* (4), 609–626.

(136) Rogers, C. E. -. In *Physics and Chemistry of the Organic Solid State*; Fox, D., Labes, M. M., Weissberger, A., Eds.; Interscience Publishers: New York, 1965; pp 509–630.

(137) Stannett, V. Simple Gases. In *Diffusion in Polymers*; Crank, J., Park, G. S., Eds.; Academic Press: London, 1968; pp 41–73.

(138) Aminabhavi, T. M.; Phayde, H. T. . Sorption, Desorption, Diffusion and Permeation of Aliphatic Alkanes into Santoprene Thermoplastic Rubber. *J. Appl. Polym. Sci.* **1995**, No. 55, 17–37.

(139) Keeffe, C. O.; Wallace, I.; Gill, P. P. Effect of Humidity on the Real-Time , Low

Temperature , Nitrocellulose Degradation by Chemiluminescence. Cranfield University.

(140) Berendsen, H. J. C.; Grigera, J. R.; Straatsma, T. P. The Missing Term in Effective Pair Potentials. *J. Phys. Chem.* **1987**, *91* (24), 6269–6271 DOI: 10.1021/j100308a038.

(141) Crank, J. (John). *The Mathematics of Diffusion*, 2nd Ed.; Oxford University Press: Oxford, 1975.

(142) Vanderkooi, W. N.; Long, M. W. The Concentration-Dependent Diffusion of Styrene in Ethyl Cellulose. *J. Polym. Sci.* **1962**, *56*, 57–68.

(143) Secor, R. M. The Effect of Concentration on Diffusion Coefficient in Polymer Solutions. *AI.ChE J.* **1965**, *11* (3), 452–456.

(144) Fox, T.; Kollman, P. A. Application of the RESP Methodology in the Parameterization of Organic Solvents. *J. Phys. Chem. B* **1998**, *102* (41), 8070–8079 DOI: Doi 10.1021/Jp9717655.

(145) Aminabhavi, T. M.; Phayde, H. T. S. Sorption, Desorption, Diffusion, and Permeation of Aliphatic Alkanes into Santoprene Thermoplastic Rubber. *J. Appl. Polym. Sci.* **1995**, *55* (1), 17–37 DOI: 10.1002/app.1995.070550103.

Appendix 1 - Construction of Simulation Cells for Parameterisation Simulations

2,4,6-TNEB

Based on monoclinic TNT unit cell reported at 100 K[123]
The lattice parameters, a = 14.9113 Å, b = 6.0340 Å, c = 20.8815 Å

The volume of the unit cell was used to calculate how many TNT molecules would fit in a 40 Å × 40 Å × 40 Å cubic box.

14.9113 Å × 6.0340 Å × 20.8815 Å = 1879 Å^3, the unit cell of this volume contains 8 TNT molecules
40 Å × 40 Å × 40 Å = 64000 Å^3, a simulation box of this size can hold 272 TNT molecules

TNT = 21 atoms 2,4,6-TNEB = 24 atoms

Number of atoms in 40 Å × 40 Å × 40 Å cubic box of TNT molecules is 272 × 21 = 5712 atoms

Estimate of the number of 2,4,6-TNEB molecules in 40 Å × 40 Å × 40 Å cubic box
5712 ÷ 24 = 238 2,4,6-TNEB molecules in 40 Å^3

2,4-DNEB

Based on monoclinic 2,4-DNT unit cell reported at 173 K[124]
The lattice parameters, a = 8.0057 Å, b = 15.1273 Å, c = 12.8853 Å

The volume of the unit cell was used to calculate how many 2,4-DNT cells would fit in a 40 Å × 40 Å × 40 Å cubic box.

8.0057 Å × 15.1273 Å × 12.8853 Å = 1561 Å^3, the unit cell of this volume contains 8 2,4-DNT molecules
40 Å × 40 Å × 40 Å = 64000 Å^3, a simulation box of this size can hold 328 2,4-DNT molecules

2,4-DNT = 19 atoms 2,4-DNEB = 22 atoms

Number of atoms in 40 Å × 40 Å × 40 Å cubic box of 2,4-DNT molecules is 328 × 19 = 6231.9 atoms

Estimate of number of 2,4-DNEB molecules in 40 Å × 40 Å × 40 Å cubic box
6231.9 ÷ 22 = 283 2,4-DNEB molecules in 40 Å^3

ethyl centralite (EC)

Unit cell dimensions (monoclinic),[115] a = 9.6990 Å, b = 16.7622 Å, c = 10.6011 Å
Z = 4 per unit cell
Cubic symmetry assumed, unit cell dimensions used to calculate volume
9.70 Å × 16.76 Å × 10.60 Å = 1723 $Å^3$
40 Å × 40 Å × 40 Å = 64,000 $Å^3$
64,000 $Å^3$ / 1723 $Å^3$ = 37.14
37.14 × 4 ~ 149 ethyl centralite molecules in 40 $Å^3$

1-nitramino-2,3-dinitroxypropane (NG-N1)

Unit cell dimensions (monoclinic),[41] a = 7.1363 Å, b = 8.6355 Å, c = 13.7048 Å
Z = 4 per unit cell
Cubic symmetry assumed, unit cell dimensions used to calculate volume
7.1 Å × 8.6 Å × 13.7 Å = 837 $Å^3$
40 Å × 40 Å × 40 Å = 64,000 $Å^3$
64,000 $Å^3$ / 837 $Å^3$ = 76.46
76.46 × 4 = ~ 306 NG-N1 molecules in 40 $Å^3$

Nitrogen Dioxide (NO_2)

Density = 0.0034 g cm^{-3} at ~ 298 K

$$\text{Density g cm}^{-3} = \frac{\text{number of molecules} \times \text{Mr of molecule}}{\text{Volume (cm}^{-3}) \times \text{Avogadro's constant}}$$

Box volume = 77 Å × 71 Å × 76 Å = 415,492 $Å^3$
= 4.15492×10^{-19} cm^{-3}

$$0.004 \text{ g cm}^{-3} = \frac{22 \text{ (molecules)} \times 46 \text{ (Mr)}}{4.15492 \times 10^{-19} \text{ cm}^{-3} \times 6.023 \times 10^{23}}$$

= 22 NO_2 molecules added to box with dimensions 77 Å × 71 Å × 76 Å

NC, NG-N1 and 2,4-DNEB binder system

NC model = 40 dimers
Mass of one dimer = 594
Mass of 1 NC model = 23,760

NC : plasticiser = 1 : 8 ratio[42]

23,760 × 8 = 190,080
Mass of plasticiser = 190,080

% mass of plasticiser that NG-N1 = 34%
190,080 × 0.34 = 64,627 ÷ NG-N1 Mr 226
= 286 NG-N1 molecules

% mass of plasticiser that 2,4-DNEB = 66%
190,080 × 0.66 = 125,453 ÷ 2,4-DNEB Mr 196
= 640 2,4-DNEB molecules

NC, 2,4-DNEB and 2,4,6-TNEB binder system

NC model = 40 dimers
Mass of one dimer = 594
Mass of 1 NC model = 23,760

NC : plasticiser = 1 : 8 ratio[42]

23,760 × 8 = 190,080
Mass of plasticiser = 190,080

% mass of plasticiser that is 2,4,6-TNEB = 35%
190,080 × 0.35 = 66,528 ÷ 2,4,6-TNEB Mr 241
= 276 2,4,6-TNEB molecules

% mass of plasticiser that 2,4-DNEB = 65%
190,080 × 0.65 = 123,552 ÷ 2,4-DNEB Mr 196
= 630 2,4-DNEB molecules

Total mass of ingredients for both binder systems = 213,840 (23,760 + 190,080)
1% 213,840 = 2138 ÷ EC Mr 268
= 8 EC molecules

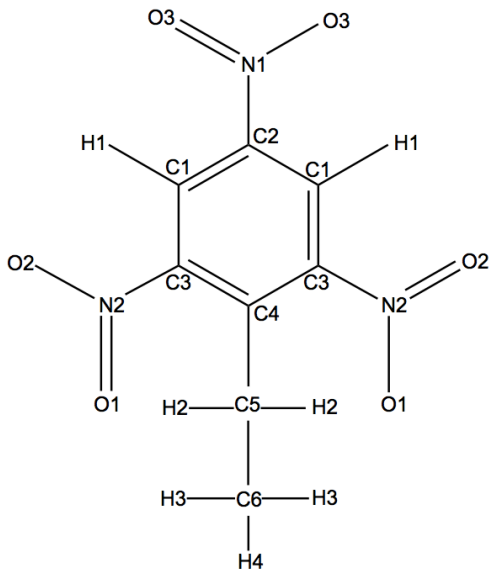

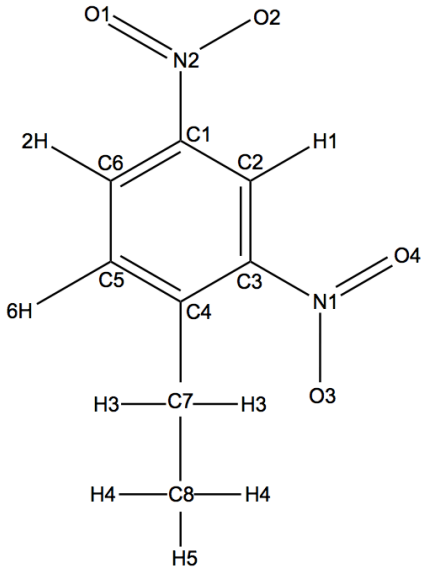

2,4,6-TNEB Force-Field Bonding Parameters

Table 1 - Bond angles, lengths and their associated force constants for 2,4,6-TNEB

angle label	angle (°)	angle force constant kcal mol^{-1}	bond label	bond length (Å)	bond force constant kcal mol^{-1}
C1-C2-C1	121.2	53.330	C1-C2	1.381	305.549
C1-C2-N1	119.4	43.139	C1-C3	1.385	343.552
C1-C3-C4	124.2	49.689	C1-H1	1.078	352.237
C1-C3-N2	114.6	50.765	C2-N1	1.477	128.720
C2-C1-C3	118.3	47.652	C3-C4	1.407	289.481
C2-C1-H1	120.8	16.581	C3-N2	1.484	151.191
C2-N1-O3	117.2	36.035	C4-C5	1.513	189.968
C3-C1-H1	120.9	67.881	C5-C6	1.541	128.785
C3-C4-C3	113.7	36.888	C5-H2	1.089	120.522
C3-C4-C5	123.1	41.074	C6-H3	1.086	134.596
C3-N2-O1	118.1	61.941	C6-H4	1.089	317.571
C3-N2-O2	116.4	57.002	N1-O3	1.222	526.127
C4-C3-N2	121.2	45.755	N2-O1	1.221	410.589
C4-C5-C6	114.2	37.247	N2-O2	1.222	325.988
C4-C5-H2	108.7	36.312			
C5-C6-H3	111.0	45.107			
C5-C6-H4	108.9	27.020			
C6-C5-H2	109.0	44.783			
H2-C5-H2	107.0	56.359			
H3-C6-H4	108.2	24.611			
H3-C6-H3	109.5	51.985			
O1-N2-O2	125.5	69.733			
O3-N1-O3	125.6	36.558			

2,4-DNEB Force-Field Bonding Parameters

Table 2 - Bond angles, lengths and their associated force constants for 2,4-DNEB

angle label	angle (°)	angle force constant kcal mol^{-1}	bond label	bond length (Å)	bond force constant kcal mol^{-1}
C1-C2-C3	118.3	45.845	C1-C2	1.381	396.060
C1-C2-H1	120.9	17.794	C1-C6	1.389	309.486
C1-C6-C5	118.7	47.814	C1-N2	1.475	147.446
C1-C6-H2	119.7	17.048	C2-C3	1.388	315.792
C1-N2-O1	117.3	46.273	C2-H1	1.077	350.855
C1-N2-O2	117.6	44.336	C3-C4	1.402	321.522
C2-C1-C6	121.4	43.961	C3-N1	1.479	110.392
C2-C1-N2	119.0	37.416	C4-C5	1.402	358.459
C2-C3-C4	122.9	47.000	C4-C7	1.510	193.014
C2-C3-N1	115.4	48.531	C5-C6	1.384	338.068
C3-C2-H1	120.8	17.266	C5-H6	1.081	339.334
C3-C4-C5	116.0	39.872	C6-H2	1.079	349.463
C3-C4-C7	125.8	37.907	C7-C8	1.538	113.742
C3-N1-O3	117.8	54.335	C7-H3	1.089	307.316
C3-N1-O4	117.2	37.037	C8-H4	1.089	320.433
C4-C3-N1	121.6	45.817	C8-H5	1.090	103.472
C4-C5-C6	122.6	54.708	N1-O3	1.225	505.821
C4-C5-H6	118.3	17.569	N1-O4	1.223	524.178
C4-C7-C8	112.9	37.238	N2-O1	1.225	518.364
C4-C7-H3	109.1	37.504	N2-O2	1.223	522.263
C5-C4-C7	118.2	35.121			
C5-C6-H2	121.6	20.554			
C6-C1-N2	119.5	46.621			
C6-C5-H6	119.1	17.672			
C7-C8-H4	111.0	23.433			
C7-C8-H5	109.9	19.696			
C8-C7-H3	109.2	22.692			
H3-C7-H3	107.3	37.665			
H4-C8-H5	108.1	20.954			
H4-C8-H4	108.5	24.058			
O1-N2-O2	125.0	39.169			
O3-N1-O4	125.0	49.379			

2,4-DNEB and 2,4,6-TNEB Force-field Non-Bonding Parameters

Table 3 Dihedral angles for 2,4-DNEB and 2,4,6-TNEB

Dihedral Angle	Number of paths [c]	$V_n/2$ [d]	γ [e]	n [f]
$C_{ar} - C_{ar} - C_{ar} - C_{ar}$	1	14.5	180.0	2.0
$C_{ar} - C_{ar} - C_{ar} - C_{al}$	1	1.10	180.0	2.0
$C_{ar} - C_{ar} - C_{ar} - N$	1	6.14	180.0	2.0
$C_{ar} - C_{ar} - C_{ar} - H$	1	1.10	180.0	2.0
$C_{ar} - C_{ar} - N - O$	4	3.68	180.0	2.0
C_{ar} - C_{ar} - C_{al} - C_{al}	1	0.00	0.000	2.0
H - C_{al} - C_{al} - H	1	0.15	0.000	3.0
$C_{ar} - O - N - O$ (improper)	-	7.28	180.0	2.0

a – $_{ar}$ = aromatic carbon atoms, b – $_{al}$ = aliphatic carbon atoms, c – number of bond paths that total V_n must be divided by, d – magnitude of the torsion in kcal mol^{-1}, e – phase angle in degrees, f – periodicity of the torsion

Table 4 Lennard-Jones parameters for 2,4-DNEB and 2,4,6-TNEB

Atom	R_{min} [a]	ε [b]
C_{ar}	1.9920	0.0700
C_{al}	1.9080	0.1094
H_{ar}	1.3580	0.0300
H_{al}	1.4870	0.0157
N	1.8240	0.1200
O	1.6610	0.1700

a - the distance where the potential reaches a minimum in Angstroms ($\sigma \times 2^{1/6}$), b - the potential well depth in kcal mol^{-1}

Figure 2 - Atom types for NC

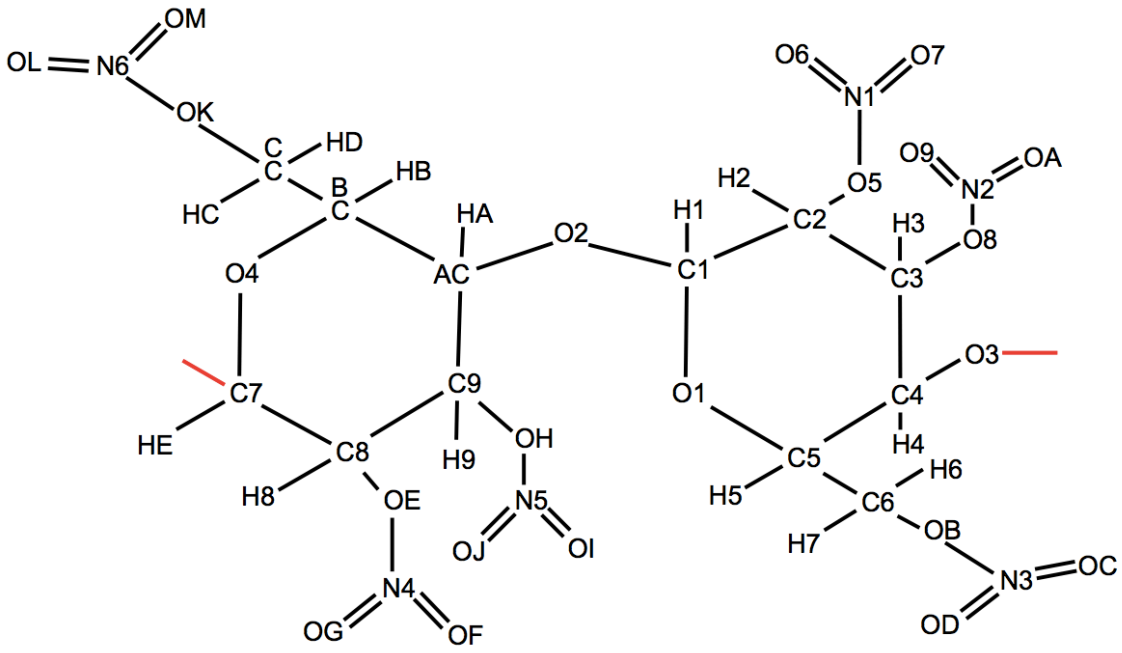

NC Force-Field Bonding Parameters

Table 5 - Bond angles and their associated force constants for NC

angle label	angle (°)	angle force constant kcal mol^{-1}	angle label	angle (°)	angle force constant kcal mol^{-1}
C1-O2-CA	119.3	40.737	C7-O3-C4	119.3	40.737
C1-O1-C5	115.2	33.674	C7-O4-CB	113.3	43.073
C1-C2-O5	108.0	43.798	C7-C8-C9	110.9	53.836
C1-C2-H2	109.0	41.389	C7-C8-H8	108.6	90.739
C1-C2-C3	110.6	48.275	C7-C8-OE	110.1	44.254
C2-O5-N1	116.6	39.885	C8-OE-N4	115.8	46.435
C2-C3-O8	108.3	34.442	C8-C9-H9	110.8	20.996
C2-C3-H3	110.3	28.754	C8-C9-CA	111.8	55.362
C2-C3-C4	111.2	36.517	C8-C9-OH	108.4	26.239
C3-O8-N2	116.5	47.412	C8-C7-HE	110.7	27.117
C3-C4-H4	109.6	56.511	C8-C7-O4	108.0	80.084
C3-C4-O3	110.4	43.839	C9-OH-N5	116.4	47.485
C3-C4-C5	108.4	43.745	C9-CA-CB	108.3	65.648
C3-C2-O5	108.1	43.652	C9-CA-HA	109.4	50.893
C3-C2-H2	111.3	25.682	CA-CB-CC	112.3	38.759
C4-O3-C7	119.3	40.737	CA-CB-HB	108.5	25.395
C4-C5-H5	108.5	30.250	CA-CB-O4	109.0	37.218
C4-C5-C6	113.1	36.787	CA-C9-H9	109.4	60.609
C4-C5-O1	110.8	43.606	CB-CC-OK	105.2	34.184
C4-C3-O8	109.1	23.300	CB-CC-HC	110.8	40.967
C4-C3-H3	109.3	26.885	CB-CC-HD	110.4	37.992
C5-C6-OB	106.8	55.967	O4-CB-CC	107.8	40.649
C5-C6-H6	109.5	65.325	O4-CB-HB	110.6	25.209
C5-C6-H7	110.8	15.878	O4-C7-HE	108.9	20.175
C5-C4-H4	109.0	42.677	O3-C7-HE	111.4	21.864
C5-C4-O3	108.3	37.763	O3-C7-O4	109.6	46.948
O1-C5-H5	110.0	21.832	O3-C4-C5	108.3	37.763
O1-C5-C6	108.2	42.454	CC-OK-N6	114.0	44.111
O1-C1-C2	109.7	44.416	O5-N1-O7	117.7	34.744
O1-C1-O2	107.4	46.583	O5-N1-O6	111.2	34.048
O1-C1-H1	110.2	39.545	O6-N1-O7	131.1	29.981
O2-CA-CB	106.9	40.242	O8-N2-OA	111.1	44.660
O2-CA-HA	110.1	29.973	O8-N2-O9	118.0	34.056
O2-CA-C9	112.8	53.169	O9-N2-OA	130.9	36.758
O2-C1-C2	108.3	48.945	OB-N3-OC	112.5	37.951
O3-C7-C8	108.2	47.206	OB-N3-OD	117.2	36.769
O3-C4-H4	111.1	21.617	OD-N3-OC	130.3	35.003
C6-OB-N3	114.2	39.895	OE-N4-OG	117.7	47.453
C6-C5-H5	106.3	30.776	OE-N4-OF	111.2	53.902

NC Force-Field Bonding Parameters

Table 5 - Bond angles and their associated force constants for NC

angle label	angle (°)	angle force constant kcal mol^{-1}	angle label	angle (°)	angle force constant kcal mol^{-1}
OE-C8-C9	106.9	36.954	H1-C1-O2	110.9	16.912
OE-C8-H8	109.9	87.142	H2-C2-O5	110.0	48.895
OF-N4-OG	131.1	69.151	H3-C3-O8	108.6	34.106
OH-N5-OI	111.2	55.446	H6-C6-OB	110.0	27.343
OH-N5-OJ	118.4	52.591	H7-C6-OB	110.0	24.304
OH-C9-H9	108.9	46.239	H7-C6-H6	109.7	31.314
OH-C9-CA	107.6	45.535	H8-C8-C9	110.5	55.266
OJ-N5-OI	130.5	82.862	HA-CA-CB	109.3	50.527
OK-N6-OM	117.1	57.325	HB-CB-CC	108.7	19.454
OK-N6-OL	112.5	57.329	HC-CC-OK	110.1	41.757
OL-N6-OM	130.4	101.28	HD-CC-OK	109.6	39.516
H1-C1-C2	110.3	50.458	HD-CC-HC	110.6	16.169

NC Force-Field Bonding Parameters

Table 6 - Bond lengths and their associated force constants for NC

bond label	bond length (Å)	bond force constant kcal mol^{-1}	bond label	bond length (Å)	bond force constant kcal mol^{-1}
C1-O1	1.418	239.053	CC-OK	1.443	215.298
C1-H1	1.099	76.391	N1-O6	1.192	606.817
C1-O2	1.398	202.201	N1-O7	1.201	569.798
C1-C2	1.538	73.590	O8-N2	1.459	41.589
C2-C3	1.529	173.643	N2-O9	1.200	513.678
C2-H2	1.090	492.373	N2-OA	1.194	134.523
C2-O5	1.436	184.887	OB-N3	1.425	86.445
C3-C4	1.533	207.598	N3-OD	1.206	547.654
C3-H3	1.092	326.109	N3-OC	1.198	589.928
C3-O8	1.438	189.688	OE-N4	1.462	25.921
C4-C5	1.543	178.092	N4-OF	1.193	518.846
C4-O3	1.424	216.279	N4-OG	1.199	454.922
C4-H4	1.095	153.217	OH-N5	1.445	51.727
C5-O1	1.432	174.002	N5-OJ	1.198	506.022
C5-C6	1.519	211.477	N5-OI	1.199	204.762
C5-H5	1.010	313.828	OK-N6	1.428	132.208
O2-CA	1.424	216.279	N6-OL	1.197	219.723
O3-C7	1.398	216.279	N6-OM	1.206	165.962
C6-H7	1.089	314.277	O5-N1	1.460	103.967
C6-H6	1.090	264.806			
C6-OB	1.446	226.092			
C7-O3	1.398	202.201			
C7-C8	1.533	106.275			
C7-O4	1.427	278.244			
C7-HE	1.104	282.007			
C8-OE	1.432	193.333			
C8-H8	1.091	336.078			
C8-C9	1.533	177.711			
C9-OH	1.442	176.667			
C9-CA	1.540	166.559			
C9-H9	1.091	147.034			
CA-HA	1.097	270.248			
CA-CB	1.545	97.561			
CB-O4	1.419	244.525			
CB-HB	1.099	294.432			
CB-CC	1.518	198.880			
CC-HD	1.089	295.255			
CC-HC	1.091	303.253			

NC Force-Field Non-Bonding Parameters

Table 7 - Dihedral angles for NC

Dihedral Angle	Number of paths [a]	V_n [b]	γ [c]	n [d]
C – O – C – C	3	1.150	0.000	3.000
C – O – C – H	3	1.150	0.000	3.000
C – C – C – C	1	0.200	180.0	1.000
C – C – C – H	1	0.160	0.000	3.000
C – C – C – O	9	1.400	0.000	3.000
C – C – O – N	3	1.150	0.000	3.000
C – O – N – O	1	1.100	180.0	2.000
C – O – C – O	9	1.400	0.000	3.000
O – C – C – O	1	1.175	0.000	2.000
O – C – C – H	1	0.250	0.000	1.000
N – O – C – H	3	1.150	0.000	3.000
H – C – C – H	0	0.150	0.000	3.000

a – number of bond paths that total V_n must be divided by, b – magnitude of the torsion in kcal mol^{-1}, c – phase angle in degrees, d – periodicity of the torsion

Table 8 - Initial Lennard-Jones parameters for NC

Atom	R_{min} [a]	ε [b]
C	1.9080	0.1094
O_{ether}	1.6837	0.1700
N	1.8240	0.1700
$O_{nitro\ grp.}$	1.6612	0.2100
H	1.4870	0.0157

a - the distance where the potential reaches a minimum in Angstroms ($\sigma \times 2^{1/6}$), b - the potential well depth in kcal mol^{-1}

Figure 3 - Atom types for NG-N1

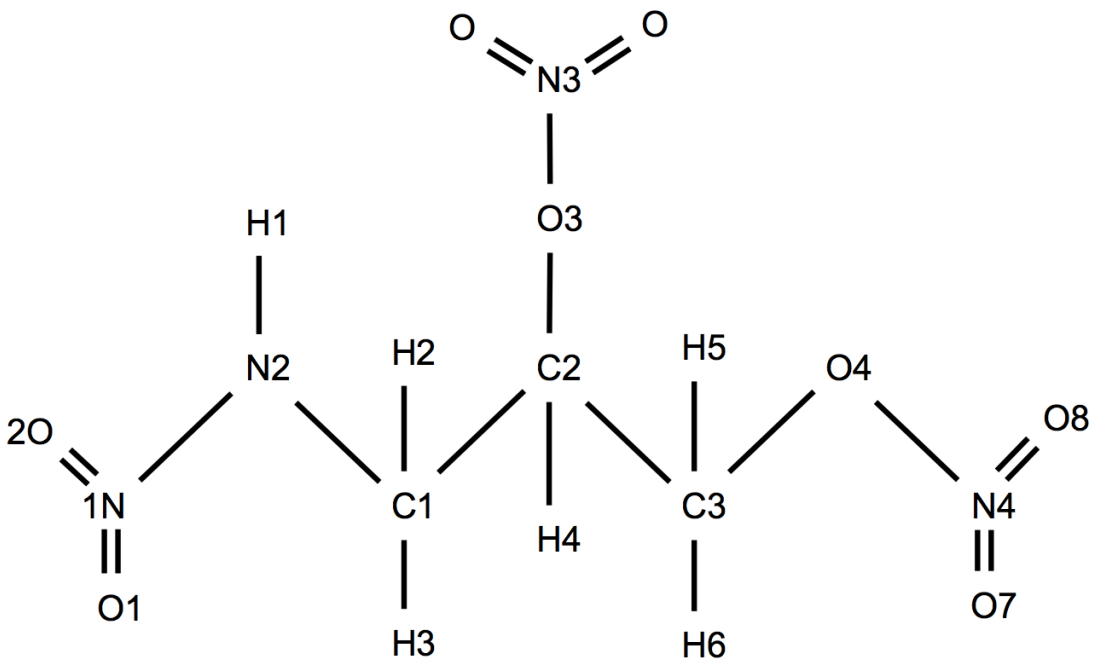

NG-N1 Force-Field Bonding Parameters

Table 9 - Bond angles and their associated force constants for NG-N1

angle label	angle (°)	angle force constant kcal mol^{-1}	angle label	angle (°)	angle force constant kcal mol^{-1}
N1-N2-H1	109.2	44.456	C2-C3-H5	110.6	40.805
N1-N2-C1	119.6	53.399	C2-C3-H6	113.9	35.379
O1-N1-O2	126.9	32.668	C2-O3-N3	114.2	36.206
O1-N1-N2	115.9	45.328	C3-C2-O3	115.1	38.968
O2-N1-N2	117.2	49.030	C3-C2-H4	105.9	20.409
N2-C1-H2	110.5	21.422	C3-O4-N4	114.2	36.206
N2-C1-H3	106.1	45.849	O3-C2-H4	99.80	42.500
N2-C1-C2	115.1	43.126	O3-N3-O5	117.0	45.368
H1-N2-C1	119.2	16.728	O3-N3-O6	112.3	40.518
H2-C1-H3	108.4	17.335	O4-C3-H5	110.0	27.784
H2-C1-C2	108.9	17.579	O4-C3-H6	109.7	40.766
H3-C1-C2	107.9	39.138	O4-N4-O7	117.0	45.368
C1-C2-C3	116.6	45.130	O4-N4-O8	112.3	40.518
C1-C2-O3	111.1	32.356	O5-N3-O6	130.5	67.287
C1-C2-H4	106.3	45.519	O7-N4-O8	130.6	58.512
C2-C3-O4	101.9	60.140	H5-C3-H6	110.4	42.5

Table 10 - Bond lengths and their associated force constants for NG-N1

bond label	bond length (Å)	bond force constant kcal mol^{-1}	bond label	bond length (Å)	bond force constant kcal mol^{-1}
N1-O1	1.220	530.96	C2-H4	1.094	88.641
N1-O2	1.222	515.10	C3-O4	1.449	144.48
N1-N2	1.388	163.58	C3-H5	1.091	262.88
N2-H1	1.012	353.36	C3-H6	1.084	241.61
N2-C1	1.459	243.44	O4-N4	1.432	115.55
H2-C1	1.093	320.79	O3-N3	1.472	115.55
H3-C1	1.091	101.87	N3-O5	1.202	590.69
C1-C2	1.537	249.54	N3-O6	1.194	383.69
C2-C3	1.536	185.49	N4-O7	1.204	568.39
C2-O3	1.448	170.08	N4-O8	1.197	598.04

NG-N1 Force-Field Non-Bonding Parameters

Table 11 - Dihedral angles for NG-N1

Dihedral Angle	Number of paths [a]	V_n [b]	γ [c]	n [d]
C – C – C – O_{ether}	1	0.300	180.0	2.000
N_{amine} – C – C – O_{ether}	1	0.300	180.0	2.000
H – C – C – H	1	0.300	180.0	2.000
N_{nitro} – N_{amine} – C – H	1	2.500	180.0	2.000
N_{nitro} – N_{amine} – C – C	1	2.500	180.0	2.000
O_{nitro} – N amine – N_{nitro} – H	1	1.150	000.0	2.000
O_{nitro} – N amine – N_{nitro} – C	1	1.150	000.0	2.000
N amine – C – C – C	1	0.300	180.0	2.000
N amine – C – C – H	1	0.300	180.0	2.000
H – N_{amine} – C – H	1	2.500	180.0	2.000
H – N_{amine} – C – C	1	2.500	180.0	2.000
H – C – C – C	1	0.300	180.0	2.000
H – C – C – O_{ether}	1	0.300	180.0	2.000
C – C – O_{ether} – N_{nitro}	3	1.150	000.0	3.000
C – O_{ether} – N_{nitro} – O_{nitro}	2	6.000	180.0	2.000
O_{ether} – C – C – O_{ether}	1	0.300	180.0	2.000
N_{nitro} – O_{ether} – C – H	3	1.150	000.0	3.000

a – number of bond paths that total V_n must be divided by, b – magnitude of the torsion in kcal mol^{-1}, c – phase angle in degrees, d – periodicity of the torsion

NG-N1 Force-Field Non-Bonding Parameters

Table 12 - Initial Lennard-Jones parameters for NG-N1

Atom	R_{min} [a]	ε [b]
N_{nitro}	1.8240	0.1200
N_{amine}	1.8240	0.1700
O_{nitro}	1.6612	0.2100
O_{ether}	1.6837	0.1700
C	1.9080	0.1094
H_{amine}	0.6000	0.0157
H	1.4870	0.0157

a - the distance where the potential reaches a minimum in Angstroms ($\sigma \times 2^{1/6}$), b - the potential well depth in kcal mol^{-1}

Figure 4 - Atom types for EC

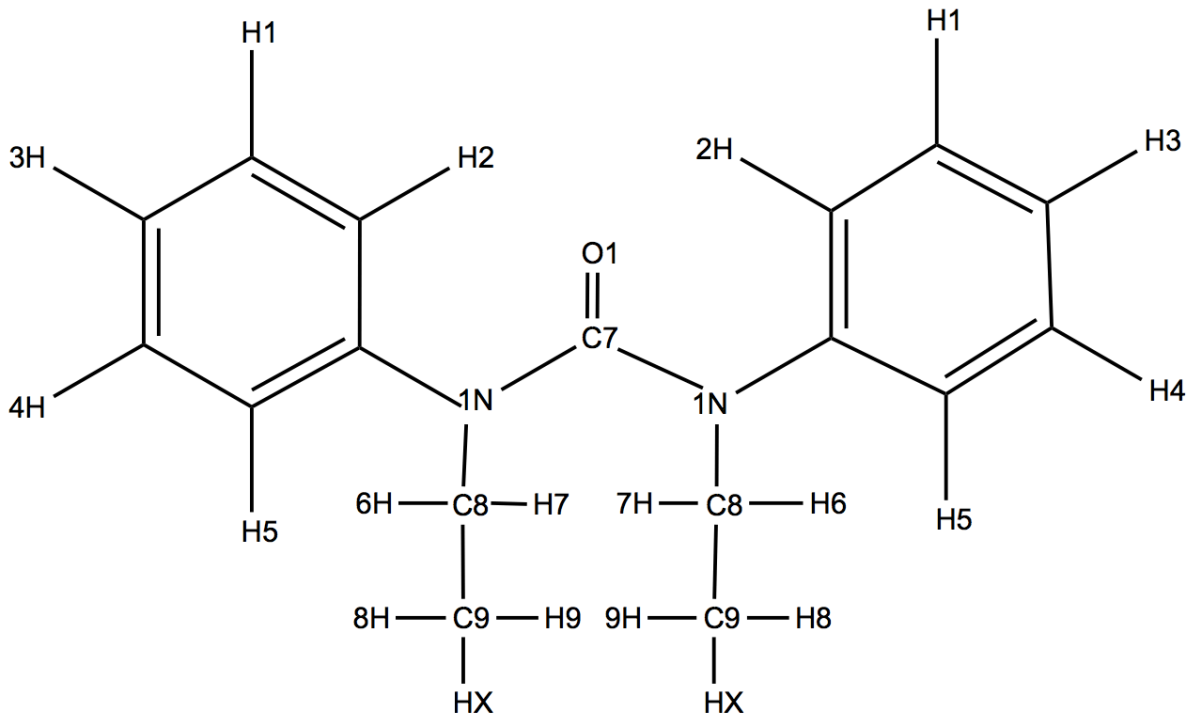

EC Force-Field Bonding Parameters

Table 13 - Bond angles and their associated force constants for EC

angle label	angle (°)	angle force constant kcal mol^{-1}	angle label	angle (°)	angle force constant kcal mol^{-1}
C4-C6-C5	120.1	50.753	C3-C4-H4	120.2	9.196
C4-C6-H5	120.1	27.276	C3-C1-H1	120.1	28.583
C4-C3-C1	119.6	53.963	N1-C7-N1	115.2	37.543
C4-C3-H3	120.1	43.327	N1-C7-O1	122.4	41.923
C6-C4-C3	120.1	67.422	N1-C8-C9	113.2	49.143
C6-C4-H4	119.7	38.032	N1-C8-H7	107.8	27.705
C6-C5-C2	119.5	74.000	N1-C8-H6	109.3	41.157
C6-C5-N1	119.8	56.555	C7-N1-C8	121.7	39.851
C5-C6-H5	119.6	28.835	C8-C9-H8	111.1	49.577
C5-C2-C1	120.1	54.231	C8-C9-HX	109.7	20.654
C5-C2-H2	119.3	35.361	C8-C9-H9	111.7	32.833
C5-N1-C7	117.3	37.401	C9-C8-H7	109.9	29.740
C5-N1-C8	115.7	36.180	C9-C8-H6	109.6	45.166
C2-C5-N1	120.8	63.310	H7-C8-H6	107.0	18.086
C2-C1-C3	120.4	51.354	HX-C9-H9	108.2	14.231
C2-C1-H1	119.6	27.167	HX-C9-H8	108.1	22.147
C1-C2-H2	120.7	39.197	H9-C9-H8	108.1	30.004
C1-C3-H3	120.3	42.653			

Table 14 - Bond lengths and their associated force constants for EC

bond label	bond length (Å)	bond force constant kcal mol^{-1}	bond label	bond length (Å)	bond force constant kcal mol^{-1}
C4-C6	1.392	280.76	C3-H3	1.084	256.40
C4-C3	1.395	211.40	N1-C7	1.402	227.41
C4-H4	1.084	187.89	N1-C8	1.478	160.70
C6-C5	1.398	280.14	C7-O1	1.219	654.10
C6-H5	1.084	112.12	C8-C9	1.529	171.52
C5-C2	1.396	248.10	C8-H7	1.088	307.06
C5-N1	1.441	229.62	C8-H6	1.097	160.82
C2-C1	1.395	278.56	C9-H8	1.093	234.00
C2-H2	1.082	173.56	C9-H9	1.091	225.00
C1-C3	1.393	334.20	C9-HX	1.094	308.57
C1-H1	1.084	125.97	C9-H9	1.093	288.02

EC Force-Field Non-Bonding Parameters

Table 15 - Dihedral angles for EC

Dihedral Angle	Number of paths [a]	V_n [b]	γ [c]	n [d]
$C_{ar} - C_{ar} - C_{ar} - C_{ar}$	1	14.50	180.0	2.000
$C_{ar} - C_{ar} - C_{ar} - N$	1	14.50	180.0	2.000
$C_{ar} - C_{ar} - C_{ar} - H$	1	1.100	180.0	2.000
$C_{ar} - C_{ar} - N - C_{carbonyl}$	4	1.800	180.0	2.000
$C_{ar} - C_{ar} - N - C_{al}$	4	1.800	180.0	2.000
C – N – C – N	4	10.00	180.0	2.000
C – N – C – O	4	10.00	180.0	2.000
$C_{ar} - N - C_{al} - C_{al}$	6	1.800	0.000	3.000
$C_{ar} - N - C_{al} - H$	6	1.800	0.000	3.000
$H - C_{ar} - C_{ar} - H$	1	1.100	180.0	2.000
$H - C_{ar} - C_{ar} - N$	1	14.50	180.0	2.000
$H - C_{al} - C_{al} - N$	1	0.300	180.0	2.000
$C_{carbonyl} - N - C_{al} - C_{al}$	6	1.800	0.000	3.000
$C_{carbonyl} - N - C_{al} - H$	6	1.800	0.000	3.000
$H - C_{al} - C_{al} - H$	1	0.300	180.0	2.000

a – number of bond paths that total V_n must be divided by, b – magnitude of the torsion in kcal mol^{-1}, c – phase angle in degrees, d – periodicity of the torsion, ar – aromatic, al – aliphatic

EC Force-Field Non-Bonding Parameters

Table 16 - Initial Lennard-Jones parameters for EC

Atom	R_{min} [a]	ε [b]
N	1.8240	0.1700
O	1.6612	0.2100
C_{ar}	1.9080	0.0860
H_{ar}	1.4590	0.0150
$C_{carbonyl}$	1.9080	0.0860
C_{al}	1.9080	0.1094
H_{al}	1.4870	0.0157

a - the distance where the potential reaches a minimum in Angstroms ($\sigma \times 2^{1/6}$), b - the potential well depth in kcal mol

Appendix 3 - Comparison of Bonding Terms with QM Terms

Comparison of QM, MD and Experimental Bond Angles for 2,4-DNEB

121.426	117.981	120.014	118.345	118.495	118.926	118.694	120.334	115.603	116.089	128.396	120.074	118.573	123.897	119.030
118.33	120.9	118.66	119.71	117.3	117.61	121.44	122.92	115.44	115	125.76	117.81	117.22	121.64	118.32
3.096	2.919	1.354	1.365	1.195	1.316	2.746	2.586	0.163	1.089	2.636	2.264	1.3534	2.257	0.710
C1C2C3	C1C2H1	C1C6C5	C1C6H2	C1N2O1	C1N2O2	C2C1C6	C2C3C4	C2C3N1	C3C4C5	C3C4C7	C3N1O3	C3N1O4	C4C3N1	C4C5H6
2.6	-2.4	1.1	-1.1	1.0	1.1	-2.3	-2.1	0.1	0.9	2.1	1.9	1.2	1.9	0.6
116.707	121.717	116.707	121.717	117.533	117.533	122.64	122.64	118.36	116.707	121.717	117.533	117.533	118.36	121.717
4.720	3.736	3.307	3.372	0.961	1.393	3.946	2.306	2.757	0.614	6.680	2.541	1.040	5.537	2.687
-4.0%	3.1%	-2.8%	2.8%	-0.8%	-1.2%	3.2%	1.9%	2.3%	0.5%	-5.5%	-2.2%	-0.9%	-4.7%	2.2%

DNEB ANGLES

MD

QM

difference between QM and MD %

DNEB ANGLES

MD

Expt

difference between MD and expt

< 3%	27/37
	difference between QM and expt

Overall bonds and angles	< 3%	66%

116.707	121.717	116.707	121.717	117.533	117.5333	122.64	122.64	118.36	116.707	121.717	117.533	117.533	118.36	121.717
118.33	120.9	118.66	119.71	117.3	117.61	121.44	122.92	115.44	115	125.76	117.81	117.22	121.64	118.32
1.623	0.817	1.953	2.007	0.233	0.077	1.2	0.280	2.92	1.707	4.0433	0.277	0.3136	-3.28	3.397
-1.39%	0.67%	-1.67%	1.65%	0.20%	-0.07%	0.98%	-0.23%	2.47%	1.46%	-3.32%	-0.24%	0.27%	-2.77%	2.79%

Comparison of QM, MD and Experimental Bond Angles for 2,4-DNEB

114.3040	109.9478	110.183	115.226	123.150	116.888	111.8087	111.9372	120.385	121.294	108.044	108.4487	104.893	107.205	107.155
112.86	107.33	110.8	118.24	122.63	119.05	111.18	110.85	120.77	121.62	109.1	109.31	107.26	112.86	107.33
1.444	2.617	0.617	3.0140	0.520	2.162	0.628	1.087	0.385	0.326	1.0564	0.862	2.367	5.655	0.175
C4C7C8	C4C7H3a	C4C7H3b	C5C4C7	C6C5C4	C6C5H6	C7C8H4a	C7C8H4b	H1C2C3	H2C6C5	H3aC7C8	H3bC7C8	H3C7H3	C4C7C8	C4C7H3a
1.3	2.4	-0.6	-2.5	0.4	-1.8	0.6	1.0	-0.3	-0.3	-1.0	-0.8	-2.2	-5.0	-0.2
112.58	110.5	109.4	121.717	116.707	121.717	109.4	111	121.717	121.717	109.3	107.9	107	112.58	110.5
1.724	0.553	0.783	6.491	6.444	4.829	2.408	0.937	1.331	0.422	1.256	0.548	2.107	5.375	3.345
-1.5%	0.5%	-0.7%	5.3%	-5.5%	4.0%	-2.2%	-0.8%	1.1%	0.3%	1.1%	-0.5%	2.0%	4.8%	3.0%
112.58	110.5	109.4	121.7177	116.7077	121.71767	109.4	111	121.7177	121.717	109.3	107.9	107	112.58	110.5
112.86	107.33	110.8	118.24	122.63	119.05	111.18	110.85	120.77	121.62	109.1	109.31	107.26	112.86	107.33
-0.280	3.17	-1.400	3.477	-5.923	2.667	-1.78	0.150	0.947	0.097	0.200	-1.41	-0.260	-0.280	3.17
-0.25%	2.87%	-1.28%	2.86%	-5.08%	2.19%	-1.63%	0.14%	0.78%	0.08%	0.18%	-1.31%	-0.24%	-0.25%	2.87%

107.805	120.777	120.353	122.255	121.026
108.55	119.04	119.52	125.09	124.96
0.745	1.737	0.8335	2.835	3.934
H4C8H4	N2C1C2	N2C1C6	O1N2O2	O3N1O4
-0.7	1.5	0.7	-2.3	-3.1
109.7	118.36	118.36	124.893	124.893
1.895	2.417	1.993	2.638	3.867
1.7%	-2.0%	-1.7%	2.1%	3.1%
109.7	118.36	118.36	124.893	124.893
108.55	119.04	119.52	125.09	124.96
1.150	0.680	-1.16	0.197	0.0676
1.05%	-0.57%	-0.98%	-0.16%	-0.05%

Comparison of QM, MD and Experimental Bond Lengths for 2,4-DNEB

1.400	1.410	1.547	1.421	1.082	1.438	1.582	1.420	1.085	1.3954	1.084	1.5587	1.091	1.091	1.091
1.38	1.39	1.47	1.39	1.08	1.4	1.48	1.4	1.08	1.38	1.08	1.54	1.09	1.08	1.09
0.020	0.020	0.077	0.031	0.002	0.038	0.102	0.020	0.005	0.015	0.0042	0.018	0.001	0.011	0.001
C1C2	C1C6	C1N2	C2C3	C2H1	C3C4	C3N1	C4C5	C5H6	C6C5	C6H2	C7C8	C7H3a	C7H3b	C8H4a
1.5	1.4	5.2	2.2	0.2	2.7	6.9	1.4	0.5	1.1	0.3	1.2	0.0	1.0	0.1
1.374	1.374	1.477	1.3743	1.032	1.374	1.477	1.374	1.0321	1.374	1.032	1.5234	0.995	0.999	1.042
0.026	0.0357	0.070	0.0466	0.050	0.063	0.105	0.046	0.0531	0.021	0.051	0.034	0.096	0.092	0.049
-1.9%	-2.6%	-4.7%	-3.4%	-4.8%	-4.6%	-7.1%	-3.3%	-5.2%	-1.5%	-5.0%	-2.3%	-9.6%	-9.2%	-4.7%

DNEB BONDS

MD

QM

difference between QM and MD %

DNEB BONDS

MD

Expt

difference between MD and expt

< 3% 12 of 22

difference between QM and expt

1.374	1.374	1.477	1.374	1.032	1.374	1.477	1.374	1.032	1.374	1.032	1.5234	0.995	0.999	1.042
1.38	1.39	1.47	1.39	1.08	1.4	1.48	1.4	1.08	1.38	1.08	1.54	1.09	1.08	1.09
0.007	0.0157	0.007	0.0157	0.048	0.026	0.003	0.026	0.048	0.006	0.0479	0.0166	0.095	0.081	-0.048
-0.41%	-1.14%	0.50%	-1.14%	-4.64%	-1.87%	-0.18%	-1.87%	-4.64%	-0.41%	-4.64%	-1.09%	-9.55%	-8.11%	-4.61%

1.091	1.097	1.226	1.227	1.229	1.226	1.539
1.09	1.09	1.22	1.22	1.22	1.22	1.51
0.004	0.007	0.006	0.007	0.009	0.006	0.029
C8H4b	C8H5	N1O3	N1O4	N2O1	N2O2	C4C7
0.1	0.6	0.5	0.6	0.7	0.5	1.9
1.011	1.02	1.208	1.208	1.208	1.208	1.5118
0.080	0.077	0.017	0.018	0.021	0.018	0.027
-7.9%	-7.5%	-1.4%	-1.5%	-1.7%	-1.5%	-1.8%
1.011	1.02	1.208	1.208	1.208	1.208	1.5118
1.09	1.09	1.22	1.22	1.22	1.22	1.51
0.079	0.070	0.012	0.012	0.012	0.012	0.002
-7.81%	-6.86%	-0.97%	-0.97%	-0.97%	-0.97%	0.12%

Comparison of QM, MD and Experimental Bond Angles for 2,4,6-TNEB

118.8421	121.5439	121.514	117.3969	112.7288	121.5433	111.4888	111.4641	118.3242	118.357	114.7422	122.4651	122.3468	120.5891	120.6422
121.21	124.2	124.2	114.56	114.56	118.3	120.79	120.79	117.18	117.18	113.69	123.09	123.09	118.07	118.07
-2.36785	-2.65614	-2.68599	2.836866	-1.83123	3.24332	-9.30119	-9.32586	1.144241	1.176954	1.052193	-0.62491	-0.74323	2.519075	2.572196
C1C2C1	C1C3C4a	C1C3C4b	C1C3N2a	C1C3N2b	C2C1C3b	C2C1H1a	C2C1H1b	C2N1O3a	C2N1O3b	C3C4C3	C3C4C5a	C3C4C5b	C3N2O1a	C3N2O1b
-2.0	-2.1	-2.2	2.5	-1.6	2.7	-7.7	-7.7	1.0	1.0	0.9	-0.5	-0.6	2.1	2.2
122.64	122.64	122.64	118.36	118.36	116.7067	121.7167	121.7167	117.5333	117.5333	116.7067	121.7167	121.7167	117.5333	117.5333
3.797853	1.096145	1.125994	0.963134	5.631234	-4.83665	10.22786	10.25253	-0.79091	-0.82362	1.964474	-0.74842	-0.6301	-3.05574	-3.10886
3.10%	0.89%	0.92%	0.81%	4.76%	-4.14%	8.40%	8.42%	-0.67%	-0.70%	1.68%	-0.61%	-0.52%	-2.60%	-2.65%

TNEB ANGLES

MD
QM
difference between QM and MD

TNEB ANGLES

MD
Expt
difference between MD and expt

< 2%	56%	22/39
< 3%	77%	30/39

Overall bonds and angles

	< 3%	67%

difference between QM and expt

122.64	122.64	122.64	118.36	118.36	116.7067	121.7167	121.7167	117.5333	117.5333	116.7067	121.7167	121.7167	117.5333	117.5333
121.21	124.2	124.2	114.56	114.56	118.3	120.79	120.79	117.18	117.18	113.69	123.09	123.09	118.07	118.07
1.43	-1.56	-1.56	3.8	3.8	-1.59333	0.926667	0.926667	0.353333	0.353333	3.016667	-1.37333	-1.37333	-0.53667	-0.53667
1.17%	-1.27%	-1.27%	3.21%	3.21%	-1.37%	0.76%	0.76%	0.30%	0.30%	2.58%	-1.13%	-1.13%	-0.46%	-0.46%

Comparison of QM, MD and Experimental Bond Angles for 2,4,6-TNEB

117.3969	117.2679	125.2263	125.1907	114.6349	110.1945	110.1663	111.6305	111.6373	108.5974	108.809	119.0718	119.039	103.4156	109.0844
116.43	116.43	121.22	121.22	114.2	108.67	108.67	111	111	109.02	109.02	120.91	120.91	107.03	108.89
0.966866	0.83794	4.006347	3.970745	0.434857	1.524546	1.496252	0.630485	0.637346	-0.42256	-0.21105	-1.83822	-1.87099	-3.61441	0.194399
C3N2O2a	C3N2O2b	C4C3N2a	C4C3N2b	C4C5C6	C4C5H2a	C4C5H2b	C5C6H3a	C5C6H3b	C6C5H2a	C6C5H2b	H1C1C3a	H1C1C3b	H2C5H2	H3C6H3
0.8	0.7	3.3	3.3	0.4	1.4	1.4	0.6	0.6	-0.4	-0.2	-1.5	-1.5	-3.4	0.2
117.5333	117.5333	118.36	118.36	112.58	109.4	110.5	111	109.4	109.3	107.9	121.7167	121.7167	107	109.7
0.136467	0.265394	-6.86635	-6.83074	-2.05486	-0.79455	0.333748	-0.63049	-2.23735	0.702565	-0.90895	2.644884	2.677653	3.584415	0.615601
0.12%	0.23%	-5.80%	-5.77%	-1.83%	-0.73%	0.30%	-0.57%	-2.05%	0.64%	-0.84%	2.17%	2.20%	3.35%	0.56%
117.5333	117.5333	118.36	118.36	112.58	109.4	110.5	111	109.4	109.3	107.9	121.7167	121.7167	107	109.7
116.43	116.43	121.22	121.22	114.2	108.67	108.67	111	111	109.02	109.02	120.91	120.91	107.03	108.89
1.103333	1.103333	-2.86	-2.86	-1.62	0.73	1.83	0	-1.6	0.28	-1.12	0.806667	0.806667	-0.03	0.81
0.94%	0.94%	-2.42%	-2.42%	-1.44%	0.67%	1.66%	0.00%	-1.46%	0.26%	-1.04%	0.66%	0.66%	-0.03%	0.74%

107.3507	107.3507	120.3679	120.3465	122.9772	121.7044	121.7725	121.5261	109.0117
108.18	108.18	119.38	119.38	125.63	125.49	125.49	118.3	109.49
-0.82935	-0.82935	0.987859	0.966502	-2.65277	-3.78556	-3.71749	3.22609	-0.47828
H3C6H4a	H3C6H4b	N1C2C1a	N1C2C1b	O3N1O3	O1N2O2a	O1N2O2b	C2C1C3a	C5C6H4
-0.8	-0.8	0.8	0.8	-2.1	-3.0	-3.0	2.7	-0.4
107.6	109.7	118.36	118.36	124.8933	124.8933	124.8933	116.7067	109.3
0.249346	2.349346	-2.00786	-1.9865	1.916108	3.188889	3.120822	-4.81942	0.288283
0.23%	2.14%	-1.70%	-1.68%	1.53%	2.55%	2.50%	-4.13%	0.26%
107.6	109.7	118.36	118.36	124.8933	124.8933	124.8933	116.7067	109.3
108.18	108.18	119.38	119.38	125.63	125.49	125.49	118.3	109.49
-0.58	1.52	-1.02	-1.02	-0.73667	-0.59667	-0.59667	-1.59333	-0.19
-0.54%	1.39%	-0.86%	-0.86%	-0.59%	-0.48%	-0.48%	-1.37%	-0.17%

Comparison of QM, MD and Experimental Bond Lengths for 2,4,6-TNEB

1.393676	1.393917	1.410093	1.410154	1.083983	1.083769	1.454637	1.454848	1.584228	1.585486	1.549098	1.559485	1.087694	1.087046	1.089741
1.38	1.38	1.38	1.38	1.08	1.08	1.41	1.41	1.48	1.48	1.51	1.54	1.09	1.09	1.09
0.013676	0.013917	0.030093	0.030154	0.003983	0.003769	0.044637	0.044848	0.104228	0.105486	0.039098	0.019485	-0.00231	-0.00295	-0.00026
C1C2a	C1C2b	C1C3a	C1C3b	C1H1a	C1H1b	C3C4a	C3C4b	C3N2a	C3N2b	C4C5	C5C6	C5H2a	C5H2b	C6H3a
1.0	1.0	2.2	2.2	0.4	0.3	3.2	3.2	7.0	7.1	2.6	1.3	-0.2	-0.3	0.0
1.374333	1.374333	1.374333	1.374333	1.032111	1.032111	1.374333	1.374333	1.477333	1.477333	1.5118	1.5234	0.999	0.995	1.011
-0.01934	-0.01958	-0.03576	-0.03582	-0.05187	-0.05166	-0.0803	-0.08051	-0.10689	-0.10815	-0.0373	-0.03609	-0.08869	-0.09205	-0.07874
-1.4%	-1.4%	-2.6%	-2.6%	-5.0%	-5.0%	-5.8%	-5.9%	-7.2%	-7.3%	-2.5%	-2.4%	-8.9%	-9.3%	-7.8%
TNEB BONDS														
	MD													
	QM													
	difference between QM and MD													
TNEB BONDS														
	MD													
	Expt													
	difference between MD and expt													
< 2%	36%	8 of 22												
< 3%	50%	12 of 24												
	difference between QM and expt													
1.374333	1.374333	1.374333	1.374333	1.032111	1.032111	1.374333	1.374333	1.477333	1.477333	1.5118	1.5234	0.999	0.995	1.011
1.38	1.38	1.38	1.38	1.08	1.08	1.41	1.41	1.48	1.48	1.51	1.54	1.09	1.09	1.09
-0.00567	-0.00567	-0.00567	-0.00567	-0.04789	-0.04789	-0.03567	-0.03567	-0.00267	-0.00267	0.0018	-0.0166	-0.091	-0.095	-0.079
-0.41%	-0.41%	-0.41%	-0.41%	-4.64%	-4.64%	-2.60%	-2.60%	-0.18%	-0.18%	0.12%	-1.09%	-9.11%	-9.55%	-7.81%

Comparison of QM, MD and Experimental Bond Lengths for 2,4,6-TNEB

1.089961	1.091148	1.567958	1.224873	1.224995	1.221604	1.221044	1.229934	1.229925
1.09	1.09	1.48	1.22	1.22	1.22	1.22	1.22	1.22
-3.9E-05	0.001148	0.087958	0.004873	0.004995	0.001604	0.001044	0.009934	0.009925
C6H3b	C6H4	N1C2	N1O3a	N1O3b	N2O1a	N2O1b	N2O2a	N2O2b
0.0	0.1	5.9	0.4	0.4	0.1	0.1	0.8	0.8
1.042	1.02	1.477333	1.208333	1.208333	1.208333	1.208333	1.208333	1.208333
-0.04796	-0.07115	-0.09062	-0.01654	-0.01666	-0.01327	-0.01271	-0.0216	-0.02159
-4.6%	-7.0%	-6.1%	-1.4%	-1.4%	-1.1%	-1.1%	-1.8%	-1.8%
1.042	1.02	1.477333	1.208333	1.208333	1.208333	1.208333	1.208333	1.208333
1.09	1.09	1.48	1.22	1.22	1.22	1.22	1.22	1.22
-0.048	-0.07	-0.00267	-0.01167	-0.01167	-0.01167	-0.01167	-0.01167	-0.01167
-4.61%	-6.86%	-0.18%	-0.97%	-0.97%	-0.97%	-0.97%	-0.97%	-0.97%

Comparison of QM and Experimental Bond Angles for EC

	C4-C6-C5	C4-C6-H5	C4-C3-C1	C4-C3-H3	C6-C4-C3	C6-C4-H4	C6-C5-C2	C6-C5-N1	C5-C6-H5	C5-C2-C1	C5-C2-H2	C5-N1-C7	C5-N1-C8
QM value	120.1	120.1	119.6	120.1	120.1	119.7	119.5	119.8	119.6	120.1	119.3	117.3	115.7
Expt betz	119.73	120.1	120.01	120	120.8	119.7	119.71	119.17	120.1	120	120.1	123.66	115.12
	119.91	120	119.97	120	120.51	120	120.02	118.95	120	119.75	120	123.78	115.16
Expt ganis	117.7		120.5		121.5		120.9	118.2		119		122.9	115.7
	119.6		118.9		120.5		120.8	118.3		119.3		123	116.2
Expt Av	119.235	120.05	119.845	120	120.8275	119.85	120.3575	118.655	120.05	119.5125	120.05	123.335	115.545
Difference QM – Expt	0.865	0.050	0.245	0.1	0.728	0.150	0.8585	1.145	0.450	0.587	-0.75	6.035	0.155
Difference / Expt %	0.73%	0.04%	-0.20%	0.08%	-0.60%	-0.13%	-0.71%	0.96%	-0.37%	0.49%	-0.62%	-4.89%	0.13%

	C2-C5-N1	C2-C1-C3	C2-C1-H1	C1-C2-H2	C1-C3-H3	C3-C4-H4	C3-C1-H1	N1-C7-N1	N1-C7-O1	N1-C8-C9	N1-C8-H7	N1-C8-H6	C7-N1-C8
QM value	120.8	120.4	119.6	120.7	120.3	120.2	120.1	115.2	122.4	113.2	107.8	109.3	121.7
Expt betz	120.96	120.06	120	120	120	119.7	120	117.25	121.51	112.95	109	109	116.5
	120.9	120.23	119.9	120.1	120	120	119.9		121.23	112.51	109.1	109.1	116.15
Expt ganis	120.7	120.6						117.8	119.9	111.5			117.3
	120.7	120.9							122.2	113.2			115.5
Expt Av	120.815	120.4475	119.95	120.05	120	119.85	119.95	117.525	121.21	112.54	109.05	109.05	116.3625
Difference QM – Expt	0.0150	0.0475	0.3509	0.6506	0.300	0.3509	0.150	-2.325	1.190	0.660	-1.25	0.25	5.338
Difference / Expt %	-0.01%	-0.04%	-0.29%	0.54%	0.25%	0.29%	0.13%	-1.98%	0.98%	0.59%	-1.15%	0.23%	4.59%

	C8-C9-H8	C8-C9-HX	C8-C9-H9	C9-C8-H7	C9-C8-H6	H7-C8-H6	HX-C9-H9	HX-C9-H8	H9-C9-H8
QM value	111.1	109.7	111.7	109.9	109.6	107	108.2	108.1	108.1
Expt betz	109.5	109.5	109.5	109.1	109.1	107.8	109.5	109.5	109.5
	109.5	109.5	109.5	109	109	107.8	109.5	109.5	109.5
Expt ganis									
Expt Av	109.5	109.5	109.5	109.05	109.05	107.8	109.5	109.5	109.5
Difference QM – Expt	1.600	0.200	2.2	0.850	0.550	0.800	-1.3	1.400	1.400
Difference / Expt %	1.46%	0.18%	2.01%	0.78%	0.50%	-0.74%	-1.19%	-1.28%	-1.28%

Comparison of QM and Experimental Bond Lengths for EC

	C4-C6	C4-C3	C4-H4	C6-C5	C5-C2	C6-H5	C5-N1	C2-C1	C2-H2	C1-C3	C1-H1	C3-H3
QM value	1.392	1.395	1.084	1.398	1.396	1.084	1.441	1.395	1.082	1.393	1.084	1.084
Expt betz	1.384	1.377	0.95	1.389	1.39	0.95	1.431	1.382	0.95	1.379	0.95	0.95
	1.385	1.385	0.95	1.382	1.386	0.95	1.435	1.384	0.95	1.378	0.95	0.95
Expt ganis	1.371	1.398		1.387	1.377		1.443	1.381		1.388		
	1.404	1.359		1.395	1.375		1.44	1.414		1.347		
Expt Av	1.386	1.37975	0.95	1.38825	1.382	0.95	1.43725	1.39025	0.95	1.373	0.95	0.95
Difference QM – Expt	0.006	0.01525	0.134	0.00975	0.014	0.134	0.00375	0.00475	0.132	0.02	0.134	0.134
Difference / Expt %	0.43%	1.11%	14.11%	0.70%	1.01%	14.11%	0.26%	0.34%	13.89%	1.46%	14.11%	14.11%

	N1-C7	N1-C8	C7-O1	C8-C9	C8-H7	C8-H6	C9-H8	C9-H9	C9-HX
QM value	1.402	1.478	1.219	1.529	1.088	1.097	1.093	1.091	1.094
Expt betz	1.38	1.473	1.227	1.507	0.99	0.99	0.98	0.98	0.98
	1.376	1.47		1.514	0.99	0.99	0.98	0.98	0.98
Expt ganis	1.374	1.469	1.217	1.505					
	1.385	1.479		1.506					
Expt Av	1.37875	1.47275	1.222	1.508	0.99	0.99	0.98	0.98	0.98
Difference QM – Expt	0.02325	0.005	-0.003	0.021	0.098	0.107	0.113	0.111	0.114
Difference QM / Expt %	1.69%	0.36%	-0.25%	1.39%	9.90%	10.81%	11.53%	11.33%	11.63%

Comparison of QM and Experimental Bond Angles for NG-N1

	N1-N2-H1	N1-N2-C1	O1-N1-O2	O1-N1-N2	O2-N1-N2	N2-C1-H2	N2-C1-H3	N2-C1-C2	H1-N2-C1	H2-C1-H3	H2-C1-C2	H3-C1-C2	C1-C2-C3
QM value	109.2	119.6	126.9	115.9	117.2	110.5	106.1	115.1	119.2	108.4	108.9	107.9	116.6
Expt alten	110.1	121.5	124.3	118.5	117.2	109	108.4	114.7	128.3	104	109	113.4	113
	110	120.8	124.9	117.3	117.7	108.7	104	112.2	125	109	113.6	109	114.3
Expt Av	110.05	121.15	124.6	117.9	117.45	108.85	106.2	113.45	126.65	106.5	111.3	111.2	113.65
Difference QM – Expt	-0.850	-1.550	2.300	-2	-0.25	1.650	-0.100	1.650	-7.45	1.900	-2.400	-3.3	2.950
Difference QM / Expt %	-0.77%	-1.28%	1.85%	-1.70%	-0.21%	1.52%	-0.09%	1.45%	-5.88%	1.78%	-2.16%	-2.97%	2.60%

	C1-C2-O3	C1-C2-H4	C2-C3-O4	C2-C3-H5	C2-C3-H6	C2-O3-N3	C3-C2-O3	C3-C2-H4	C3-O4-N4	O3-C2-H4	O3-N3-O5	O3-N3-O6
QM value	111.1	106.3	101.9	110.6	113.9	114.2	115.1	105.9	114.2	99.8	117	112.3
Expt alten	105.8	111.8	104.1	124	112	115.7	111.1	107.5	115	107.7	118	111.7
	104.7	115	100.5	107.3	108	115	110	101	109.3	112	117.8	112.8
			115						115.1			
Expt Av	105.25	113.4	106.5	115.65	110	115.35	110.55	104.25	113.13	109.85	117.9	112.25
Difference QM – Expt	5.850	-7.1001	-4.633	-5.0501	3.900	-1.150	4.55	1.650	1.067	-10.05	-0.900	0.050
Difference QM / Expt %	5.56%	-6.26%	-4.35%	-4.37%	3.55%	-1.00%	4.12%	1.58%	0.94%	-9.15%	-0.76%	0.04%

	O4-C3-H5	O4-C3-H6	O4-N4-O7	O4-N4-O8	O5-N3-O6	O7-N4-O8	H5-C3-H6
QM value	110	109.7	117	112.3	130.5	130.6	110.4
Expt alten	97	106	116.8	112.8	130.3	130.4	111
	125	114	119.6	121.1	129.3	113.3	101
	94	127	106.9	106.4		130.3	
			112.2	104.4		127.8	
Expt Av	105.3	115.7	113.875	111.175	129.8	125.45	106
Difference QM – Expt	4.667	-5.967	3.125	1.125	0.670	5.1509	4.4001
Difference QM / Expt %	4.43%	-5.16%	2.74%	1.01%	0.54%	4.11%	4.15%

Comparison of QM and Experimental Bond Lengths for NG-N1

	N1-O1	N1-O2	N1-N2	N2-C1	H2-C1	H3-C1	C1-C2	C2-C3	C2-O3	C3-O4	C3-H5	O4-N4	O3-N3	N3-O5	N3-O6	N4-O7	N4-O8
QM value	1.22	1.222	1.388	1.459	1.093	1.091	1.537	1.536	1.448	1.449	1.091	1.432	1.472	1.202	1.194	1.204	1.197
Expt alten	1.23	1.237	1.33	1.431	0.99	1.04	1.506	1.503	1.445	1.45	0.99	1.386	1.416	1.187	1.193	1.17	1.216
	1.224	1.238	1.323	1.438	1.01	0.9	1.517	1.503	1.454	1.529	0.95	1.396	1.402	1.188	1.203	1.173	1.115
										1.4		1.428				1.286	1.156
Expt Av	1.227	1.2375	1.3265	1.4345	1	0.97	1.5115	1.503	1.4495	1.4895	0.97	1.391	1.409	1.1875	1.198	1.1715	1.1655
Difference QM – Expt	-0.007	-0.0155	0.0615	0.0245	0.093	0.121	0.0255	0.033	-0.0015	-0.0405	0.121	0.041	0.063	0.0145	-0.004	0.0325	0.0315
Difference / Expt	-0.0057	-0.0125	0.0464	0.0170	0.093	0.1247	0.01687	0.0220	-0.0010	-0.0272	0.1247	0.0295	0.0447	0.0122	-0.0033	0.0277	0.0270
Difference / Expt %	-0.57%	-1.25%	4.64%	1.71%	9.30%	12.47%	1.69%	2.20%	-0.10%	-2.72%	12.47%	2.95%	4.47%	1.22%	-0.33%	2.77%	2.70%

Comparison of QM and Experimental Bond Angles for NC

	HB-CB-CC	CB-CC-HD	CB-CC-HC	HC-CC-OK	HD-CC-OK	CC-OK-N6	OK-N6-OM	OK-N6-OL	C8-OE-N4	OE-N4-OG	OE-N4-OF	C9-OH-N5
QM value	108.7	110.4	110.8	110.1	109.6	114	112.5	117.1	115.8	117.7	111.2	111.2
Expt	109.47	109.47	109.47	109.47	109.47	111	110.5	118.5	112.7	118.1	112.4	112.7
Expt	109.47	109.47	109.47	109.47	109.47	111	110.5	118.5	112.7	118.1	112.4	112.7
Difference QM – Expt	-0.770	0.930	1.33	0.630	0.130	3	2	-1.400	3.1009	-0.400	-1.2	-1.5
Difference QM / Expt %	-0.70%	0.85%	1.21%	0.58%	0.12%	2.70%	1.81%	-1.18%	2.75%	-0.34%	-1.07%	-1.33%

	OG-N4-OF	OI-N5-OJ	C2-O5-N1	O5-N1-O7	O5-N1-O6	O6-N1-O7	C3-O8-N2	O8-N2-OA	O8-N2-O9	OA-N2-O9	H5-C5-C6	OH-N5-OI
QM value	131.1	130.5	116.6	111.2	117.7	131.1	116.5	111.1	118	130.9	106.3	116.4
Expt	129.5	129.5	112.7	112.3	118.1	129.5	112.7	112.4	118.1	129.4	109.47	118.1
Expt	129.5	129.5	112.7	112.3	118.1	129.5	112.7	112.4	118.1	129.4	109.47	118.1
Difference QM – Expt	1.600	1	3.900	-1.100	-0.400	1.600	3.8	-1.300	-0.100	1.5	-3.17	-1.700
Difference QM / Expt %	1.24%	0.77%	3.46%	-0.98%	-0.34%	1.24%	3.37%	-1.16%	-0.08%	1.16%	-2.90%	-1.44%

	C5-C6-OB	C5-C6-H7	C5-C6-H6	H6-C6-OB	H7-C6-OB	C6-OB-N3	OB-N3-OC	OB-N3-OD	CB-CC-OK
QM value	106.8	110.8	109.5	110	110	114.2	117.2	112.5	105.2
Expt	109.47	109.47	109.47	109.47	109.47	111	118.5	110.5	109.47
Expt	109.47	109.47	109.47	109.47	109.47	111	118.5	110.5	109.47
Difference QM – Expt	-2.67	1.33	0.030	0.530	0.530	3.2	-1.3	2	-4.27
Difference QM / Expt %	-2.44%	1.21%	0.03%	0.48%	0.48%	2.88%	-1.10%	1.81%	-3.90%

Comparison of QM and Experimental Bond Lengths for NC

	C8-OE	OE-N4	N4-OF	N4-OG	C9-OH	OH-N5	N5-OI	N5-OJ	C2-O5	O5-N1	N1-O6
QM value	1.432	1.462	1.193	1.199	1.442	1.445	1.199	1.198	1.436	1.46	1.192
Expt	1.437	1.402	1.208	1.205	1.437	1.402	1.205	1.208	1.437	1.402	1.208
Expt	1.437	1.402	1.208	1.205	1.437	1.402	1.205	1.208	1.437	1.402	1.208
Difference QM – Expt	-0.005]	0.060	-0.0150	-0.006	0.0059	0.043	-0.006	-0.01	-0.001	0.058	-0.016
Difference QM / Expt %	-0.35%	4.28%	-1.24%	-0.50%	0.35%	3.07%	-0.50%	-0.83%	-0.07%	4.14%	-1.32%

	N1-O7	C3-O8	O8-N2	N2-OA	N2-O9	C5-H5	C5-C6	C6-H6	C6-H7	C6-OB	OB-N3
QM value	1.201	1.438	1.459	1.194	1.2	1.01	1.519	1.09	1.089	1.446	1.425
Expt	1.205	1.437	1.402	1.205	1.208	1.089	1.528	1.089	1.089	1.43	1.407
Expt	1.205	1.437	1.402	1.205	1.208	1.089	1.528	1.089	1.089	1.43	1.407
Difference QM – Expt	-0.004	0.001	0.057	-0.011	-0.008	-0.079	-0.009	0.001	0	0.016	0.018
Difference QM / Expt %	-0.33%	0.07%	4.07%	-0.91%	-0.66%	-7.25%	-0.59%	0.09%	0.00%	1.12%	1.28%

	N3-OC	N3-OD	CB-HB	CB-CC	CC-HC	CC-HD	CC-OK	OK-N6	N6-OL	N6-OM
QM value	1.198	1.206	1.099	1.518	1.091	1.089	1.443	1.428	1.197	1.206
Expt	1.215	1.215	1.089	1.528	1.089	1.089	1.43	1.407	1.215	1.215
Expt	1.215	1.215	1.089	1.528	1.089	1.089	1.43	1.407	1.215	1.215
Difference QM – Expt	-0.017	-0.009	0.01	-0.01	0.002	0	0.013	0.021	-0.018	-0.009
Difference QM / Expt %	-1.40%	-0.74%	0.92%	-0.65%	0.18%	0.00%	0.91%	1.49%	-1.48%	-0.74%

Appendix 4 - Refined Lennard-Jones A and B Coefficients

2,4-DNEB – LJ A and B Coefficients

```
%FLAG LENNARD_JONES_ACOEF
%FORMAT(5E16.8)
 2.58295201E+05  2.51540433E+04  1.83040314E+03  2.31070169E+05  2.22182399E+04
 2.04880834E+05  0.58502908E+05  0.30388921E+04  0.38645875E+05  4.50572207E+04
%FLAG LENNARD_JONES_BCOEF
%FORMAT(5E16.8)
 1.28145282E+02  4.73564996E+01  0.41591691E+01  1.17422201E+02  4.53998826E+01
 1.06886505E+02  0.88940538E+02  3.87246323E+01  1.78564142E+02  1.46675021E+02
```

2,4,6-TNEB – LJ A and B Coefficients

```
%FLAG LENNARD_JONES_ACOEF
%FORMAT(5E16.8)
 2.58295201E+05  2.51540433E+04  2.53040314E+03  4.29831603E+05  4.35335119E+04
 6.04308023E+05  3.55482321E+04  2.63199013E+03  5.71708117E+04  3.51607703E+03
 2.31070169E+05  2.22182399E+04  3.96031998E+05  3.20911590E+04  2.04880834E+05
 0.58502908E+05  1.30388921E+04  1.83154328E+05  1.94051493E+04  1.38645875E+05
 0.10572207E+05
%FLAG LENNARD_JONES_BCOEF
%FORMAT(5E16.8)
 2.30145282E+02  5.75564996E+01  0.53591691E+01  3.06222485E+02  7.11230755E+01
 3.92612247E+02  7.26425128E+01  0.89424645E+01  7.43919150E+01  0.34257828E+01
 2.19422201E+02  5.55998826E+01  2.94098026E+02  7.23892175E+01  2.08886505E+02
 1.90940538E+02  4.89246323E+01  2.63636834E+02  6.96295664E+01  0.80564142E+02
 1.48675021E+02
```

NG-N1 – LJ A and B Coefficients

```
%FLAG LENNARD_JONES_ACOEF
%FORMAT(5E16.8)
 6.36559929E+05  4.79838626E+05  3.49876399E+05  7.63365004E+05  5.76829342E+05
 9.14293233E+05  1.48620720E+03  0.72595236E+03  1.82601181E+03  1.09982777E-01
 7.23443375E+04  5.14261042E+04  8.66776989E+04  0.77193646E+02  7.21607703E+03
 8.06370883E+05  6.17841731E+05  9.65480466E+05  2.26678134E+03  9.41708117E+04
 0.74308023E+06  4.65546481E+05  3.40622491E+05  5.59818288E+05  0.73954408E+03
 5.03379252E+04  5.98541240E+05  3.31397723E+05
%FLAG LENNARD_JONES_BCOEF
%FORMAT(5E16.8)
 6.65640138E+02  6.68979341E+02  6.64885984E+02  7.73246427E+02  7.77220874E+02
 9.01323529E+02  2.76102750E+01  2.53505284E+01  3.09604198E+01  9.37598976E-02
 2.14373531E+02  2.11805549E+02  2.36131731E+02  3.59456373E+00  3.17257828E+01
 7.19126068E+02  7.26720080E+02  8.36907417E+02  3.06278363E+01  2.26919150E+02
 7.75612247E+02  6.32083432E+02  6.29252520E+02  7.33305958E+02  2.46567808E+01
 2.04986921E+02  6.85549272E+02  5.95732238E+02
```

EC – LJ A and B Coefficients

```
%FLAG LENNARD_JONES_ACOEF
%FORMAT(5E16.8)
 8.11971662E+05  7.54451550E+04  5.63629601E+03  8.74619071E+05  7.83627154E+04
 9.36293233E+05  5.66393458E+05  4.69908183E+04  5.98829342E+05  3.71876399E+05
 9.16822270E+05  8.51947003E+04  9.87480466E+05  6.39841731E+05  0.96308023E+06
 8.53541883E+04  6.47825601E+03  8.88776989E+04  5.36261042E+04  9.63708117E+04
 7.43607703E+03
%FLAG LENNARD_JONES_BCOEF
%FORMAT(5E16.8)
 5.79102864E+02  1.52660679E+02  2.33196588E+01  7.01361429E+02  1.74451907E+02
 8.49323529E+02  6.03666448E+02  1.51580945E+02  7.25220874E+02  6.12885984E+02
 6.47015525E+02  1.66043746E+02  7.84907417E+02  6.74720080E+02  7.23612247E+02
 1.60529845E+02  2.48642027E+01  1.84131731E+02  1.59805549E+02  1.74919150E+02
 2.65257828E+01
```

NC – LJ A & B Coefficients, the original LJ GAFF A & B Coefficients which were not altered

```
%FLAG LENNARD_JONES_ACOEF
%FORMAT(5E16.8)
 1.04308023E+06  6.28541240E+05  3.61397723E+05  9.95480466E+05  5.89818288E+05
 9.44293233E+05  6.47841731E+05  3.70622491E+05  6.06829342E+05  3.79876399E+05
 9.71708117E+04  5.33379252E+04  8.96776989E+04  5.44261042E+04  7.51607703E+03
%FLAG LENNARD_JONES_BCOEF
%FORMAT(5E16.8)
 6.75612247E+02  5.85549272E+02  4.95732238E+02  7.36907417E+02  6.33305958E+02
 8.01323529E+02  6.26720080E+02  5.29252520E+02  6.77220874E+02  5.64885984E+02
 1.26919150E+02  1.04986921E+02  1.36131731E+02  1.11805549E+02  2.17257828E+01
```

NO_2 – LJ A & B Coefficients, the original LJ GAFF A & B Coefficients which were not altered

```
%FLAG LENNARD_JONES_ACOEF
%FORMAT(5E16.8)
 9.44293233E+05  6.06829342E+05  3.79876399E+05
%FLAG LENNARD_JONES_BCOEF
%FORMAT(5E16.8)
 8.01323529E+02  6.77220874E+02  5.64885984E+02
```

K10 and R8002 – LJ A and B Coefficients

```
%FLAG LENNARD_JONES_ACOEF
%FORMAT(5E16.8)
 3.98295201E+05  3.81540433E+04  3.93040314E+03  5.59831603E+05  5.75335119E+04
 7.91308023E+05  4.85482321E+04  3.83199013E+03  6.91708117E+04  4.91607703E+03
 3.91070169E+05  3.92182399E+04  5.96031998E+05  4.60911590E+04  3.64880834E+05
 1.88502908E+05  2.90388921E+04  3.03154328E+05  3.14051493E+04  2.68645875E+05
 1.70572207E+05
%FLAG LENNARD_JONES_BCOEF
%FORMAT(5E16.8)
 3.93145282E+02  6.88564996E+01  106591691E+01   4.49222485E+02  7.64230755E+01
 4.95612247E+02  0.87425128E+02  1.02424645E+01  0.96919150E+02  1.90257828E+01
 3.42422201E+02  6.48998826E+01  3.97098026E+02  8.26892175E+01  2.91586505E+02
 2.95940538E+02  6.02246323E+01  3.96636834E+02  7.89295664E+01  2.95564142E+02
 2.81675021E+02
```

NC binder, EC, 2,4-DNEB and 2,4,6-TNEB – LJ A and B Coefficients

%FLAG LENNARD_JONES_ACOEF
%FORMAT(5E16.8)
 1.04308023E+06 6.28541240E+05 3.61397723E+05 9.95480466E+05 5.89818288E+05
 9.44293233E+05 6.47841731E+05 3.70622491E+05 6.06829342E+05 3.79876399E+05
 9.71708117E+04 5.33379252E+04 8.96776989E+04 5.44261042E+04 7.51607703E+03
 9.16822270E+05 5.57281136E+05 8.74619071E+05 5.66393458E+05 8.61541883E+04
 8.11971662E+05 8.51947003E+04 4.68711055E+04 7.83627154E+04 4.69908183E+04
 6.47825601E+03 7.54451550E+04 5.63629601E+03 5.59831603E+05 4.94288582E+05
 7.88668117E+05 5.08834397E+05 4.85482321E+04 7.35750447E+05 6.67431709E+04
 3.98295201E+05 5.75335119E+04 4.64541893E+04 7.74535450E+04 4.74688095E+04
 3.83199013E+03 7.40630009E+04 5.79840054E+03 3.81540433E+04 5.83040314E+03
 5.96031998E+05 4.72903691E+05 7.55824921E+05 4.86681987E+05 4.60911590E+04
 7.05782832E+05 6.36637279E+04 3.91070169E+05 3.92182399E+04 3.64880834E+05
 3.03154328E+05 3.35024951E+05 5.47065415E+05 3.43546042E+05 3.14051493E+04
 5.17039910E+05 4.34097263E+04 1.88502908E+05 2.90388921E+04 2.68645875E+05
 1.70572207E+05
%FLAG LENNARD_JONES_BCOEF
%FORMAT(5E16.8)
 6.75612247E+02 5.85549272E+02 4.95732238E+02 7.36907417E+02 6.33305958E+02
 8.01323529E+02 6.26720080E+02 5.29252520E+02 6.77220874E+02 5.64885984E+02
 1.26919150E+02 1.04986921E+02 1.36131731E+02 1.11805549E+02 2.17257828E+01
 6.47015525E+02 5.19163331E+02 7.01361429E+02 6.03666448E+02 1.12529845E+02
 5.79102864E+02 1.66043746E+02 9.73010751E+01 1.74451907E+02 1.51580945E+02
 2.48642027E+01 1.52660679E+02 2.33196588E+01 4.49222485E+02 5.07729638E+02
 6.41341537E+02 5.43091556E+02 0.87425128E+02 5.22420097E+02 1.01684844E+02
 3.93145282E+02 7.64230755E+01 8.27803323E+01 1.06889580E+02 8.82188690E+01
 1.02424645E+01 8.81511044E+01 1.59396732E+01 6.88564996E+01 1.36591691E+01
 3.97098026E+02 4.96625000E+02 6.27845563E+02 5.31138100E+02 1.06892175E+02
 5.11670235E+02 9.93113403E+01 3.42422201E+02 6.48998826E+01 2.91586505E+02
 3.96636834E+02 4.62597858E+02 5.91132274E+02 4.93855744E+02 9.79295664E+01
 4.84662543E+02 9.07547049E+01 2.95940538E+02 6.02246323E+01 2.95564142E+02
 4.31675021E+02

NC binder, EC, 2,4-DNEB and NG-N1 – LJ A and B Coefficients

%FLAG LENNARD_JONES_ACOEF
%FORMAT(5E16.8)
1.00508023E+06 6.25541240E+05 3.57897723E+05 9.91980466E+05 5.86318288E+05
9.40793233E+05 6.44341731E+05 3.67122491E+05 6.03329342E+05 3.76376399E+05
9.68208117E+04 5.29879252E+04 8.93276989E+04 5.40761042E+04 7.48107703E+03
9.21322270E+05 5.53781136E+05 8.79119071E+05 5.70893458E+05 8.58541883E+04
8.16471662E+05 8.59947003E+04 4.68711055E+04 7.91627154E+04 4.77908183E+04
6.52325601E+03 7.58951550E+04 5.68129601E+03 8.26331603E+05 4.90788582E+05
7.85168117E+05 5.05334397E+05 7.51982321E+04 7.32250447E+05 6.63931709E+04
6.54795201E+05 8.31835119E+04 4.61541893E+04 7.71535450E+04 4.71188095E+04
6.59699013E+03 7.37130009E+04 5.76340054E+03 6.48540433E+04 5.79540314E+03
7.92531998E+05 4.69403691E+05 7.52324921E+05 4.83181987E+05 7.17411590E+04
7.02282832E+05 6.33137279E+04 6.27570169E+05 6.18682399E+04 6.01380834E+05
5.79654328E+05 3.31524951E+05 5.43565415E+05 3.40046042E+05 4.90551493E+04
5.13539910E+05 4.30597263E+04 4.55002908E+05 4.26888921E+04 4.35145875E+05
3.07072207E+05 8.32870883E+05 4.92046481E+05 7.89865004E+05 5.06338626E+05
7.49943375E+04 7.38048344E+05 6.61599843E+04 6.59113754E+05 6.47239939E+04
6.31519950E+05 4.56126883E+05 6.63059929E+05 2.53178134E+03 1.00454408E+03
2.09101181E+03 0.99095236E+03 1.03693646E+02 2.24077561E+03 8.87487508E+01
1.81828768E+03 0.99885611E+02 1.70366606E+03 9.54165009E+02 1.75120720E+03
1.36482777E-01
%FLAG LENNARD_JONES_BCOEF
%FORMAT(5E16.8)
6.99612247E+02 6.09549272E+02 5.19732238E+02 7.60907417E+02 6.57305958E+02
8.25323529E+02 6.50720080E+02 5.53252520E+02 7.01220874E+02 5.88885984E+02
1.50919150E+02 1.28986921E+02 1.60131731E+02 1.35805549E+02 2.41257828E+01
6.23015525E+02 5.43163331E+02 6.77361429E+02 5.79666448E+02 1.36529845E+02
5.55102864E+02 1.42043746E+02 9.97010751E+01 1.50451907E+02 1.27580945E+02
2.24642027E+01 1.28660679E+02 2.09196588E+01 6.13222485E+02 5.31729638E+02
6.65341537E+02 5.67091556E+02 1.33425128E+02 5.46420097E+02 1.25684844E+02
5.37145282E+02 1.01830755E+02 8.51803323E+01 1.30889580E+02 9.06188690E+01
1.96424645E+01 9.05511044E+01 1.83396732E+01 8.82564996E+01 1.60591691E+01
6.01098026E+02 5.20625000E+02 6.51845563E+02 5.55138100E+02 1.30892175E+02
5.35670235E+02 1.01713403E+02 5.26422201E+02 8.62998826E+01 5.15886505E+02
5.70636834E+02 4.86597858E+02 6.15132274E+02 5.17855744E+02 1.00325664E+02
5.08662543E+02 9.31547049E+01 4.97940538E+02 7.96246323E+01 4.87564142E+02
4.55675021E+02 6.43126068E+02 5.56083432E+02 6.97246427E+02 5.92979341E+02
1.38373531E+02 5.72933398E+02 1.30240852E+02 5.62834669E+02 9.22052105E+01
5.51495783E+02 5.20650450E+02 5.89640138E+02 2.30278363E+01 1.70567808E+01
2.33604198E+01 1.77505284E+01 2.83456373E+00 2.06891803E+01 2.57864085E+00
1.95386389E+01 2.39281869E+00 1.90001876E+01 1.60343530E+01 2.00102750E+01
9.61598976E-02

Appendix 5 - Calculation of Self-diffusion Coefficients for 2,4-DNEB and 2,4,6-TNEB and Calculation of Diffusion Coefficients for 2,4-DNEB and 2,4,6-TNEB in K10 and R8002.

	slope	std. error of slope	D	D	D std. error	D std. error
	(Å2/ps)	(Å2/ps)	(Å2/ps)	(m2/s)	(Å2/ps)	(m2/s)
DNEB self - diffusion coefficient	0.04961	0.0003246	0.008268333	8.26833E-11	0.0000541	5.41E-13
TNEB self- diffusion coefficient	0.003492	0.00003313	0.000582	5.82E-12	5.52167E-06	5.52167E-14
TNEB diffusion coeffcient in K10	0.006111	0.00006787	0.0010185	1.0185E-11	1.13117E-05	1.13117E-13
DNEB diffusion coeffcient in K10	0.008513	0.00003632	0.001418833	1.41883E-11	6.05333E-06	6.05333E-14
TNEB diffusion coeffcient in R8002	0.002719	0.00003724	0.000453167	4.53167E-12	6.20667E-06	6.20667E-14
DNEB diffusion coeffcient in R8002	0.004767	0.0000737	0.0007945	7.945E-12	1.22833E-05	1.22833E-13

Appendix 6 - Calculation of Diffusion Coefficients for the Plasticiser Molecules and the NC in the NC Binder Systems

Table 1 Calculation of diffusion coefficients, their associated errors and ln D for 2,4-DNEB and NG-N1 in the NC, 2,4-DNEB and NG-N1 binder

	slope	std. error of slope	D	D	D std. error	D std. error	D	D	D std. error	T	1/T	ln D
	($Å^2$/ps)	($Å^2$/ps)	($Å^2$/ps)	(m^2/s)	($Å^2$/ps)	(m^2/s)	(cm^2/s)	(cm^2/s) 10^7	(cm^2/s)	(K)	(K)	(cm^2/s)
DNEB 298K	0.000987	0.0000188	0.000164467	1.645E-12	3.1333E-06	3.1333E-14	1.64E-08	0.164	3.13E-10	298	0.00336	-17.92
NGN1 298K	0.001109	3.38E-05	0.000184833	1.848E-12	5.6317E-06	5.6317E-14	1.85E-08	0.185	5.63E-10	298	0.00336	-17.81
DNEB 323K	0.002698	8.94E-05	0.000449667	4.497E-12	1.4902E-05	1.4902E-13	4.50E-08	0.450	1.49E-09	323	0.00310	-16.92
NGN1 323K	0.001301	1.855E-05	0.000216833	2.168E-12	3.0917E-06	3.0917E-14	2.17E-08	0.217	3.09E-10	323	0.00310	-17.65
DNEB 348K	0.005122	9.173E-05	0.000853667	8.537E-12	1.5288E-05	1.5288E-13	8.54E-08	0.854	1.53E-09	348	0.00287	-16.28
NGN1 348K	0.003381	3.94E-05	0.0005635	5.635E-12	6.5633E-06	6.5633E-14	5.64E-08	0.564	6.56E-10	348	0.00287	-16.69
DNEB 373K	0.00901	3.701E-05	0.001501667	1.502E-11	6.1683E-06	6.1683E-14	1.50E-07	1.502	6.17E-10	373	0.00268	-15.71
NGN1 373K	0.005754	2.14E-05	0.000959	9.59E-12	3.5717E-06	3.5717E-14	9.59E-08	0.959	3.57E-10	373	0.00268	-16.16
DNEB 398K	0.02027	5.199E-05	0.003378333	3.378E-11	8.665E-06	8.665E-14	3.38E-07	3.378	8.67E-10	398	0.00251	-14.90
NGN1 398K	0.01486	6.18E-05	0.002476667	2.477E-11	1.0302E-05	1.0302E-13	2.48E-07	2.477	1.03E-09	398	0.00251	-15.21

Table 2 Calculation of diffusion coefficients, their associated errors and ln D for 2,4-DNEB and 2,4,6-TNEB in the NC and K10 binder

	slope	std. error of slope	D	D	D std. error	D std. error	D	D	D std. error	T	1/T	ln D
	(Å2/ps)	(Å2/ps)	(Å2/ps)	(m2/s)	(Å2/ps)	(m2/s)	(cm2/s)	(cm2/s) 107	(cm2/s)	(K)	(K)	(cm2/s)
DNEB 298K	0.00198	1.63E-05	0.00032967	3.3E-12	2.7233E-06	2.72333E-14	3.30E-08	0.330	2.72E-10	298	0.00336	-17.23
TNEB 298K	0.00181	2.80E-05	0.000302	3E-12	4.6633E-06	4.66333E-14	3.02E-08	0.302	4.66E-10	298	0.00336	-17.32
DNEB 323K	0.01299	0.000312	0.002165	2.2E-11	0.000052	5.2E-13	2.17E-07	2.165	5.20E-09	323	0.00310	-15.35
TNEB 323K	0.00762	0.0001247	0.00127017	1.3E-11	2.0783E-05	2.07833E-13	1.27E-07	1.270	2.08E-09	323	0.00310	-15.88
DNEB 348K	0.02247	0.0002556	0.003745	3.7E-11	0.0000426	4.26E-13	3.75E-07	3.745	4.26E-09	348	0.00287	-14.80
TNEB 348K	0.01111	0.00008555	0.00185167	1.9E-11	1.4258E-05	1.42583E-13	1.85E-07	1.852	1.43E-09	348	0.00287	-15.50
DNEB 373K	0.02577	0.00005581	0.004295	4.3E-11	9.3017E-06	9.30167E-14	4.30E-07	4.295	9.30E-10	373	0.00268	-14.66
TNEB 373K	0.01845	0.00006755	0.003075	3.1E-11	1.1258E-05	1.12583E-13	3.08E-07	3.075	1.13E-09	373	0.00268	-14.99
DNEB 398K	0.05584	5.94E-05	0.00930667	9.3E-11	9.895E-06	9.895E-14	9.31E-07	9.307	9.90E-10	398	0.00251	-13.89
TNEB 398K	0.03454	0.00008873	0.00575667	5.8E-11	1.4788E-05	1.47883E-13	5.76E-07	5.757	1.48E-09	398	0.00251	-14.37

Table 3 Calculation of diffusion coefficients and their associated errors for NC in the NC, 2,4-DNEB and NG-N1 binder

	slope	std. error of slope	D	D	D std. error	D std. error	D	D	D std. error
	(Å2/ps)	(Å2/ps)	(Å2/ps)	(m2/s)	(Å2/ps)	(m2/s)	(cm2/s)	(cm2/s) 107	(cm2/s)
NC in NCDNNG 298K	0.0002032	1.08E-05	3.38667E-05	3.38667E-13	0.000001805	1.805E-14	3.39E-09	0.034	1.81E-10
NC in NCDNNG 323K	0.0007918	3.42E-05	0.000131967	1.31967E-12	5.70667E-06	5.70667E-14	1.32E-08	0.132	5.71E-10
NC in NCDNNG 348K	0.001156	7.49E-05	0.000192667	1.92667E-12	0.000012485	1.2485E-13	1.93E-08	0.193	1.25E-09
NC in NCDNNG 373K	0.001903	3.43E-05	0.000317167	3.17167E-12	5.71667E-06	5.71667E-14	3.17E-08	0.317	5.72E-10
NC in NCDNNG 398K	0.002818	6.46E-05	0.000469667	4.69667E-12	0.00001077	1.077E-13	4.70E-08	0.470	1.08E-09

Table 4 Calculation of diffusion coefficients and their associated errors for NC in the NC and K10 binder

	slope	std. error of slope	D	D	D std. error	D std. error	D	D	D std. error
	(Å2/ps)	(Å2/ps)	(Å2/ps)	(m2/s)	(Å2/ps)	(m2/s)	(cm2/s)	(cm2/s) 107	(cm2/s)
NC in NCDNTN 298K	0.001176	4.21E-05	0.000196	1.96E-12	7.0117E-06	7.0117E-14	1.96E-08	0.196	7.01E-10
NC in NCDNTN 323K	0.001315	3.33E-05	0.000219167	2.192E-12	5.545E-06	5.545E-14	2.19E-08	0.219	5.55E-10
NC in NCDNTN 348K	0.001785	0.0001087	0.0002975	2.975E-12	1.8117E-05	1.8117E-13	2.98E-08	0.298	1.81E-09
NC in NCDNTN 373K	0.002172	7.01E-05	0.000362	3.62E-12	1.1688E-05	1.1688E-13	3.62E-08	0.362	1.17E-09
NC in NCDNTN 398K	0.007152	3.34E-04	0.001192	1.192E-11	5.5633E-05	5.5633E-13	1.19E-07	1.192	5.56E-09

Appendix 7 - The Natural Logarithms of the Diffusion Coefficients vs. 1/T for each Plasticiser Molecule in the NC Binder Systems and Calculation of Activation Energies of Diffusion

Table 5 Natural logarithms of the diffusion coefficients of 2,4-DNEB and 2,4 TNEB in an NC binder.

		ln D ($cm^2 s^{-1}$) for 2,4-DNEB and 2,4 TNEB in an NC binder	
T (K)	1/T (K)	2,4-DNEB	2,4,6-TNEB
298	0.00336	-17.23	-17.32
323	0.00310	-15.35	-15.88
348	0.00287	-14.80	-15.50
373	0.00268	-14.66	-14.99
398	0.00251	-13.89	-14.37

Table 6 Natural logarithms of the diffusion coefficients of 2,4-DNEB and NG-N1 in an NC binder.

		ln D ($cm^2 s^{-1}$) for 2,4-DNEB and NG-N1 in an NC binder	
T (K)	1/T (K)	2,4-DNEB	NG-N1
298	0.00336	-17.92	-17.81
323	0.00310	-16.92	-17.65
348	0.00287	-16.28	-16.69
373	0.00268	-15.71	-16.16
398	0.00251	-14.90	-15.21

Calculation of Activation Energies of Diffusion of the Plasticiser Molecules with their errors

$$lnD = lnD_0 - \frac{E_a}{RT}$$

Slope lnD versus 1/T = $-E_a/R$
E_a = - Slope × R

2,4-DNEB and 2,4,6-TNEB in the NC and K10 binder

2,4-DNEB
E_a = - Slope × R
E_a = - (- 3214 K × 8.314 J mol^{-1} K^{-1})
E_a = 26721.196 J mol^{-1}
E_a = 26.7 kJ mol^{-1}

2,4,6-TNEB
E_a = - Slope × R
E_a = - (- 3368 K × 8.314 J mol^{-1} K^{-1})
E_a = 28001.552 J mol^{-1}
E_a = 28.0 kJ mol^{-1}

2,4-DNEB and NG-N1 in the NC, 2,4-DNEB and NG-N1 binder

2,4-DNEB
E_a = - Slope × R
E_a = - (- 3042 K × 8.314 J mol^{-1} K^{-1})
E_a = 25291.188 J mol^{-1}
E_a = 25.3 kJ mol^{-1}

NG-N1
E_a = - Slope × R
E_a = - (- 3355 K × 8.314 J mol^{-1} K^{-1})
E_a = 27893.47 J mol^{-1}
E_a = 27.9 kJ mol^{-1}

Calculation of Errors

2,4-DNEB and 2,4,6-TNEB in the NC and K10 binder

2,4-DNEB
E_a = - Error of Slope × R
E_a = - (± 339.7 K × 8.314 J mol^{-1} K^{-1})
E_a = 2824.3 J mol^{-1}
E_a = 2.8 kJ mol^{-1}

2,4,6-TNEB
E_a = - Error of Slope × R
E_a = - (± 204.7 K × 8.314 J mol^{-1} K^{-1})
E_a = 1701.9 J mol^{-1}
E_a = 1.7 kJ mol^{-1}

2,4-DNEB and NG-N1 in the NC, 2,4-DNEB and NG-N1 binder

2,4-DNEB
E_a = - Error of Slope × R
E_a = - (± 145.8 K × 8.314 J mol^{-1} K^{-1})
E_a = 1212.2 J mol^{-1}
E_a = 1.2 kJ mol^{-1}

NG-N1
E_a = - Error of Slope × R
E_a = - (± 267.3 K × 8.314 J mol^{-1} K^{-1})
E_a = 2222.3 J mol^{-1}
E_a = 2.2 kJ mol^{-1}

Appendix 8 - Construction of Simulation Cells with Water

2,4,6-TNEB
238 molecules in 40 $Å^3$ simulation box
Total mass = 238 × 241.16 = 57,396
Total mass of 155 water molecules = 2790/57396 × 100 = 4.8%

2,4-DNEB
283 molecules in 40 $Å^3$ simulation box
Total mass = 283 × 196 = 55,468
Total mass of 155 water molecules = 2790/55,468 × 100 = 5%

K10
78 2,4,6-TNEB molecules in 40 $Å^3$ simulation box, 144 2,4-DNEB molecules in 40 $Å^3$ simulation box
Total mass = 47,034
Total mass of 155 water molecules = 2790/47,034 × 100 = 5.9%

R8002
111 2,4,6-TNEB molecules in 40 $Å^3$ simulation box, 111 2,4-DNEB molecules in 40 $Å^3$ simulation box
Total mass = 48,524.76
Total mass of 155 water molecules = 2790/48,534.76 × 100 = 5.7%

NG-N1
306 NG-N1 molecules in 40 $Å^3$ simulation box
Total mass = 306 × 226 = 69,156
5% mass of 69,156 = 3457.8/18
= 192 water molecules, 190 added to simulation box

NG-N1 and 2,4-DNEB
208 2,4-DNEB molecules in 40 $Å^3$ simulation box, 90 NG-N1 molecules in 40 $Å^3$ simulation box
Mass of 2,4-DNEB = 208 × 196 = 40,768, Mass of NG-N1 = 90 × 226 = 20,340
Total mass = 61,108
5% mass of 61,108 = 3055/18
= 169.7 water molecules, 170 added to simulation box

NC, 2,4-DNEB and NG-N1 binder system
mass of NC in mixture = 23,760
Ethyl C Mr = 268.36 × 8 = 2146.88
2,4-DNEB = 196 × 640 = 125,440
NG-N1 = 226 × 286 = 64,636
Total = 215,982 × 0.05 = 10,799/18 = 600 molecules

NC, 2,4-DNEB and 2,4,6-TNEB binder system
mass of NC in mixture = 23,760
Ethyl C Mr = 268.36 × 8 = 2146.88
2,4-DNEB = 196 × 630 = 123,480
2,4,6-TNEB = 241.16 × 276 = 66,560.16
Total = 215,947 × 0.05 = 10,797/18 = 600 molecule

Appendix 9 - Diffusion Coefficients for NO_2 in the NC Binders and for Water in the Plasticisers and NC Binders

Table 1 Calculation of Diffusion Coefficients for Different Concentrations of NO_2 (%) in the NC Binder Plasticised with K10

	Conc. Of NO_2	slope	std. err. slope	D	D	D std. error	D std. error	D	D	D std. error
		(Å2/ps)	(Å2/ps)	(Å2/ps)	(m2/s)	(Å2/ps)	(m2/s)	(cm2/s)	(cm2/s) 107	(cm2/s)
298 K	5%	0.009432	0.0001378	0.001572	1.572E-11	2.2967E-05	2.2967E-13	1.57E-07	1.572	2.30E-09
	15%	0.006691	0.0002935	0.00111517	1.1152E-11	4.8917E-05	4.8917E-13	1.12E-07	1.115	4.89E-09
	40%	0.01363	0.0001151	0.00227167	2.2717E-11	1.9183E-05	1.9183E-13	2.27E-07	2.272	1.92E-09
	75%	0.02033	0.0002462	0.00338833	3.3883E-11	4.1033E-05	4.1033E-13	3.39E-07	3.388	4.10E-09
	100%	0.02504	8.91E-05	0.00417333	4.1733E-11	1.4843E-05	1.4843E-13	4.17E-07	4.173	1.48E-09
323 K	5%	0.007704	0.0004307	0.001284	1.284E-11	7.1783E-05	7.1783E-13	1.28E-07	1.284	7.18E-09
	15%	0.02456	0.0002749	0.00409333	4.0933E-11	4.5817E-05	4.5817E-13	4.09E-07	4.093	4.58E-09
	40%	0.05224	0.0001383	0.00870667	8.7067E-11	0.00002305	2.305E-13	8.71E-07	8.707	2.31E-09
	75%	0.05419	0.0001605	0.00903167	9.0317E-11	0.00002675	2.675E-13	9.03E-07	9.032	2.68E-09
	100%	0.0938	0.0002196	0.01563333	1.5633E-10	0.0000366	3.66E-13	1.56E-06	15.633	3.66E-09
348 K	5%	0.06725	0.001744	0.01120833	1.1208E-10	0.00029067	2.9067E-12	1.12E-06	11.208	2.91E-08
	15%	0.08812	0.001078	0.01468667	1.4687E-10	0.00017967	1.7967E-12	1.47E-06	14.687	1.80E-08
	40%	0.1468	0.0007074	0.02446667	2.4467E-10	0.0001179	1.179E-12	2.45E-06	24.467	1.18E-08
	75%	0.1774	0.001341	0.02956667	2.9567E-10	0.0002235	2.235E-12	2.96E-06	29.567	2.24E-08
	100%	0.2235	0.0009725	0.03725	3.725E-10	0.00016208	1.6208E-12	3.73E-06	37.250	1.62E-08

Table 2 Calculation of Diffusion Coefficients for Different Concentrations of NO_2 (%) in the NC Binder Plasticised with 2,4-DNEB and NG-N1

	Conc. Of NO_2	slope	std. error of slope	D	D	D std. error	D std. error	D	D	D std. error
		(Å2/ps)	(Å2/ps)	(Å2/ps)	(m2/s)	(Å2/ps)	(m2/s)	(cm2/s)	(cm2/s) 107	(cm2/s)
298 K	5%	0.0003195	0.004272	0.00005325	5.325E-13	0.000712	7.12E-12	5.33E-09	0.053	7.12E-08
	15%	0.0001047	1.50E-05	0.00001745	1.745E-13	2.5033E-06	2.5033E-14	1.75E-09	0.017	2.50E-10
	40%	0.005616	0.0001052	0.000936	9.36E-12	1.7533E-05	1.7533E-13	9.36E-08	0.936	1.75E-09
	75%	0.009847	0.000112	0.00164117	1.6412E-11	1.8667E-05	1.8667E-13	1.64E-07	1.641	1.87E-09
	100%	0.0131	0.0002138	0.00218333	2.1833E-11	3.5633E-05	3.5633E-13	2.18E-07	2.183	3.56E-09
323 K	5%	0.002157	0.000282	0.0003595	3.595E-12	0.000047	4.7E-13	3.60E-08	0.360	4.70E-09
	15%	0.003737	0.0001783	0.00062283	6.2283E-12	2.9717E-05	2.9717E-13	6.23E-08	0.623	2.97E-09
	40%	0.005178	8.85E-05	0.000863	8.63E-12	0.00001475	1.475E-13	8.63E-08	0.863	1.48E-09
	75%	0.01394	7.30E-05	0.00232333	2.3233E-11	1.2158E-05	1.2158E-13	2.32E-07	2.323	1.22E-09
	100%	0.02234	0.0001762	0.00372333	3.7233E-11	2.9367E-05	2.9367E-13	3.72E-07	3.723	2.94E-09
348 K	5%	0.005619	0.0002019	0.0009365	9.365E-12	0.00003365	3.365E-13	9.37E-08	0.937	3.37E-09
	15%	0.01876	0.0003926	0.00312667	3.1267E-11	6.5433E-05	6.5433E-13	3.13E-07	3.127	6.54E-09
	40%	0.02891	8.87E-05	0.00481833	4.8183E-11	1.4782E-05	1.4782E-13	4.82E-07	4.818	1.48E-09
	75%	0.06014	8.07E-05	0.01002333	1.0023E-10	1.3445E-05	1.3445E-13	1.00E-06	10.023	1.34E-09
	100%	0.06501	9.05E-05	0.010835	1.0835E-10	0.00001508	1.508E-13	1.08E-06	10.835	1.51E-09

Table 3 Calculation of Diffusion Coefficients for Water in the Plasticisers

	slope	std. error of slope	D	D	D std. error	D std. error	D	D	D std. error
	(Å2/ps)	(Å2/ps)	(Å2/ps)	(m2/s)	(Å2/ps)	(m2/s)	(cm2/s)	(cm2/s) 107	(cm2/s)
DNEB 298 K	0.2648	0.001554	0.044133333	4.41333E-10	0.000259	2.59E-12	4.41E-06	44.133	2.59E-08
DNEB 338 K	0.4956	0.001313	0.0826	8.26E-10	0.000218833	2.18833E-12	8.26E-06	82.600	2.19E-08
TNEB 298 K	0.05138	0.000247	0.008563333	8.56333E-11	4.11667E-05	4.11667E-13	8.56E-07	8.563	4.12E-09
TNEB 338 K	0.06202	0.0008206	0.010336667	1.03367E-10	0.000136767	1.36767E-12	1.03E-06	10.337	1.37E-08
K10 298 K	0.1305	0.0005878	0.02175	2.175E-10	9.79667E-05	9.79667E-13	2.18E-06	21.750	9.80E-09
K10 338 K	0.2221	0.0007505	0.037016667	3.70167E-10	0.000125083	1.25083E-12	3.70E-06	37.017	1.25E-08
R8002 298 K	0.1231	0.0006572	0.020516667	2.05167E-10	0.000109533	1.09533E-12	2.05E-06	20.517	1.10E-08
R8002 338 K	0.3312	0.003311	0.0552	5.52E-10	0.000551833	5.51833E-12	5.52E-06	55.200	5.52E-08
NG-N1 298 K	0.0001421	9.952E-07	2.36833E-05	2.36833E-13	1.65867E-07	1.65867E-15	2.37E-09	0.024	1.66E-11
NG-N1 338 K	0.0009412	0.000004706	0.000156867	1.56867E-12	7.84333E-07	7.84333E-15	1.57E-08	0.157	7.84E-11
2,4-DNEB & NG-N1 298 K	0.02429	0.0002229	0.004048333	4.04833E-11	0.00003715	3.715E-13	4.05E-07	4.048	3.72E-09
2,4-DNEB & NG-N1 338 K	0.111	0.0008199	0.0185	1.85E-10	0.00013665	1.3665E-12	1.85E-06	18.500	1.37E-08

Table 4 Calculation of Diffusion Coefficients for Water in the NC Binder Plasticised with K10

	slope	std. error of slope	D	D	D std. error	D std. error	D	D	D std. error
	(Å2/ps)	(Å2/ps)	(Å2/ps)	(m2/s)	(Å2/ps)	(m2/s)	(cm2/s)	(cm2/s) 107	(cm2/s)
298 K	0.05025	0.0005712	0.008375	8.375E-11	0.0000952	9.52E-13	8.38E-07	8.375	9.52E-09
323 K	0.06042	0.0004933	0.01007	1.007E-10	8.2217E-05	8.2217E-13	1.01E-06	10.070	8.22E-09
338 K	0.07316	0.0005962	0.01219333	1.2193E-10	9.9367E-05	9.9367E-13	1.22E-06	12.193	9.94E-09
348 K	0.1369	0.00128	0.02281667	2.2817E-10	0.00021333	2.1333E-12	2.28E-06	22.817	2.13E-08

Table 5 Calculation of Diffusion Coefficients for Water in the NC Binder Plasticised with 2,4-DNEB and NG-N1

	slope	std. error of slope	D	D	D std. error	D std. error	D	D	D std. error
	(Å2/ps)	(Å2/ps)	(Å2/ps)	(m2/s)	(Å2/ps)	(m2/s)	(cm2/s)	(cm2/s) 107	(cm2/s)
298 K	0.0141	0.00007523	0.00235	2.35E-11	1.2538E-05	1.2538E-13	2.35E-07	2.350	1.25E-09
323 K	0.04401	0.0002251	0.007335	7.335E-11	3.7517E-05	3.7517E-13	7.34E-07	7.335	3.75E-09
338 K	0.03437	0.0002457	0.005728333	5.7283E-11	0.00004095	4.095E-13	5.73E-07	5.728	4.10E-09
348 K	0.102	0.0009837	0.017	1.7E-10	0.00016395	1.6395E-12	1.70E-06	17.000	1.64E-08

Table 6 Calculation of Diffusion Coefficients for Water in the NC Binder Plasticised with K10 containing Water and 40% NO_2

H_2O in NO_2 NCDNTN	slope	std. error of slope	D	D	D std. error	D std. error	D	D	D std. error
	(Å2/ps)	(Å2/ps)	(Å2/ps)	(m2/s)	(Å2/ps)	(m2/s)	(cm2/s)	(cm2/s) 107	(cm2/s)
298 K	0.02353	0.0002904	0.00392167	3.9217E-11	0.0000484	4.84E-13	3.92E-07	3.922	4.84E-09
323 K	0.04497	0.0008061	0.007495	7.495E-11	0.00013435	1.3435E-12	7.50E-07	7.495	1.34E-08
338 K	0.1116	0.0006879	0.0186	1.86E-10	0.00011465	1.1465E-12	1.86E-06	18.600	1.15E-08
348 K	0.1764	0.002355	0.0294	2.94E-10	0.0003925	3.925E-12	2.94E-06	29.400	3.93E-08

Table 7 Calculation of Diffusion Coefficients for NO_2 in the NC Binder Plasticised with K10 containing Water and 40% NO_2

NO_2 in H_2O NCDNTN	slope	std. error of slope	D	D	D std. error	D std. error	D	D	D std. error
	(Å2/ps)	(Å2/ps)	(Å2/ps)	(m2/s)	(Å2/ps)	(m2/s)	(cm2/s)	(cm2/s) 107	(cm2/s)
298 K	0.01666	0.0001659	0.00277667	2.7767E-11	0.00002765	2.765E-13	2.78E-07	2.777	2.77E-09
323 K	0.06345	0.0001577	0.010575	1.0575E-10	2.6283E-05	2.6283E-13	1.06E-06	10.575	2.63E-09
338 K	0.1169	0.0000635	0.01948333	1.9483E-10	1.0583E-05	1.0583E-13	1.95E-06	19.483	1.06E-09
348 K	0.2068	0.0008631	0.03446667	3.4467E-10	0.00014385	1.4385E-12	3.45E-06	34.467	1.44E-08

Table 8 Calculation of Diffusion Coefficients for Water in the NC Binder Plasticised with 2,4-DNEB and NG-N1 containing Water and 40% NO_2

H_2O in NO_2 NCDNNG	slope	std. error of slope	D	D	D std. error	D std. error	D	D	D std. error
	(Å2/ps)	(Å2/ps)	(Å2/ps)	(m2/s)	(Å2/ps)	(m2/s)	(cm2/s)	(cm2/s) 107	(cm2/s)
298 K	0.0186	0.0001119	0.0031	3.1E-11	0.00001865	1.865E-13	3.10E-07	3.100	1.87E-09
323 K	0.02337	9.70E-05	0.003895	3.895E-11	1.6167E-05	1.6167E-13	3.90E-07	3.895	1.62E-09
338 K	0.04682	0.0001913	0.00780333	7.8033E-11	3.1883E-05	3.1883E-13	7.80E-07	7.803	3.19E-09
348 K	0.0486	0.0005869	0.0081	8.1E-11	9.7817E-05	9.7817E-13	8.10E-07	8.100	9.78E-09

Table 9 Calculation of Diffusion Coefficients for NO_2 in the NC Binder Plasticised with 2,4-DNEB and NG-N1 containing Water and 40% NO_2

NO_2 in H_2O NCDNNG	slope	std. error of slope	D	D	D std. error	D std. error	D	D	D std. error
	(Å2/ps)	(Å2/ps)	(Å2/ps)	(m2/s)	(Å2/ps)	(m2/s)	(cm2/s)	(cm2/s) 107	(cm2/s)
298 K	0.00758	0.00009001	0.0012635	1.2635E-11	1.5002E-05	1.5002E-13	1.26E-07	1.264	1.50E-09
323 K	0.00982	0.00008607	0.001637	1.637E-11	1.4345E-05	1.4345E-13	1.64E-07	1.637	1.43E-09
338 K	0.02096	0.00006963	0.00349333	3.4933E-11	1.1605E-05	1.1605E-13	3.49E-07	3.493	1.16E-09
348 K	0.0627	0.000218	0.01045	1.045E-10	3.6333E-05	3.6333E-13	1.05E-06	10.450	3.63E-09